ALO-5391-T2

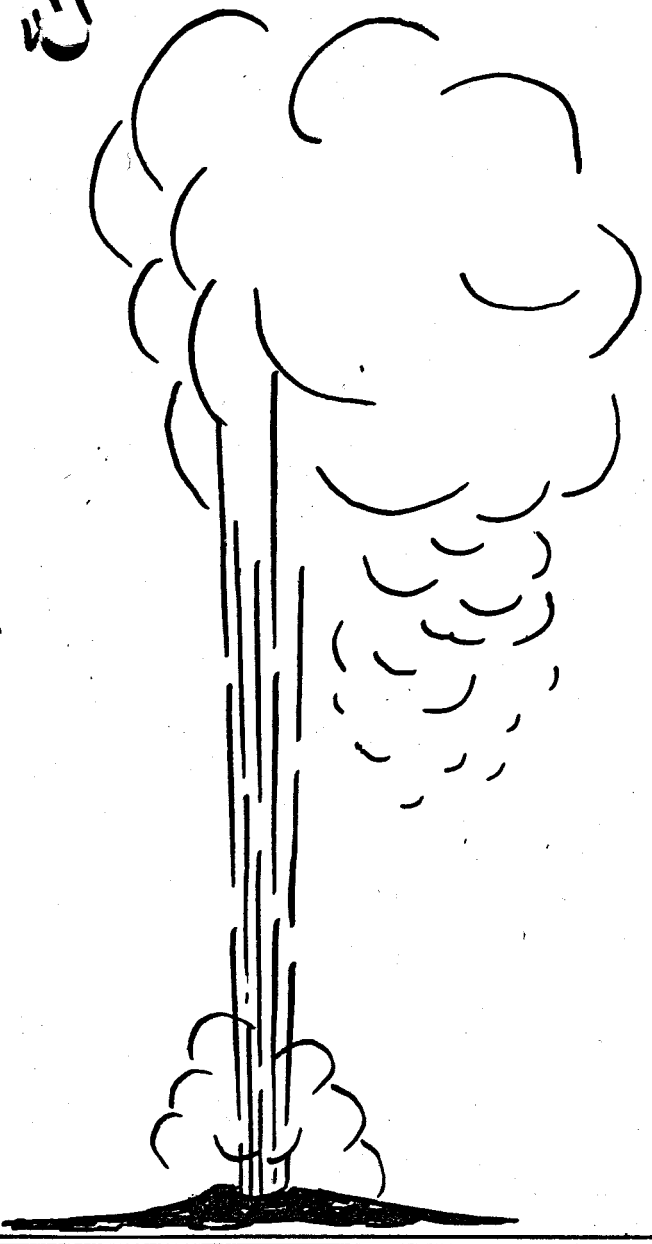

DEVELOPMENT OF AN ACOUSTIC SENSOR FOR A GEOTHERMAL BOREHOLE TELEVIEWER

By
J. W. Wonn

March 1979

Work Performed Under Contract No. ET-76-C-04-5391

Westinghouse Electric Corporation
Research and Development Laboratories
Pittsburgh, Pennsylvania

U. S. DEPARTMENT OF ENERGY

Geothermal Energy

DISCLAIMER

DISCLAIMER

ALO-5391-T2
Distribution Category UC-66b

Development of an Acoustic Sensor for a Geothermal Borehole Televiewer

U. S. Department of Energy
Division of Geothermal Energy

Contract DE-AC04-76ET15391

by

J. W. Wonn

March 1979

Westinghouse Electric Corporation
Research and Development Laboratories
Pittsburgh, PA 15235

TABLE OF CONTENTS

SUMMARY

The objective of this project is to upgrade acoustic sensor technology such that appropriate well logging instruments can be made to operate under the hostile environment conditions anticipated in geothermal resource exploration and evaluation. The Borehole Televiewer (BHTV) was selected as the vehicle for this sensor improvement work, primarily because of its demonstrated ability to detect and characterize fractures under sub-geothermal conditions. This Final Technical report describes the work done toward providing an improved sensor for the televiewer. An experimental sensor concept was devised, incorporating a thin metal acoustic window, an improved, high-temperature internal coupling fluid, and thermally resistant sensor internals.

During an autoclave test, it was successfully demonstrated that the resulting experimental sensor design concept provides the basic target detection and characterization functions required of a fracture mapping, Borehole Televiewer under simulated goethermal conditions. In particular, the experimental sensor remained operational at 275°C and 7000 psi.

1. INTRODUCTION

Fundamental to the exploration and development of geothermal energy resources is the availability of well logging instrumentation for measuring the down-hole physical parameters. The need has been recognized for extending the hostile environment capabilities of existing well logging tools and for developing new tools and methods where necessary.

In a geothermal workshop report[1] issued in 1975, the geothermal instrumentation problem was addressed. The report discusses and rank-orders eight parameters considered essential for evaluation of most geothermal reservoirs. Traditional tools for measuring three of these essential parameters either require or could make use of acoustic sensors: flow rate, fracture system (characterization), and formation depth and thickness. From a list of six important but lower priority parameters, severe environment acoustic sensors can aid in measuring three: lithology and minerology, P and S wave velocities, and hole size (caliper).

Since September 1976, Westinghouse has been under contract with DOE/ERDA to provide improved acoustic sensor technology for geothermal well logging instrumentation. The work plan identified three sequential tasks:

Task 1 - Sensor Application Survey

Task 2 - Geothermal Sensor Development

Task 3 - Sensor Demonstration Under Simulated Geothermal Conditions

The major goal of the Task 1 survey was to identify the most appropriate sensor type to carry into Task 2 (development) and Task 3 (demonstration). Subject logging tools of the Task 1 survey were borehole

[1] All references given in Section 14.

televiewer, acoustic caliper, acoustic velocity logger, down-hole flow meter, and passive listening (fracture) monitor. Efforts included a study of tool capabilities, applications, operation, and geothermal limitations as discussed in the Task 1 - Technical Report[2], issued in May 1977. Based upon Task 1 findings it was concluded that the Borehole Televiewer could make the most effective use of the severe environment acoustic sensor development work.

This Final Technical Report describes the development and demonstration work done under Task 2 and Task 3. Sections 2 and 3 describe the borehole televiewer tool, its acoustic sensor, and the geothermal deficiencies of the sensor. The approach toward solving the sensor problems is discussed in Section 4. Sections 5 through 10 review the work done to provide a televiewer sensor capable of withstanding simulated geothermal fluid at 275°C and 7000 psi.

2. BHTV TOOL DESCRIPTION

The borehole televiewer (BHTV) is an important well logging tool for characterizing geothermal resources, identifying (locating) production zones, studying the down-hole geology and lithology, and for maintaining production wells. Its demonstrated capacity for locating, mapping, and characterizing fractures makes it especially relevant to geothermal researchers charged with resource assessment. Such fracture information can be combined with other data for estimating porosity of potential production zones and therefore the production capacity of the geothermal well.

The televiewer provides an acoustic image of the bore hole surface, delineating such important features as wall discontinuities, formation dip, fracture patterns, vugs, and washouts. Demonstrated capabilities include mapping of fracture zones, bedding planes, and other borehole manifestations of the geology. BHTV has also been used in cased wells as an inspection tool to map cavitation, pitting, perforation plugging or enlargement, case breaches, and other production-related parameters.

Figure 2.1 shows the down-hole portion of a televiewer tool. The upper 2/3 of the cylindrical tool body contains the electronic circuitry and the lower 1/3 contains the acoustic sensor as indicated in the figure. The schematic block diagram of Figure 2.2 indicates the operation of the down-hole televiewer tool in conjunction with surface electronics and a display.

Within the down-hole sensor compartment, a piezoelectric transducer is rotated (180 RPM) by an electric motor to provide a scan of a line around the borewall. The transducer emits high-frequency, narrow beam acoustic pulses. The emitted pulses are reflected from the borewall

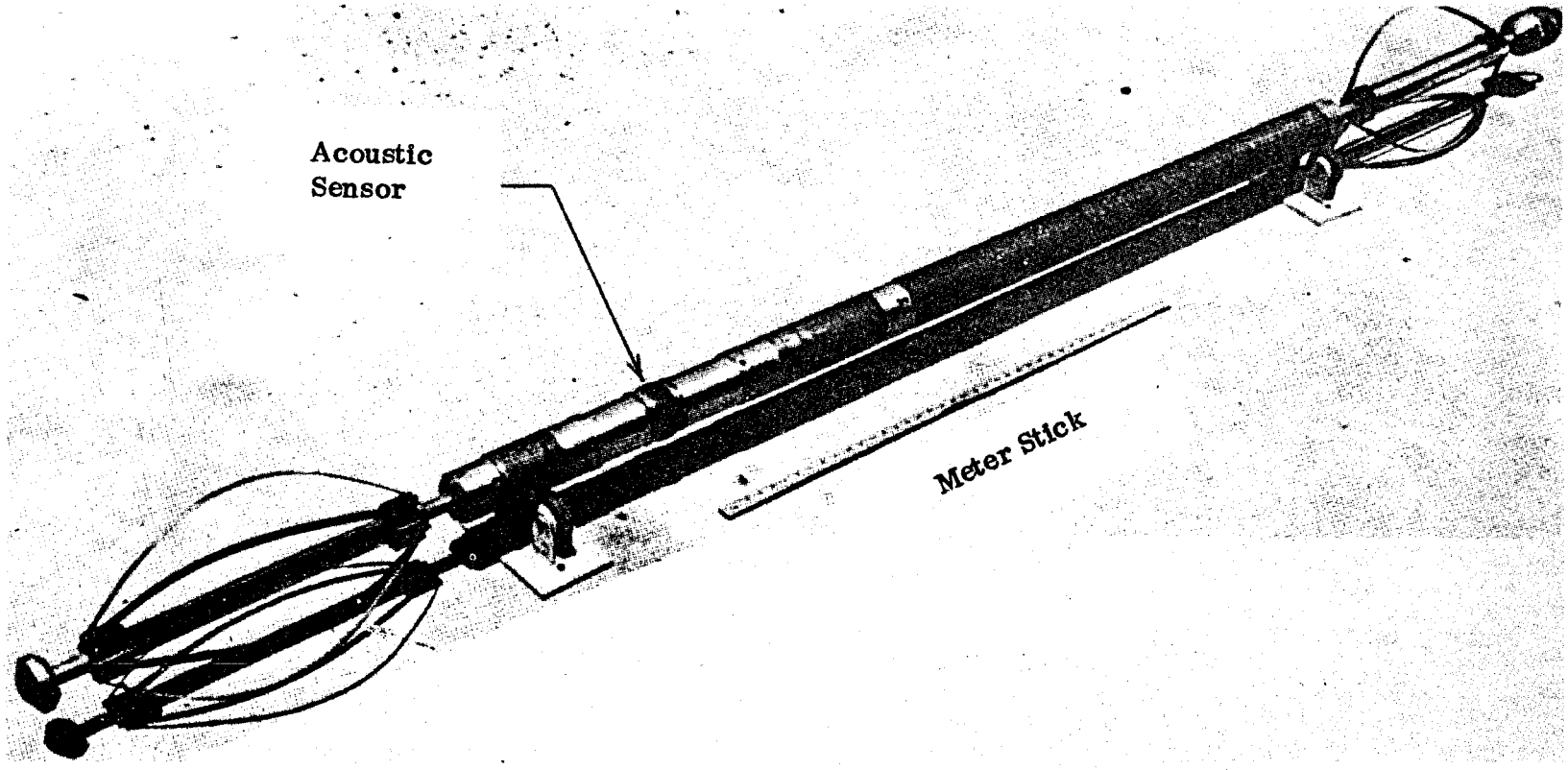

Figure 2.1. Typical down-hole "sonde" of borehole televiewer, showing location of acoustic sensor. Bow-spring centralizers top and bottom.

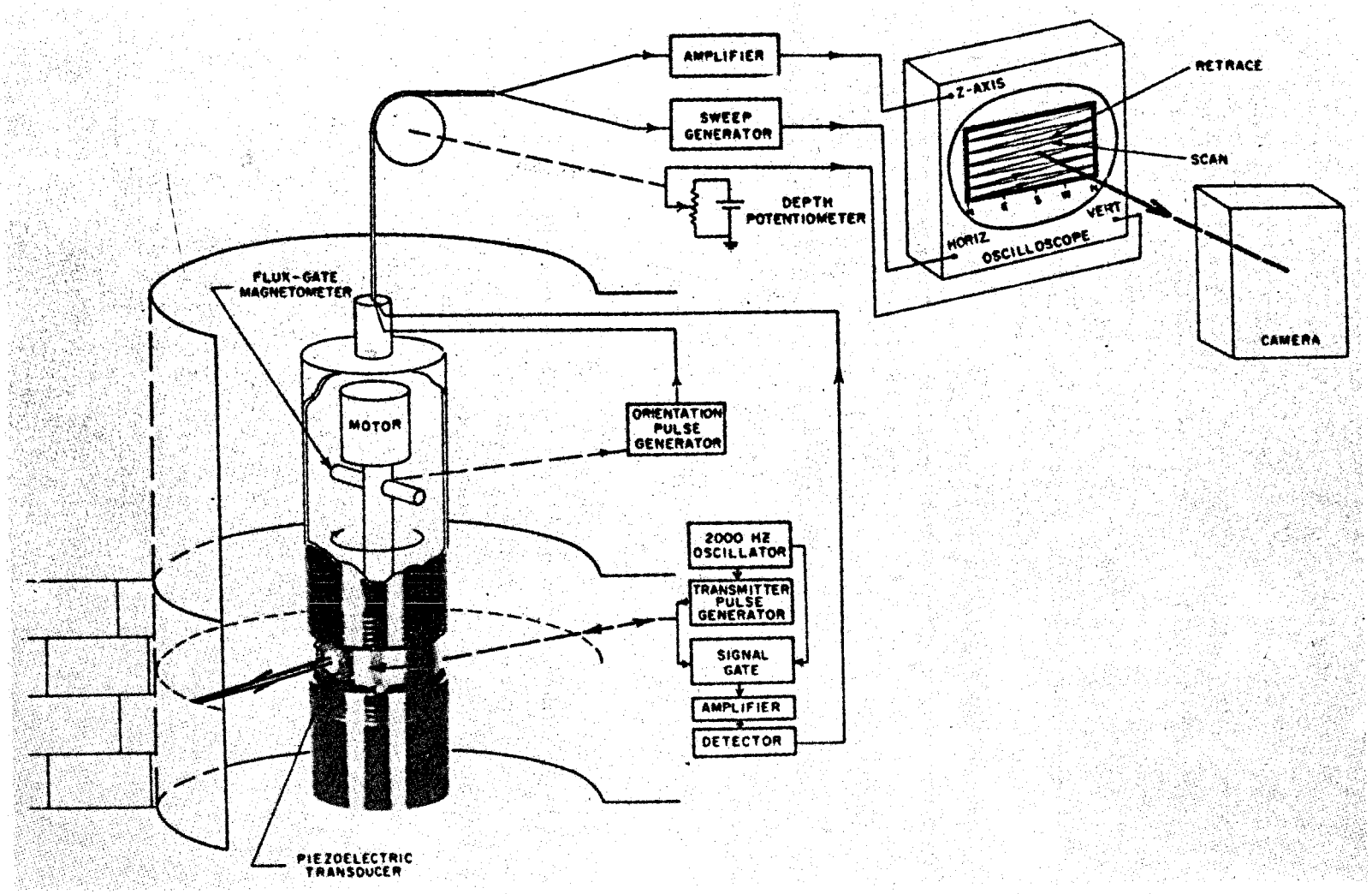

Figure 2.2. Schematic block diagram of BHTV system and operation. (Reproduced from and with permission of Journal of Petroleum Technology[3]).

and are detected by the transducer. Scattering due to irregularities in the wall geometry varies the amplitude of the received signals. The received signals are amplified and detected by the down-hole electronics and the envelope of the signal is sent to the surface via the logging cable. At the surface, the envelope is used to Z-axis modulate a CRT display. A pulse is also generated by the flux gate magnetometer each time the acoustic beam passes magnetic north. This pulse is multiplexed to the surface on the logging cable to provide a trigger for the display horizontal sweep. Blanking and horizontal retrace are automatic parts of the sweep. The vertical beam position on the CRT display is determined by vertical position of the tool in the bore as measured by the depth potentiometer. The camera shutter remains open to record the display over each successive vertical segment of well. The result is an oriented acoustic image, providing a direct and descriptive reproduction of the borehole wall split along a known line.

Figure 2.3 shows 3 examples of typical televiewer output data. Each example consists of a composite of successive individual pictures to form a continuous log. Fractures appear as characteristic lines, and bedding planes appear as sinusoidal curves with a single maximum and minimum point providing dip information.

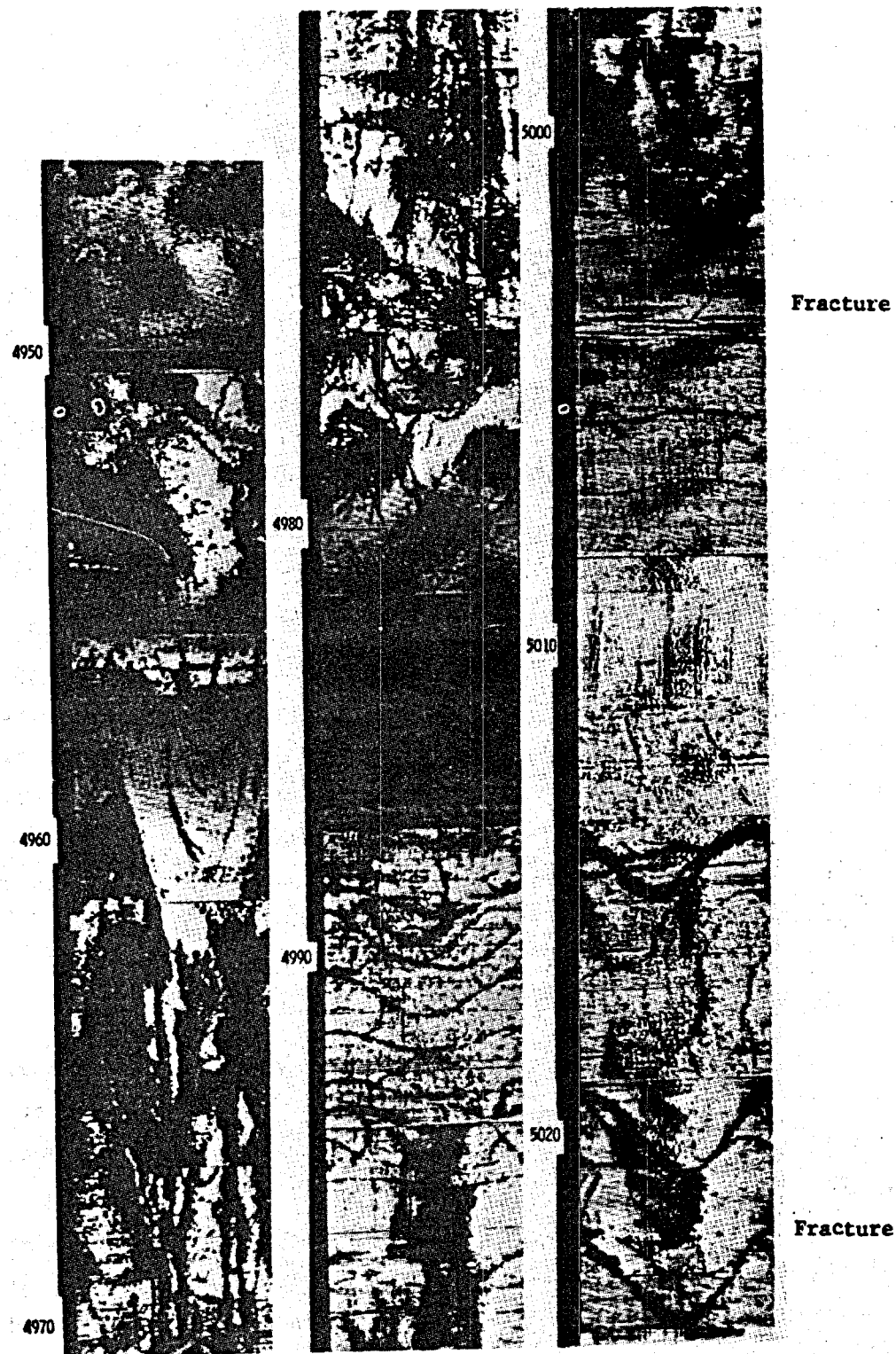

Figure 2.3. Three borehole televiewer logs in fractured West Texas Precambrian Formation. Wellbore filled with drilling mud. (Reproduced from and with permission of Journal of Petroleum Technology[3]).

3. PROBLEM DEFINITION

The borehole televiewer (BHTV) was originally developed for use in relatively cool petroleum reservoirs. As such, the traditional BHTV has a temperature limitation of approximately 150°C. The objective of this project is to develop an improved BHTV sensor concept, capable of withstanding the caustic geothermal well fluid at 275°C and 7000 psi.

USGS/Water Resources Department has been conducting field evaluations of BHTV in geothermal reservoirs for some time. Their cooperative efforts with Simplec have resulted in an improved BHTV with extended temperature tolerance. However, efforts to operate the improved tool at temperatures as high as 500°F have been largely unsuccessful to date. Some of the most serious geothermal tool deficiencies appear to be concentrated in the acoustic sensor portion of the tool, as it must withstand direct exposure to the borehole fluid.

The Acoustic Sensor

Figure 3.1 shows a cross-sectional diagram of a traditional BHTV acoustic sensor in typical proximity with its surrounds. A piezoceramic disc is used as a transducer element which launches and receives acoustic pulses. The piezoceramic disc is mounted on a damping material to minimize structural reverberation within the tool which could mask weak received signals. Acoustic communication between the piezoceramic disc and the borehole fluid is accomplished through an acoustic window and an intermediate coupling fluid. The acoustic window must efficiently pass acoustic energy, maintain a barrier against the borehole fluid environment, and be durable enough to withstand the rigors of logging as well as a certain amount of abuse through surface handling. The acoustic sensor also includes electrical wires which must be attached to the piezoelectric disc and some means for holding the disc in place.

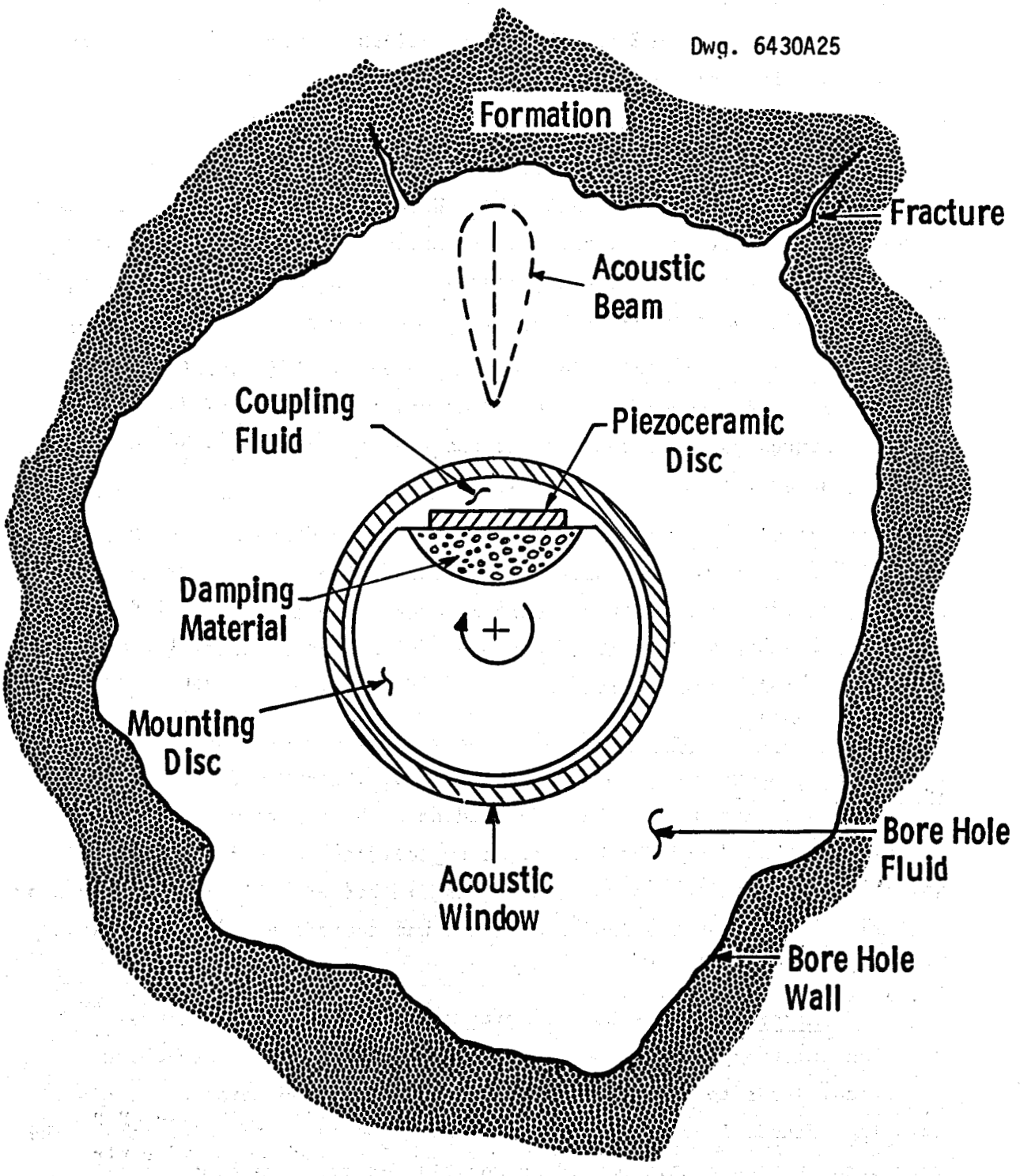

Fig. 3.1—Cross-section diagram indicating construction of conventional BHTV tools

Sensor Deficiencies

Following a functional analysis of the various sensor components, a preliminary assessment was made of deficiencies which could hinder operation under anticipated geothermal conditions.

Piezoceramic Disc - Lead metaniobate piezoceramic is the material used on the traditional BHTV. With a curie temperature in excess of 400°C, this material has been widely accepted as a transducer material for similar applications at temperatures of 275°C and higher. Therefore, no major design problem was anticipated in this area.

Damping Material - The commonly used damping material is an absorptive rubber compound. This rubber was expected to be unsatisfactory at temperatures as high as 275°C and the need for a replacement material was identified.

Coupling Fluid - Mobil Jet Oil II is used in the conventional televiewer. This is a synthetic oil formulated for jet engine lubrication applications. Contact with the manufacturer suggested uncertain performance under geothermal conditions. A potential coupling fluid problem was therefore identified.

Acoustic Window - Traditionally, BHTV windows have been fabricated from temperature intolerant elastomers. Recent efforts toward higher temperature windows have focused on high-temperature polyimide plastics such as Vespel by DuPont. A typical window thickness is 0.10". While this material has permitted logging in hotter wells, frequent window failure has been reported and the window was therefore viewed as a likely problem.

Miscellaneous - Contact with the televiewer manufacturer revealed existing fabrication difficulties in the area of attaching electrical leads to the silver electrodes of the lead metaniobate disc. Existing methods involved soldering wires directly to the electrode. The manufacturer viewed this method as unsatisfactory. Availability of suitable wire with high-temperature insulation was also viewed as a potential problem.

4. PROJECT APPROACH

Strategy - The sensor development approach selected was to provide geothermal replacement components for the existing televiewer embodiment rather than completely redesigning the sensor configuration. This decision was made for several reasons: 1) identified sensor problems appear to be material problems and solutions were considered to be realizable, 2) the basic BHTV sensor configuration was expected to suffice for a geothermal tool, 3) a BHTV tool was available for experimentation, 4) the approach permits testing an improved BHTV in the geothermal environment in the shortest time.

An engineering analysis of the BHTV was done to justify the replacement component approach. Although some parts of the following analysis require approximations, the technique provides a semi-quantitative approach to extrapolating BHTV performance to the geothermal environment.

Engineering Analysis of Existing BHTV Operation

Introduction: This section describes an analytical method for relating tool and borehole parameters to BHTV performance. The analytical basis is provided by the classical active sonar equation.[4] The terms comprising the equation will be discussed, their significance reviewed, and relationship to the various system parameters identified. By comparing parameters for known operating conditions with those anticipated under geothermal conditions, this analytical method is then used to predict satisfactory performance capabilities of a geothermal BHTV.

The Active Sonar Equation: The monostatic active sonar equation has been developed to describe the acoustic operation of a simple pulse-echo system such as is illustrated in Figure 4.1. A transducer, acting as

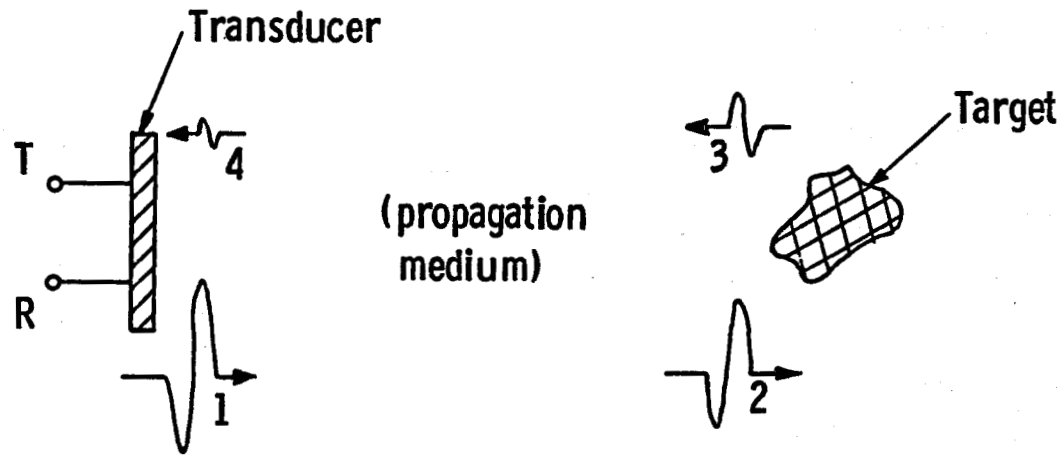

Fig. 4.1—A combination transmit/receive (i.e, monostatic) transducer used in pulse-echo mode to detect a target. Numbered waveforms discussed in text

a sound source (T) as well as a receiver (R), launches an acoustic pressure wave (1) in accordance with electrical excitation applied at T. The intensity of the launched sound is characterized by a quantity called the source level (SL). In traveling from the source to some distant target, the signal level is reduced by the transmission loss (TL) and at (2) becomes SL - TL. (Quantities are expressed in decibels, a logarithmic notation, such that addition and subtraction within expressions imply multiplication and division, respectively.) This signal impinges on some object which has a target strength (TS), giving rise to a backscattered or reflected level (3) of SL-TL + TS. Traveling back toward the source, this level is again decreased by the transmission loss (TL) in the medium. Thus the signal (echo) level (4) arriving at the receiving transducer is SL - 2TL + TS. The receiving transducer converts this pressure wave to an electrical signal which appears at R.

Once the echo (4) is received, it must compete with various noise signals in order to be recognized or detected. The three most common noise sources are 1) isotropic noise coming from the medium, 2) electrical noise in the receiver, and 3) reverberation noise. At typical BHTV operating frequencies, the isotropic noise in a borehole is expected to be negligible. It is further assumed that suitably low-noise receiver circuitry can be provided. It is expected that reverberation noise represents the predominant noise source competing with and masking echo signals at R. Denoting the reverberation level as RL, an expression for the signal-to-noise ratio (SNR) at R, the receiver input can be written:

$$SNR = SL - 2TL + TS - RL \qquad (4.1)$$

Reliable discrimination of bona fide echos in the presence of masking noise requires that the SNR exceeds some minimum value which can be called the detection threshold (DT). The detection threshold is determined by specific signal parameters, noise characteristics, and signal processing techniques incorporated into the receiver. It suffices to say that given a system, satisfactory operation can be expected whenever the following inequality is satisfied:

$$DT \leq SL - 2TL + TS - RL \qquad (4.2)$$

This form of the active sonar equation provides the basis for relating BHTV performance to various operating conditions.

Terms of the Active Sonar Equation: Before equation (4.2) can be put to use, it is necessary to have a basic understanding of the various physical parameters which influence the actual values of the terms in the right half of the equation.

Source Level (SL) - is basically determined by the electrical excitation level and the electroacoustic efficiency of the transducer. Other factors such as directivity also affect SL but can be ignored for reasons explained later.

Transmission Loss (TL) - is caused by interface reflections, absorption, scattering, and spreading (divergence) of the traveling acoustic waves. Interface reflections are the result of acoustic impedance mismatches. They occur at the boundaries between two elastically dissimilar materials such as between an acoustic window and a borehole fluid. Minimizing impedance mismatch minimizes this source of TL. Absorption describes the process of converting the acoustic energy to some other non-acoustic form such as heat thereby introducing loss. Scattering can be a major source of loss in fluids containing sediments or gas voids suspended in the solution. As the acoustic wave encounters each particle, some portion of the propagating energy is scattered off in non-useful directions. Spreading or divergence losses occur beyond the near-field of the sonic beam.

Target Strength (TS) - is essentially determined by the geometry of the target and the wavelength of the acoustic energy. Size, roughness, and orientation of reflecting surfaces relative to the acoustic wavelength (λ) establish the magnitude of this terms. Large (compared with λ), smooth (compared with λ), perpendicular target surfaces exhibit the highest target strengths.

Reverberation Level (RL) - Of particular concern is reverberation caused by acoustic energy which is launched by the transmitter, finds its way into the structure surrounding the transducer, and is still

rattling around in the structure at the time the target echo returns to the receiving transducer. Thus structural reverberation level is a function of the amount of energy launched into the structure, and the acoustic loss mechanisms built into the structure.

RL is also related to acoustic window performance. Acoustic energy reflected from the window back toward the sensor internals can introduce significant reverberation problems.

Table 4-I summarizes the preceeding discussion.

TABLE 4-I

SONAR EQUATION TERM	INFLUENTIAL SENSOR & BOREHOLE PARAMETERS
Source Level (SL)	Electrical Excitation Level. Electroacoustic Efficiency. Directivity Index.
Transmission Loss (TL)	Reflections at interfaces. Absorption and scattering in the medium. Spreading Loss (divergence).
Target Strength (TS)	Target Geometry (size, shape, orientation). Wavelength of acoustic energy.
Reverberation Level (RL)	Materials and construction of sensor and adjacent structures. Acoustic window performance.
Detection Threshold (DT)	Determined by signal, noise, and receiver characteristics

BHTV Performance Reference - There exists a reasonable body of information regarding performance of BHTV as a function of influential parameters. More specially, the HT-BHTV available for experimentation is known to reach a marginal SNR condition under the following conditions:

Tool:	Hi-Temperature (HT) BHTV
Sensor:	H-T Construction
Borehole:	12 #/gallon mud-filled hole of optimum tool/borehole diameter relationship.
Targets:	Fractures and other typical borehole features.

Let us say that for the above "reference" conditions, the left side of equation (4.2) just equals the right (i.e., barely marginal performance).

Geothermal BHTV Performance Extrapolation - It is now possible to hypothetically place the same tool in a geothermal environment by using approximations to establish system parameters. Translating parameter variations into changes in the sonar equation terms then permits estimating overall impact on performance under geothermal conditions.

A representative set of geothermal conditions might be as follows:

Tool:	Geothermal BHTV
Sensor:	Improved HT Construction
Borehole:	1% sediment by volume in caustic borehole fluid; same optimum tool/borehole diameter relationship.
Targets:	"Typical" geothermal fractures.

We can now look at changes in the various terms of the sonar equation introduced by tool operation in a geothermal well.

Source Level - The general form of the geothermal sensor is assumed to mimmick the design of the "reference" sensor. The peizoelectric element is assumed to be the same material with the same dimensions and operating (resonant) frequency. The directivity of the sensor is therefore unchanged. Sensor efficiency should not be adversely affected at 275°C. It is also assumed that a comparable electrical transmit pulse level is applied to the sensor. Under these assumed conditions, there should be no change in source level when compared with the reference case.

Transmission Loss - Acoustic window losses for a geothermal sensor are expected to be essentially unchanged. Assume the tool-to-borehole distance for both tools is approximately 1". Total path in the borehole fluid is therefore 2". At the assumed operating frequency the approximate attenuation through 1" of 12 #/gallon mud is calculated to be 30 dB/inch while only 6 dB/inch in a 1% sediment (geothermal) solution. The difference represents a 48 dB decrease in loss compared with the round-trip path loss of the reference case. Acoustic path length, wavelength, and acoustic beam characteristics are assumed to be the same. The losses due to divergence should also be the same.

Target Strength - Little is known about the geometrical features of significant targets in geothermal well logging. Some initial investigation may suggest that "significant" geothermal fractures, for example, may be smaller than the "typical fractures" of the reference case. It is simply assumed that the strengths of significant geothermal targets are lower by 20 dB.

Reverberation Level - An acoustic window material capable of withstanding the geothermal environment is likely to cause measurable increases in structural reverberation compared with the reference case. It is also expected to be somewhat challenging to provide a geothermal damping material for piezoelectric elements. It is therefore assumed that the reverberation level may increase by 10 dB.

The accompanying Table 4.II summarizes the changes in the various sonar equation terms and shows that a geothermal BHTV, constructed and used according to the listed assumptions would actually outperform the reference televiewer. Looking at it a different way, the signal to noise ratio could deteriorate an additional 18 dB before the geothermal BHTV would be as marginal as the reference case. For example this could mean that even smaller geothermal fractures may be resolvable, all other parameters kept equal.

Various other geothermal BHTV scenarios could also be constructed and contrasted with the reference case to get a rough approximation of their viability.

While portions of this analysis involve approximations, it is believed that the results provide reasonable assurance that a geothermal version of the present BHTV is sound in principle.

TABLE 4.II

SONAR EQUATION	CHANGE EXPECTED IN THESE PARAMETERS	NET EFFECT ON SNR (dB)
Source Level (SL)	No change expected	0
Transmission Loss (2 TL)	Amount of particulate in borehole fluid;	+48
Target Strength (TS)	Size and shape of significant borehole features	-20
Reverberation Level (RL)	Window performance; damping characteristics of backing block	-10
		+18 OVERALL EFFECT ON SNR

Work Plan

Initial project efforts involved identifying candidate materials which potentially offered an acceptable combination of improved immunity to the geothermal environment and satisfactory functional characteristics. The survivability of promising materials was then tested by exposing them to a simulated geothermal environment. Lab measurements were also made to establish basic acoustic properties of key materials. The materials, components, and fabrication techniques which showed promise at the completion of these tests would be considered as candidates for designing a functional acoustic sensor, suitable for testing in a simulated geothermal environment.

Special Facilities

Autoclave: Fundamental to the development program is availability of specialized autoclave facilities. A commercial autoclave service was located, having a 316 stainless steel vessel capable of achieving 275°C, 7000 psi, and tolerant to simulated geothermal brine. The 10 gallon vessel (Figure 4.2) is cylindrical with interior dimensions of 11-1/2" diameter and 19" height. The vessel is resistance-heated from the outside and the internal temperature is controlled by circulating a moderating fluid through spiral wound tubing coils suspended inside the vessel. Continuous or intermittent mixing of autoclave fluid is provided by an agitator affixed to a rotary shaft which penetrates the autoclave head. Temperature and pressure within the vessel can be continuously monitored.

An argon cover gas is used to pressurize the autoclave fluid. Exact volumes of brine and cover gas under room conditions are noted to permit computation of dissolved gas liquid-vapor phase partition at elevated temperature and pressure.

Simulated Geothermal Brine: It was equally important to formulate an autoclave fluid representative of the borehole environment. DOE/DGE provided the essentials of a recipe developed for similar evaluations of other geothermal components (elastomers). The following composition is being used:

H_2O	=	990 g/l
NaCl	=	25.4 g/l
$NaHCO_3$	=	1.94 g/l (0.023 M)
$Na_2S \cdot 9H_2O$	=	2.15 g/l (0.00895 M)
HCl (1M)	=	41.0 ml/l (0.041 M)

Electro-Acoustic Characterization of BHTV

During the latter part of the project, the plan called for performance demonstration of an operating sensor in a simulated geothermal environment. An important part of the planned demonstration would be to

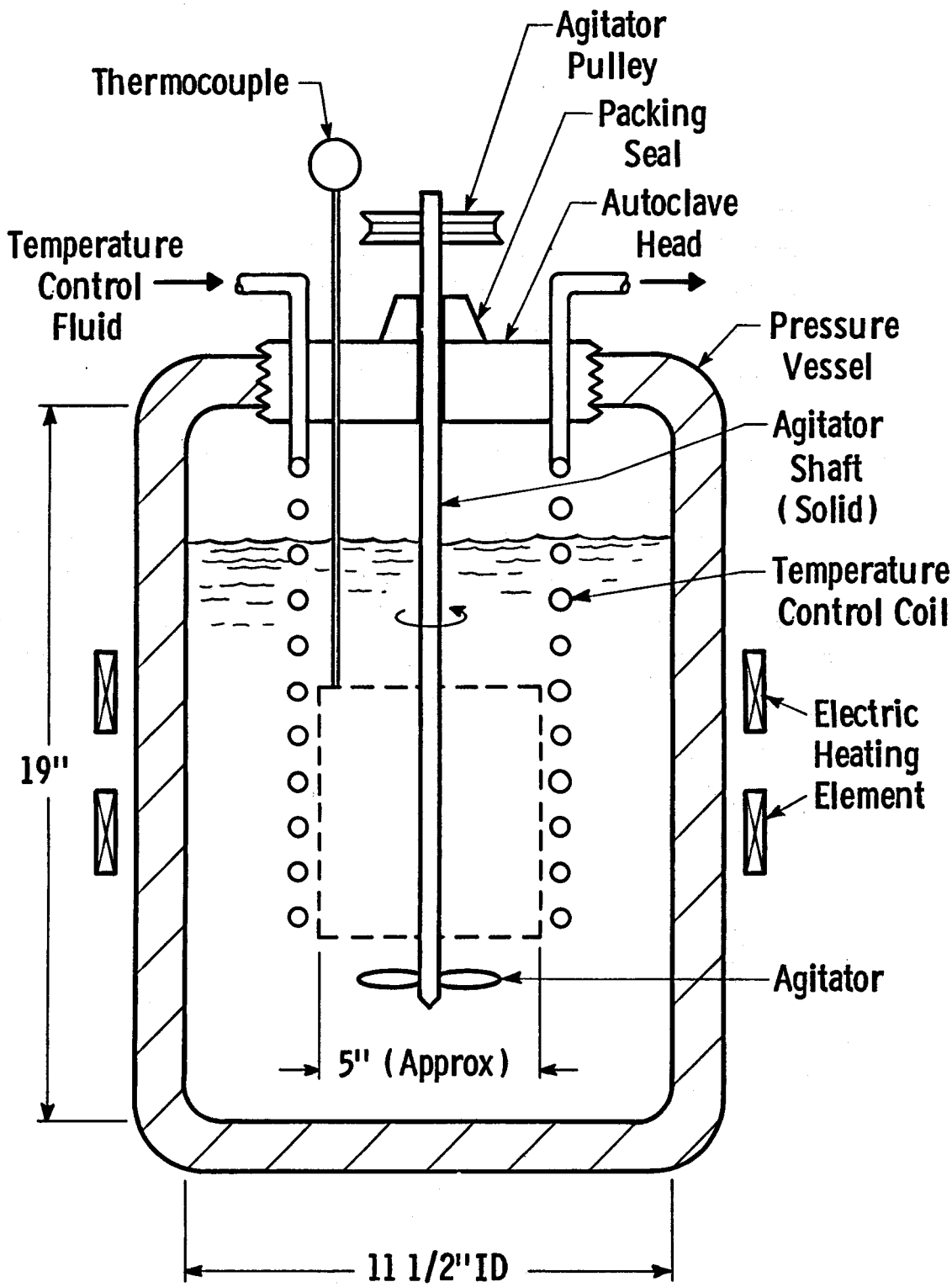

Fig. 4. 2— Diagram of 10-gallon autoclave vessel used for geothermal simulation testing

show that the experimental sensor exhibits those electroacoustic characteristics necessary for a BHTV sensor. As such, a set of baseline performance characteristics for the more conventional BHTV were viewed essential for comparison purposes.

An investigation revealed that electroacoustic performance data available for existing BHTV tools was qualitative and difficult to relate to useful performance reference techniques. Therefore, quantitative characterization of two borehole televiewer tools at USGS (Denver) was undertaken. Both tools incorporated Vespel acoustic windows which represented the high-temperature state of the art at the initiation of this project. Details of the characterization methods, apparatus, and results are presented in Appendix I. The results satisfied the need for baseline performance comparison data and may represent the first documentation of quantitative relationships between BHTV electrical signals and pressure fields in the surrounding medium.

5. SENSOR REPLACEMENT MATERIALS INVESTIGATION

Screening Tests

Considerable effort went into evaluating replacement materials from the standpoint of environmental immunity, sonic properties, and non-acoustic functions. Immunity to the geothermal environment and non-acoustic functions were evaluated by autoclave screening tests.

Phase I - Screening Test: A capsule (Figure 5.1) was designed to expose candidate sensor materials and components to service-simulative conditions. Capsules were fabricated from 6-inch lengths of 1-inch, Schedule 80, SS 316 pipe, threaded on both ends to accept threaded caps. The end caps compress the perimeter of the candidate window material against a series of concentric sealing grooves machined in the pipe end faces. One-inch diameter axial holes through the center of the end caps provide simultaneous exposure of window materials to internal coupling fluid on one face and autoclave fluid on the other. The capsule interior is charged with various samples of candidate sensor internal components and then filled with a candidate coupling fluid. Total fluid volume was minimized to reduce volume expansion and the accompanying risk of window rupture. This was done by charging the capsule interior with tabular alumina before installing the coupling fluid.

Free-flooding capsules were also constructed by replacing the window disc with a perforated stainless steel disc. These capsules were used to evaluate survivability of numerous items requiring direct exposure to the corrosive fluid.

Two iterations of autoclave screening tests were accomplished, involving a wide range of candidate materials. Appendix II contains details of the test procedures, materials tested, and results. One of the more significant results of the early materials screening tests was

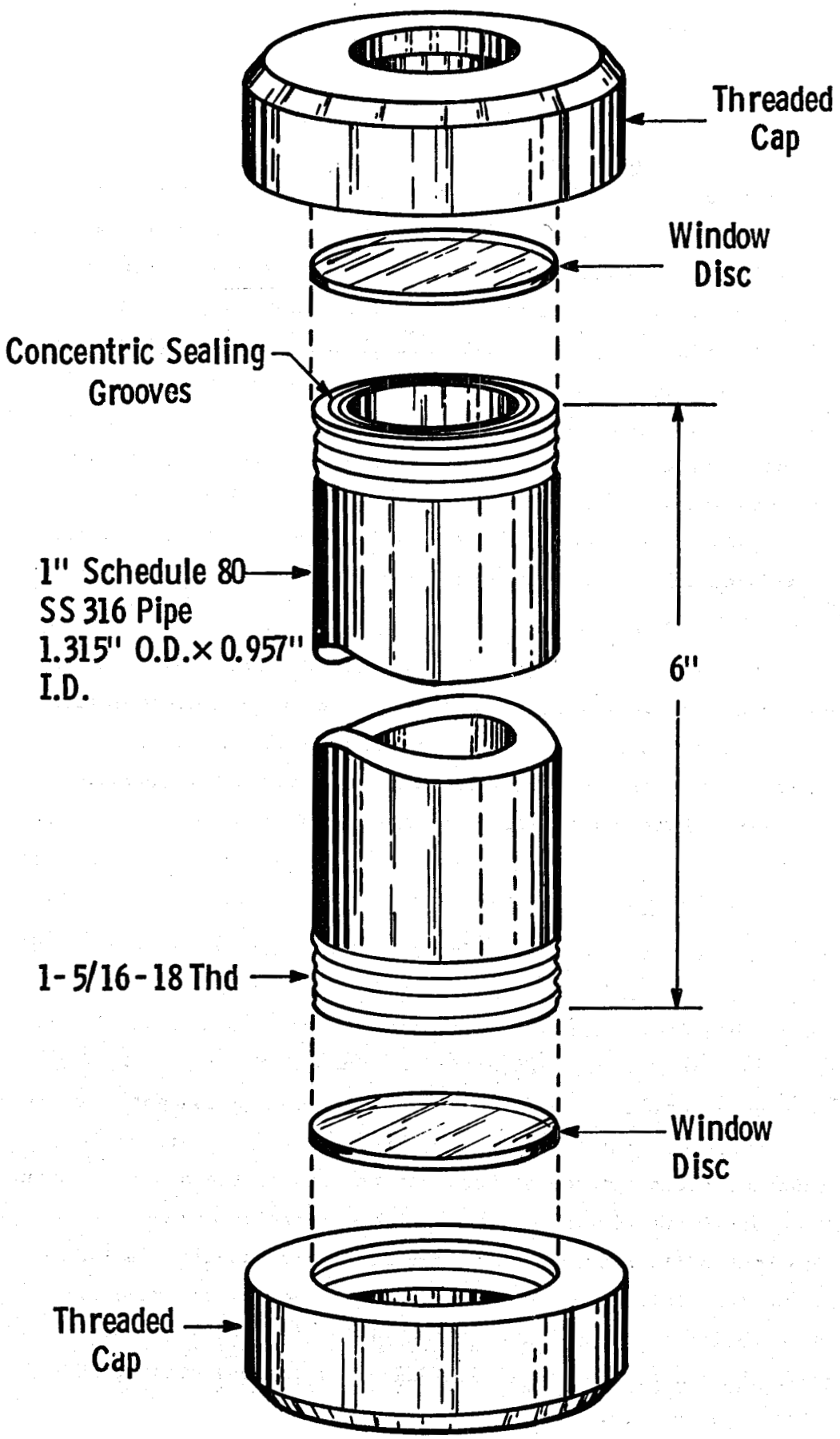

Fig. 5.1—Assembly drawing of capsule for early screening tests

verification that Vespel is a high-risk acoustic window material. This result is illustrated in Figure 5.2 which shows severe decomposition of a Vespel block and wafer (coupon) resulting from one autoclave screening test. Information available at the end of the two screening tests indicated that a replacement window material would be a major problem. The two window materials which showed marginal promise were Kalrez 1050 (DuPont) and TFE Teflon (DuPont). Screening tests also indicated that lead metaniobate piezoceramic bonded to a newly developed tungsten-filled cement backing material using a conductive epoxy could survive not only the temperature, but direct exposure to the simulated geofluid as well. This was also found to be the case for at least one type of TFE Teflon insulated hook-up wire.

The simple capsule design of Figure 5.1 did not provide an adequate seal between the window and the metal housing. Therefore fluid communication of varying degrees was a problem throughout the two screening tests. As a result, the screening test provided little new data regarding improved high temperature coupling fluids.

Advanced Screening Tests

Recognizing the limitations of the simple screening test capsule of Figure 5.1, it was decided that an improved test capsule was needed. An improved capsule was designed, incorporating a cylindrical shell window and improved means of sealing between the window and the housing. Figure 5.3 shows a cross-section of the improved capsule design concept. An SS 316 spool is enveloped by a cylindrical shell window. The window is sealed around the circumference of both end flanges of the spool using an SS hose clamp or similar device. The resulting interior chamber is charged with prototypical transducer assemblis and a coupling fluid. A bellows is used to minimize pressure differential across the acoustic window and to permit free expansion of the fluid at elevated temperatures. Such a bellows is also widely used in conventional BHTV tools for the same purpose.

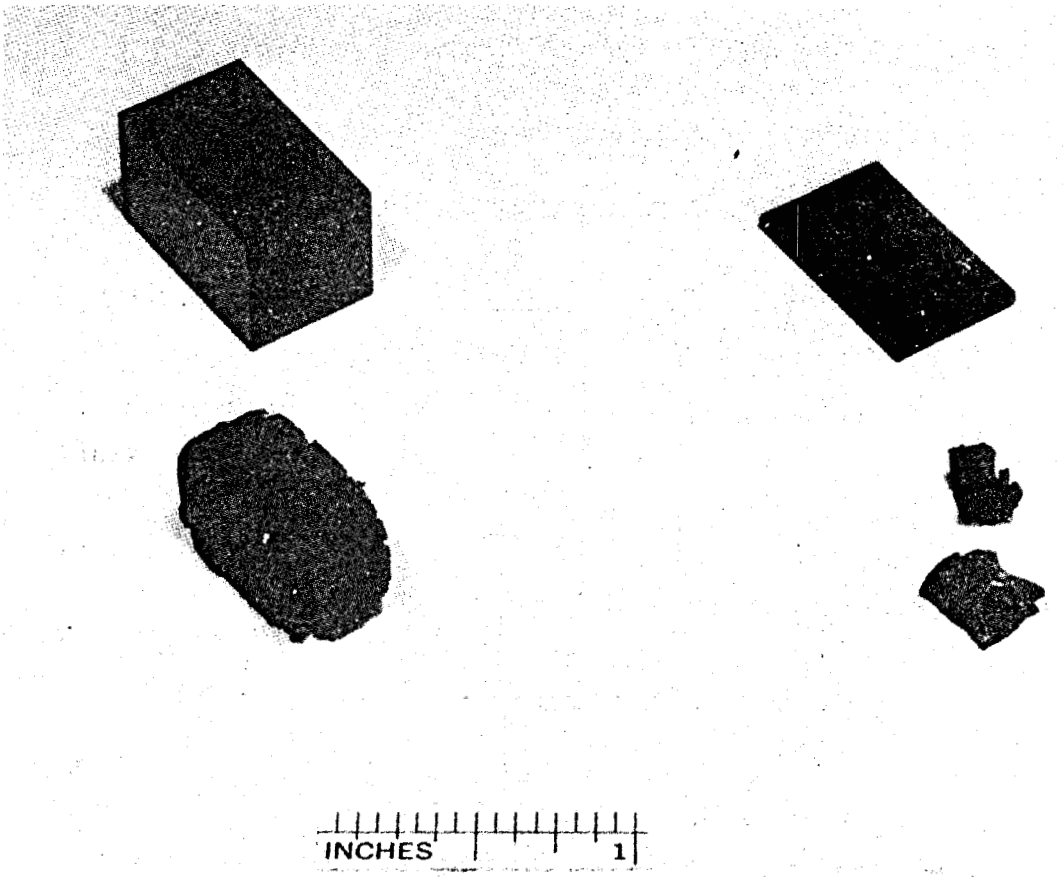

Figure 5.2 Photograph showing decomposition of Vespel after exposure to simulated geothermal conditions. Block and coupon control specimens (above) are compared with their autoclaved counterparts (below).

Dwg. 6428A69

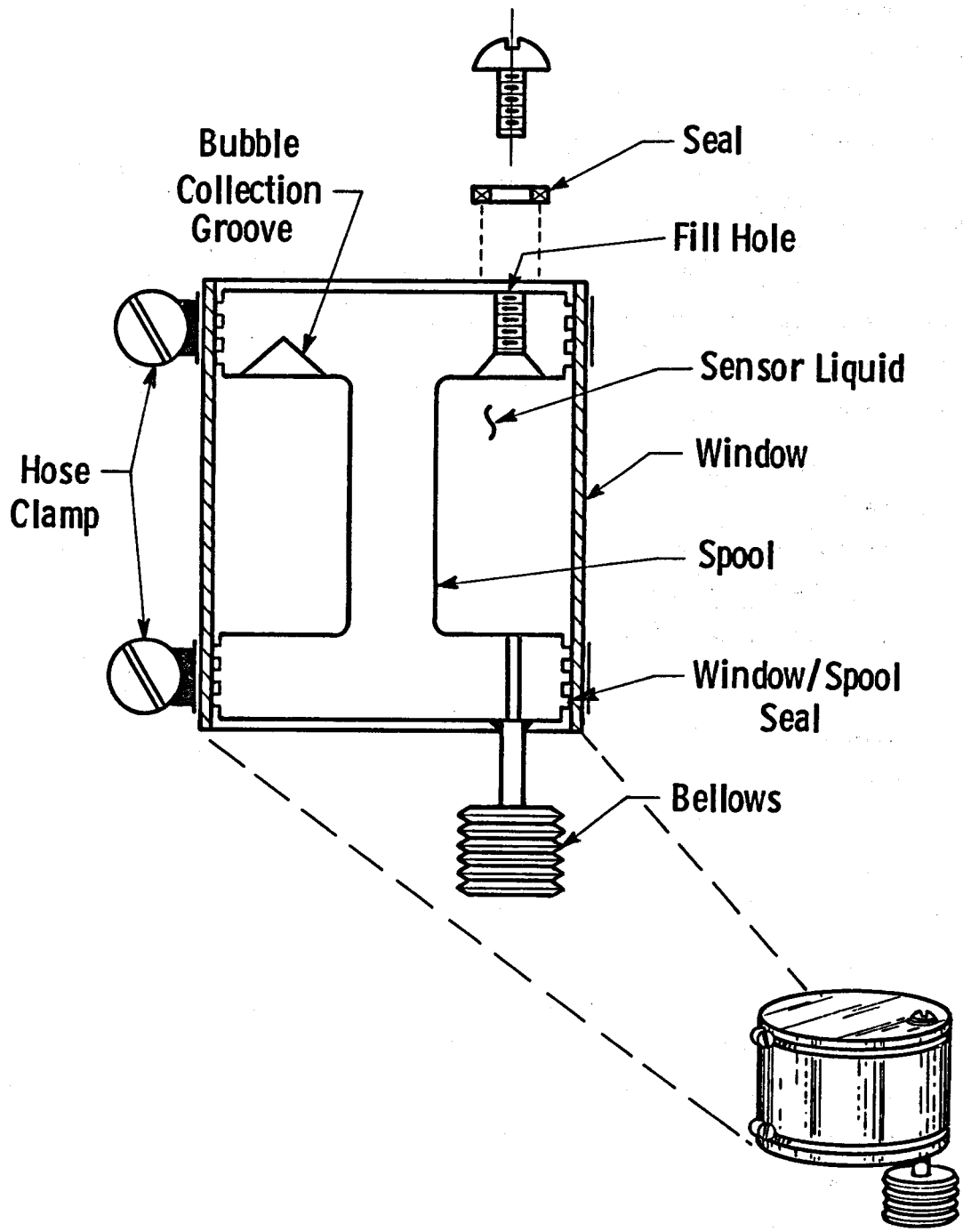

Fig. 5. 3— Diagram of improved capsule for advanced screening tests

Three such improved test capsules were designed around the window materials considered most promising at that point in the investigation: Kalrez 1050 (DuPont) perfluoroelastomer, Teflon TFE (DuPont) tetrafluorethylene, and Ryton R-171 (International Polymer Corporation) 40% glass-filled polyphenylene sulfide. The internal fluid for all three capsules was DC-710 (Dow Corning) high-phenylated silicone oil.

Figure 5.4 shows the three capsules, assembled and ready for autoclave testing. Figures 5.5, 5.6 and 5.7 show the condition of capsules after autoclaving. Figures 5.8 and 5.9 are close-ups of the Ryton and Teflon windows.

With regard to the performance of DC-710 fluid, autoclaving resulted in extensive gas formation in the Teflon capsule, causing the bellows to rupture upon return to atmospheric pressure. In the Ryton capsule, the DC-710 fluid apparently reacted with the window material to form a consolidated white powder as is shown in Figure 5.10.

These results raised serious doubt about the existence of a suitable non-metallic window material. It was also clear that some additional work was needed in the area of high temperature coupling fluids. It was concluded that geothermal BHTV window development should be redirected toward metal designs and that identification and screening of better coupling fluids were needed.

Acoustic Properties of Materials

Concurrent with the preliminary and advanced materials screening tests, data was collected regarding the sonic properties of the various subject materials. Of particular interest are sonic velocity (compressional) and specific acoustic impedance. Data was readily available for some materials. In other cases the parameters were from lab measurements. Table 5-I summarizes certain acoustic properties of materials examined. Figure 5.11 relates acoustic losses through various thicknesses of window materials immersed in transformer oil.

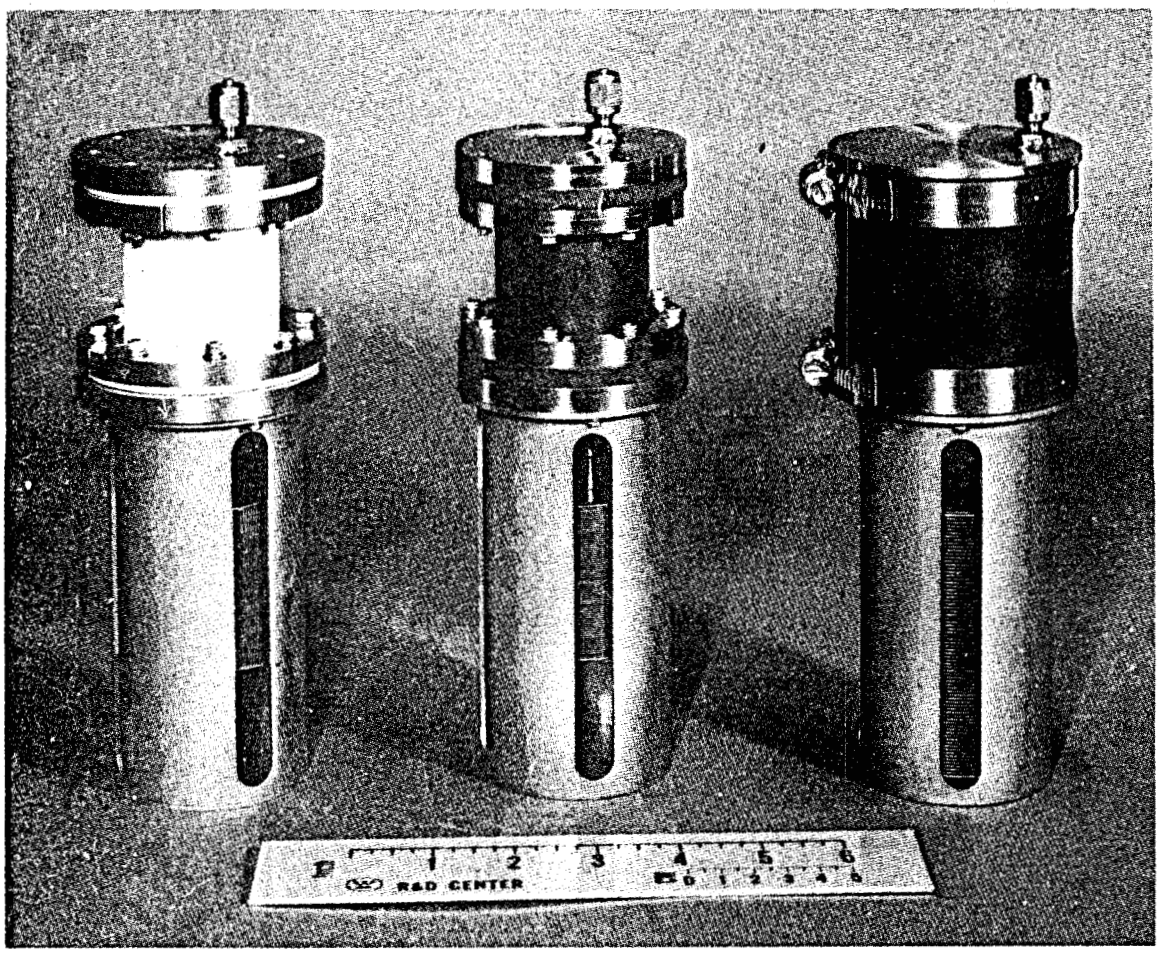

Figure 5.4. The three advanced screening test capsules ready for autoclave testing. Window materials are TFE Teflon (left), Ryton 171 (center), and Kalrez 1050 (right).

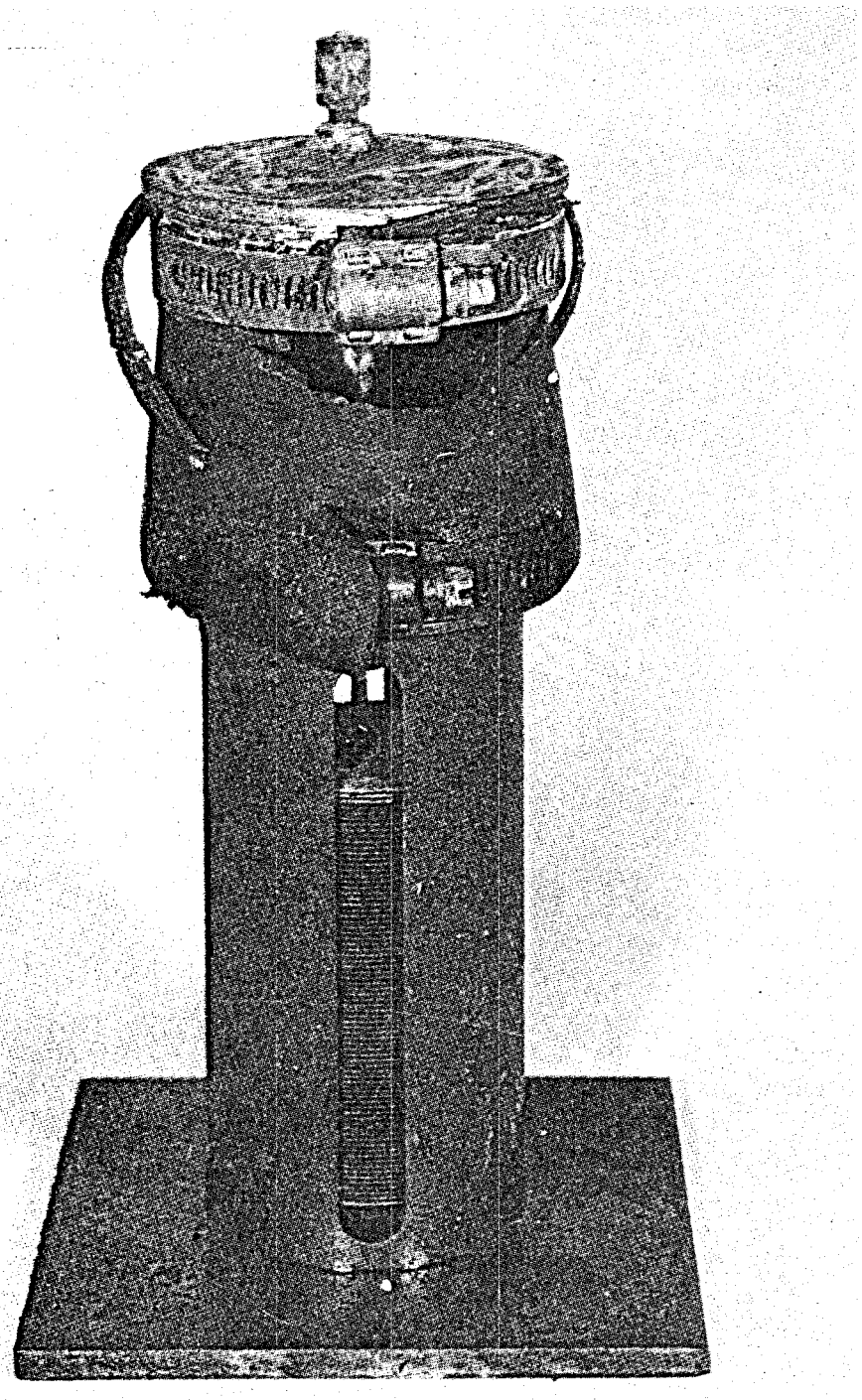

Figure 5.5 Photo showing the post-autoclave condition of the Kalrez window.

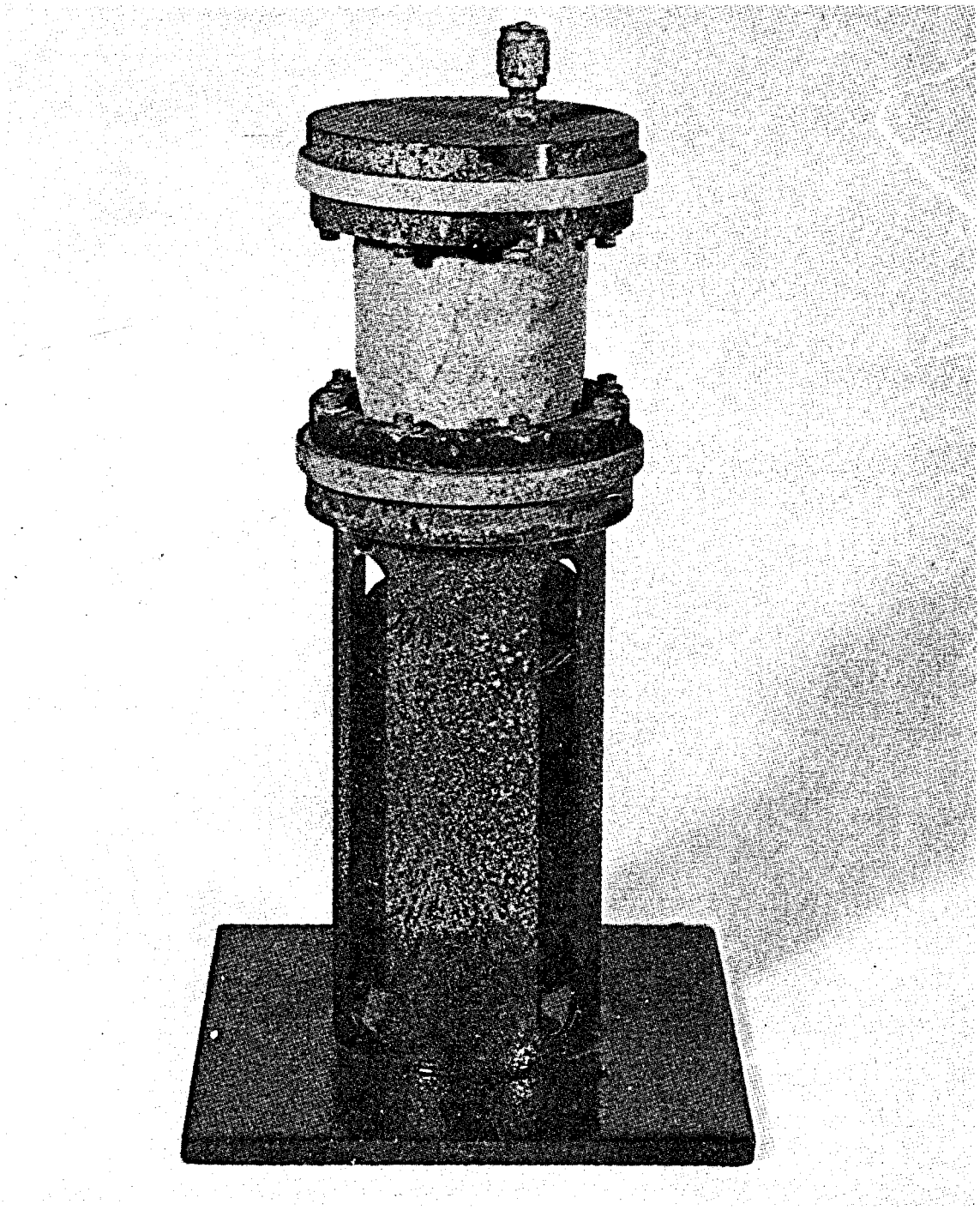

Figure 5.6 Photo showing the post-autoclave condition of the Ryton window. Note deformed bellows top and swollen window.

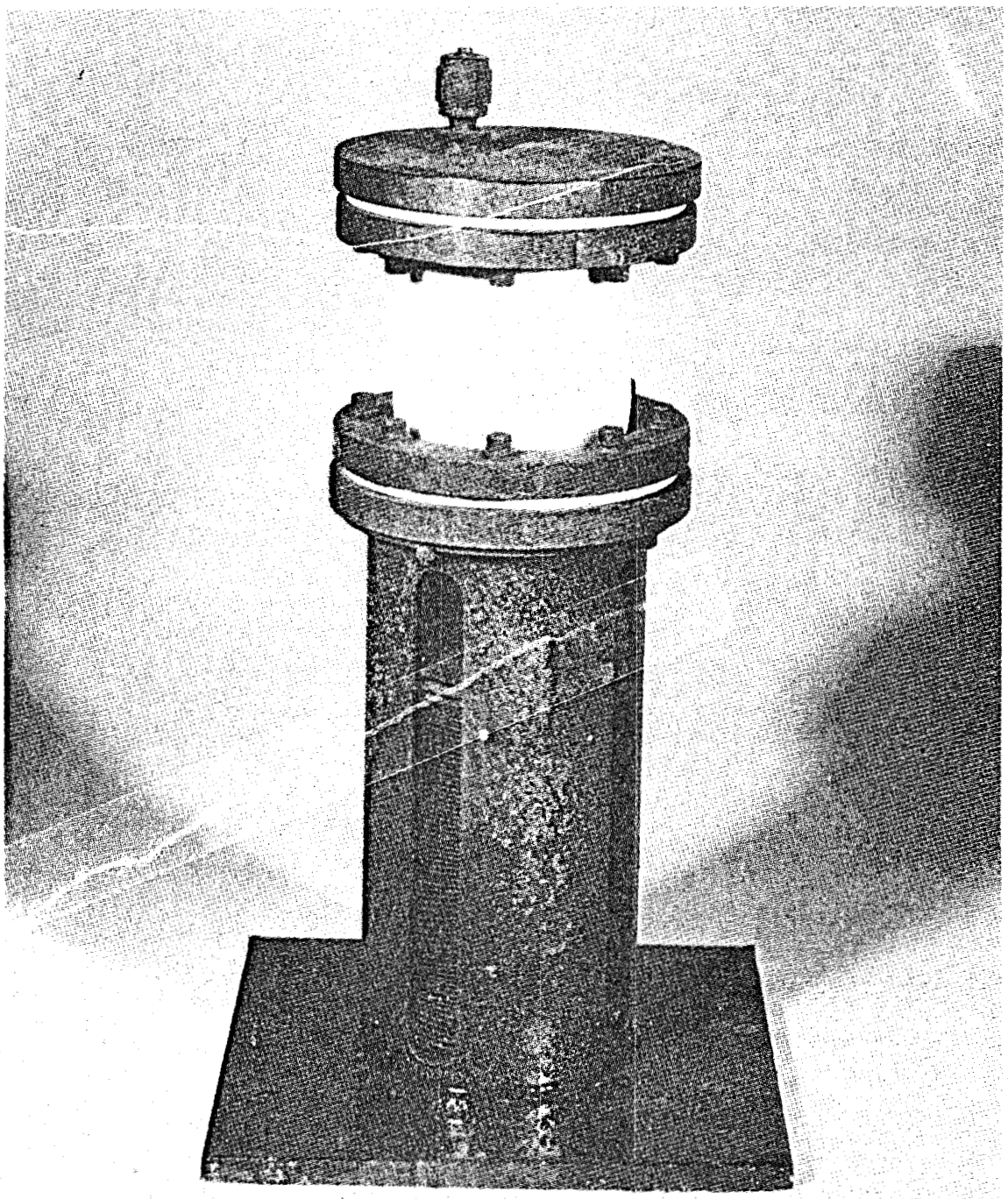

Figure 5.7 Photo showing the post-autoclave condition of the Teflon window. Note deformed bellows top and window indention on right side.

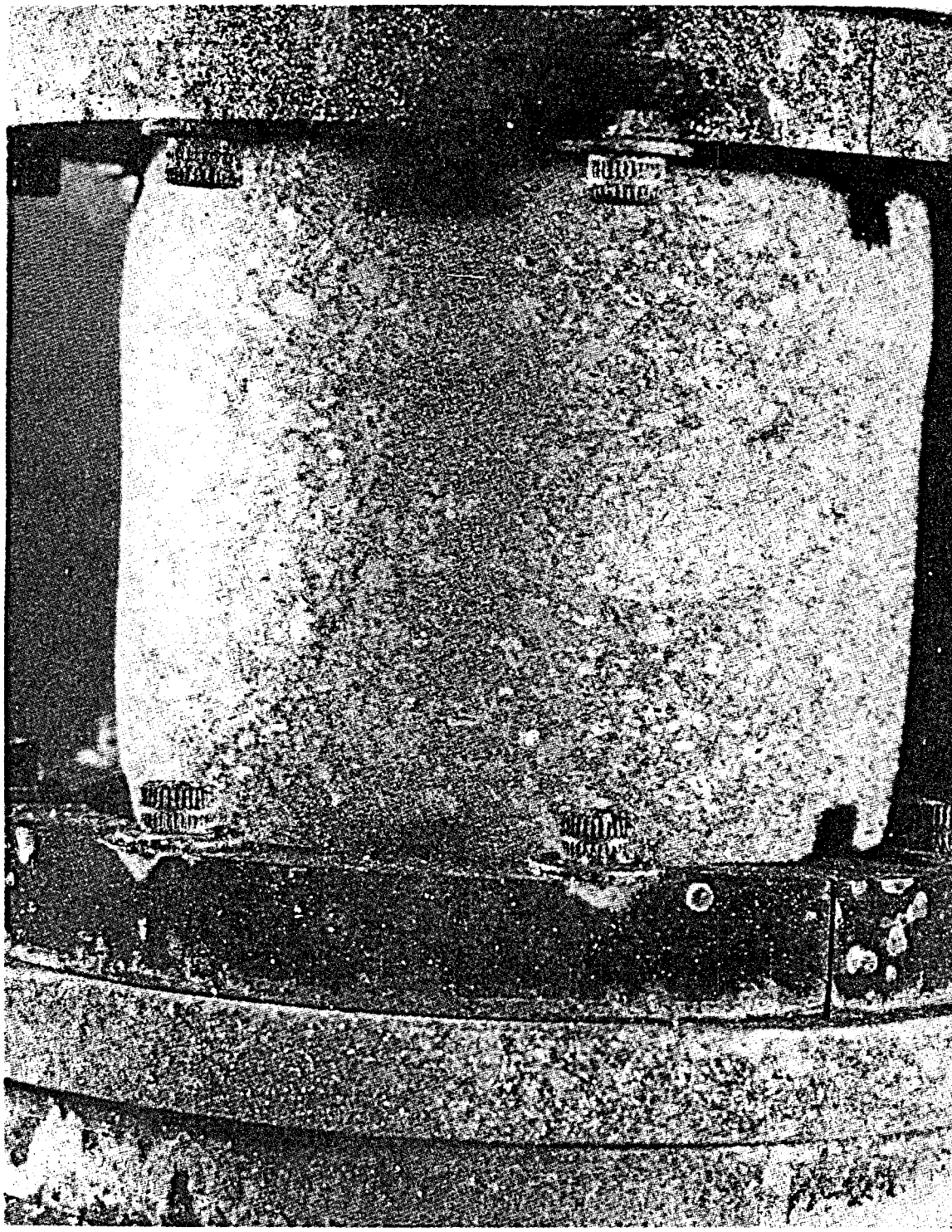

Figure 5.8 Close-up of post-autoclave Ryton window. Surface pinholes do not penetrate window.

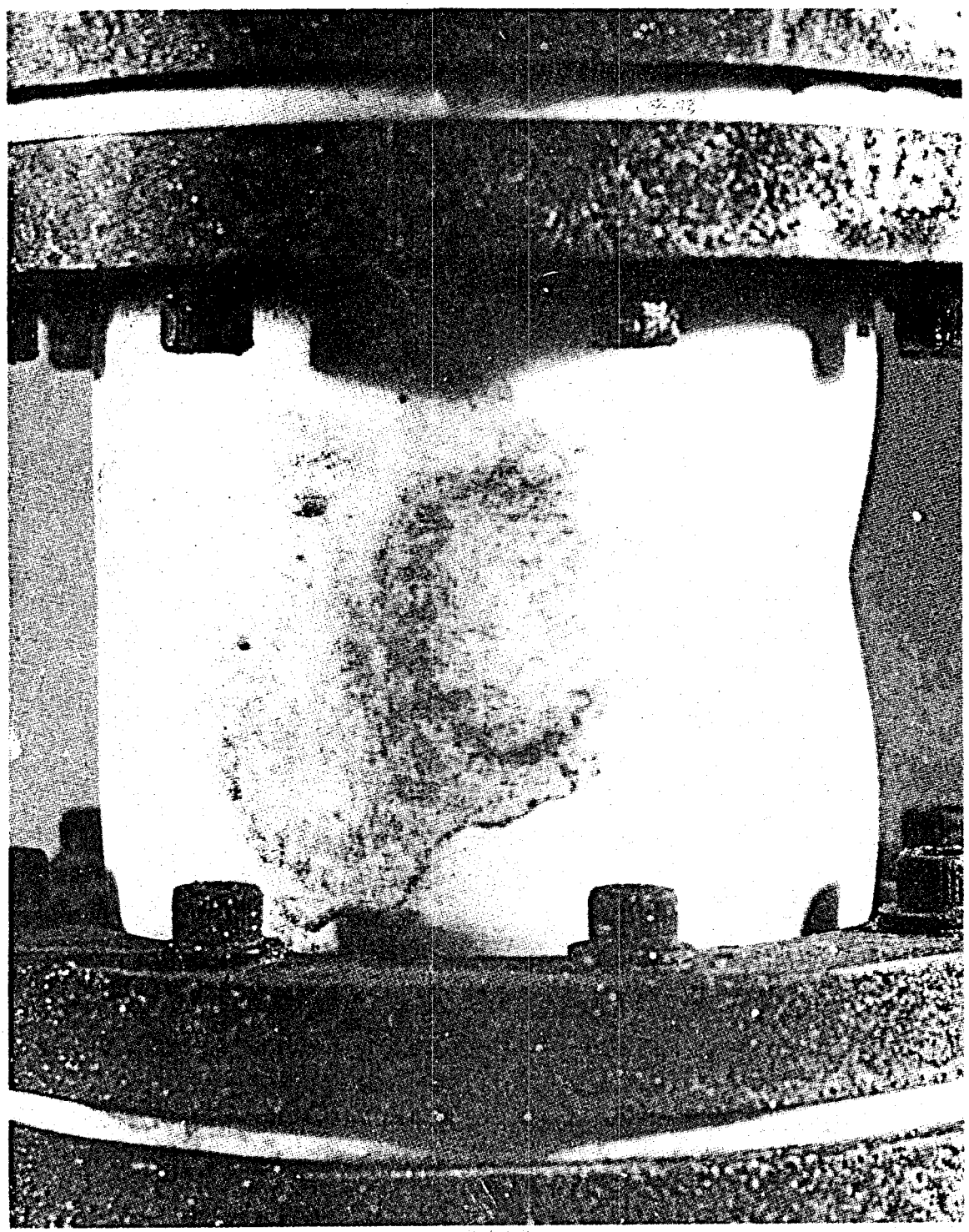

Figure 5.9 Close-up view post-autoclave Teflon window.

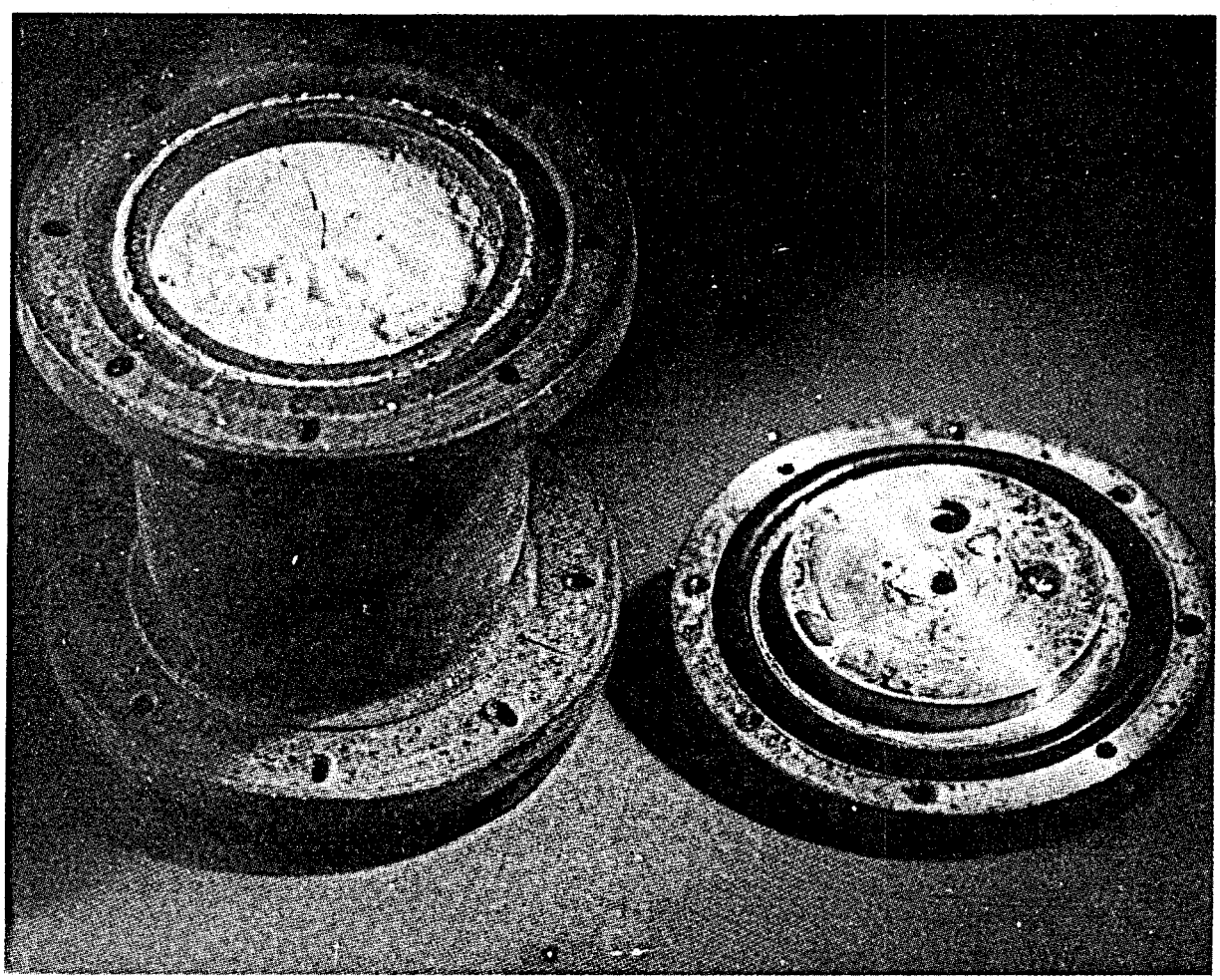

Figure 5.10 Although the Ryton window (left) remained intact, the DC-710 internal fluid apparently reacted with the window, forming the white powder shown in photo. Flange retainer screw holes and o-ring (Kalrez 1050) seal surface show evidence of considerable plastic deformation. Top flange with o-ring shown at right.

TABLE 5-I

	Compressional Velocity (C_o) m/sec	Density (ρ) kg/m^3	Acoustic Impedance (ρC_o) MKS rayls
MACOR (ceramic)	5.9×10^3	2.51×10^3	14.9×10^6
VESPEL	2.5×10^3	1.43×10^3	3.6×10^6
KALREZ	1.35×10^3	2.01×10^3	2.71×10^6
E/C 2762 FT Epoxy	3.02×10^3	2.14×10^3	6.47×10^6
Cotronics Epoxy (Duralco 700)	2.55×10^3	1.94×10^3	4.9×10^6
(1)TUNGSTEN/EPOXY	2.32×10^3	6.76×10^3	15.7×10^6
(2)TRANSFORMER OIL	1.41×10^3	0.88×10^3	1.24×10^6
Mobil Jet Oil II	1.36×10^3	1.0035×10^3	1.37×10^6
WATER (typical)	1.5×10^3	1.0×10^3	1.5×10^6
ALUMINUM (typical)	6.3×10^3	2.7×10^3	17×10^6
STEEL (typical)	6.1×10^3	7.7×10^3	47×10^6
Lead Metaniobate (Keramos K-81)	3.3×10^3	6.2×10^3	20.5×10^6
TFE Teflon	1.25×10^3	2.2×10^3	2.75×10^6
Ryton (R-100)	2.3×10^3	1.34×10^3	2.99×10^6
Ryton (R-171) (40% glass fiber-filled)	2.35×10^3	1.60×10^3	3.76×10^6
Brayco 812 (fluid)	0.7×10^3	2.0×10^3	1.4×10^6
Inconel 718 (approx. values)	5.9×10^3	8.9×10^3	52×10^6

(1)3:1 Ratio by weight Tungsten powder: Emerson Cumming 1762 FT Epoxy.

(2)Oil used to simulate typical internal fluid (WEMCO-C) Insulating Oil.

Curve 715659-A

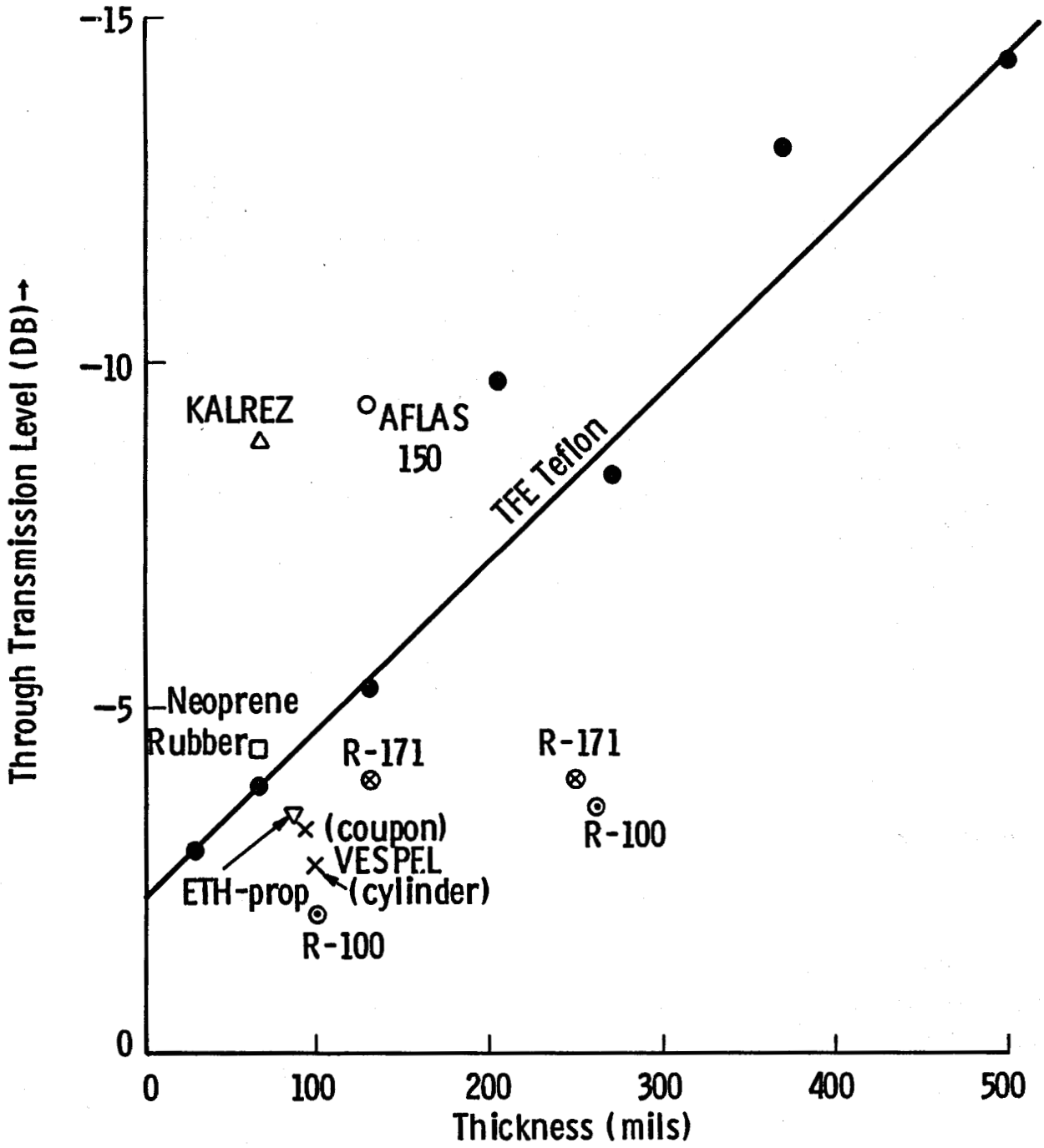

Fig. 5.11—Data showing signal drop through certain window materials of various thicknesses. Solid line depicts drop through TFE Teflon. Measured with specimens immersed in transformer oil. Data generally indicates Ryton is low-loss, high temperature material

6. ADVANCED FLUID SCREENING TESTS

As a result of the problems encountered with DC-710, additional sources of high temperature fluids were sought and a method for screening new candidates was needed.

The additional fluids considered were as follows:

KRYTOX 143 (DuPont) - perfluoroalkylpolyether
Santovac 5, 6 (Monsanto) - polyphenylether
Therminol 66 (Monsanto)
BRAYCO 810, 812 (Bray Oil Co.) - perfluoroalkylpolyether
FOMBLIN Y-25 (Mon-Edison) - perfluorinated polyether
BRAYCO 815Z (Bray Oil Co.) - perfluorinated polyether

Three representative fluids were selected from this list for follow-on screening tests.

The major concern regarding fluid properties were chemical compatibility with the sensor components and decomposition to a gas phase at high temperature.

A simple capsule was designed to provide for testing these fluids in a small autoclave. The test capsule is approximately 6-inches long and the design is indicated in Figure 6.1. One end of a 3/8" tube (1) is capped (2) and the other end is terminated in a 3/8" x 1/4" tubing adaptor (3). A metal bellows (4) is connected to the adaptor (3) by a short length of 1/4" tubing (5). The bellows allows for thermal expansion of the fluid and provides an indication of residual gas generation after autoclaving. Figure 6.2 shows an assembled capsule.

To include possible chemical effects on the sensor internals, a miniature transducer assembly was also constructed to fit into the capsule. The assembly design is shown in Figure 6.3 and consists of a 0.10" diameter disc of K-81 lead metaniobate, bonded to a rectangular

Dwg. 7690A42

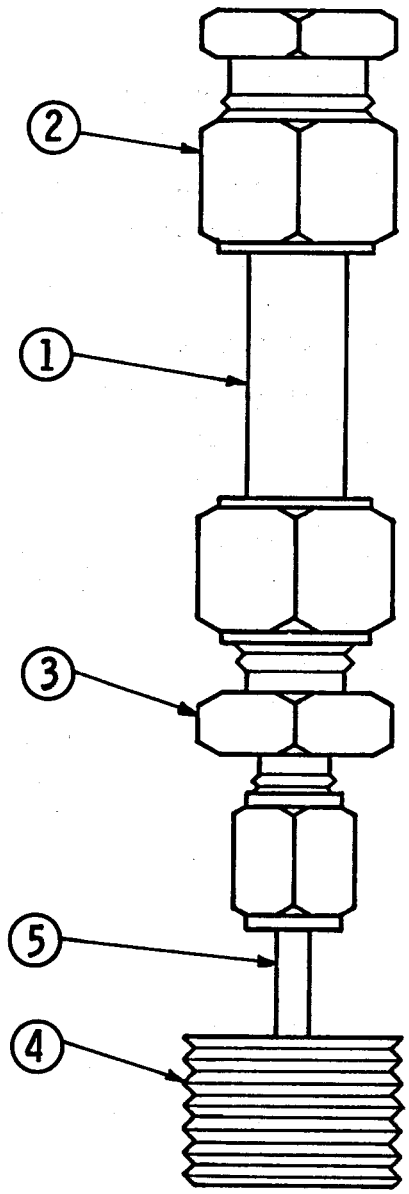

Fig. 6.1—Diagram of advanced fluid screening test capsule design

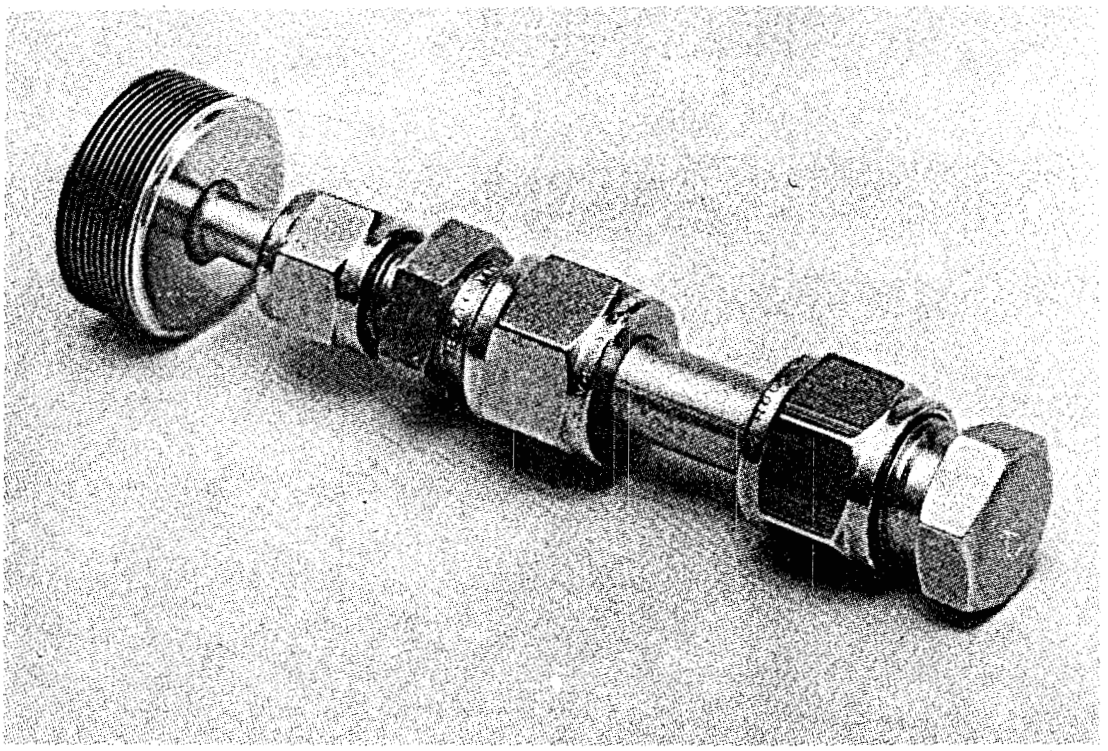

Figure 6.2 Photo of an assembled advanced fluid screening test capsule.

Dwg. 7690A43

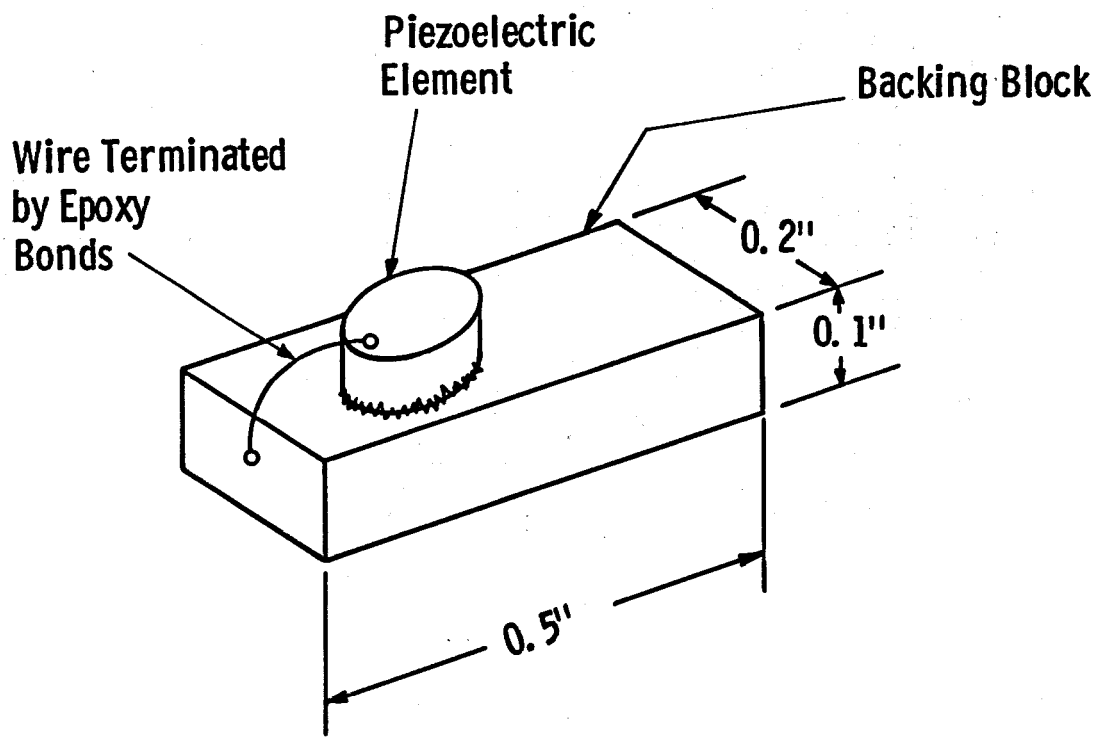

Fig. 6.3—Design details of the miniature transducer assembly for advanced fluid screening tests

piece of tungsten powder filled alumina cement (backing material). A short piece of TFE Teflon insulated copper wire is prototypically connected to the silver electrode of the K-81 piezoceramic. The adhesive used for the wire and the disc is Epotek H20E silver conductive epoxy. A completed assembly is shown in Figure 6.4.

Temperature was expected to be the most significant test parameter with regard to fluid performance. Pressure was expected to be of little importance and caustic geofluid should not affect the internals of a properly assembled capsule. Therefore the three capsules were tested in a water autoclave with cylindrical dimensions of 12" high and 5" diameter. The autoclave is rated at 650°F (343°C) and 5000 psi.

The test procedure was as follows: 1) capsules were charged with a miniature transducer assembly and approximately 7 ml of candidate fluid and then sealed, 2) capsules were autoclaved at 275°C and 2000 psi for a period of 4-hours.

Fluid performance was assessed by two methods. First, evidence of residual fluid outgassing was checked by comparing pre- and post-autoclave capsule volumes. Significant gas generated due to fluid breakdown or reaction with internals would result in measurable increases in bellows length and capsule volume. Second, the condition of the fluids and the miniature transducer assemblies were carefully inspected and compared with pre-test conditions.

The results of these tests for all three fluids showed no detectable sign of residual gas formation, revealed no chemical attack of internals, and produced no apparent changes in color or appearance of fluids or materials.

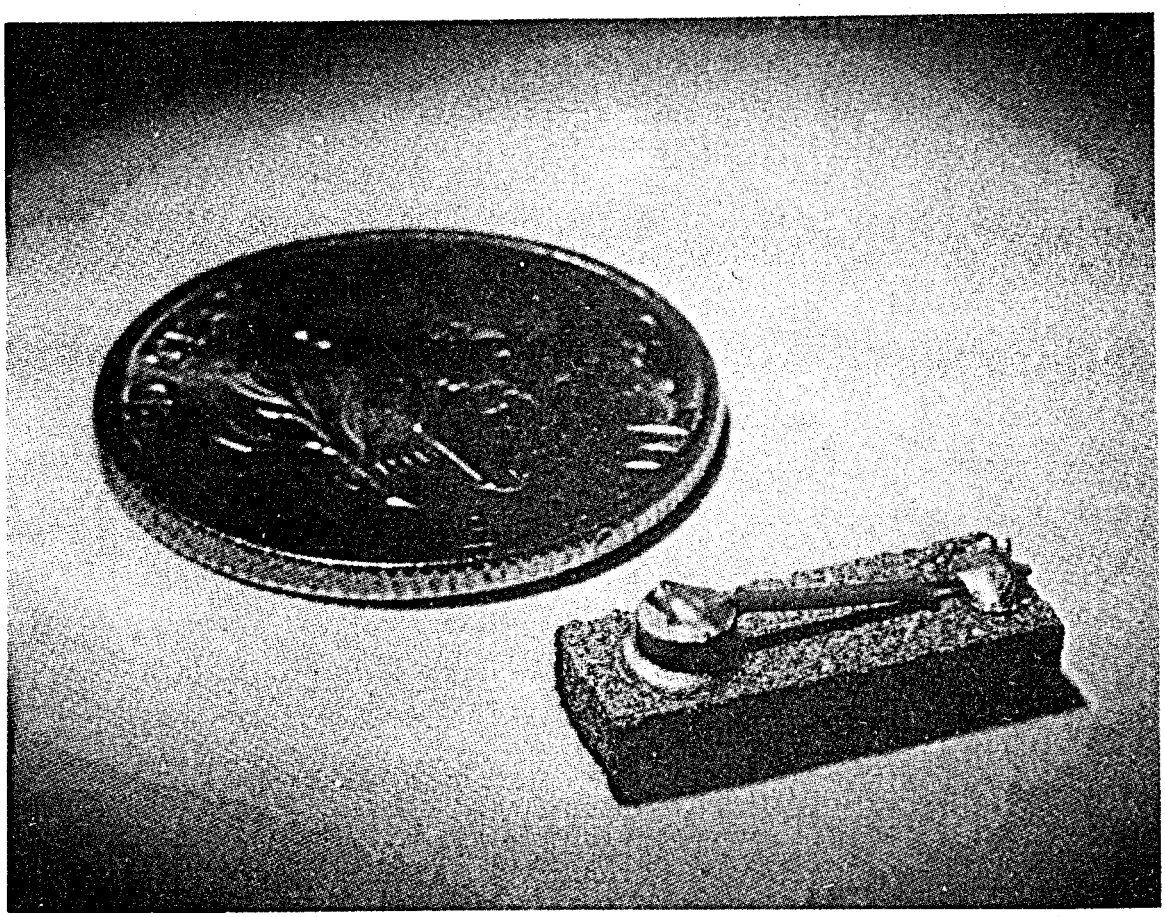

Figure 6.4 Photo of fabricated miniature transducer assembly.

7. METAL ACOUSTIC WINDOW DESIGNS

The results of preliminary and advanced window material screening tests did not provide the confidence viewed necessary for designing a geothermal BHTV sensor. It was therefore decided that a metal window design should be investigated. The following sections describe analytical and experimental work to identify and test solutions to the metal window problem.

Design Problem Defined

Referring to Figure 7.1A, we are given:

1) piezoelectric crystal
2) coupling fluid
3) acoustic window material (metal)
4) geometric constraints (e.g., ℓ_c is fixed)
5) approximate acoustic properties of the two fluids.

The problem to be solved is to determine what can be done with window thickness (ℓ_w) to provide acceptable acoustic signal transfer between the crystal and the geofluid.

Analytical Solutions

Solution #1): Transmission line theory provides a convenient analytical approach to this problem. Referring to Figure 7.1-B, let Z_c and Z_w be the characteristic (or "specific") acoustic impedances of the coupling fluid and the window material respectively. The coupling fluid can be modeled by a fixed length of line (ℓ_c) having a characteristic impedance Z_c. Similarly, the acoustic window is modeled by a variable length (ℓ_w) of transmission line having characteristic impedance Z_w.

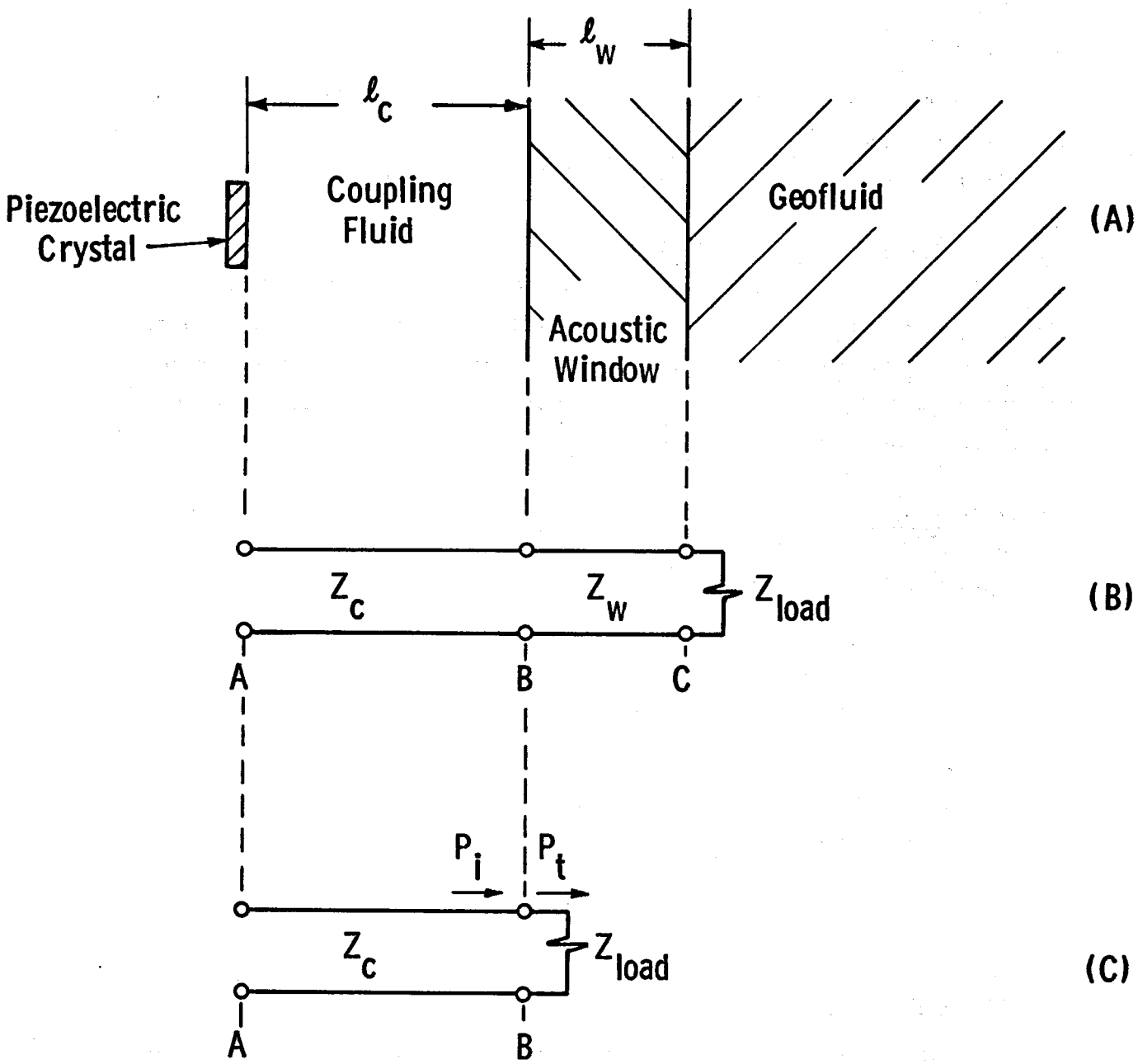

Fig. 7.1—Transmission-line equivalents of the BHTV sensor: (A) the physical embodiment, (B) a generalized transmission line analog, (C) the transmission line analog for special case of a half-wave window

The purposes of this analysis are served by representing the geofuid as a "lumped" load impedance (Z_{LOAD}) which terminates the window transmission line at "C".

The specified piezoelectric crystal determines the nature of the energy pulse launched into the coupling fluid section at "A". Maximum power is delivered to the load (Z_{LOAD}) when ℓ_w is equal to one half wavelength. It can be shown that under these conditions, the acoustic window essentially "disappears" (except for the effects of absorption loss in the window which in our case is small). Power transfer can now be examined using the simplified analog shown in Figure 7.1-C where the coupling fluid is terminated at "B" by the geofluid load impedance (Z_{LOAD}).

The actual coupling fluid to be used has not been specified so that exact acoustic impedance (Z_c) is not known. Similarly, the acoustic impedance of the geofluid (Z_{LOAD}) is not well known. However, based upon conservative estimates, we expected that:

$$0.5 \leq \frac{Z_{LOAD}}{Z_c} \leq 2.0 \qquad (7.1)$$

Another formula[5] can now be used to calculate the ratio of power transmitted (delivered) to the load (P_t), to the power incident (P_i) from the left on the boundary at "B":

$$\frac{P_t}{P_i} = \frac{4R}{(R+1)^2} \qquad (7.2)$$

Substituting the limiting R values of (7.1) into Equation (7.2), the power transmitted will be greater than or equal to 89% of the incident power. It may be tentatively concluded that from a power transmission standpoint, a half-wavelength window is certainly worth pursuing. However, there are some potential difficulties associated with half-wavelength (or tuned) windows.

First, the above analysis can be extended to show that as much as 11% of the incident energy is reflected back toward the source (crystal). Such reflected energy must be reduced to an acceptably low level by the time that echoes are returning from the borewall targets. This puts additional demands on methods for controlling internal reverberation.

Second, a half-wavelength window is a resonant device, valid at a single frequency. The bandwidth of the "half-wavelength solution" is related to the Q of the mechanically resonant system. High acoustic impedance metal windows in conjunction with the relatively low impedances of the subject fluids result in a high Q resonance and therefore relatively narrow bandwidth.

The acoustic pulse emitted by the conventional BHTV has considerable bandwidth and we would expect that a half-wave window would essentially narrow-band-filter this pulse. The anticipated result would be an output pressure pulse of longer duration due to "ringing" in the resonant window.

Solution #2). Electrical transmission line theory also predicts that even for severe impedance mismatches, power transmission through a window can approach unity for arbitrarily thin windows. In practice, satisfactory power transmission can often be obtained through windows with thicknesses on the order of 1/10 wavelength.

The thickness of a typical 1/10 wavelength metal window can be calculated using the basic equation

$$f\lambda = c \qquad (7.3)$$

where f = frequency

λ = wavelength

c = speed of sound in window.

It is apparent that

$$\frac{\lambda}{10} = \frac{c}{10f} \tag{7.4}$$

A typical sonic velocity for metals is 5×10^3 m/sec and the dominant BHTV frequency is 1.3×10^6 Hz so that

$$\frac{\lambda}{10} \approx \frac{5 \times 10^3 \text{ m/sec}}{(10)(1.3 \times 10^6)/\text{sec}} = 3.85 \times 10^{-4} \text{meters} \tag{7.5}$$

This is equivalent to approximately 0.015 inches.

Inspection of these equations shows the advantage of using a high sonic velocity window material. That is, the $\lambda/10$ criteria can be met with a thicker and therefore more durable window.

Experimentation:

These solutions were examined experimentally using the apparatus diagrammed in Figure 7.2. A commercial BHTV transducer (Simplec) was used to launch pulses into an oil bath in the direction of a broadband Automation Industries receiver with flat response though 5 MHz. Transmitter to receiver orientation and separation were held constant at 6-inches. Various experimental windows were inserted at the location indicated and the effect(s) on received signal level was determined. Window performance is characterized by calculating the signal loss (in decibels) compared with no window present and is plotted in Figure 7.3. For reference, the loss through the existing high-temperature BHTV Vespel window (0.10" thick) is also included.

Discussion of Results: The data for brass of varying thicknesses demonstrates the low loss expected from thin (in wavelengths) metal windows. The 1.3 MHz wavelength in brass is approximately 0.142". A brass window of 1.5 mils (0.0015") of $\lambda/100$ nearly duplicates the loss of the 0.1" Vespel window. Transmission line theory would predict maximum

Dwg. 7690A40

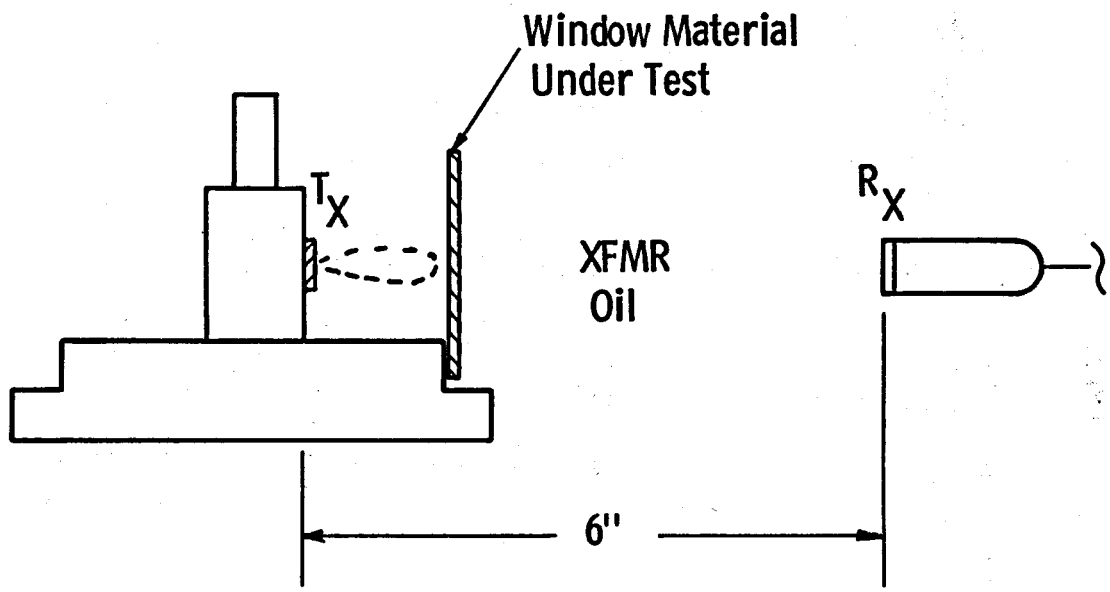

T_X = Simplec XDCR

R_X = Auto. Ind. 10 - mHz

XMTR = Panametrics 5050 PR
Energy = 1
Damping = 0
Atten = 20 db

Fig. 7.2 — Diagram of experimental set-up used to evaluate acoustic window performance

Curve 715661-A

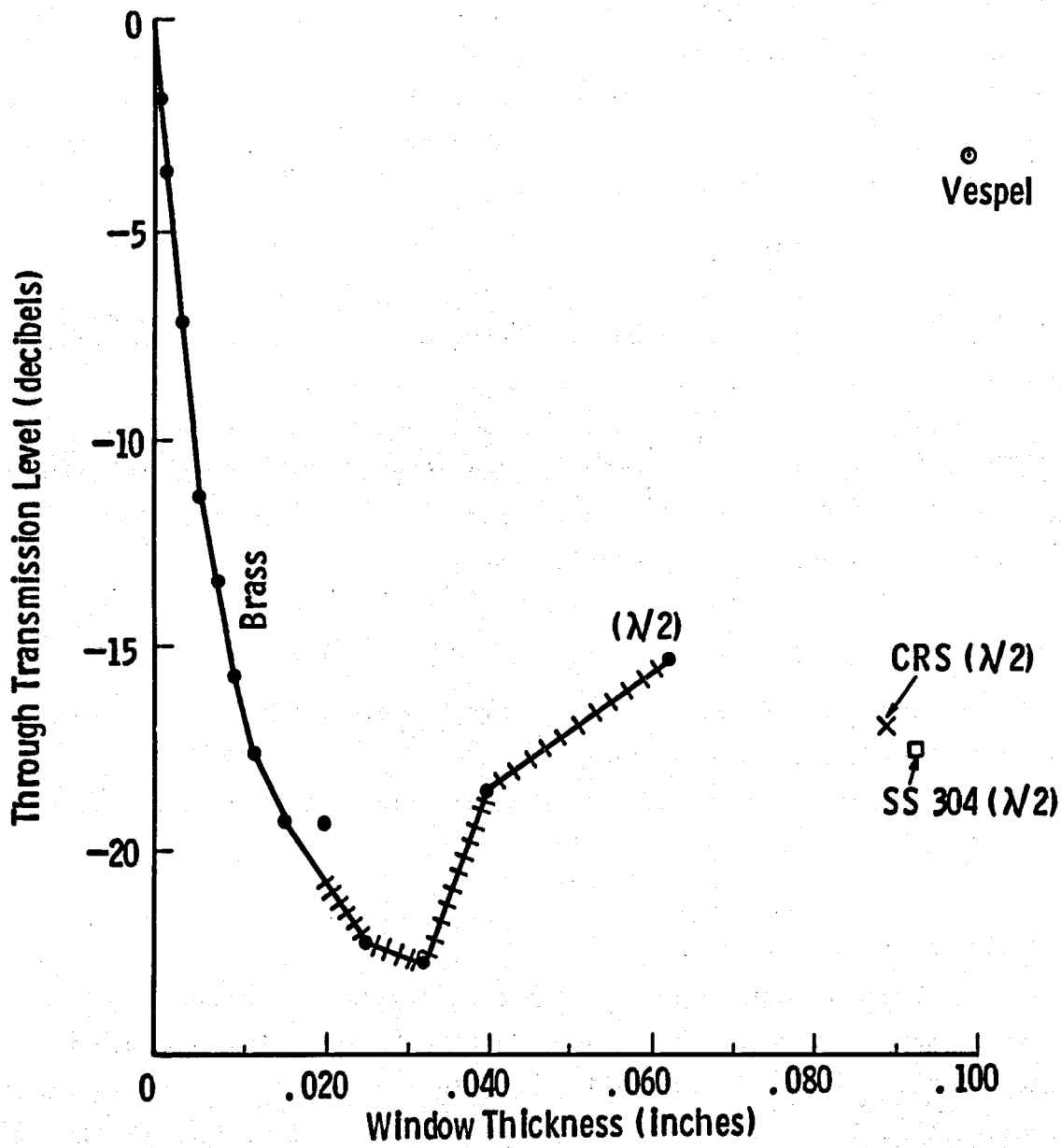

Fig. 7.3—Experimental verification of window performance predicted from analytical solutions. Solid line is for brass shim-stock of various thicknesses up to 0.062-inches. Waveform phase distortions occur in region of herring-bone. Performance of half-wavelength carbon and stainless steels also plotted along with that of a commercial Vespel BHTV window

loss at $\lambda/4$ or ~ 35 mils. The data agrees well, showing a maximum loss at ~ 32 mils. The approximate loss for a $\lambda/2$ brass window is the 63 mil data point or about 15 dB. Approximate half-wavelength windows of cold rolled steel (CRS) and SS 304 (higher sonic velocity materials) are also shown with losses of 17 to 18 dB.

Signals through all three $\lambda/2$ windows showed definite ringing and therefore pulse spreading, as anticipated. Pulses through the brass windows of increasing thickness were reduced in amplitude but undistorted from 1 mil through 20 mil (~ 0.14λ) thickness. (Solid line in Figure 7.3.) Phase distortion begins at ~ 20 mils and results in pulse elongation by 63 mils ($\lambda/2$). (The region of pulse distortion is indicated in Figure 7.3 by herring-bone line.) Both steel $\lambda/2$ windows also exhibited the expected pulse elongation.

Sampling of Data

A series of selected oscillograph photos (Figures 7.4 through 7.11) is included for demonstrating some of the aforementioned effects. In each of these cases, pertinent received signals are found in the left half of the delayed sweep oscillographs.

Additional Tests

These encouraging results obtained with thin brass sheet prompted some revised fixturing and additional tests with some other alloys. The improved fixturing is shown in Figure 7.12 and provides for covering a window port with a segment of metallic cylindrical shell. The radius of the metal acoustic window port covering is made to be the same as the reference Vespel window (3-3/8" Dia.).

Pulse-echo tests were then made in an oil bath to further demonstrate the viability of a thin metal window. For these tests, metal window materials were 0.002" thick SS 301 and Inconel 718. The performance of these window materials was compared with the standard (Simplec) Vespel window by echo-ranging off of a 0.024" diameter wire

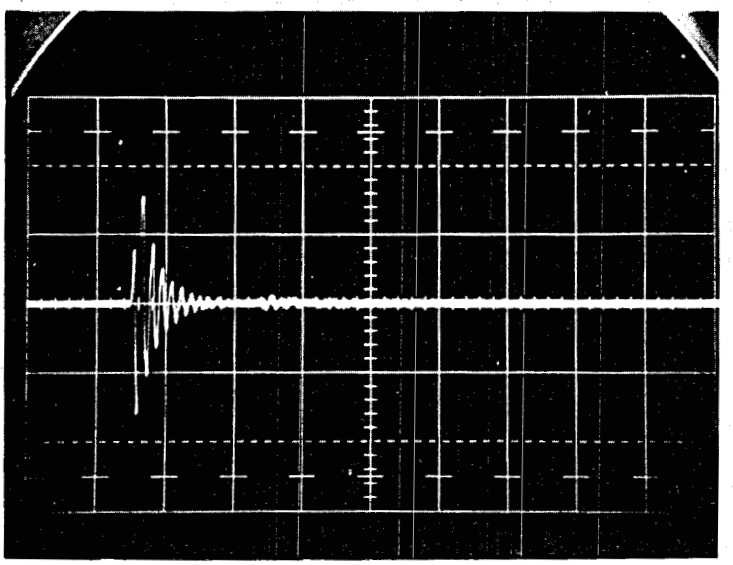

Figure 7.4. Received signal through oil; no window present. (0.5 V/cm vert., 5 μsec/cm horiz.)

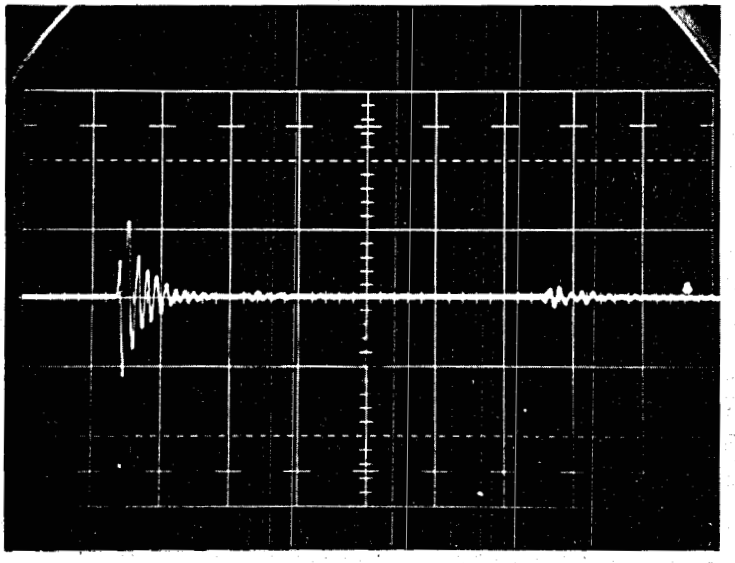

Figure 7.5. Received signal through 0.10" cylindrical shell Vespel window. (0.5 V/cm vert., 5 μsec/cm horiz.)

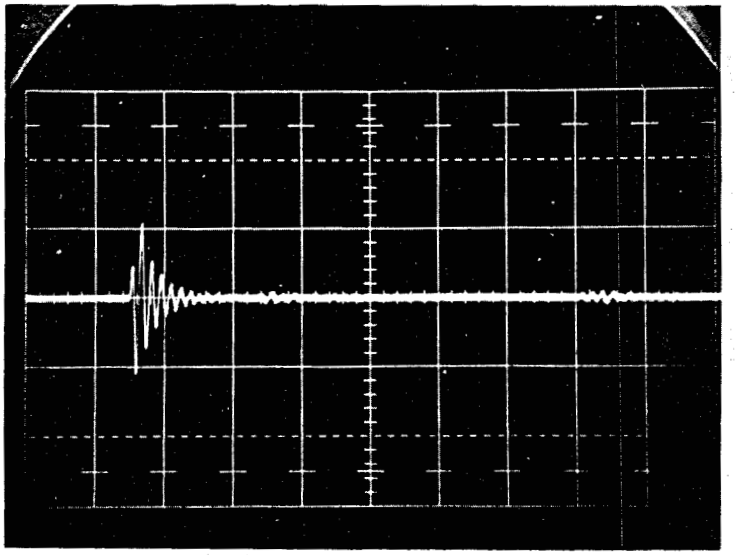

Figure 7.6. Received signal through 0.0015" brass window. (0.5 V/cm vert., 5 μsec/cm horiz.)

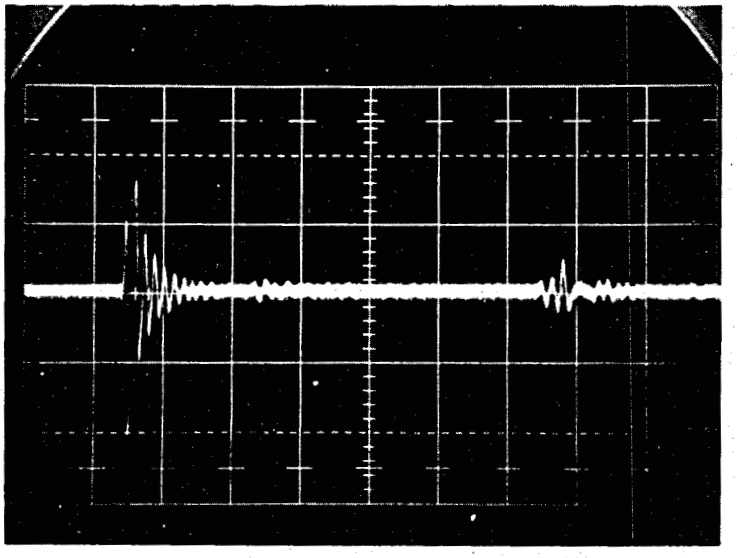

Figure 7.7. Received signal through 0.015" brass window. (0.05 V/cm vert., 5 μsec/cm horiz.)

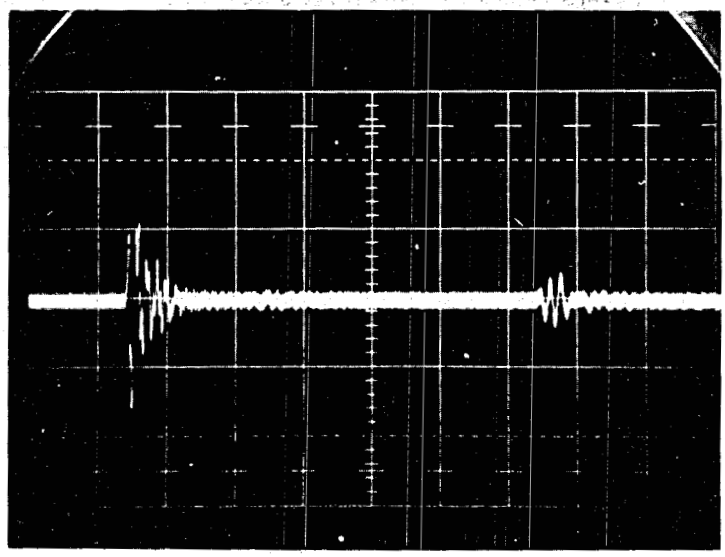

Figure 7.8. Received signal through 0.025" brass window, showing phase distortion (0.05 V/cm vert., 5 μsec/cm horiz.)

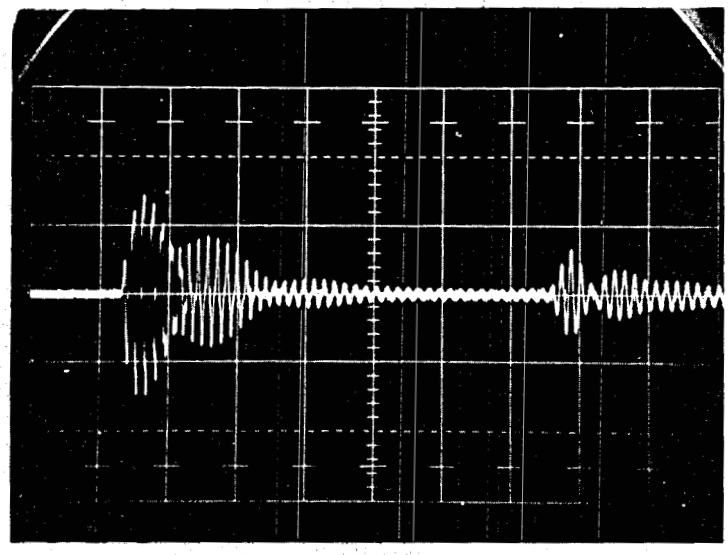

Figure 7.9. Received signal through 0.063" brass window, showing pulse elongation associated with $\lambda/2$ thickness. (0.1 V/cm vert., 5 μsec/cm horiz.)

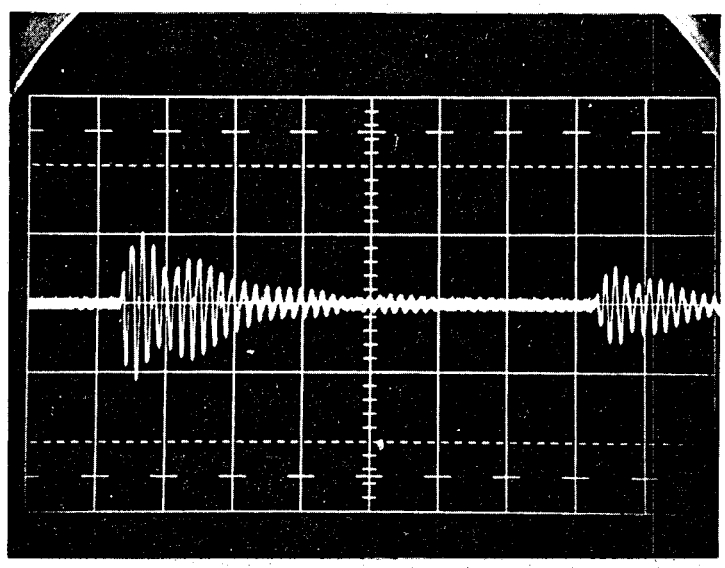

Figure 7.10. Received signal through 0.093" stainless steel window, showing pulse elongation associated with $\lambda/2$ thickness. (0.1 V/cm vert., 5 μsec/cm horiz.)

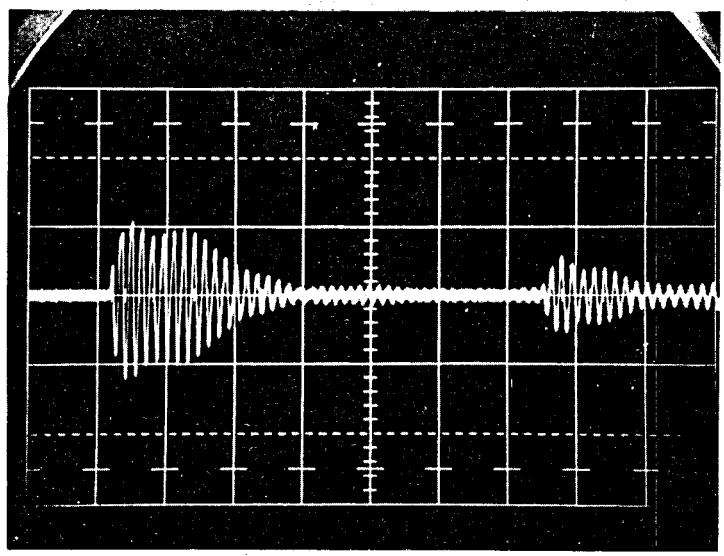

Figure 7.11. Received signal through 0.089" Cold Rolled Steel window, showing pulse elongation associated with $\lambda/2$ thickness. (0.1 V/cm vert., 5 μsec/cm horiz.)

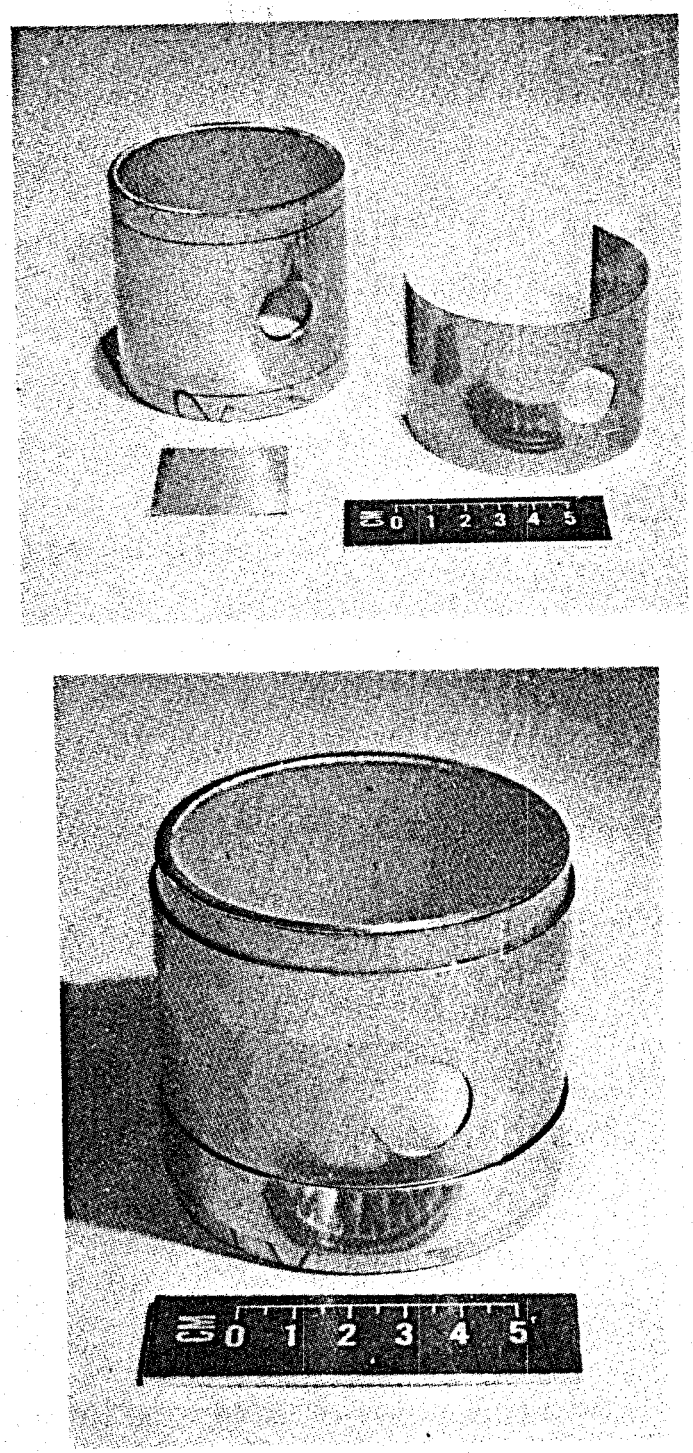

Figure 7.12. Fixturing for evaluating thin metal acoustic windows.

target located 1.5" from the outside window radius. A standard (Simplec) transducer assembly was placed against the inside radius of the test windows for transmitting and receiving acoustic pulses from the wire target through the windows. This test arrangement roughly simulates a conventional BHTV sensor, including the effects of reverberation, window reflections, window absorption, and reflection from a target.

Figures 7.13 and 7.14 show the results for the 0.1" thick Vespel and the 0.002" thick SS 301 windows, respectively. Both oscillograms show the superimposed effects of 1) transducer ring-down (internal reverberations, window reflections) and 2) the target echo. The target echo occurs at the 3 cm mark, corresponding to the target range of 1.5 inches. The first 2 cm are occupied by transducer ring-down. Acceptably low level residuals of the ring-down persist beyond the 2 cm mark. Comparing the two oscillograms, it is apparent that the metal window produces increased reverberation as expected, however does not result in a target echo masking problem. The received echo level through the metal window is only 4 dB down from that obtained through the Vespel window. The data for the 0.002" Inconel 718 window is essentially identical to that shown for the SS-301.

These results are significant since both Inconel 718 and 300-series stainless steels are expected to be tolerant to corrosive geothermal borehole fluids.

Summary

1) Loss and pulse shape for the Vespel window can be duplicated with metal windows having thicknesses of about $\lambda/100$ to $\lambda/50$.

2) Metal window thicknesses between 0.15λ and 0.40λ should be avoided to eliminate difficulties with phase distortion.

3) Half-wavelength metal windows represent considerable loss (12 to 15 dB worse than Vespel) and produce pulse elongation. Pulse elongation tends to reduce distance resolution. The major practical concern with the $\lambda/2$ window is that most of the "lost" energy actually goes into internal sensor reverberation.

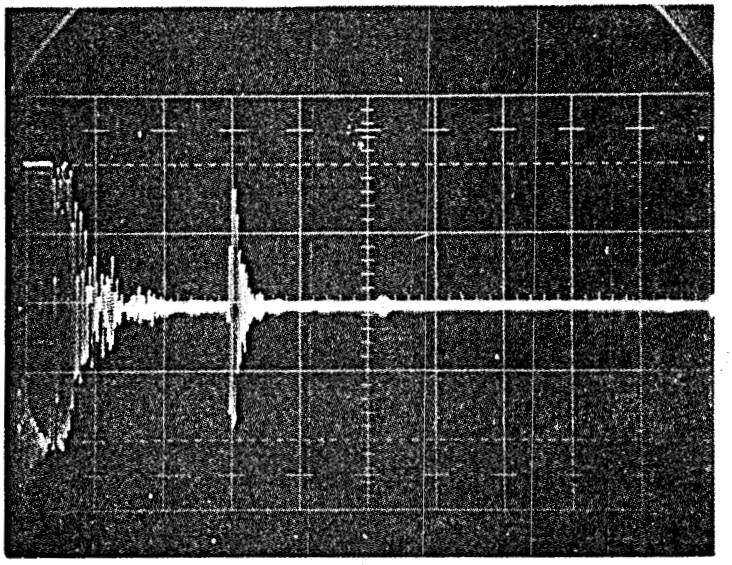

Figure 7.13. Pulse-echo oscillogram of 0.024" wire target through 0.1" Vespel window.

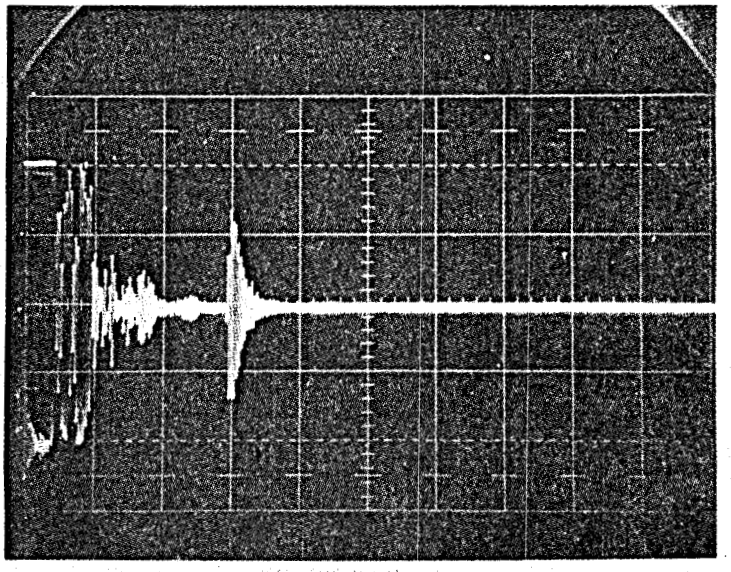

Figure 7.14. Pulse-echo oscillogram of 0.0.24" wire target through 0.002" SS301 window.

8. EXPERIMENTAL SENSOR DESIGN

Results of investigations of materials, components, and fabrication techniques were now sufficiently promising to permit proceeding with an experimental sensor design for autoclave testing. A transducer assembly consisting of lead metaniobate bonded to a tungsten powder-filled refractory cement looked promising. Advanced fluid screening tests had identified three candidate coupling fluids, Santovac 5, Krytox 143, and Brayco 812. Of the three, some successful work had been reported in operating an electric motor in contact with 812 at high temperature. As this feature is relevant to the televiewer, Brayco 812 was selected for evaluation in the experimental sensor design. Considerable analytical and experimental work had also shown the promise of thin metal acoustic windows. Inconel 718 was selected for the experimental sensor because it was readily available in thin sheets, had a favorably high sonic velocity (~5900 m/sec), and had demonstrated good corrosion resistance during prior autoclave screening tests. These major design elements were essentially specified at the outset of designing the experimental BHTV test sensor. The rest of the sensor design involved determining how the elements could be placed in available autoclave space while maintaining those features necessary for evaluation testing. Identifying certain hardware support items was also involved.

The basic test plan for the experimental sensor concept is indicated in Figure 8.1. An autoclave was available which had provisions for a rotary shaft penetration in the head to permit fluid agitation. The test plan called for replacing the conventional rotary shaft with a special shaft which would include a housing for the experimental sensor package. In effect then, this approach permits rotating the sensor and "scanning" targets as the BHTV does.

Dwg. 6428A70

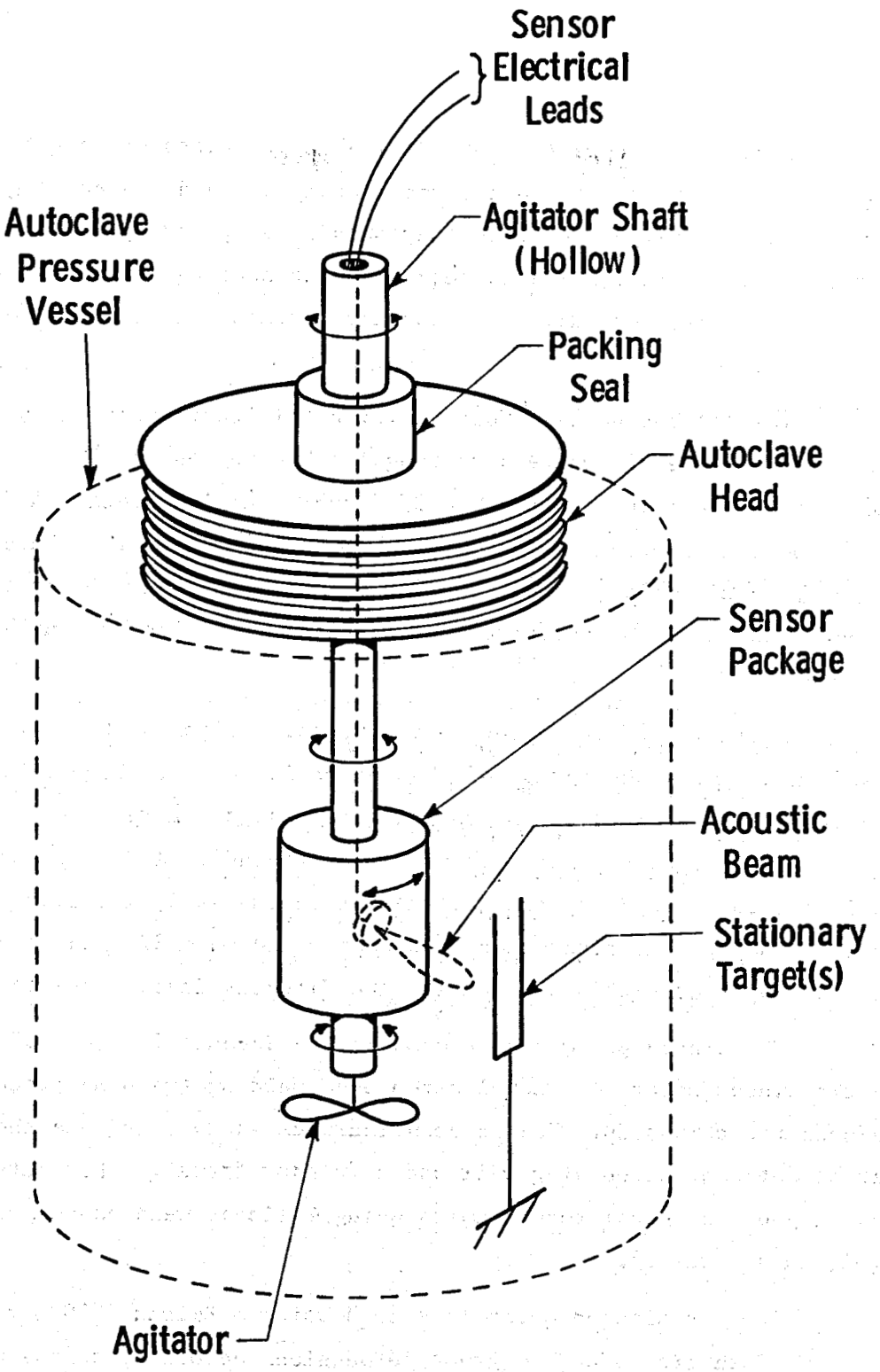

Fig. 8.1—Basic test concept for evaluating experimental sensor

Figure 8.2 shows the most desirable locations of targets and the sensor element with respect to the rotational axis and the cooling coil. To insure "clean" target returns, they should be spaced approximately 1/2" from the cooling coil I.D. A target-to-sensor spacing of approximately 1-1/2" is realistic for BHTV operation and defines the rest of the basic geometry.

The concept devised for realizing this configuration is indicated in Figure 8.3 where a rectangular housing encloses the 1/2" diameter piezoelectric disc and the 3/4" cubic damping block. A 3/4" diameter port hole provides for passage of acoustic signals. This port is to be covered by a flat, 0.002" thick metal window. Other bench testing has shown insignificant performance variations with flat vs. curved, thin metal windows.

A drawing of the experimental sensor design is shown in Figure 8.4 and an assembly photograph of the sensor is shown in Figure 8.5. There are several points of interest in the design. A rectangular tubing section is welded to top and bottom flanges (round). A 3/4" diameter port hole is cut in one side of the rectangular tubing wall, locating the acoustic window. The piezoelectric disc mounted on a 3/4" cubic damping block is supported within the housing and directly inside the window port.

The window port is covered with the Inconel 718 (0.002") acoustic window material. An electron beam welding (vacuum) process was developed for this step. The process includes sandwiching the thin window material between the housing wall and a "window frame". This method provided good and consistent results using 4 linear weld passes which are visible in Figure 8.5.

The top flanged joint is sealed using a Kalrez 1050 o-ring. Grooves deviate from standard groove dimensions according to the manufacturers recommendations. The top flange also contains the necessary electrical feed through. The sensor housing interior is filled with coupling fluid. The electrical feedthrough used was specially designed and manufactured by Ceramaseal Corp. and was welded into the top flange.

Dwg. 7690A44

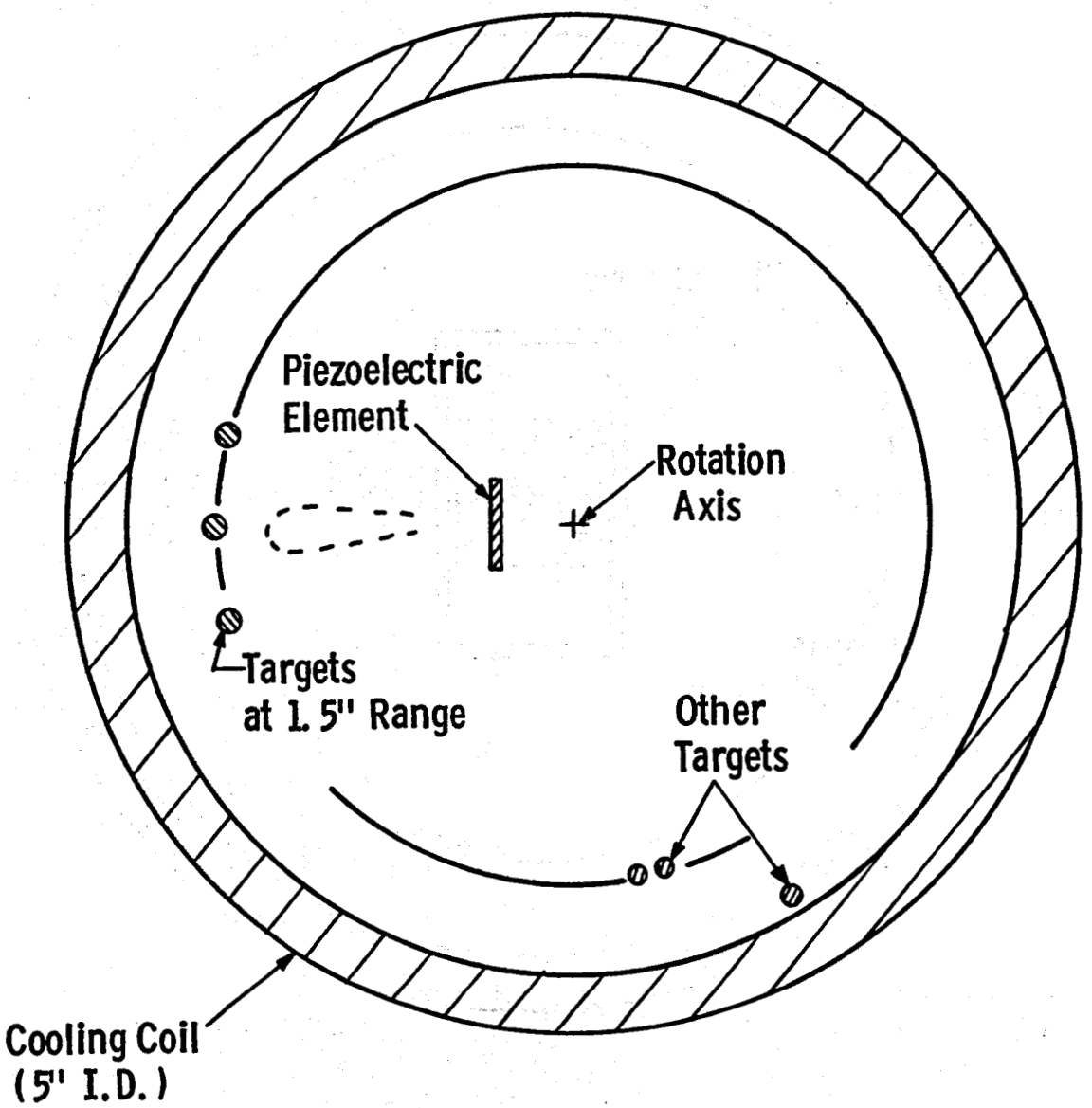

Fig. 8.2— Diagram showing desired placement of piezoelectric element and targets within available autoclave space

Dwg. 7690A45

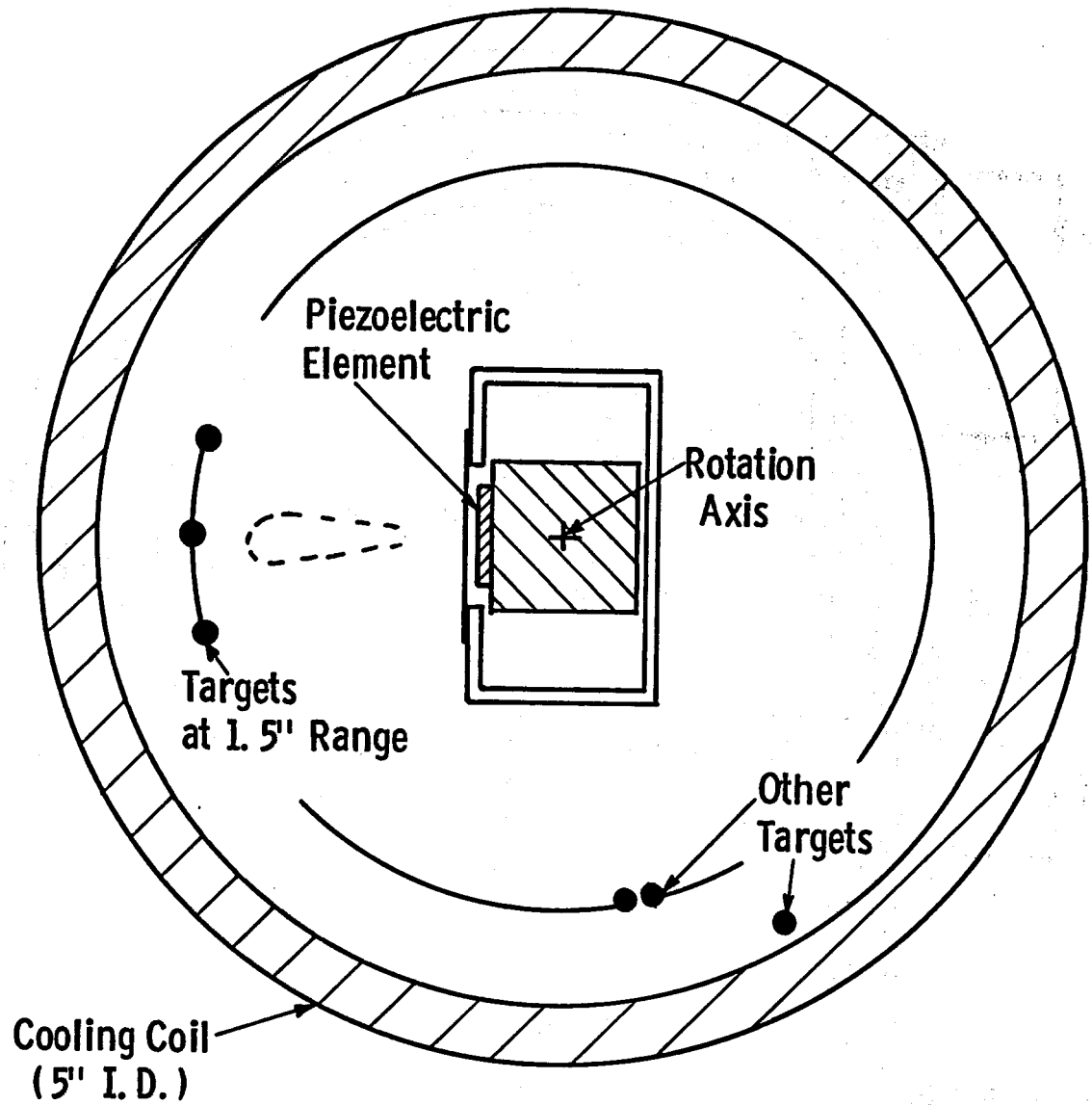

Fig. 8.3— Diagram of sensor and housing design used to realize desired element/target geometry

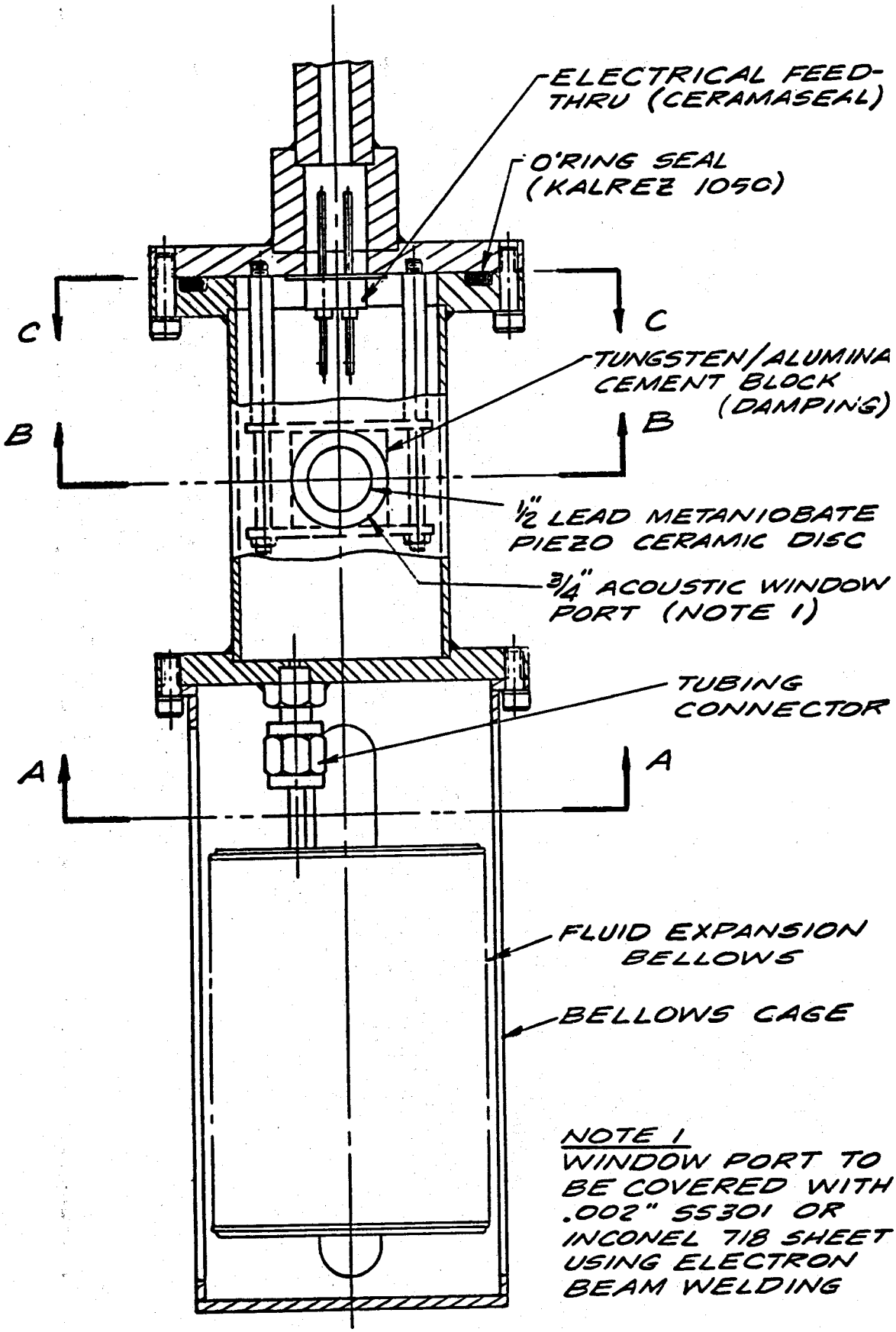

Figure 8.4. Resulting sensor design, including internal supports, housing, acoustic window, electrical feed-through, seal, and volume expansion bellows.

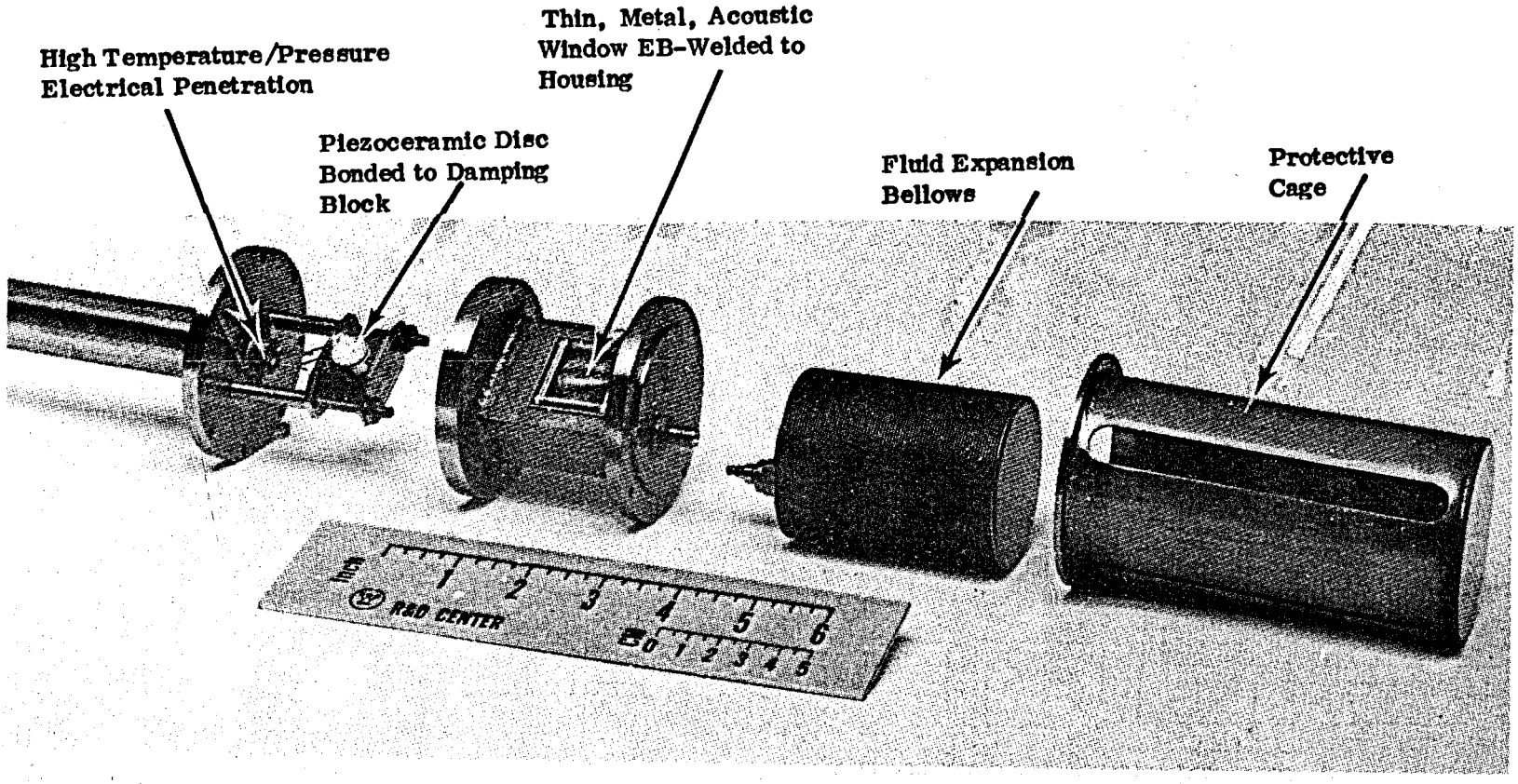

Figure 8.5. Assembly photograph of the experimental BHTV sensor.

The feedthrough uses 0.035" diameter nickel wires. The other wires were attached to the feedthrough wires by spot welding.

A tubing connector is welded to the bottom flange of the sensor housing for attachment of the fluid expansion bellows. Fluid volume increases on the order of 20% are expected at 530°F (275°C). The bellows also serves to pressure balance the housing so that the differential pressure across the thin acoustic window is very small. A bellows is used in the conventional televiewer tool for the same reason. A protective cage surrounds the bellows. Figure 8.6 shows a photograph of the assembled sensor ready for evaluation testing.

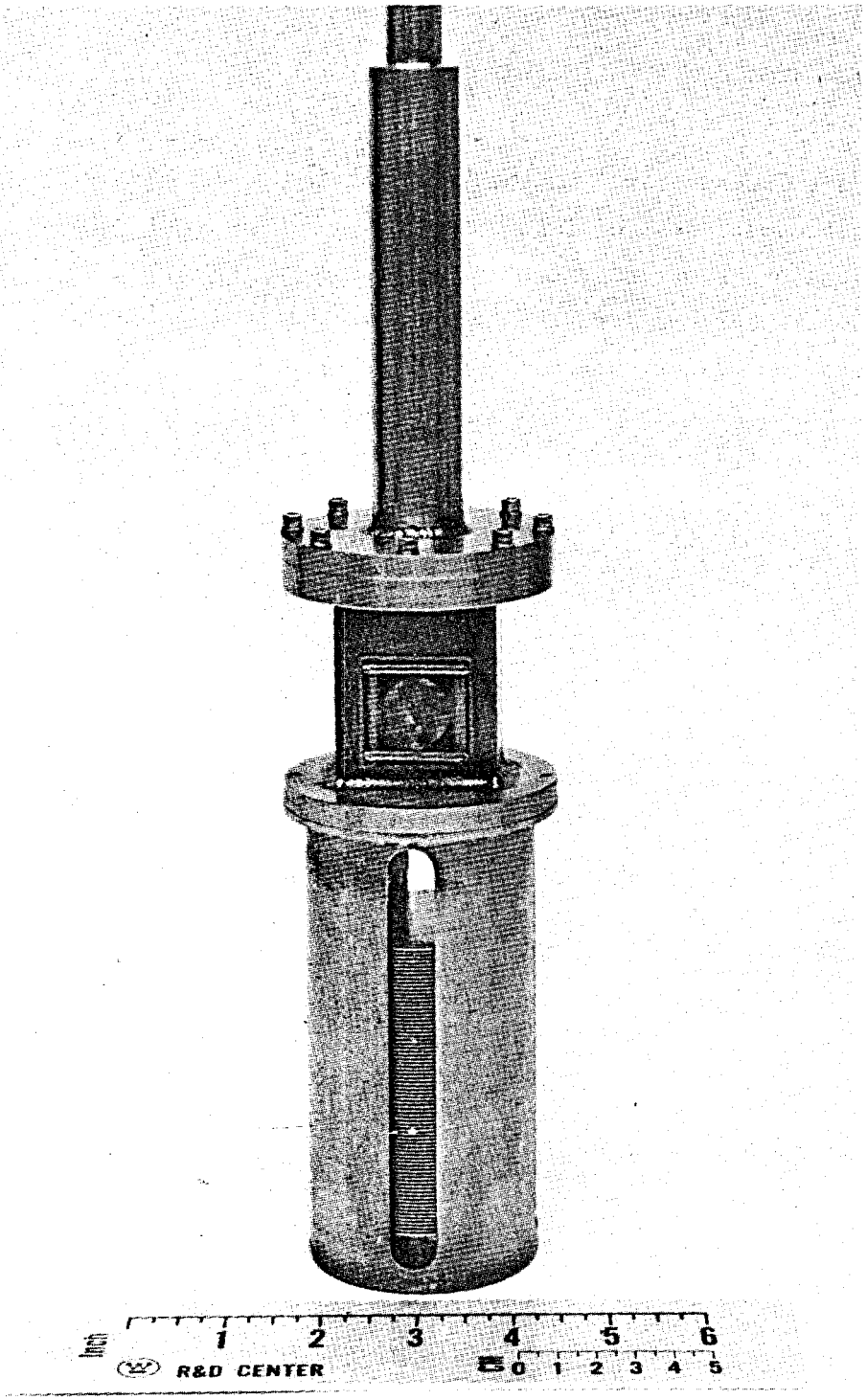

Figure 8.6. Photograph of fabricated experimental acoustic sensor concept.

9. PRELIMINARY SENSOR TESTING

The experimental sensor was fabricated along with a set of identical spare transducer and housing parts. The spare parts were used to perform some of the following bench tests. Performance and characteristic comparisons were made relative to standard televiewer parts supplied for this project by Simplec Manufacturing. Beam patterns, reverberation levels, and sensitivities were measured and compared as described in the following sections. The section describing sensitivity measurements indicates the effects of certain individual acoustic elements.

Beam Pattern - The assembled experimental sensor, filled with Brayco 812, was immersed in an oil bath and used in the pulse-echo mode to detect a 3/32" diameter steel rod target at a range of 1-1/8". The test apparatus is shown in Figure 9.1. A Panametrics 5050 PR pulser/receiver was used in conjunction with the sensor. The resulting beam pattern is plotted Figure 9.2. The half-power (-3 dB) beam width is 3.2^{o}. This compares favorably with the 3^{o} beam width measured during tests (see Appendix I) on an actual BHTV tool. The beam pattern measured on that tool is shown in Figure 9.3. It is apparent that the experimental design does not degrade the beam pattern.

Reverberation - Measurements were also made to compare the reverberation levels of the assembled geothermal sensor and a (reference) mock-up of a conventional BHTV sensor. The reference sensor mock-up consisted of a set of conventional sensor internals (Simplec) and a Vespel window (Simplec) in appropriate proximity to each other as shown in Figure 9.4. Although the reference sensor mock-up shown in Figure 9.4 consists of a window from a 3 3/8" diameter tool and a transducer assembly from a 1 7/8" diameter tool, this arrangement does put the piezoelectric transducer assembly in close proximity with the window and is therefore believed to be representative of an actual BHTV sensor.

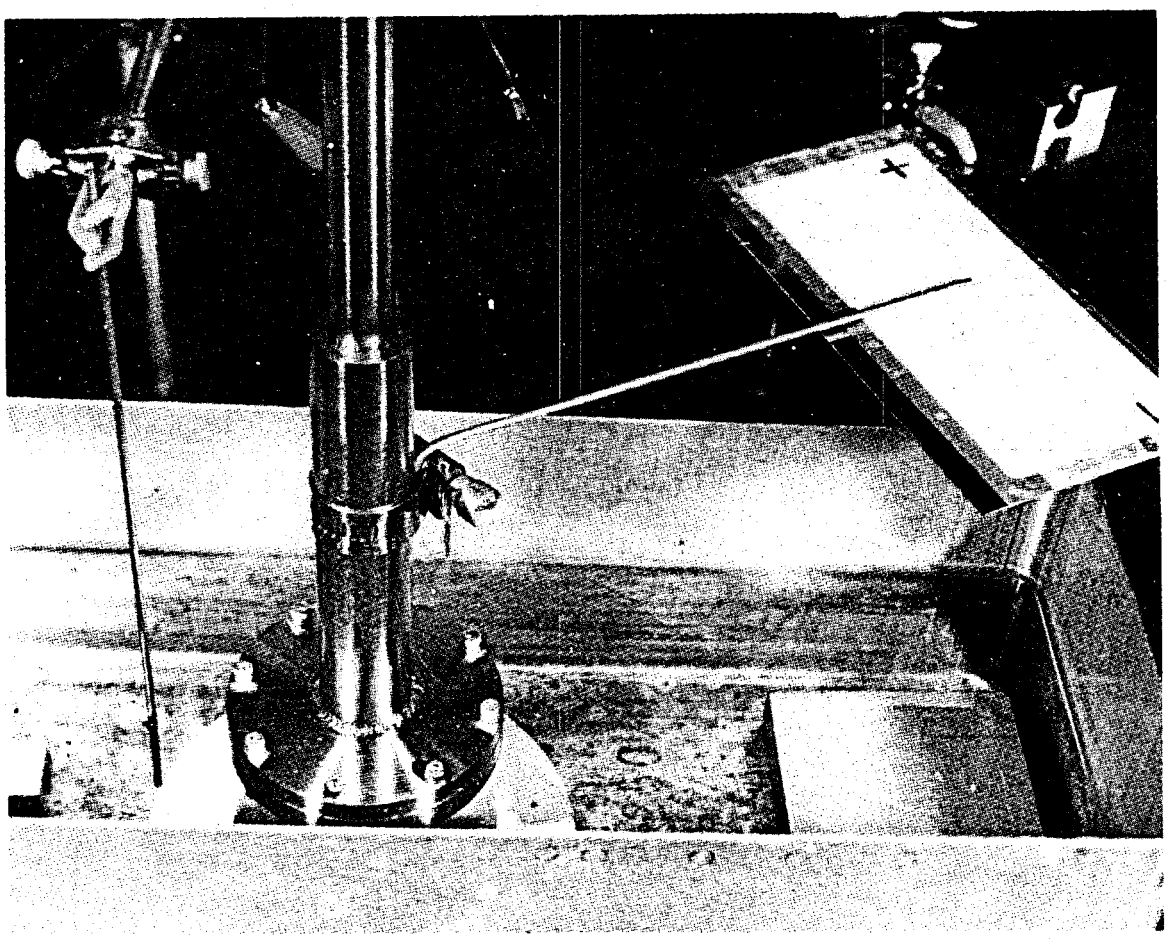

Figure 9.1. Apparatus used to measure beam pattern of Experimental Geothermal Sensor.

Curve 715663-A

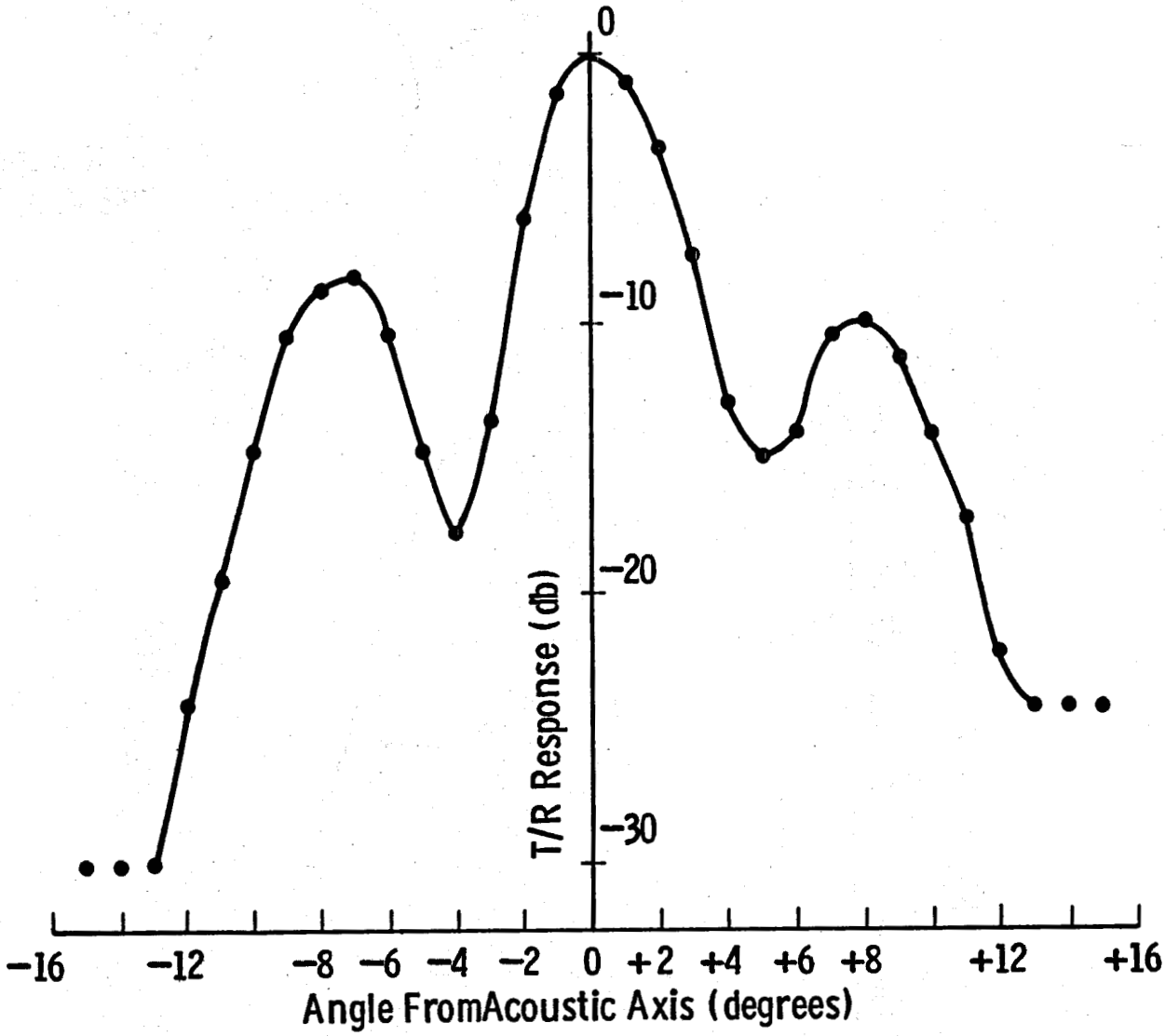

Fig. 9. 2—Transmit-receive beam pattern for experimental sensor, measured in room temperature transformer oil. Half-power beam-width is 3. 2°

Curve 715666-A

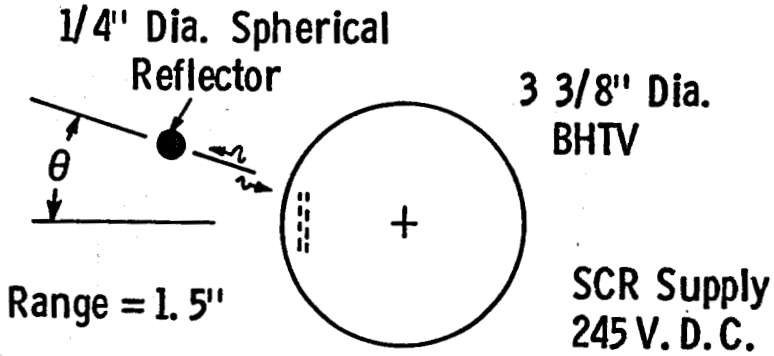

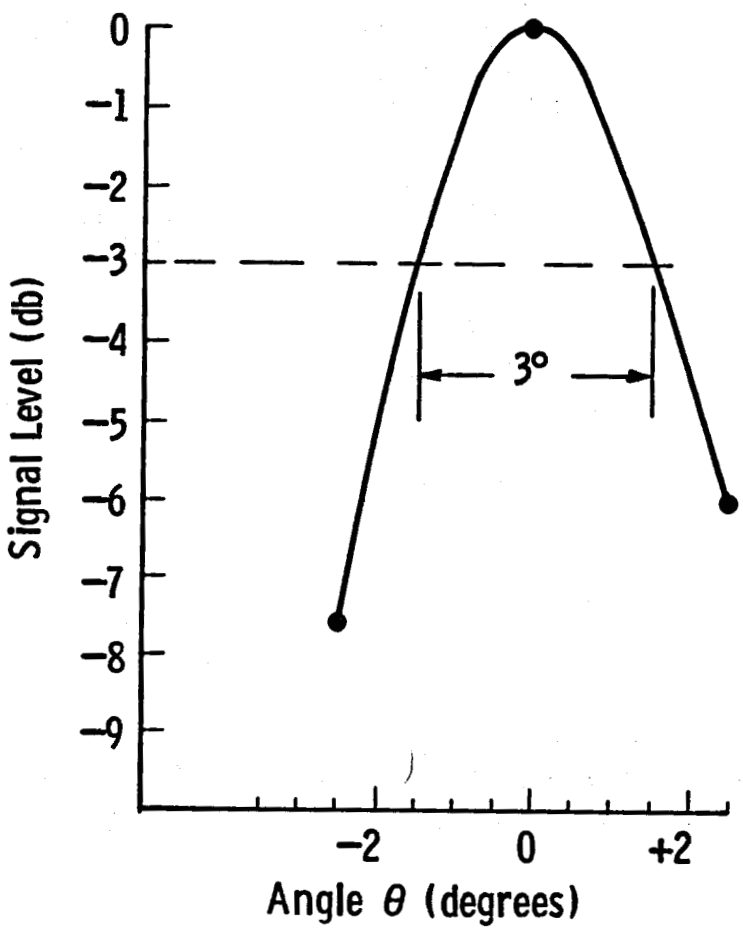

Fig. 9.3—Transmit-receive pattern for a USGS BHTV sensor, measured in room-temperature water

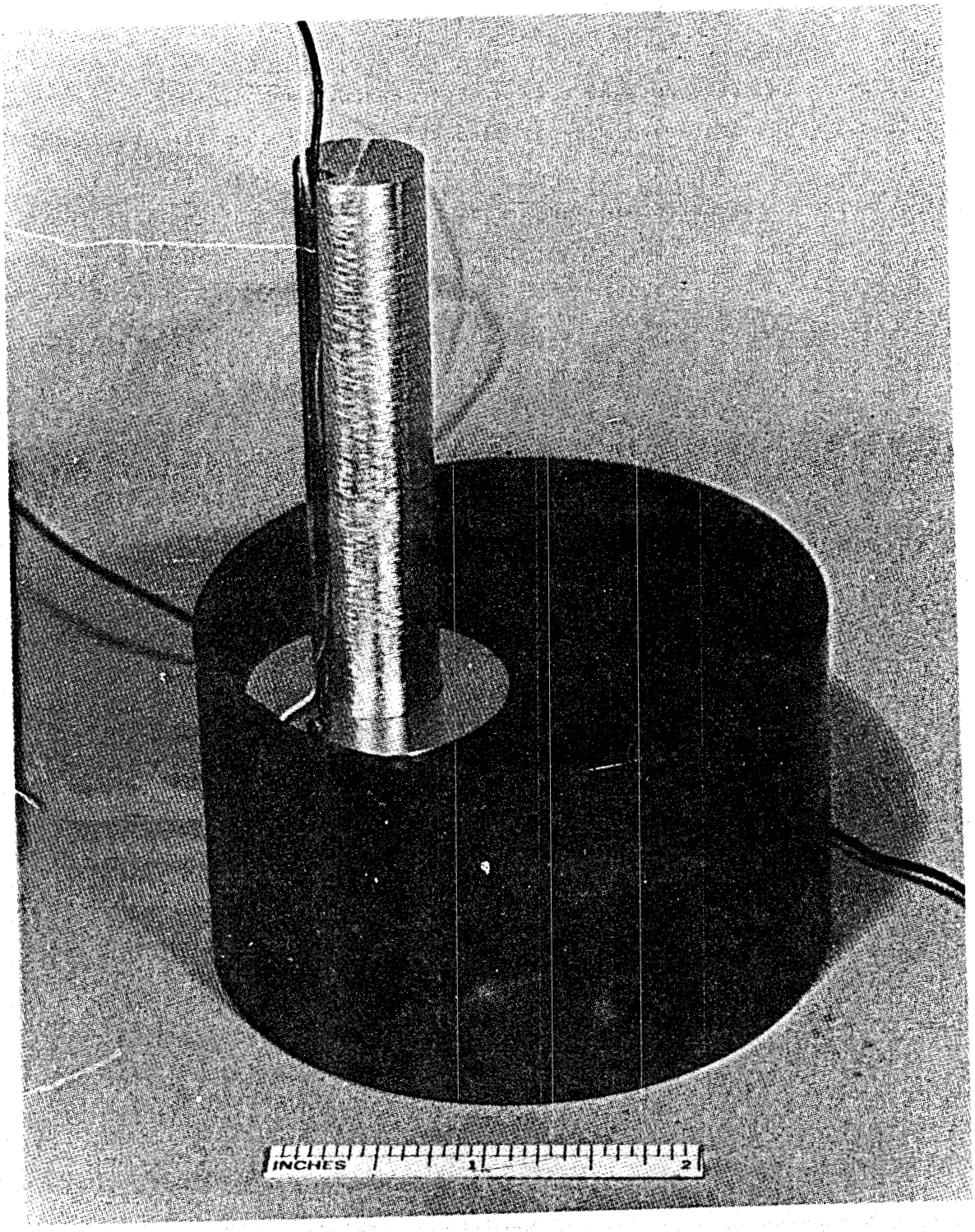

Figure 9.4. Reference transducer assembly in prototypical proximity with Vespel (reference) window.

Two comparative sets of data are presented. Again, the Panametric 5050 PR pulser/receiver was used. Figure 9.5 compares the reverberation levels immediately after the transmitted pulse. Figure 9.6 displays the same reverberation over a longer time interval. There are no targets in the sound field for these measurements. It is concluded that 1.) both sensors are reverberation-noise-limited and 2.) the geothermal sensor offers an improvement (decrease) in reverberation level by a factor of approximately 2.

Sensitivity - Detailed measurements were made to compare the transmit/receive sensitivity of the geothermal sensor and the (reference) conventional BHTV sensor mock-up. For the following tests, the target was a large, flat, metal reflector (tank wall) at a range of 1" and the Panametrics 5050 PR pulser/receiver was used. The propagation medium was transformer oil.

Transducer Assembly - Figures 9.7 and 9.8 show the two transducer assemblies used to generate and receive the acoustic signals. Figure 9.9 shows a 2.65 Volt (p-p) wall echo using the reference transducer immersed in oil. Figure 9.10 shows a 1.32 Volt (p-p) wall echo using the goethermal transducer assembly immersed in oil. This shows that the basic geothermal transducer assembly response is down by 6 dB compared with the reference. At least part of this performance difference was expected. The reference transducer has a layer of epoxy over the crystal for the purpose of improving coupling to liquids. Lacking a high-temperature equivalent of the epoxy, this feature is not easily realized in the geothermal unit and was therefore omitted. Also, the geothermal backing material is higher density and therefore has a higher acoustic impedance than the reference unit. The high density is a result of the tungsten powder which helps to control transducer Q, promotes attenuation and therefore reduces transducer reverberation. (The improved reverberation performance is also evident in comparing Figures 9.9 and 9.10.) The relatively higher impedance of the backing materials was expected to decrease the output pressure somewhat. It is estimated that between 2 and 4 of the 6 dB performance differential could be recovered by

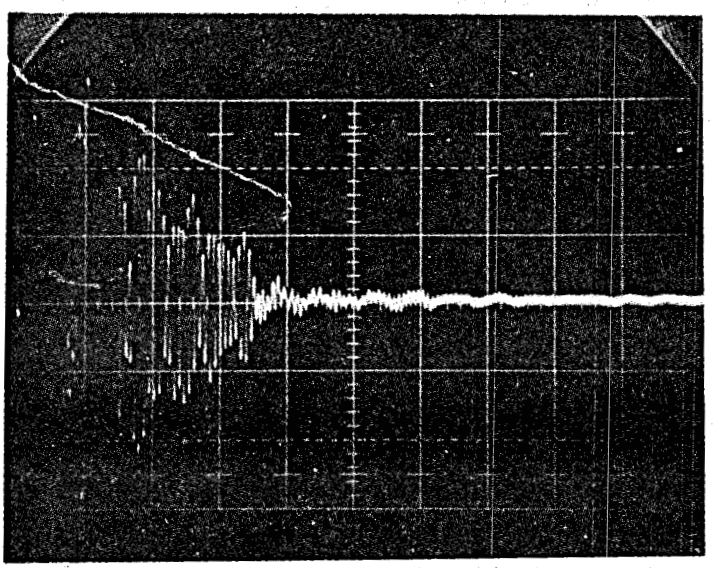

(A) Experimental Geothermal Sensor

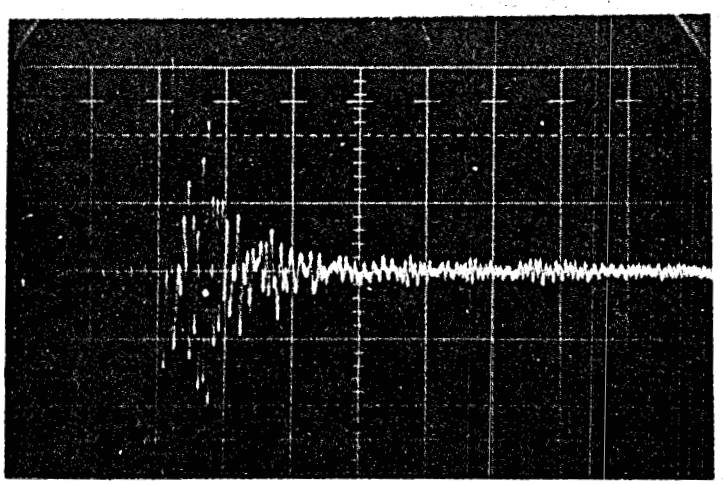

(B) Reference Sensor

Figure 9.5. Reverberation comparison beteween (A) experimental geothermal sensor and (B) reference sensor. Scale factors are 0.1 V/div. (vertical) and 10 μsec/div. (horizontal). Panametrics 5050 PR settings: Energy = 4, Attenuation = 20 dB.

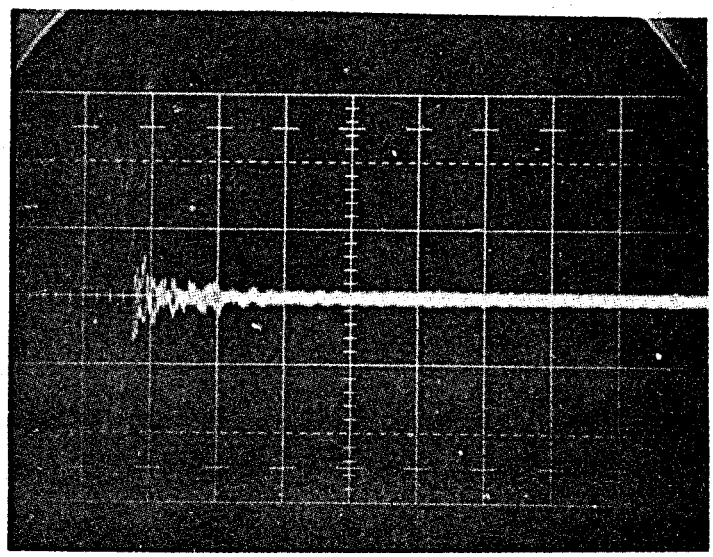

(A) Experimental Geothermal Sensor

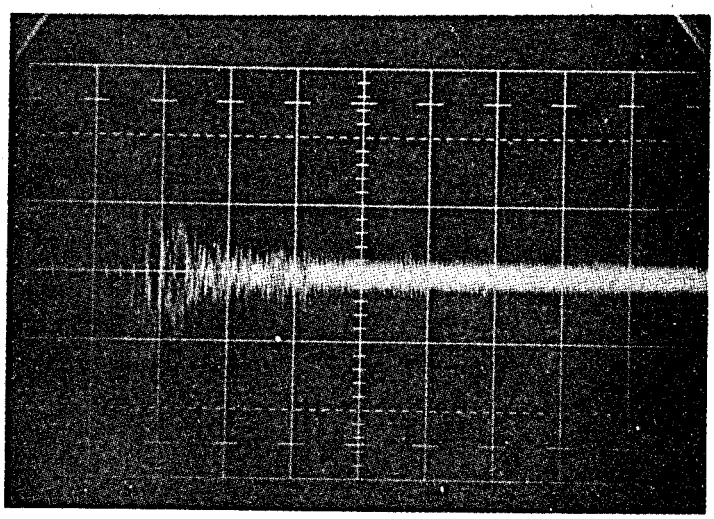

(B) Reference Sensor

Figure 9.6. Reverberation comparison between (A) experimental goethermal sensor and (B) reference sensor. Scale factors are 0.2 V/div. (vertical) and 20 μsec (horizontal). Panametrics 5050PR settings: Energy = 4, Attenuation = 0 dB.

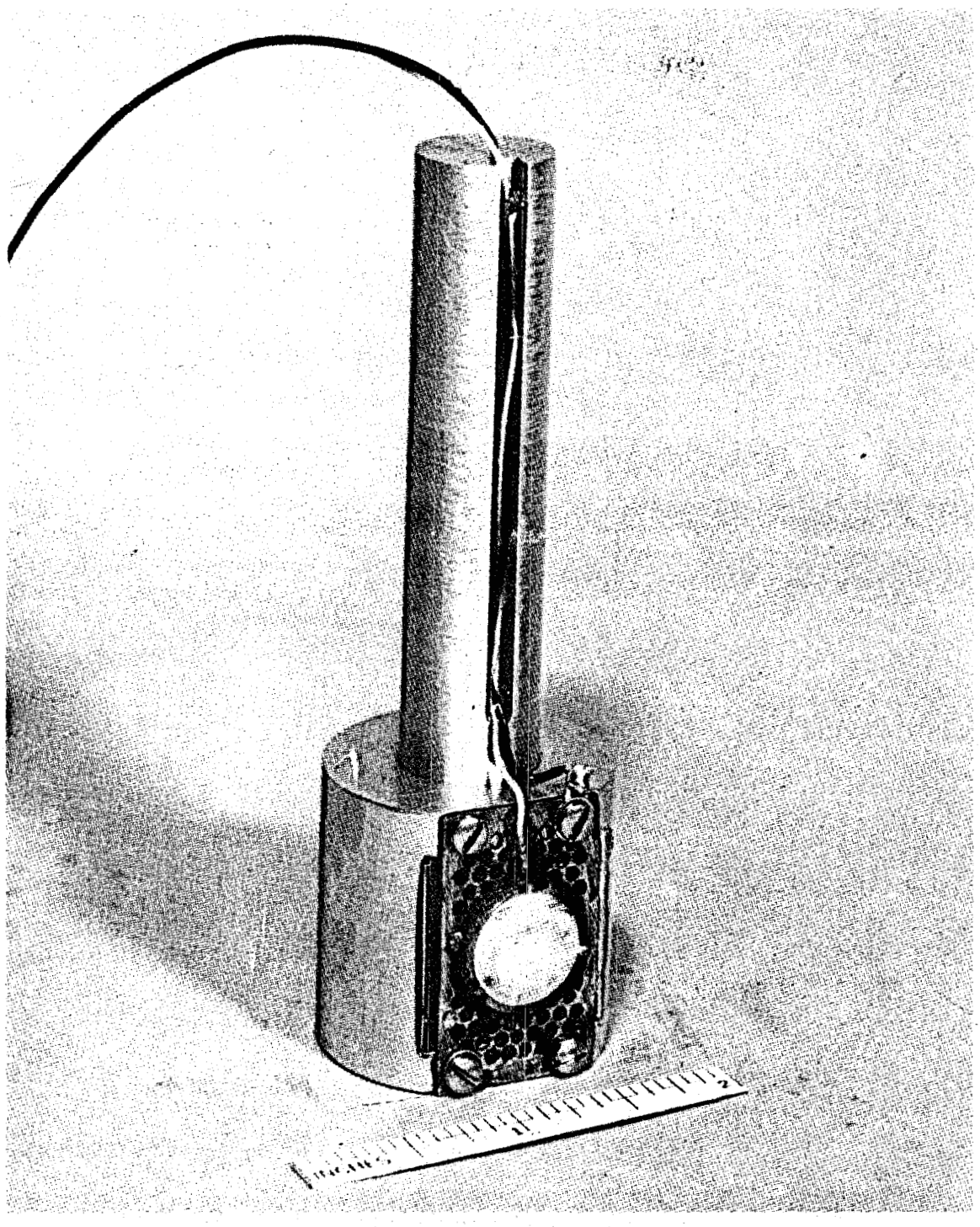

Figure 9.7. Reference transducer assembly by Simplec, using lead-metaniobate crystal and rubber backing material behind perforated brass mounting plate.

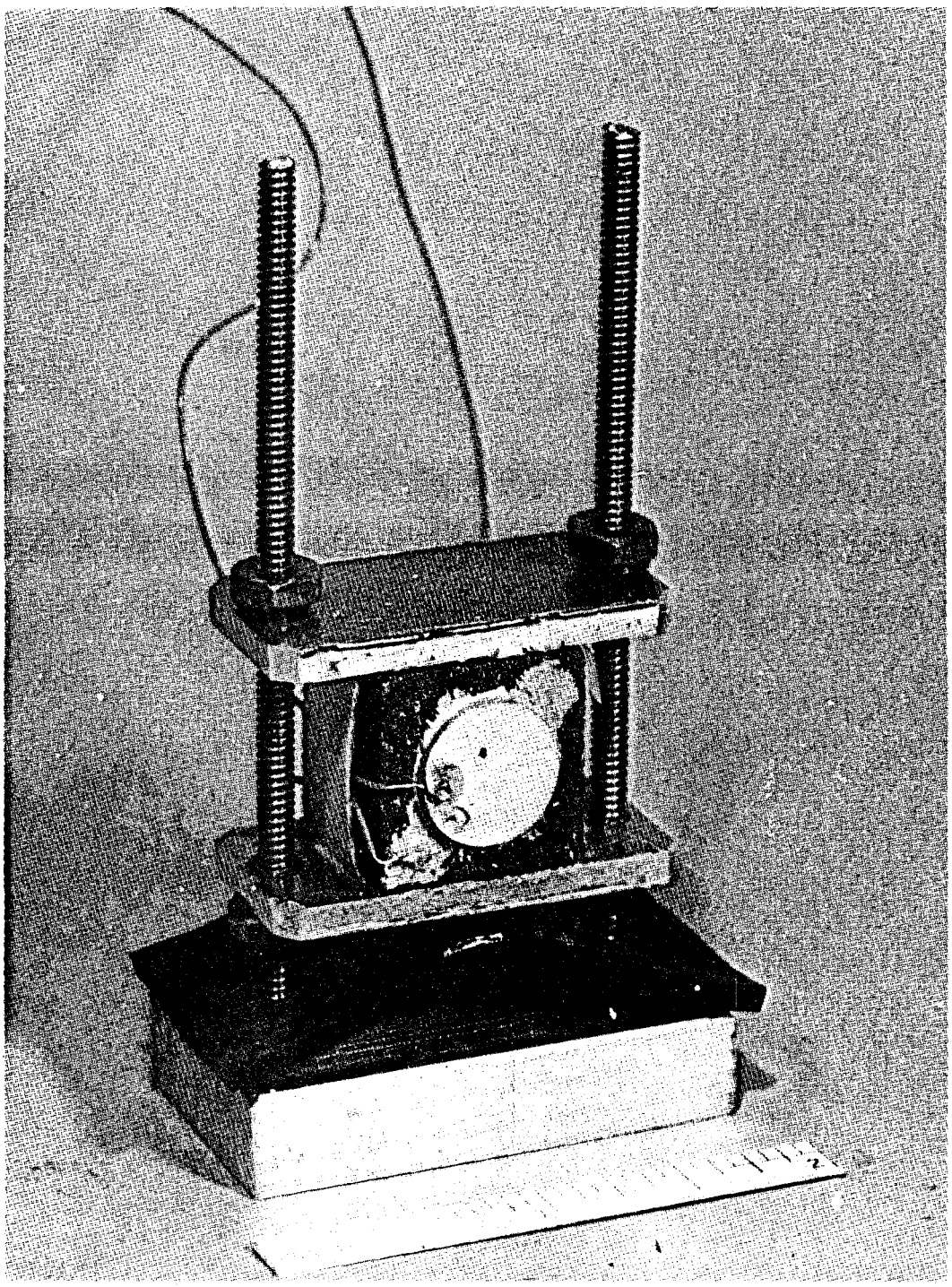

Figure 9.8. Experimental geothermal transducer assembly, using lead-metaniobate crystal bonded to tungsten-filled, refractory cement backing block.

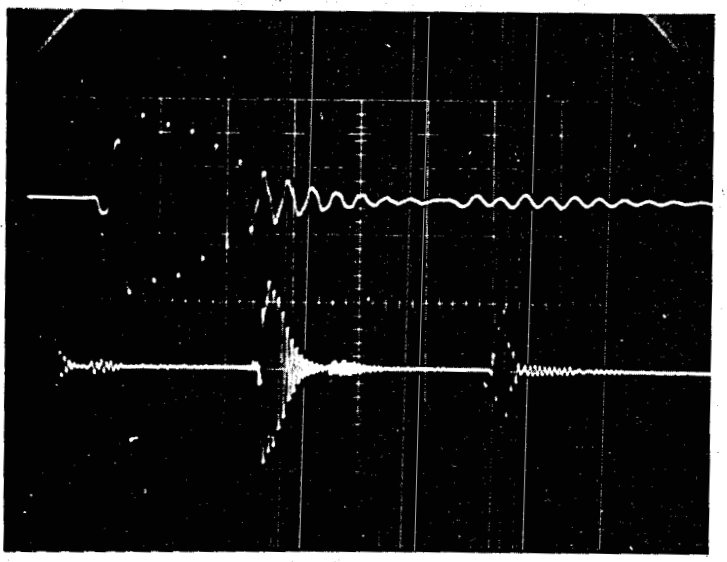

Figure 9.9. Wall echo using reference transducer. Wall echo appears at 3.5 div. on lower trace (10 μsec/div) and is expanded (2 μsec/div) in upper trace. Vertical scale factor is 1 Volt/div. Panametrics 5050 PR settings, Energy = 4, Attenuation = 40 dB.

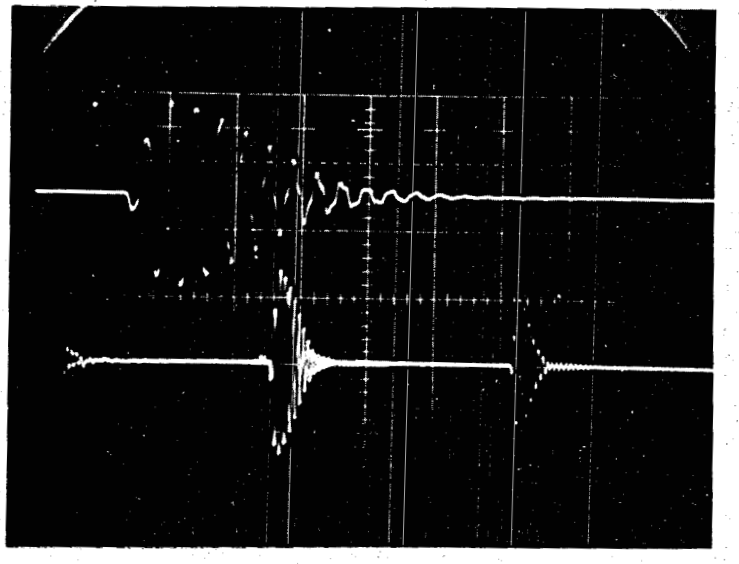

Figure 9.10. Wall echo using geothermal transducer. Wall echo appears at 3.5 div on lower trace (10 μsec/div) and is expanded (2 μsec/div) in upper trace. Vertical scale factor is 0.5 Volt/div. Panametrics 5050 PR settings: Energy = 4, Attenuation = 40 dB.

sacrificing some Q and/or reverberation performance. Omitting the tungsten powder from the backing material should go toward realizing this trade-off.

Transducer with Window - The two transducer assemblies were then put in appropriate conjunction with their respective acoustic windows of Vespel and Inconel 718. The two assemblies are shown in Figures 9.11 and 9.12. For this test, transformer oil was used both inside the outside transducer housings. Figure 9.13 and 9.14 show the target echoes for the geothermal (0.51 Volts) and the reference unit (1.675 Volts) respectively. This data shows that the metal geothermal window causes 4 dB more attenuation than the reference (Vespel) window. While little can be done to mitigate this 4 dB acoustic performance decrement, mechanical durability and thermal immunity of the window have been greatly improved.

High-Temperature Fluid - The final test involved filling the goethermal sensor the Brayco 812 instead of transformer oil. The resulting target echo is shown in Figure 9.15. The echo amplitude is 0.27 Volts (p-p) which is 6 dB worse than the same apparatus filled with transformer oil.

Comparing Signal-to-Noise Ratios (SNR) - Comparing Figures 9.14 and 9.15 shows the geothermal sensor to be lower sensitivity than the reference sensor by 16 dB. However, sensitivity is not viewed as the ultimate figure of merit for the BHTV sensor. The most significant sensor characteristic is SNR. High sensitivity to targets is irrelevant if the masking noise is extreme. Similarly, less sensitive sensors with low masking noise levels can usually be improved by simply increasing receiver amplifier gain.

Both the geothermal and reference sensors are reverberation-noise-limited and from Figures 9.5 and 9.6 it is evident that the reverberation noise in the geothermal sensor is down by a factor of 2. Therefore, the voltage gain of a geothermal BHTV receiver input amplifier can be doubled (+6 dB) to make the reverberation level of the geothermal sensor equal to that of the reference sensor at some detector input. The

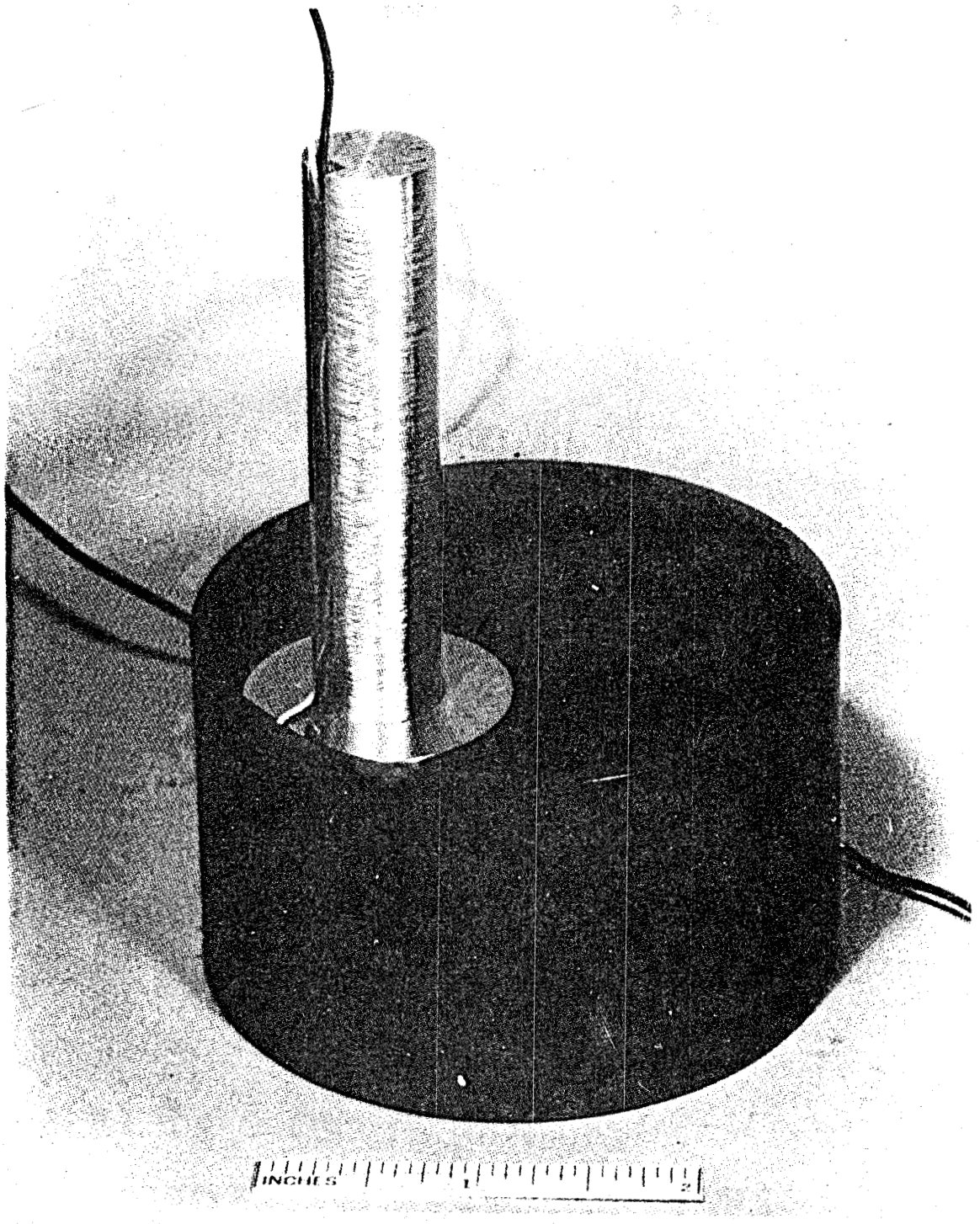

Figure 9.11. Reference transducer assembly in prototypical proximity with Vespel (reference) window.

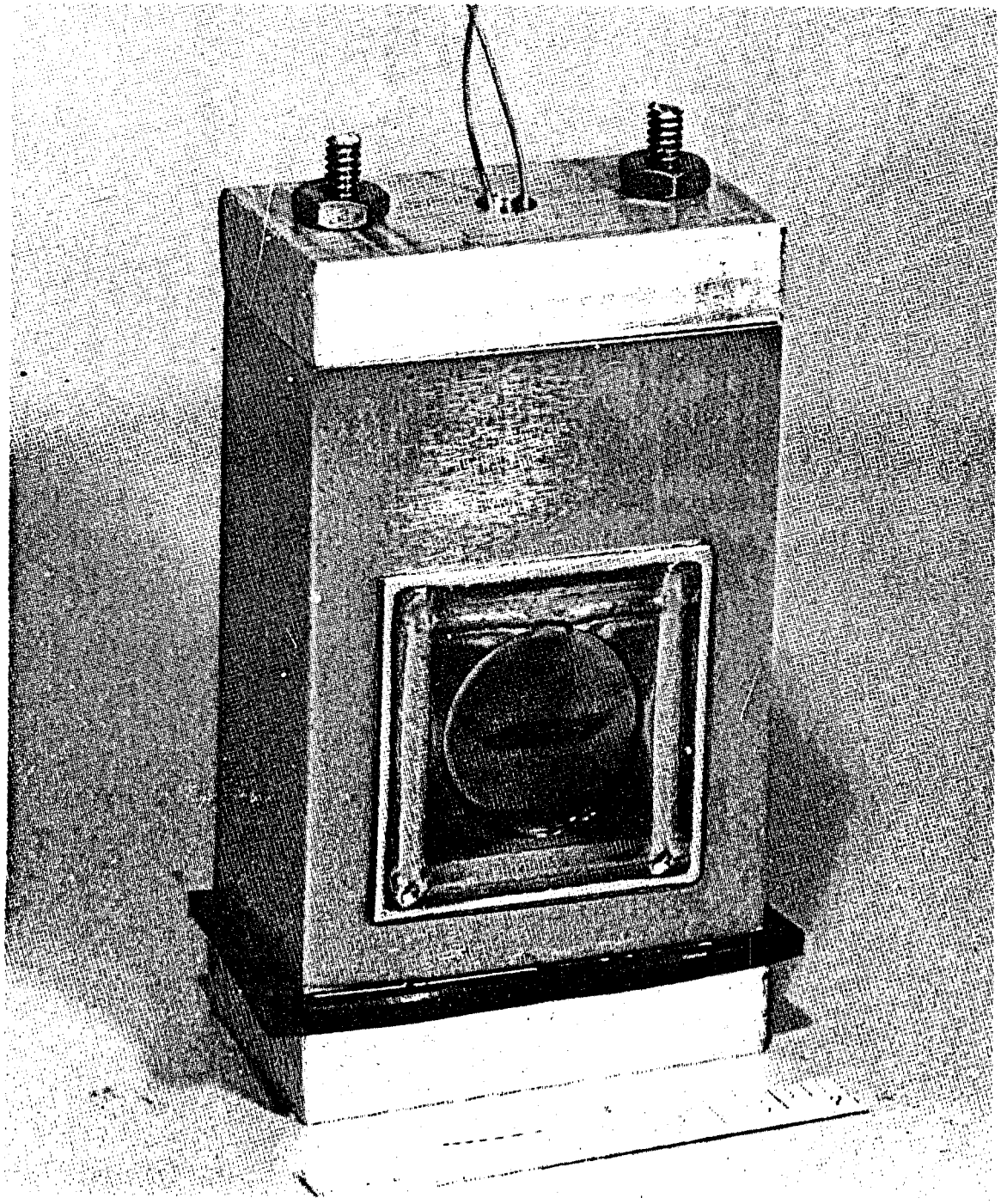

Figure 9.12. Experimental geothermal transducer installed in housing with 0.002" Inconel 718 window.

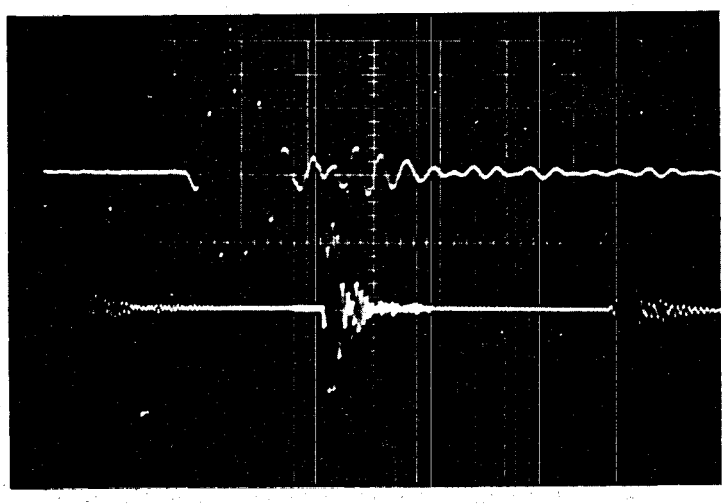

Figure 9.13. Wall echo using transformer oil-filled geothermal sensor mock-up shown in Figure 9.12. Wall echo appears at 4.2 div. on lower trace (10 μsec/div) and is expanded (2 μsec/div) in upper trace. Vertical scale factor is 0.2 Volts/div. Panametrics 5050 PR settings: Energy = 4, Attenuation = 40 dB.

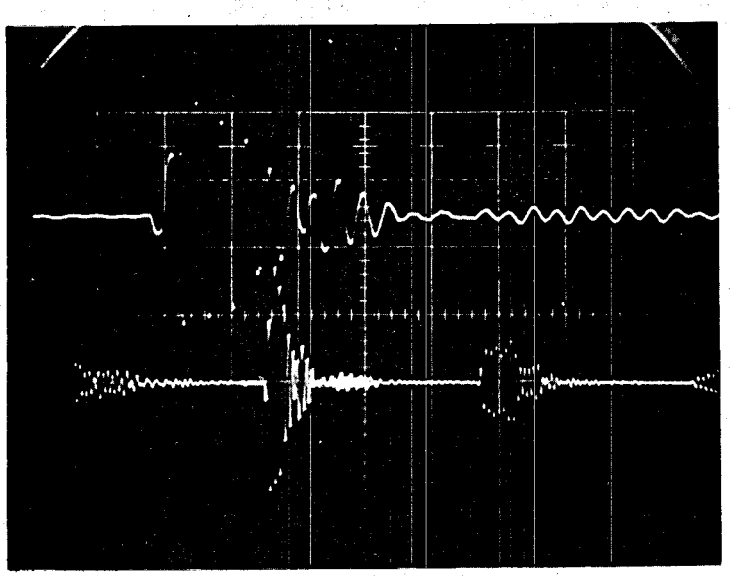

Figure 9.14 Wall echo suing reference sensor mock-up shown in Figure 9.11. Wall echo appears at 3.5 div. on lower trace (10 μsec/div) and is expanded (2 μsec/div) in upper trace. Vertical scale factor is 0.5 Volts/div. Panametrics 5050 PR settings: Energy = 4, Attenuation = 40 dB.

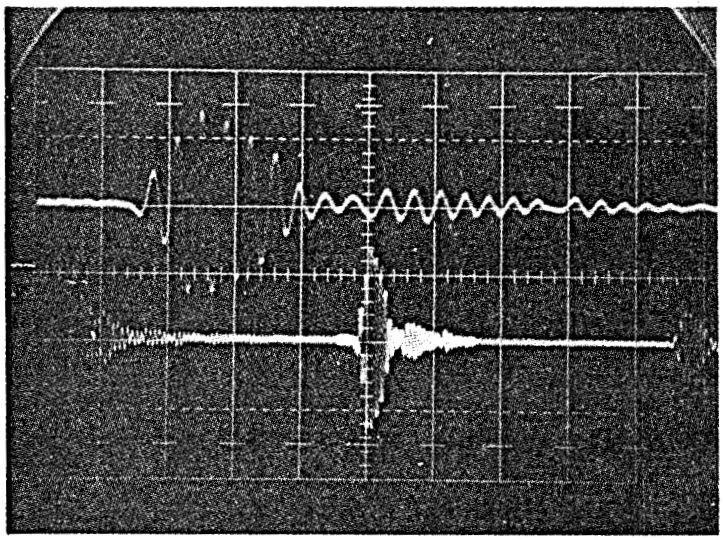

Figure 9.15. Wall echo using Brayco 812-filled geothermal sensor mock-up shown in Figure 9.12. Wall echo appears at 5 div. on lower trace (10 μsec/div) and is expanded (2 μsec/div) in upper trace. Vertical scale factor is 0.1 Volt/div. Panametrics 5050 PR settings: Energy = 4, Attenuation = 40 dB.

2X voltage gain also increases the level of all geothermal target echoes by 6 dB. Therefore the 16 dB performance differential based on target sensitivity is reduced by 6 dB from a SNR standpoint. On a SNR figure of merit basis, the geothermal sensor is therefore only about 10 dB worse than the reference sensor.

Conclusion. The conventional BHTV has demonstrated acceptable fracture imaging performance in mud-filled boreholes where target echo attenuation is relatively high. The geothermal BHTV is expected to encounter relatively "clean" borehole fluid which should cause much less target echo attenuation. Referring to Section 4, attenuations in mud-filled boreholes may be as much as 50 dB higher. Meanwhile, reverberation levels in the sensors remain fixed. Therefore as a practical matter, the (-10 dB) geothermal sensor design should produce satisfactory results in a geothermal BHTV tool.

10. AUTOCLAVE DEMONSTRATION TEST OF EXPERIMENTAL SENSOR

Over the period of December 18-20, 1978, an experimental acoustic sensor was tested at Pressure Chemical Co. (Pittsburgh) during autoclaving under simulated geothermal conditions according to Test Plan No. ST-005 (see Appendix III). The primary objective of the test was to demonstrate acoustic sensor operation at 275°C, 7000 psi, and in simulated geothermal fluid.

Test Apparatus and Methods - Figure 10.1 shows the experimental sensor designed for this test. The acoustic window is fabricated from 0.002" Inconel 718. Transducer internals consist of a lead metaniobate piezoceramic element (disc) bonded to a cube (3/4") of tungsten-powder-filled refractory cement. The internal coupling fluid selected was Brayco 812. A special high-temperature and pressure electrical feedthrough (Ceramaseal) provided electrical contact with the sensor internals. The housing design included a flanged joint which was sealed using a Kalrez o-ring.

The housing was designed to be an integral part of a shaft which penetrates a gland seal in the autoclave head. This permits rotation of the sensor housing to aim the acoustic beam in various directions.

The autoclave and the simulated geothermal fluid used was the same as had been used in all prior tests.

Figure 10.2 shows the type of acoustic target installed in the autoclave for evaluating sensor performance. Three targets were installed with rod diameters of 0.096", 0.124", and 0.188".

Figure 10.3 shows the test sensor installed in the autclave head just prior to installing the head on the autoclave vessel. The electrical leads can be seen coming out of the top of the hollow support shaft. The acoustic targets are wired in place on the inside of the spiral cooling coil.

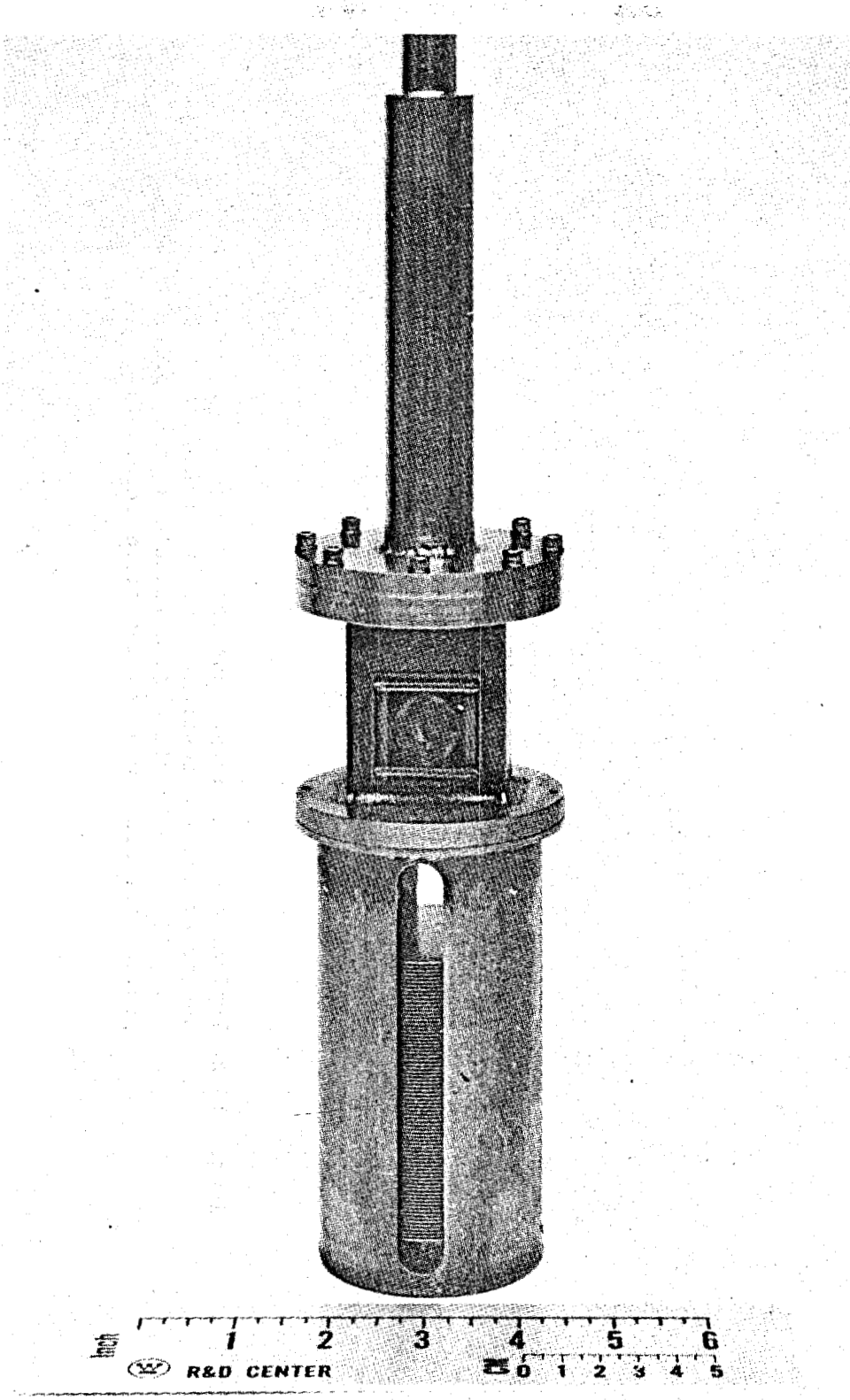

Figure 10.1 Photograph of assembled experimental BHTV sensor, designed for operation under simulated geothermal conditions.

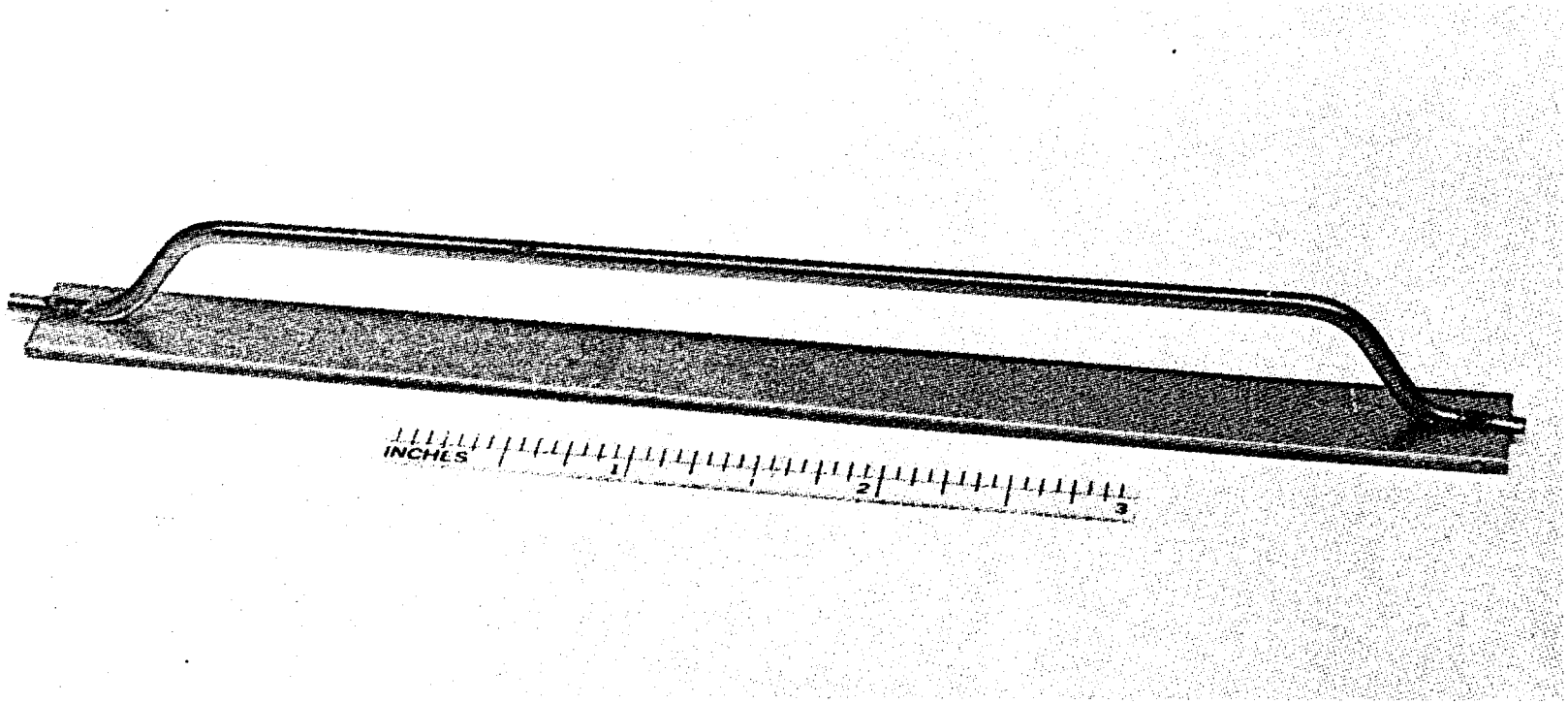

Figure 10.2. Typical acoustic target assembly designed for autoclave sensor evaluation testing. The stainless steel rod (target) is spot-welded to a stainless steel plate to provide for attachment to autoclave internals.

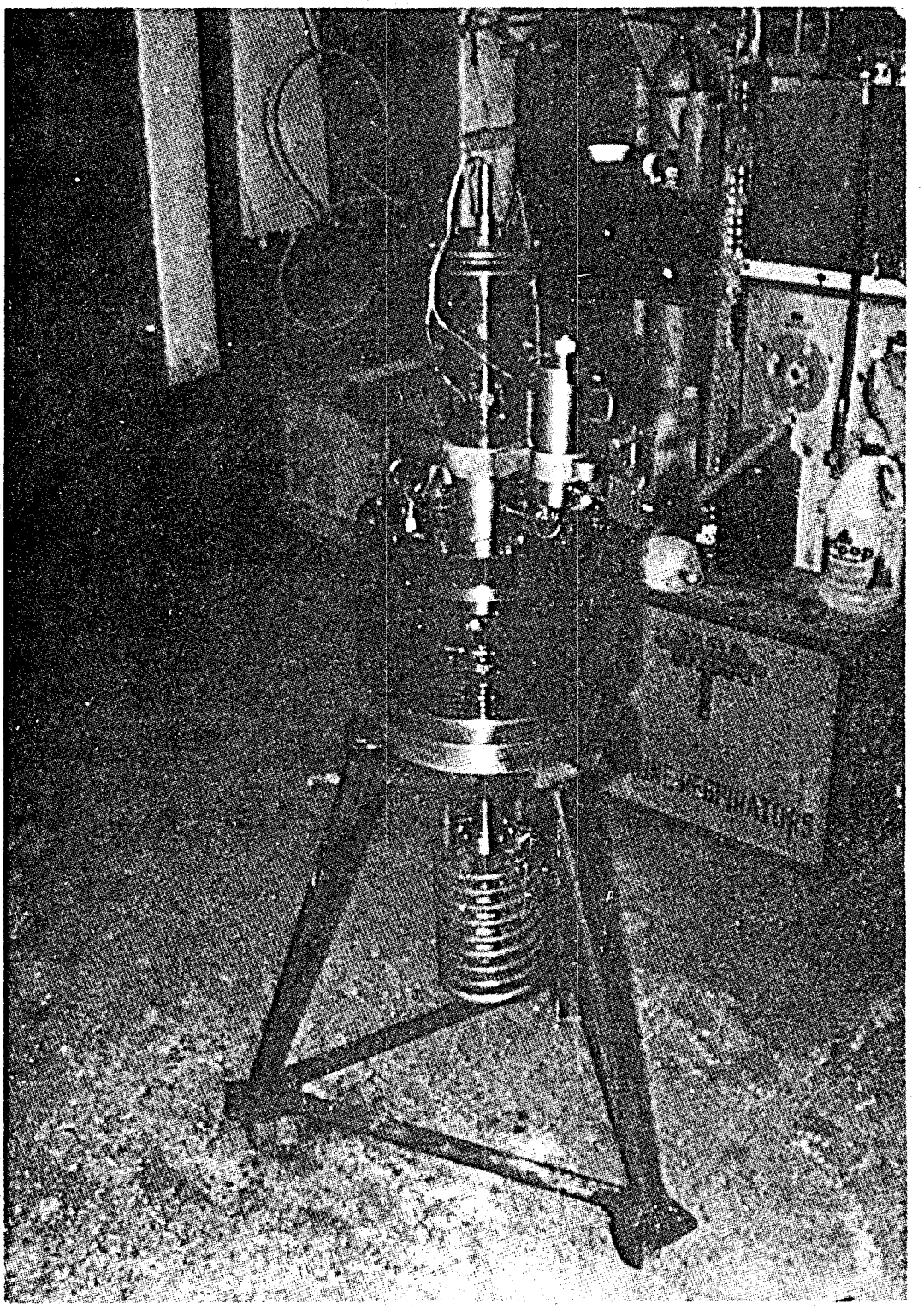

Figure 10.3. Experimental sensor and three targets shown installed (inside cooling coil) in the autoclave head assembly prior to testing. Electrical leads can be seen coming out of the top of the hollow support shaft.

A list of specific electro-acoustic test parameters was identified for monitoring and recording at various times during the autoclave test. The plan called for recording the parameters intially, at temperature/presssure, and at test conclusion. Polaroid photographs of oscilloscope CRT would provide permanent records.

1.) Sensor ring-down (reverberation) - This measurement may aid in diagnosing sensor problems which could arise during the test and is significant in its own right.

2.) Target echo levels (on-axis) - Provides overall performance indication.

3.) Half-power (-3 dB) beam width and levels/angles of sidelobes - Provides overall performance indication.

4.) Echo travel times - Provides data for calculating sonic velocity in simulated geofluid.

5.) Sensor element (D.C.) resistance - Aid in diagnosing possible transducer integrity problems.

An electronic diagram of the test apparatus is shown in Figure 10.4. A Panametrics Model 5050PR pulser/receiver was used to transmit and receive acoustic pulses which were displayed on an oscilloscope. A Polaroid camera was used for recording waveforms. Provisions for measuring the D.C. resistance of the sensor are also shown. Safety consideration dictated that the sensor be remotely operated over a 100' length of coaxial cable. A room temperature bench test indicated that this was acceptable practice.

Figure 10.5 shows the test sensor and the three targets about to be immersed in water for the purpose of preliminary base line measurements. Following thse measurements the autoclave head and test apparatus was installed on the vessel and a direction indicator was installed on the shaft pulley as shown in Figure 10.6. The direction indicator provided "aiming" information for the sensor and is graduated in degrees.

Dwg. 7690A39

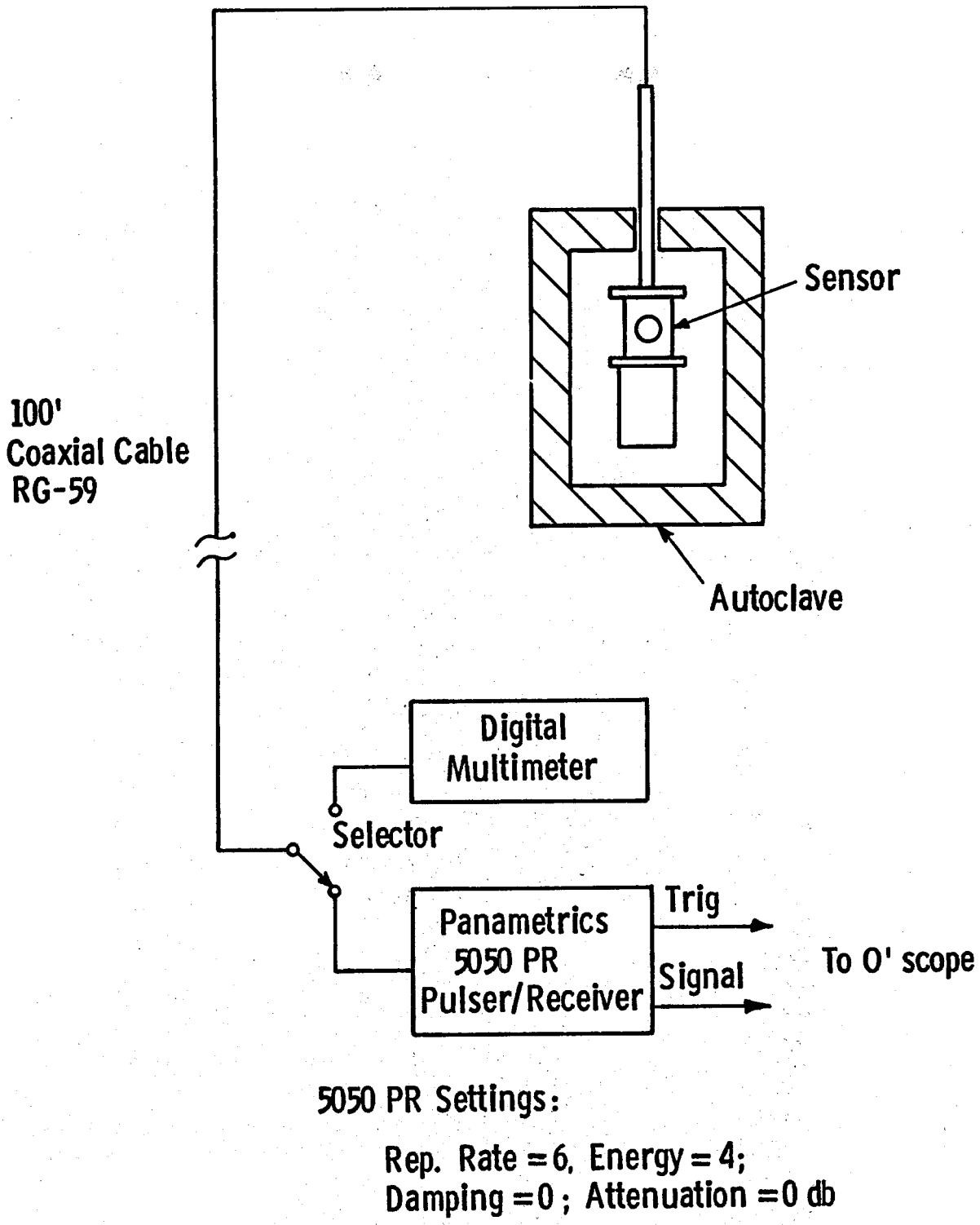

Fig. 10.4— Diagram of electronic test apparatus used during autoclave testing

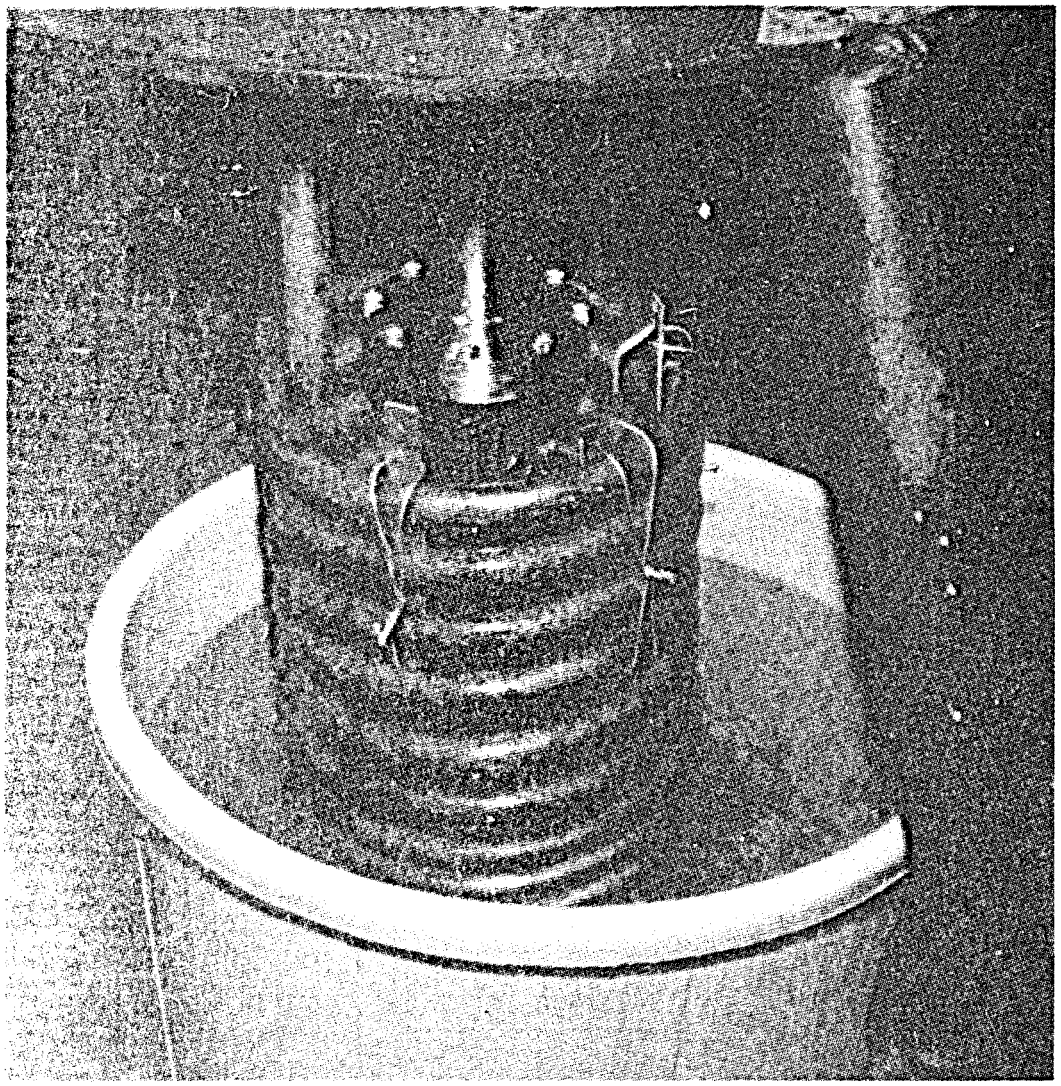

Figure 10.5. Close-up view of sensor and targets about to be immersed in water for preliminary base-line measurements.

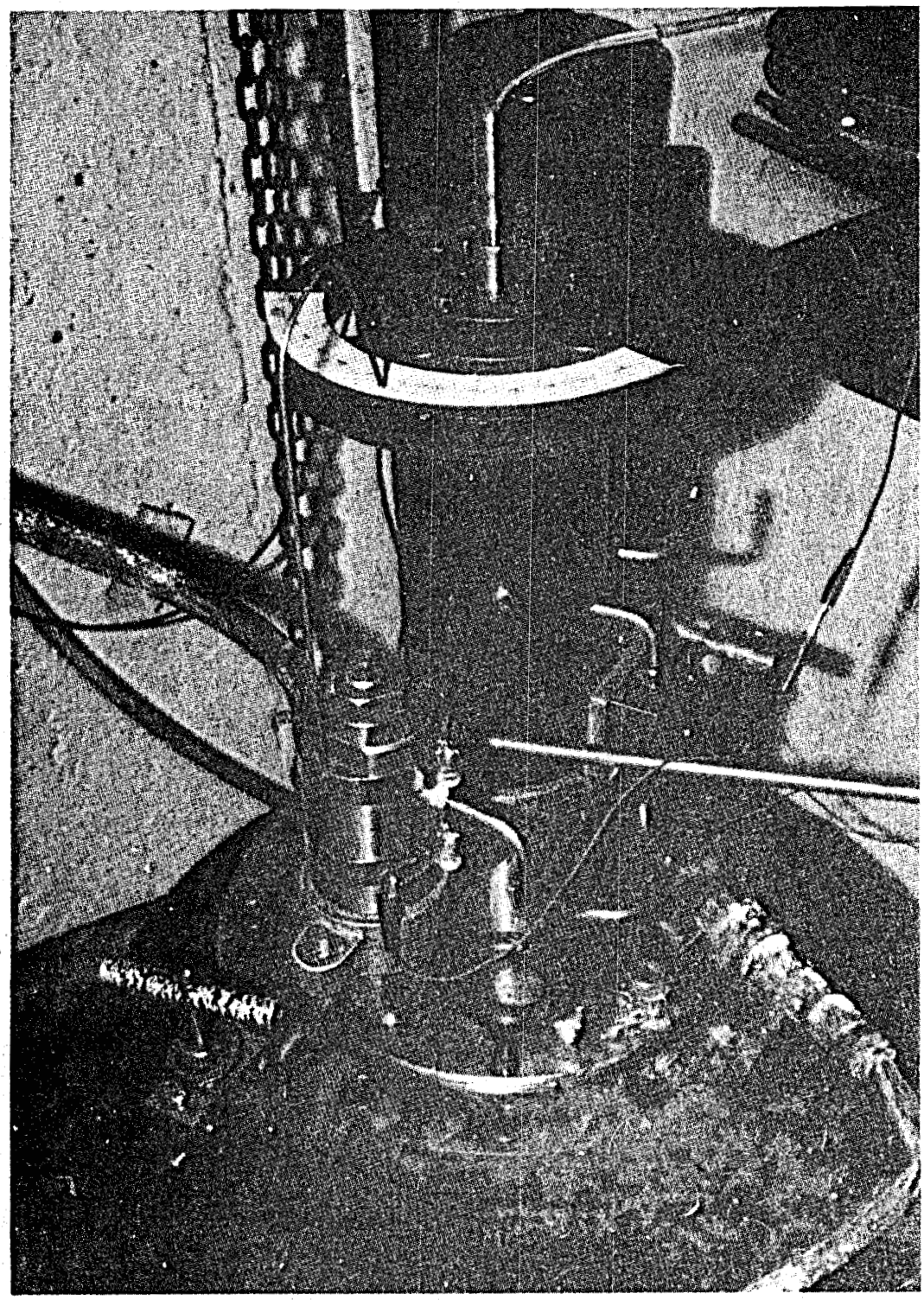

Figure 10.6. Photograph of autoclave head finally installed in the vessel, showing direction indicator attached to "beam-stearing" pulley.

Test Problems - Several difficulties developed over the course of the autoclave testing. As temperature increased, the sensor susceptibility to RFI (radio frequency interference) also increased. RFI from AM radio broadcasts as well as high frequency interference synchronized with 60-Hertz power line were observed.

Increased sensor temperature also resulted in an apparent decrease in the sensor target sensitivity. This sensitivity decrease was accompanied by a dramatic decrease in the D.C. resistance of the sensor. The resistance went from greater than 20 megohms at room temperature to 170 Ω at 540°F. One effect of these electrical problems is manifest in the base-line distortion of CRT photographs. The causes of these test problems were investigated and are decribed later (see Section 11).

Sensor Acoustic Performance - The RFI problems made signal-to-noise ratios (SNR) marginal for the two smaller targets (0.094" and 0.125" diameter). However, echoes from these smallest tarets remained detectable even at 275°C.

The SNR for the 3/16" diameter target remained high enough to provide confirmation of sensor operation at 275°C. The range of this target from the sensor window was 1.77".

Figure 10.7 is an oscillogram of the echoes from the 3/16" target rod at room temperature just before the autoclave was ready to begin heating. The data of Figure 10.8 also includes the effects of the chemicals and a hydrostatic pressure of 295 psi. The first 2.5 divisions are occupied by transducer ring-down. The wire rod target echo occurs at 5.8 divisions and an echo from the rod mounting plate appears at 7.8 divisions. Although the mounting plate is a "stronger" target, its echo is lower because it is "shadowed" by the wire rod.

Figure 10.8 shows an oscillogram with the sensor "aimed" at the same target but with an autoclave temperature of 480°F and pressure of 5725 psi. The echo from the wire rod target is lower level, has shifted to the right due to temperature dependence of sonic velocity, and now occurs at 6.8 divisions. The echo from the rod mounting plate is still

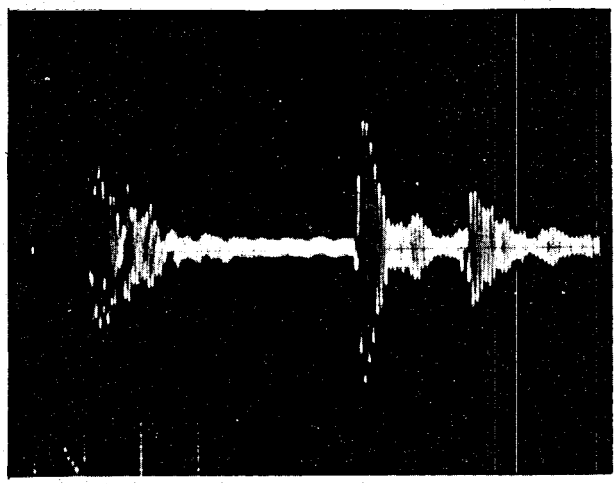

Figure 10.7. Echo pattern from 3/16" dia. rod in simulated geogluid. T = 70°F; P = 295 psi.
Horizontal = 10 μsec/div.
Vertical = 0.5 Volt/div.

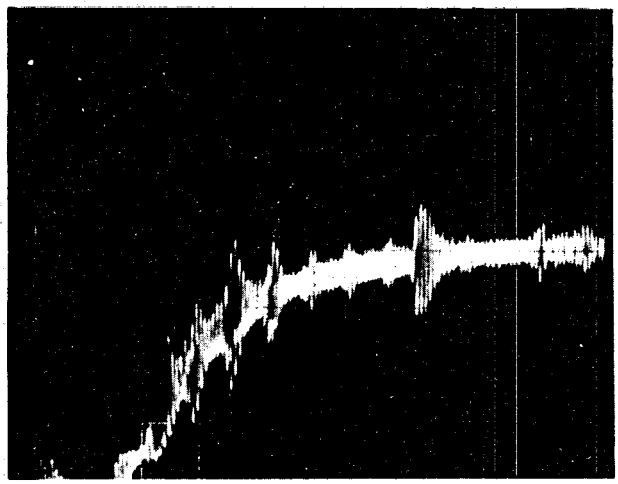

Figure 10.8. Echo pattern from 3/16" dia. rod in simulated geofluid. T = 480°F; P = 5725 psi
Horizontal = 10 μsec/div.
Vertical = 0.5 Volt/div.

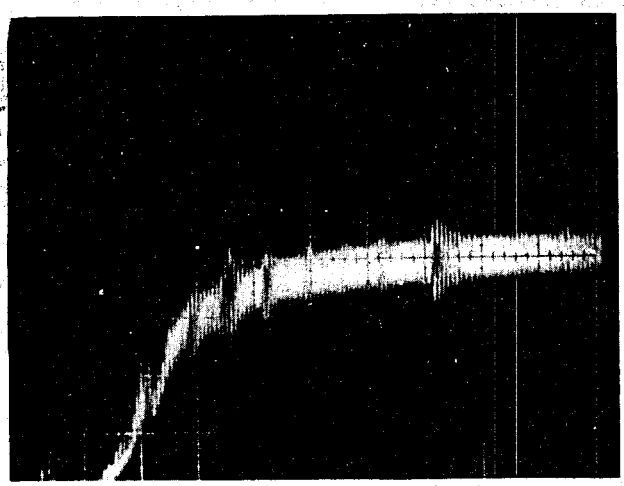

Figure 10.9. Echo pattern from 3/16" dia. rod in simulated geofluid. T = 350°F (275°C) P = 6500 pss.
Horizontal = 10 μsec/div.
Vertical = 0.5 Volt/div.

distinguishable at 8.8 divisions. Figure 10.9 also shows the aforementioned distortion in the base-line and reveals an apparent increase in the sensor reverberation level.

Figure 10.9 shows similar data under maximum test conditions of 530°F (275°C) and 6500 psi. The wire rod target echo is lower level and occurs at 7.1 divisions and the mounting plate echo is masked by the increasd background electrical noise level. The base-line distortion is still apparent and the sensor reverberation appears to be about the same as that of Figure 10.8.

The acoustic beam shape was measured with the sensor in the autoclave at both room temperature and at 300°F. The resulting data is plotted in Figure 10.10 and shows that the beam shape is essentially unaltered from RT through 300°F. The plots also reflect the overall decrease in sensitivity previously discussed. Decreased SNR made similar beam shape measurements at high temperatures difficult. However, steering the beam $\pm 2^{\circ}$ of the target did cause echos to drop into the noise level even at 275°C, confirming the basic target discrimination feature.

Pose-Test Examination - Figure 10.11 shows the condition of the experimental sensor after the autoclave test. Examination of the sensor housing exterior revealed no mechanical damage to the window or the bellows, although something (presumably internal fluid decomposition to gas) had caused the room-temperature bellows length to increase. The Inconel 718 acoustic window was still shiny. In Figure 10.12, the top flange is removed, showing the post-test condition of the Kalrez o-ring and a contrast between the general condition of interior and exerior surfaces. All interior stainless steel surfaces were bright and shiny and there was no sign of autoclave fluid invasion. Carbon steel all-thread inside the housing was corroded as is evident in the post-test photo of Figure 10.13. The piezoceramic element remained bonded to the backing (damping) block and all electrical wire connections were intact. The piezoceramic material appears to have turned grey instead of its original light tan color. The exposed silver electrode was in good condition.

Curve 716364-A

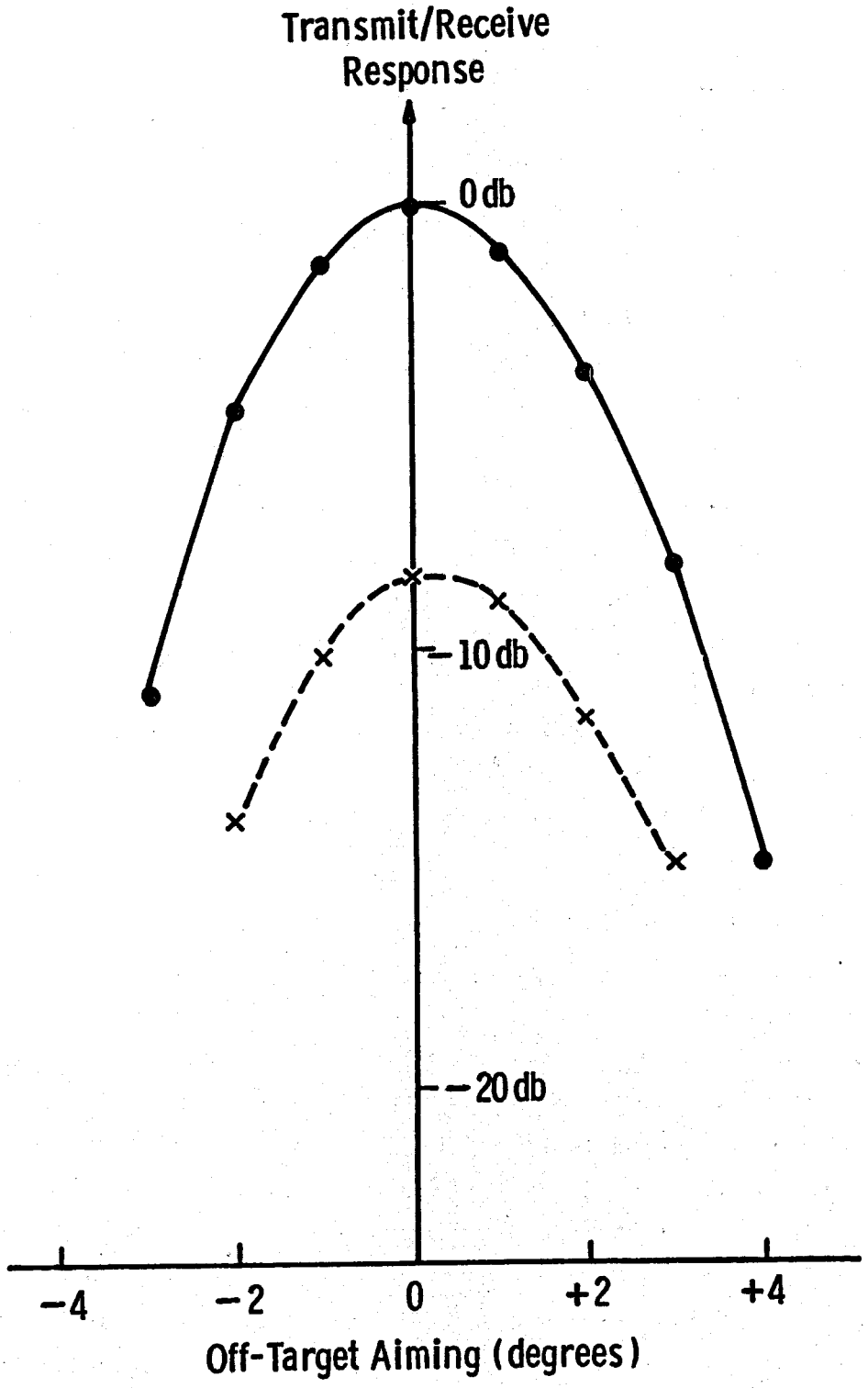

Fig. 10.10—Transmit/receive beam pattern for experimental sensor at R.T. (solid) and at 300°F (broken)

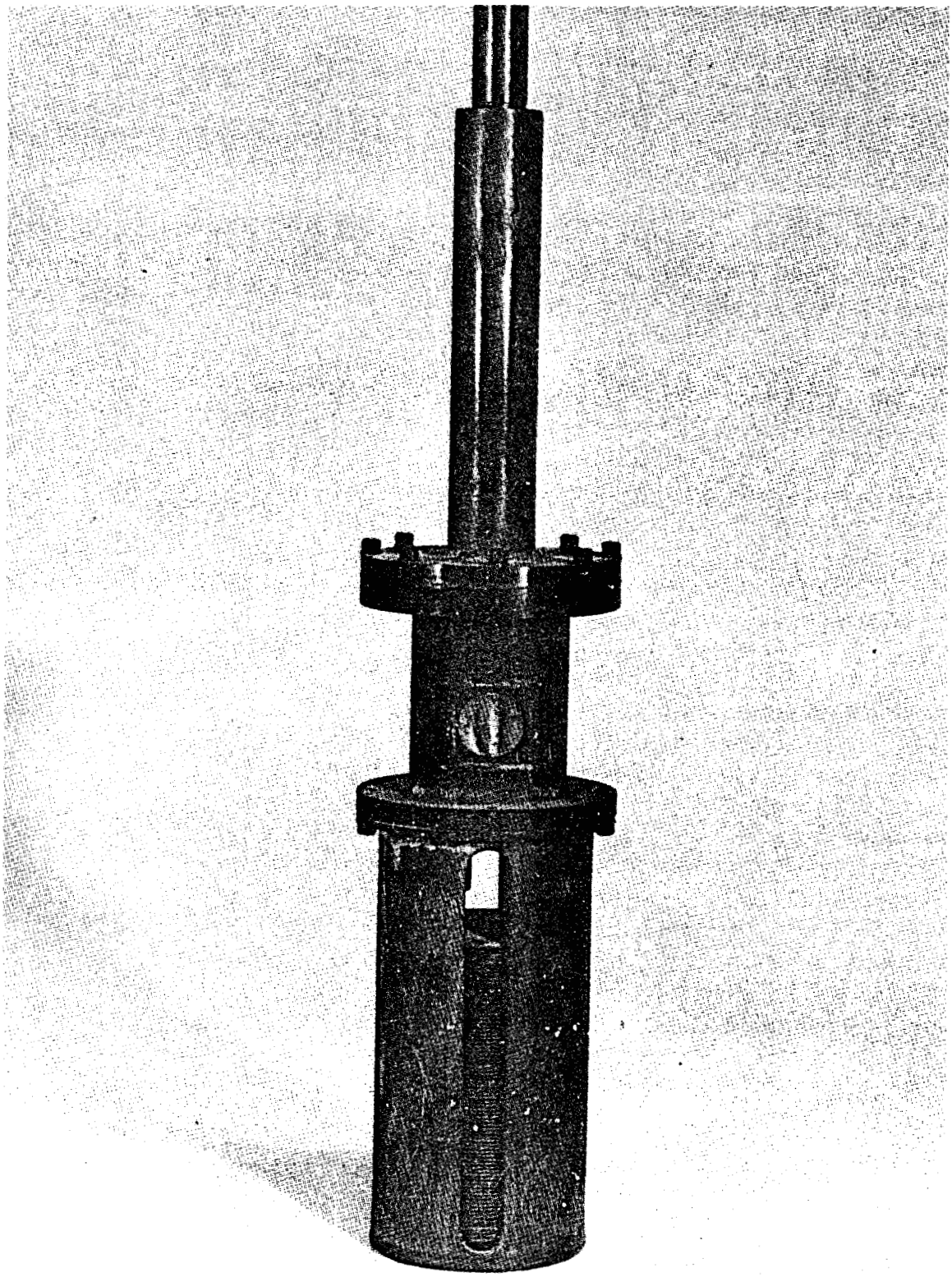

Figure 10.11 Photo showing post-test condition of the sensor housing. No sign of mechanical damage is evident.

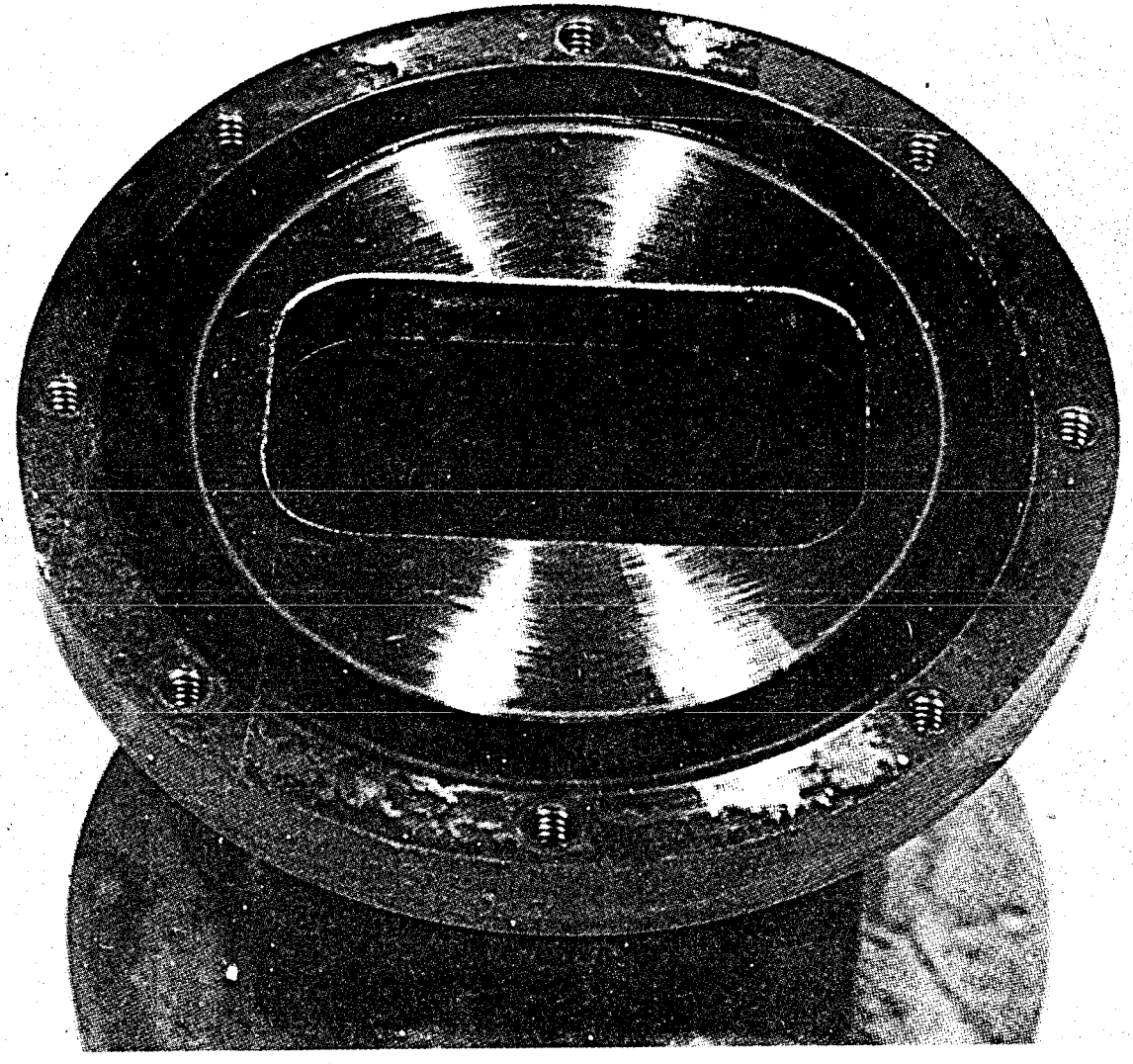

Figure 10.12. Photo of the disassembled flanged joint, showing post-test condition of the Kalrez o-ring and untarnished interior stainless steel surfaces.

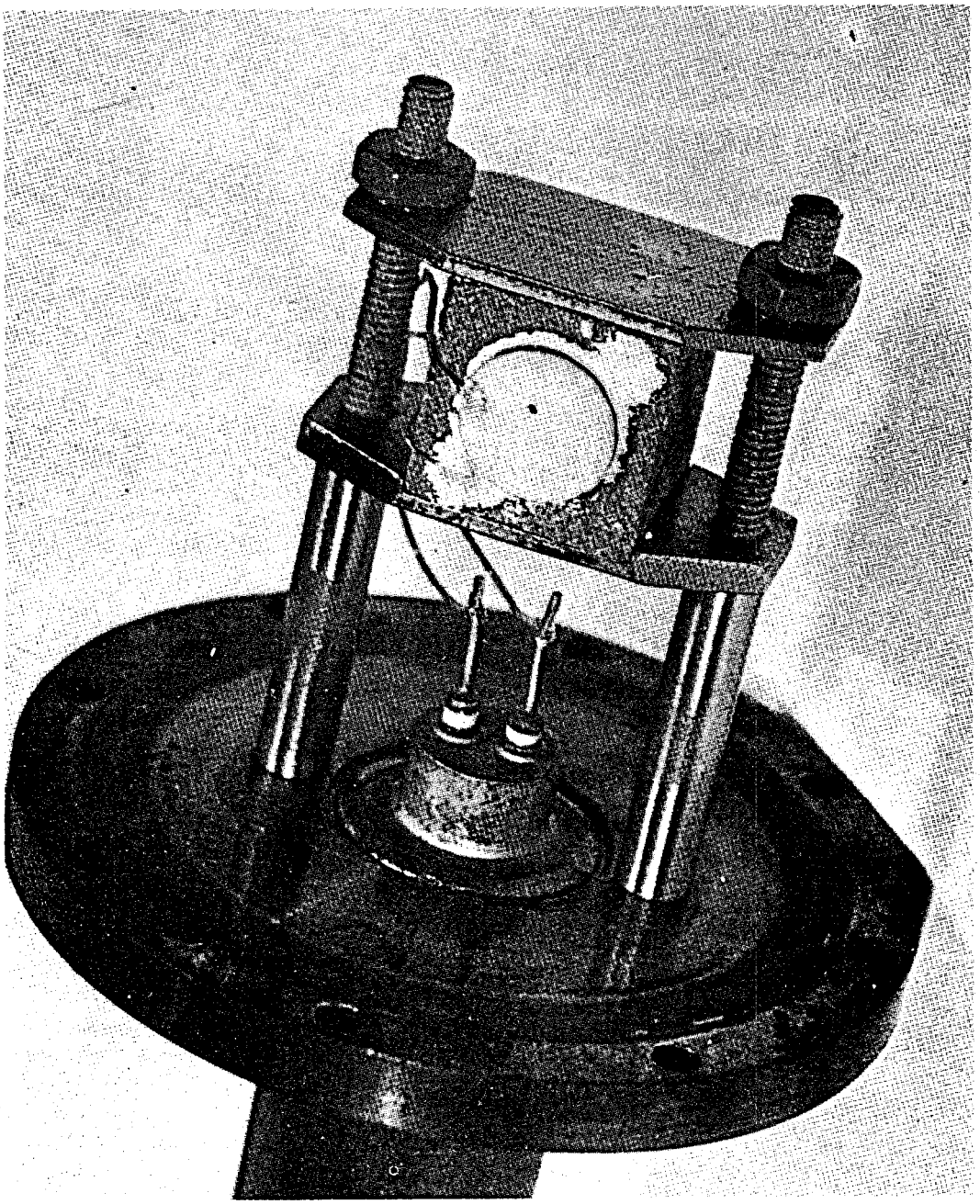

Figure 10.13 Post-test photo of sensor internals, including transducer assembly, wiring, all-thread, and electrical penetration.

Some concern was registered over the condition of the internal coupling fluid (Brayco 812) which had changed from clear to slightly cloudy. This suggests some degree of chemical instability in Brayco 812 which was not observed during earlier fluid qualification tests at 275°C and 2000 psi. Discussion of this problem is found in Section 11.

Post-test D.C. resistance of the sensor recovered to 3.3 Megohms. The internal gas generated during the autoclaving was of sufficient volume (at room temperature and 1 atm) to void the critical region between the piezoceramic and the acoustic window. This rendered the upright sensor inoperative immediately after the test. To permit post-autoclave bench tests (acoustic), fluid was forced out of the bellows and into the critical region and then the housing was resealed.

It was then possible to confirm that both target sensitivity and reverberation level recovered to near pre-test conditions. The re-assembled sensor was immersed in a water bath and connected to the 5050 PR to permit measurement of reverberation and target sensitivity. Pre-autoclaving measurements under identical R.T. (room temperature) conditions were avilable for comparison. Before and after R.T. target sensitivities were determined using a reference target (3/32" diameter rod) hose-clamped to the sensor housing flange and positioned to produce the highest echo level. Figure 10.14 shows the pre-autoclave test data with a 3.4 Volt (peak-to-peak) target echo at 3.8 horizontal divisions. Figure 10.15 shows the echo from the same target after autoclaving. The post-autoclaving echo level is 3.5 Volt (peak-to-peak). This test shows that autoclaving did not cause any appreciable permanent change in R.T. target sensitivity.

Reverberation level was checked by simply removing the target from the test apparatus. Pre- and post-autoclaving reverberation levels can be compared directly in Figures 10.16 and 10.17. If anything, autoclaving has decreased the high-frequency reverberation between 2 and 4 horizontal divisions. Autoclaving has slightly exaggerated the low-frequency reverberation between 5 and 7 divisions, but this can be

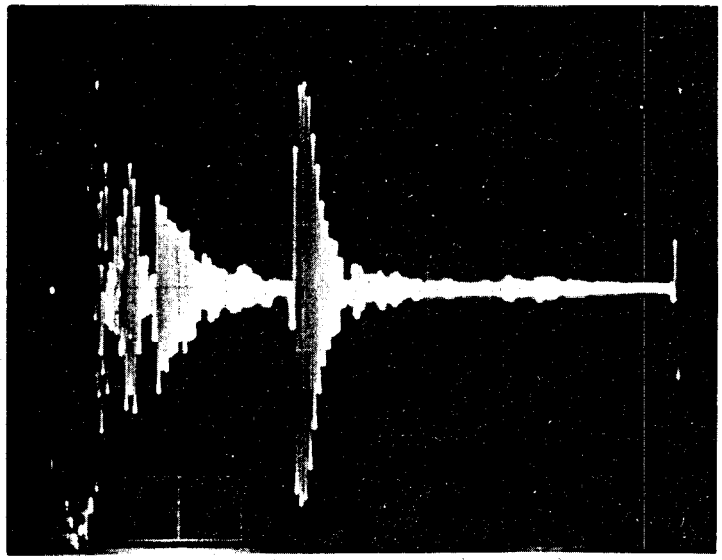

Figure 10.14. Pre-autoclave R.T. target sensitivity data. Target: 3/32" dia. rod @ 1-1/2" range (3.8 div.)
Vertical = 0.5 Volt/div
Horizontal = 10 μsec/div.

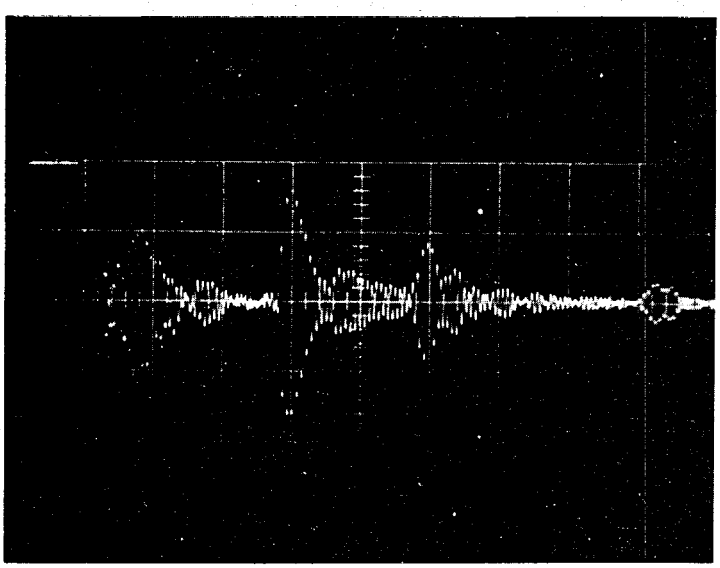

Figure 10.15. Post-autoclave R.T. target sensitivity data. Target: 3/32" dia. rod @ 1-1/8" range (3.8 div.)
Vertical = 1 Volt/div
Horizontal = 10 μsec/div.

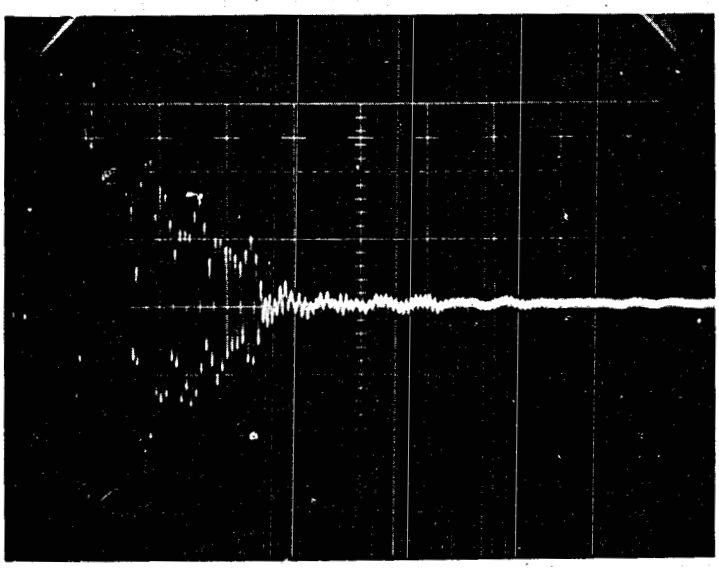

Figure 10.16. Pre-autoclave sensor reverberation characteristics. Vertical = 0.1 Volt/div; Horizontal = 10 msec/div.

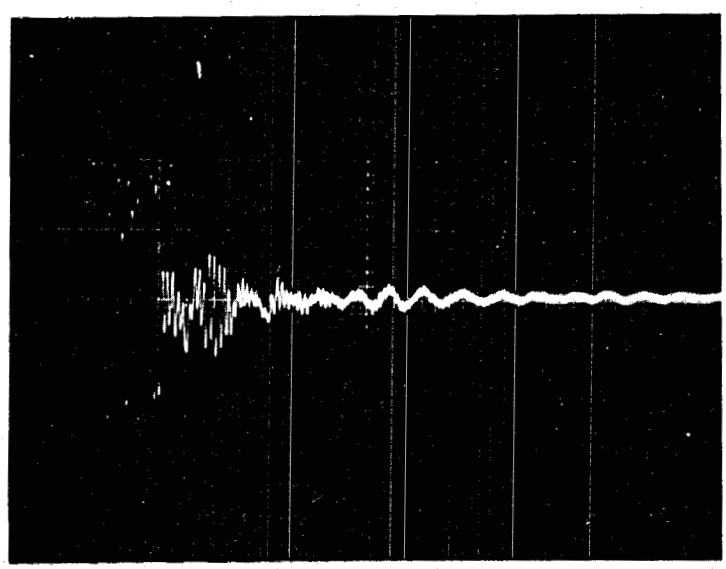

Figure 10.17. Post-autoclave sensor reverberation characteristics. Vertical 0.1 Volt/div; Horizontal = 10 msec/div.

filtered out. This test shows that no significant change in R.T. reverberation characteristics has resulted from autoclaving.

Sonic Velocity in Geofluid - The successful operation of the sensor in the simulated geothermal fluid provided an opportunity to measure the sonic velocity of the fluid at various temperatures and pressures. In Figure 10.18, this sonic velocity (c) data is plotted and compared with known sonic velocity of pressurized water. Figure 10.18 indicates that the chemistry of the simulated geothermal fluid has a relatively small effect on the sonic velocity as a function of temperature.

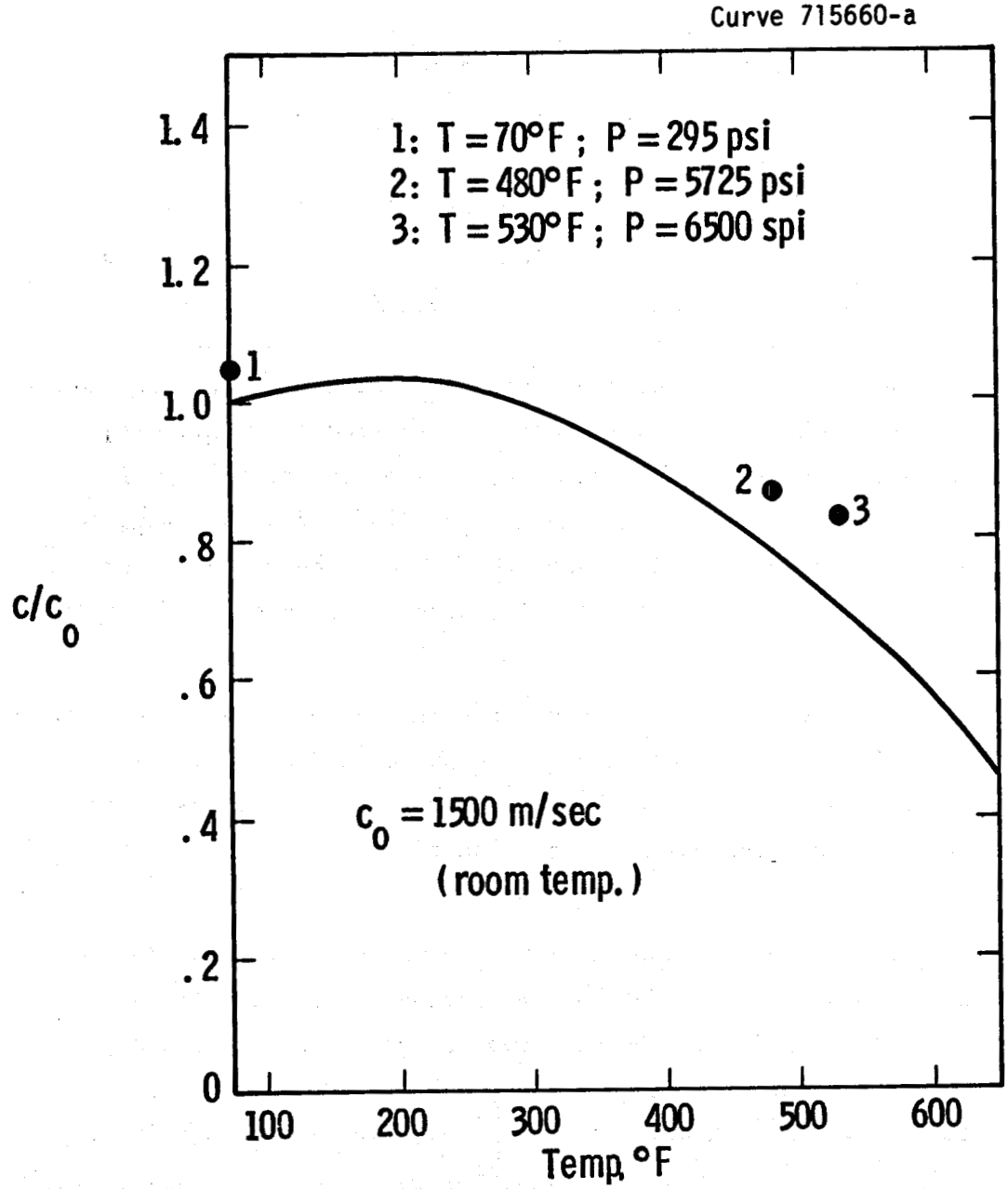

Fig. 10.18—Variation of sonic velocity vs temperature for pressurized water (line) and simulated geofluid (points)

11. DISCUSSION OF RESULTS

The major objective of the autoclave test was to demonstrate operation of those electro-acoustic features required of a BHTV sensor. Although degraded from room temperature operation, the sensor remained functional at contract-specified conditions of 275°C, 7000 psi, and in the presence of a simulated geofluid. The other major requirement which was also demonstrated is that it maintains its directionally-selective beam characteristics.

The major difficulties encountered during autoclave testing were 1) coupling fluid depolymerization to a gas phase, and 2) certain electronic problems related to high temperature characteristics of the piezoelectric sensor material. A discussion of these two difficulties follows.

Coupling Fluid Decomposing to Gas - The gas found inside the post-autoclave sensor compartment was unexpected. The approximate volume of Brayco 812 fluid inside the housing was 150 cc. The post-autoclave bellows length had increased about 3.8 cm, corresponding to a net volume increase of 68 cc. This amounts to 45% of the original fluid volume.

Consultation with polymer fluids expertise has provided insight into the problem of fluid depolymerization during autoclaving. The gas produced during autoclaving is almost certain to be related to the unfortunate use of carbon steel all-thread inside the sensor compartment. This conclusion is reached based upon a technical publication[6] DuPont's Krytox, which is also a perfluoroalkylpolyether like Brayco 812. At temperatures above about 550°F these fluids begin to react with some metals and/or their oxides. Figure 11.1 is copied from the reference and quantifies the reaction problem for several metal alloys. Presumably, positive slopes correspond to reaction products deposited on

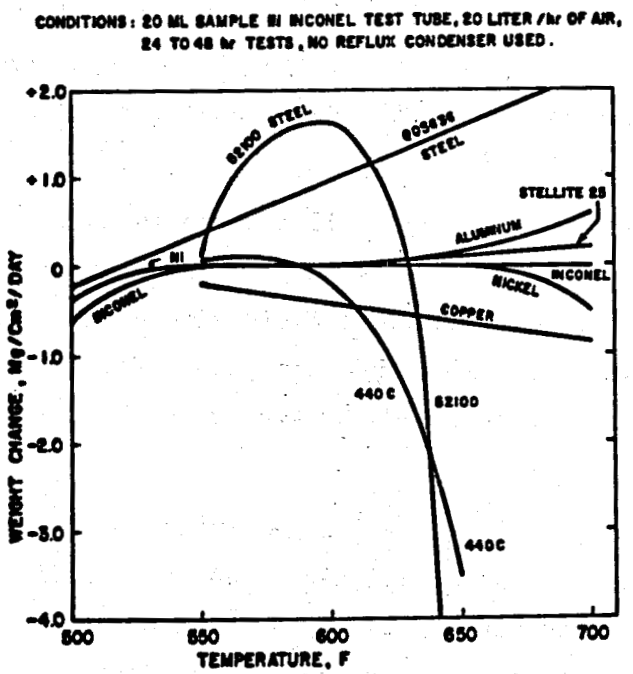

Figure 11.1. Corrosion of metals by KRYTOX 143AC fluorinated oil at elevated temperatures (from Ref. 6).

the specimens and negative slopes indicate conditions of specimen decomposition. These curves confirm that carbon steels are particularly problematical.

Table 11-I, also copied from the reference, lists alloys better suited for exposure to high temperature perfluoroalkylpolyether. The reference also describes work toward developing certain additives which can decrease the reaction rate.

A reaction between Brayco 812 and the tungsten powder in the backing material is not considered likely since no significant gas was generated during the latest autoclave fluid screening tests. During those screening tests, (see Section 6) tungsten powder filled backing material was exposed to Brayco 812 at 275°C for 4-hours without evidence of gas generation.

It is concluded that the gas generation problem encountered during sensor autoclave tests could have been avoided if the carbon steel all-thread were replaced with a stainless steel or an Inconel. As such perfluoroalkylpolyethers such as Brayco 812 and Krytox 143 would appear to be acceptable from the standpoint of the geothermal acoustic sensor concept.

Electronic Problems

Following the autoclave testing, several lab investigations were conducted to locate the source of electronic problems. The first test was aimed at determining if autoclaving had resulted in permanent (residual) changes in room-temperature sensor operation. These lab investigations were also aimed at a better phenomenological understanding of the test results.

It has been mentioned that autoclaving caused some coupling fluid degradation to the gas phase. This gas did not preclude sensor operation in the autoclave because of the very high pressure. However, at room temperature and pressure the increased gas volume voided the acoustic path between the piezoelectric disc and the acoustic window, making the

METALS AND ALLOYS SUITABLE FOR USE WITH KRYTOX® 143 OILS AT ELEVATED TEMPERATURES

Test Conditions: 72 hours at 5 liters dry gas/hr.

Qualifying Corrosion Rate: $\leq$ 0.4 mg/cm -day.

TEMP., F	ATMOSPHERE	
	AIR	INERT GAS
700	Nickel alloys Cobalt alloys AMS-5547 steel	Nickel alloys Cobalt alloys AMS-5547 steel
650	AMS-5525 steel Ti (6Al 6V 2Sn) Mg, Ag, Cr, V	304, 446 stainless steel
600	301, 304, 310, 316, 321, 446 stainless steels N-155 Ti (13V 11Cr 3Al) Ti (6Al 4V) Al (QQ-A-355) Bearing Bronze	440C High-speed stainless steel (14.5Cr 4.0Mo 1.2V 1.15C bal. Fe) QQ-S-636, M-1, M-50, WB-49, 52100 steels Ti (8Mn), Cu
550	405, 410, 440 stainless steels High Speed stainless steel (14.5Cr 4.0Mo 1.2V 1.15C bal. Fe) QQS-636, M-1, M-50, WB-49, 52100 steels Ti (8Mn), Cu	Ti (7Al 4Mo)

NOTE: Any metal or alloy suitable at one temperature is also suitable at all lower temperatures. Any metal suitable in air is also suitable in inert atmosphere.

TABLE 11-I
(from Ref. 6)

sensor inoperative. This was overcome by removing the top flange, forcing coupling fluid out of the bellows, and then replacing and re-sealing the top flange. The D.C. resistance of the sensor was then checked at 3.3 Megohms, the same as before resolving the gas void problem.

The re-assembled sensor was then immersed in a water bath and connected to the 5050 PR to permit measurement of reverberation and target sensitivity. Pre-autoclaving measurements under identical R.T. (room temperature) conditions were available for comparison.

Before and after R.T. target sensitivities were determined using a reference target (3/32" diameter rod) hose-clamped to the sensor housing flange and positioned to produce the highest echo level. Figure 11.2 shows the pre-autoclave test data with a 3.4 Volt (peak-to-peak) target echo at 3.8 horizontal divisions. Figure 11.3 shows the echo from the same target after autoclaving. The post-autoclaving echo level is 3.5 Volt (peak-to-peak). This test shows that autoclaving did not cause any appreciable permanent change in R.T. target sensitivity

Reverberation level was checked by simply removing the target from the test apparatus. Pre- and post-autoclaving reverberation levels can be compared directly in Figures 11.4 and 11.5. If anything, autoclaving has decreased the high-frequency reverberation between 2 and 4 horizontal divisions. Autoclaving has slightly exaggerated the low-frequency reverberation between 5 and 7 divisions, but this can be filtered out. This test shows that no significant change in R.T. reverberation characteristics has resulted from autoclaving.

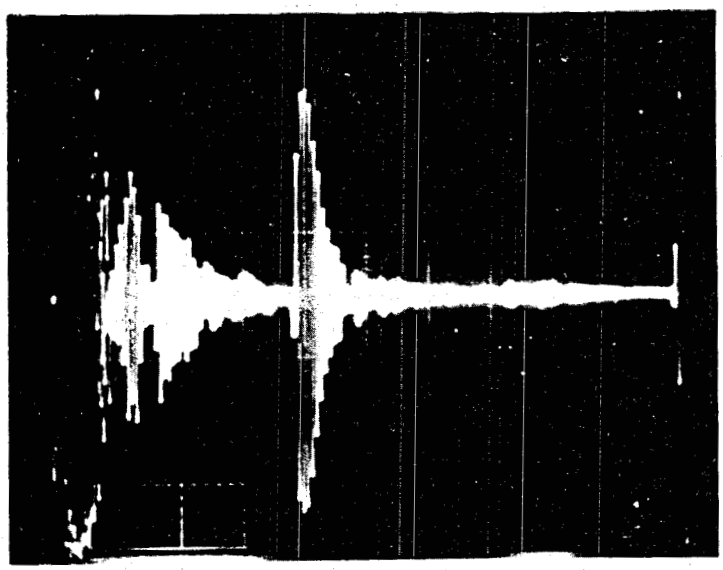

Figure 11.2. Pre-autoclave R.T. target sensitivity data. Target: 3/32" dia. rod @ 1-1/2" range (3.8 div.)
Vertical = 0.5 Volt/div.
Horizontal = 10 μsec/div.

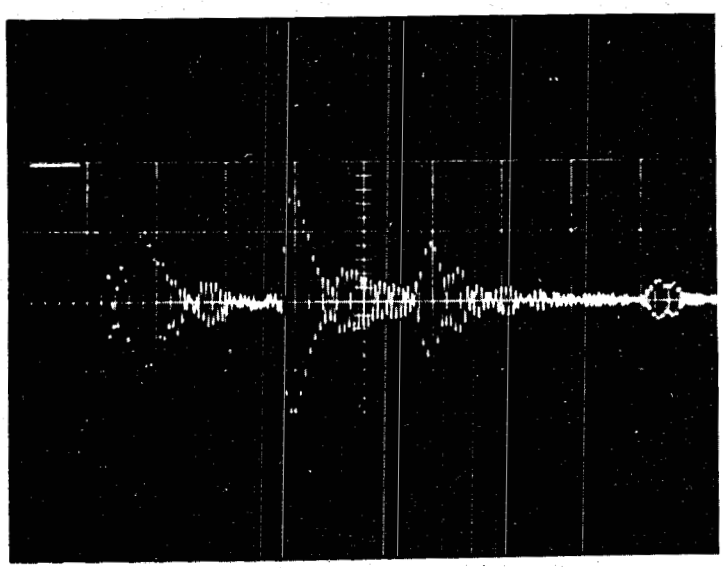

Figure 11.3. Post-autoclave R.T. target sensitivity data. Target: 3/32" dia. rod @ 1-1/8" range (3.8 div.)
Vertical = 1 Volt/div
Horizontal = 10 μsec/div.

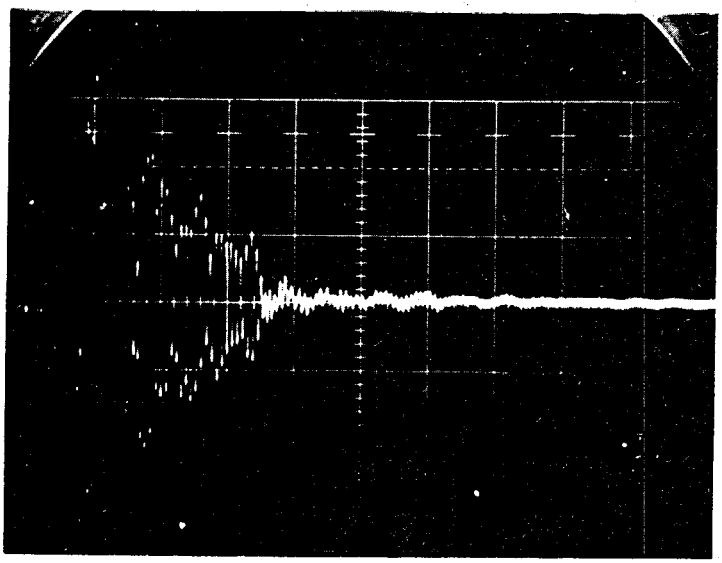

Figure 11.4. Pre-autoclave sensor reverberation characteristics. Vertical = 0.1 Volt/div; Horizontal = 10 μsec/div.

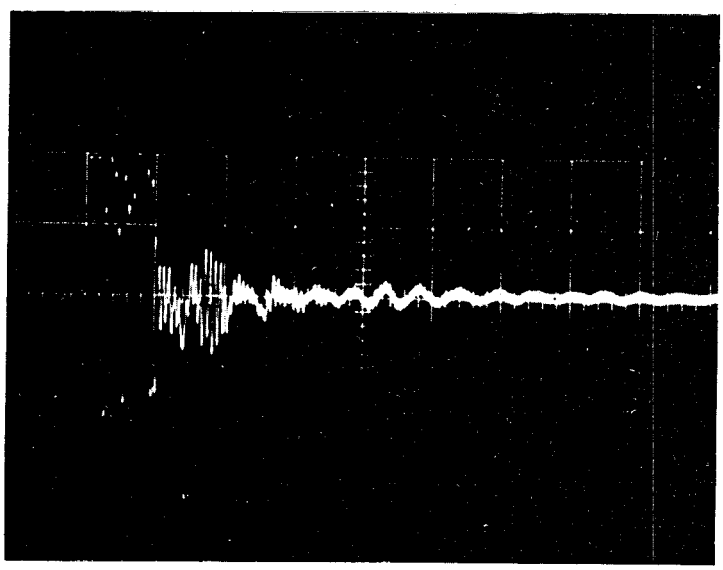

Figure 11.5. Post-autoclave sensor reverberation characteristics. Vertical = 0.1 Volt/div; Horizontal = 10 μsec/div.

Investigating Sources of Autoclave Test Problems

After determining that no permanent acoustic performance damage was done to the sensor as measured at room temperature, attention turned to understanding the autoclave test difficulties and accounting for decreased sensitivity at 530°F (275°C). The planned tests would require heating sensor test apparatus to 600°F in a nitrogen-atmosphere furnace. In the interest of preserving the condition of the autoclaved sensor, it was decided that all testing requiring heating sensors should be done using the "spare" transducer assembly, fabricated identically to the autoclaved unit. This assembly is shown in Figure 11.6.

Initial efforts focused on the cause of the exponential base-line observed during high temperatures in the autoclave. At first it was suspected that the 170 Ω D.C. resistance measured at 550° during autoclaving could cause the problem. Shunting the R.T. sensor with a 170 Ω resistor did not change the base-line but did decrease echoes by 2:1. This helps account for part of the lost sensor sensitivity noted at 530°F.

Further efforts to understand the exponential base-line revealed that shunting the sensor with .01 mF capacitor could force an exponential base-line condition on the scope trace. This is a major departure from the few hundred picofarads measured across the sensor element at room temperature.

Toward understanding how this dramatic change could come about at elevated temperature, pursuant investigations focused on the detailed electro-mechanical characteristics of the sensor at high temperature. Specific attention was given to the sensor capacitance. The testing again involved the non-autoclaved transducer mock-up in the nitrogen-atmosphere furnace. This testing involved three kinds of measurements at various temperatures:

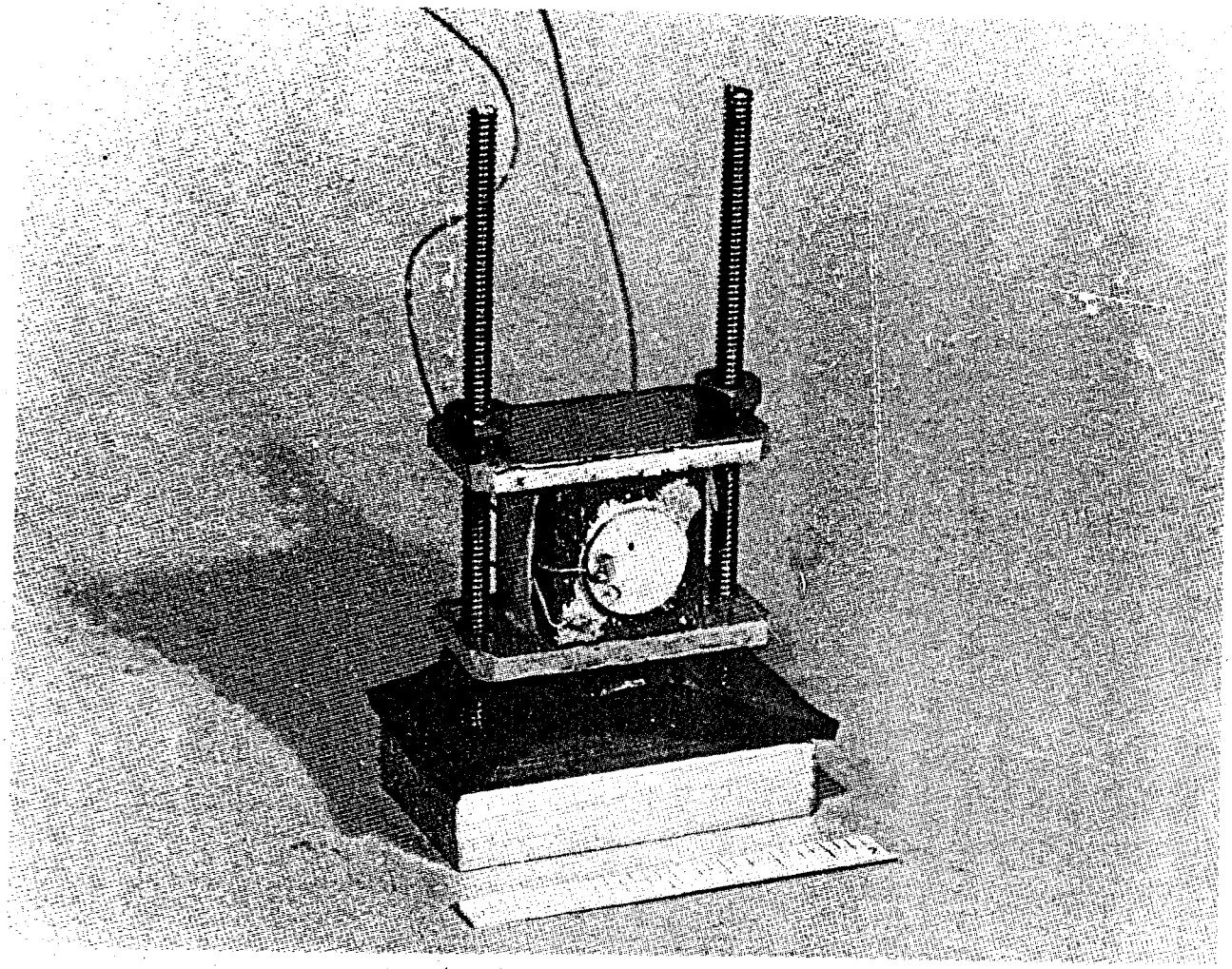

Figure 11.6. "Spare" transducer assembly used for investigations requiring large thermal excursions.

1) the 5050 PR and the scope could be connected to the transducer to observe exponential base-line distortion,
2) a special instrument was used to measure the vector impedance of the sensor vs. frequency,
3) an impedance bridge was used to measure the low-frequency (1 kHz) capacitance of the sensor.

The "spare" transducer was put into the nitrogen furnace and heated to 633°F. At that temperature, the exponential base-line distortion was apparent using the 5050 PR and scope. Figure 11.7 shows the base-line distortion at that time and temperature. This is an important result in that it shows that the exponential base-line at high temperature is not related to pressure or the presence of coupling fluid. It was then hypothesized that the base-line distortion could be eliminated by a parallel (shunt) inductor across the sensor, forming a high-pass filter. While the conditions of Figure 11.7 were maintained, such an inductor was installed. The effect of the shunt inductor is evident in Figure 11.8 showing the desired straight, horizontal base-line. This demonstrates that the base-line distortion problem can be easily overcome with a simple parallel inductor.

The capacitance of the transducer assembly was also measured vs. temperature, using a General Radio Bridge (Model 1650-A). Figure 11.9 shows the capacitance data plotted. The plot shows that the capacitance of the sensor element is relatively stable until about 450°F and then takes a dramatic upturn toward many thousands of picofarads. This is just the kind of shunt capacitance that was required to force an exponential base-line condition at room temperature.

Presumably, something happens to the molecular structure of the lead metaniobate (the capacitor dielectric) at high temperature which dramatically increases its effective dielectric constant. The increased capacitance at high temperature should contribute to the decreased sensor sensitivity during autoclaving. It is believed that this enormous high temperature shunt capacitor "swamps" much of the current produced by the

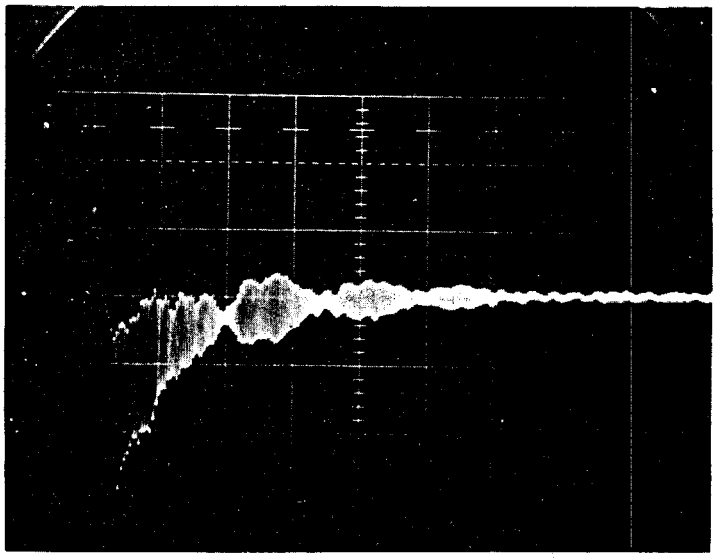

Figure 11.7. Ring-down pattern of "spare" assembly in 633°F furnace, showing exponential scope baseline.

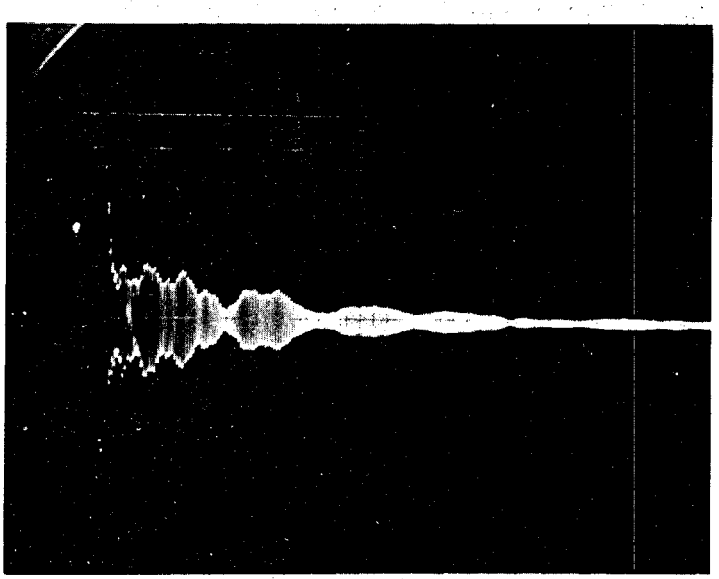

Figure 11.8. Same conditions as Figure 6, except with inductor in parallel with sensor element.

Curve 715662-A

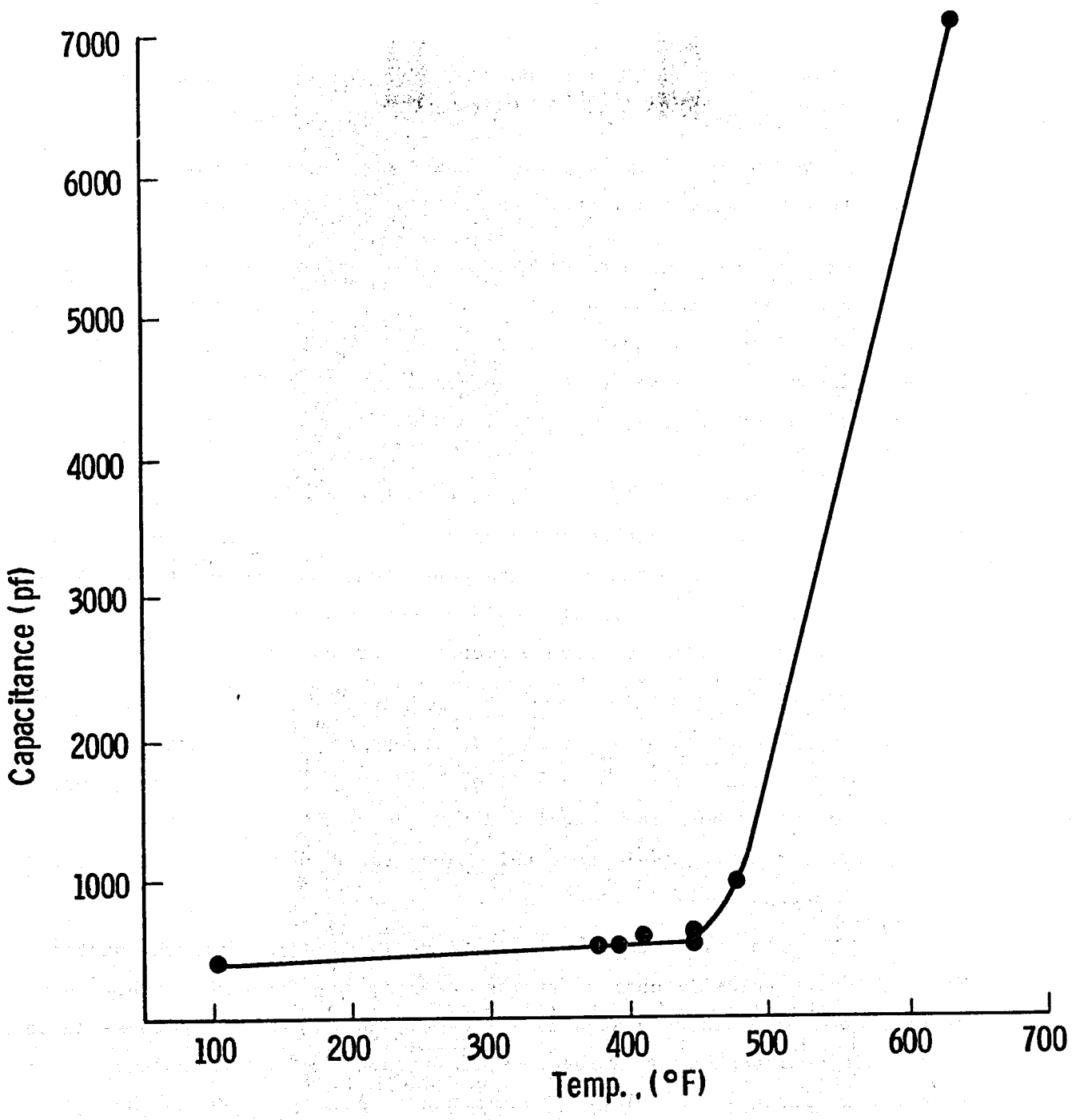

Fig. 11.9— Plot of measured transducer capacitance vs temperature

electro-acoustic transduction process. One way of alleviating this problem would be to use a very low input impedance receiver.

Numerous other capacitance measurements were also made on room temperature devices toward further understanding in this area:

Unmounted lead metaniobate disc 1	261 pf
Unmounted lead metaniobate disc 2	261 pf
Unmounted lead metaniobate disc 3	269 pf
Autoclaved sensor disc (post-autoclaving)	420 pf
"Spare" sensor disc, after several 600°F excursions	450 pf

Calculated capacitance, based on actual dimensions and manufacturers published dielectric constant, is 257 pf. It is clear that the capacitance of unmounted discs are consistent, unit-to-unit, and agree with the calculations. It is also evident that elements which were exposed to high-temperatures have permanent increase (approximately doubled) in R.T. capacitance.

Subsequent thermal cycles did not apper to cause further room temperature capacitance increase. Also, the R.T. capacitance change was about the same for both the autoclaved transducer and the "spare" transducer, suggesting again that this capacitance shift is attributable to thermal effects only.

The final test to be described involved special instrumentation for electromechanically characterizing resonant devices such as the sensor transducer. The data generated is a plot of the magnitude and phase angle of the sensor impedance as a function of frequency. An x-y plotter permanently records this plot. These measurements were made on the various available transducer devices over a range of temperatures as an additional aid in understanding the autoclave test results. The predominant plot characteristic of a resonant device is a "loop" whose features provide quantitative performance data.

Figure 11.10 shows a typical impedance vs. phase angle plot. This plot is for a 1/2" dia. x 1.3 MHz, unmounted lead metaniobate disc (Keramos K-81) identical to those used in the autoclaved sensor and the transducer mock-up. Figure 11.11 shows the plot for the "spare" transducer assembly at R.T. prior to a 650°F thermal excursion. The most notable differences are a smaller size loop and a slightly lower resonant frequency. Both of these effects are typical of piezoelectric elements tightly coupled (bonded) to high-Z backing materials.

Figure 11.12 through 11.16 show similar plots for the "spare" transducer assembly at various temperatures up to 604°F. The plot of Figure 11.17 was made after the assembly had returned to room temperature. The consistency of the "loop" characteristics over the test temperature range indicates a stable electro-acoustic transduction process which is maintained at high temperature and is essentially unaltered upon return to room temperature.

Figure 11.18 shows a R.T. plot of the sensor (in air) which had undergone the autoclave test. The plot departs from the othes in that the "loop" is considerably smaller and the resonance frequency has increased. These differences are thought to be due to the unique conditions of the autoclave test. Specifically, it is believed that the internal coupling fluid under the 7000 psi pressure may have been forced into the porosity of the lead metaniobate and/or the backing material. This may explain the smaller loop because the loss mechanisms could be modified (increased). Permanent invasion of fluid into the lead metaniobate could modify the sonic velocity in the material and therby change the resonant frequency. This effect would have to decrease the sonic velocity in the lead metaniobate by approximately 18%.

Table 11-II compiles relevant features of the impedance plots for the various test transducers mentioined above.

Curve 594612-A

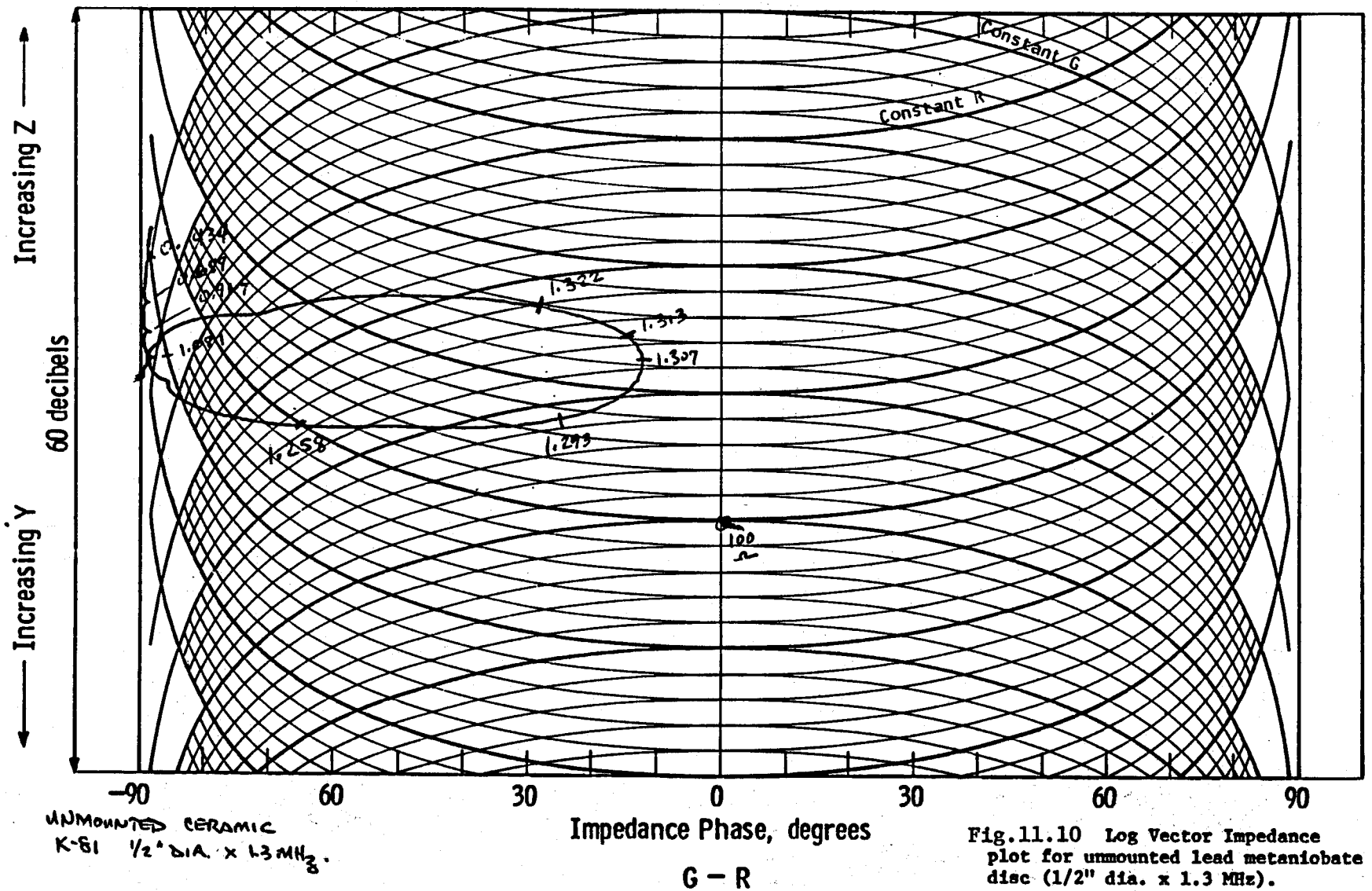

Fig.11.10 Log Vector Impedance plot for unmounted lead metaniobate disc (1/2" dia. x 1.3 MHz). Frequency Sweep Range: 0.3 MHz to 1.5 MHz.

Curve 594612-A

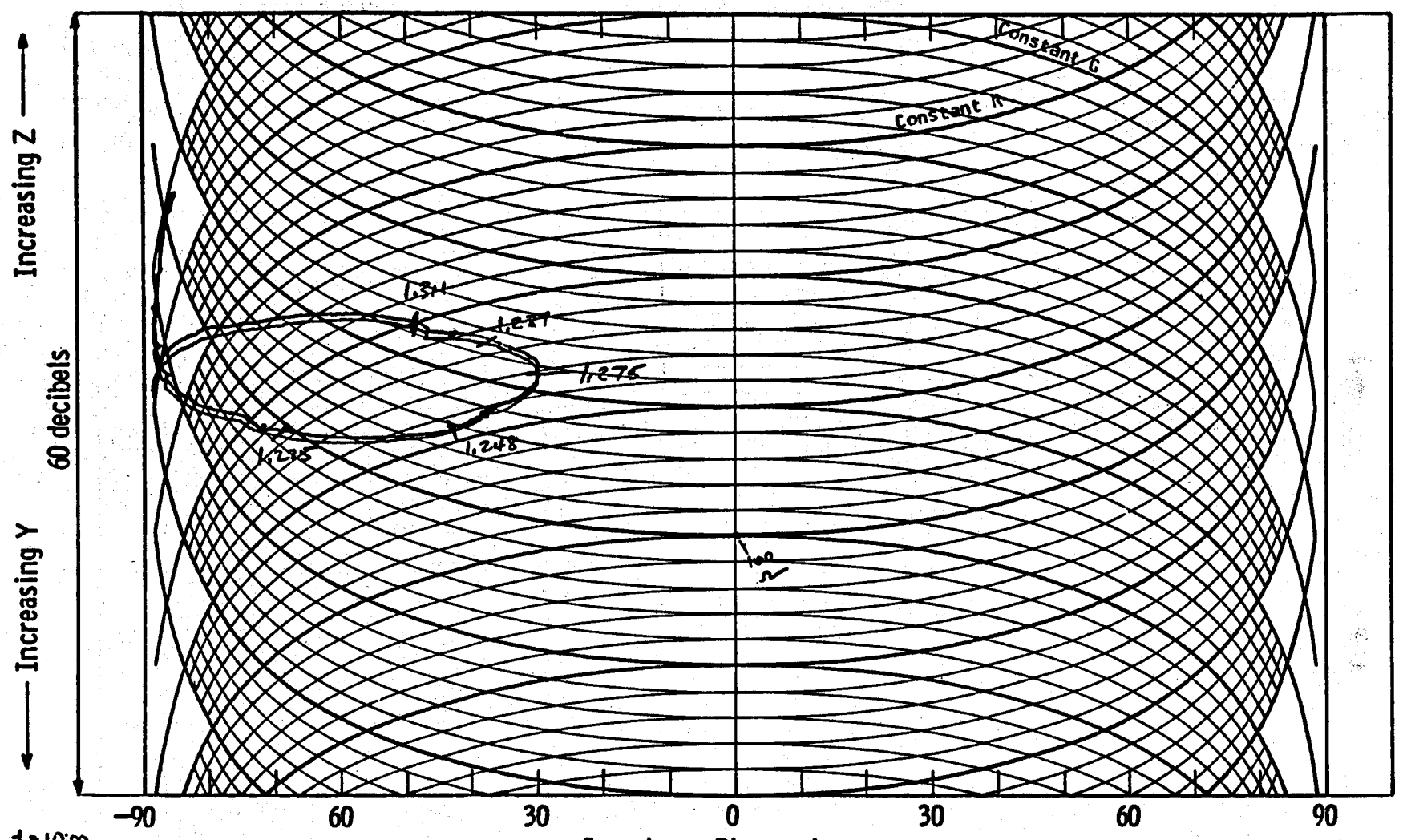

t-10:00

R.T. MOCK-UP.
IN FURNACE
1.3 mV (70°F)

20 db = 10:1 Change

4 JAN 79

Log Z - Phase Angle Diagram

Fig.11.11 Log Vector Impedance Plot (0.3 - 1.5 MHz) for "spare" transducer assembly of Fig. 5, at R.T., before 650°F thermal cycle test.

Curve 594612-A

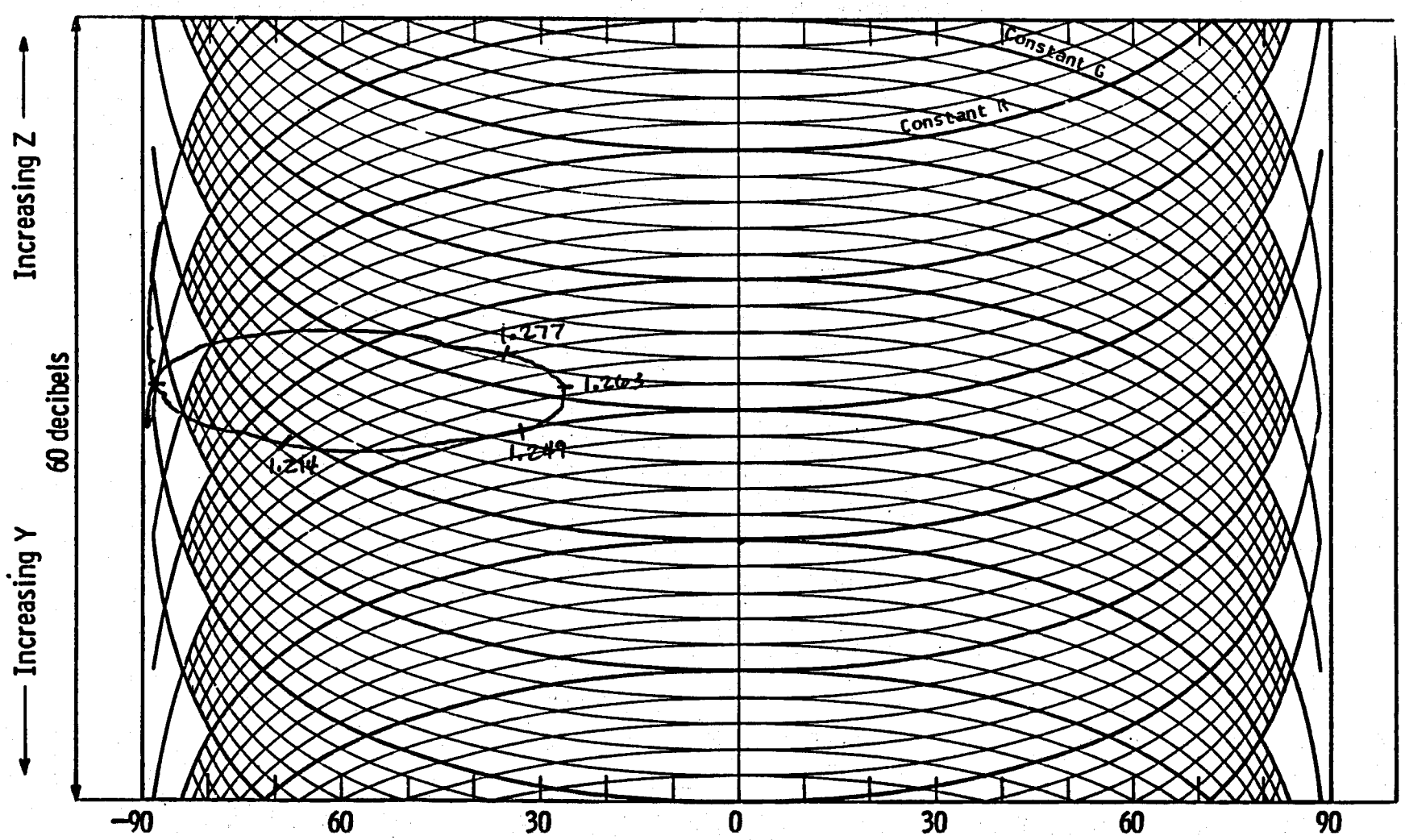

t-1041
mock-up in
furnace
5.3 mV. (214°F)
4 JAN 79

20 db = 10:1 Change

Log Z - Phase Angle Diagram

Fig.11.12 Log Vector Impedance Plot (0.3 - 1.5 MHz) for "spare" transducer assembly of Fig. 5. Temperature = 214°F.

Curve 594612-A

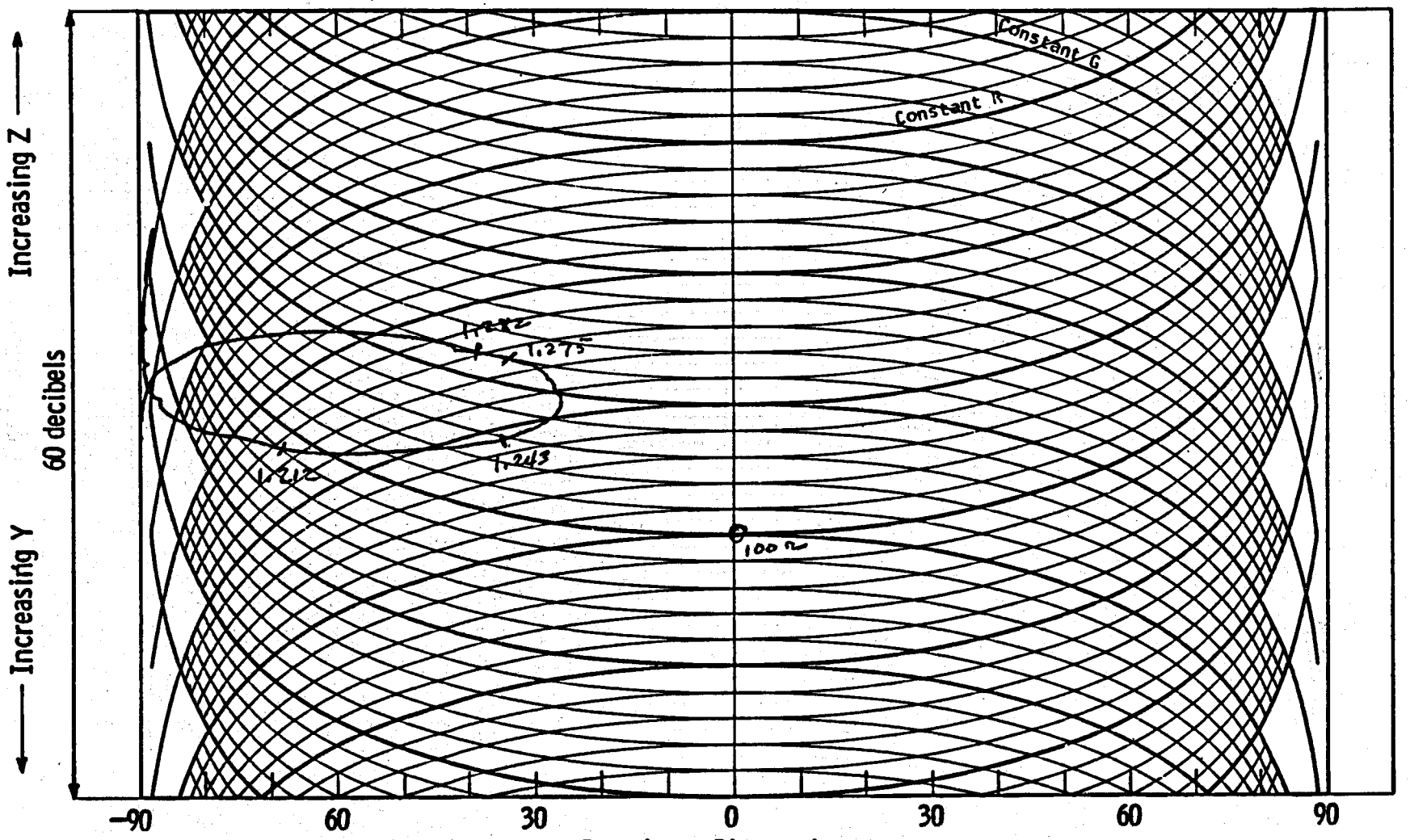

t= 1049
MOCK-UP
IN FURNACE
9.0 mV (335°F)

20 db = 10:1 Change

4 JAN 79

Log Z - Phase Angle Diagram

Fig.11.13 Log Vector Impedance Plot (0.3 - 1.5 MHz) for "spare transducer assembly of Fig. 5. Temperature = 335°F.

Curve 594612-A

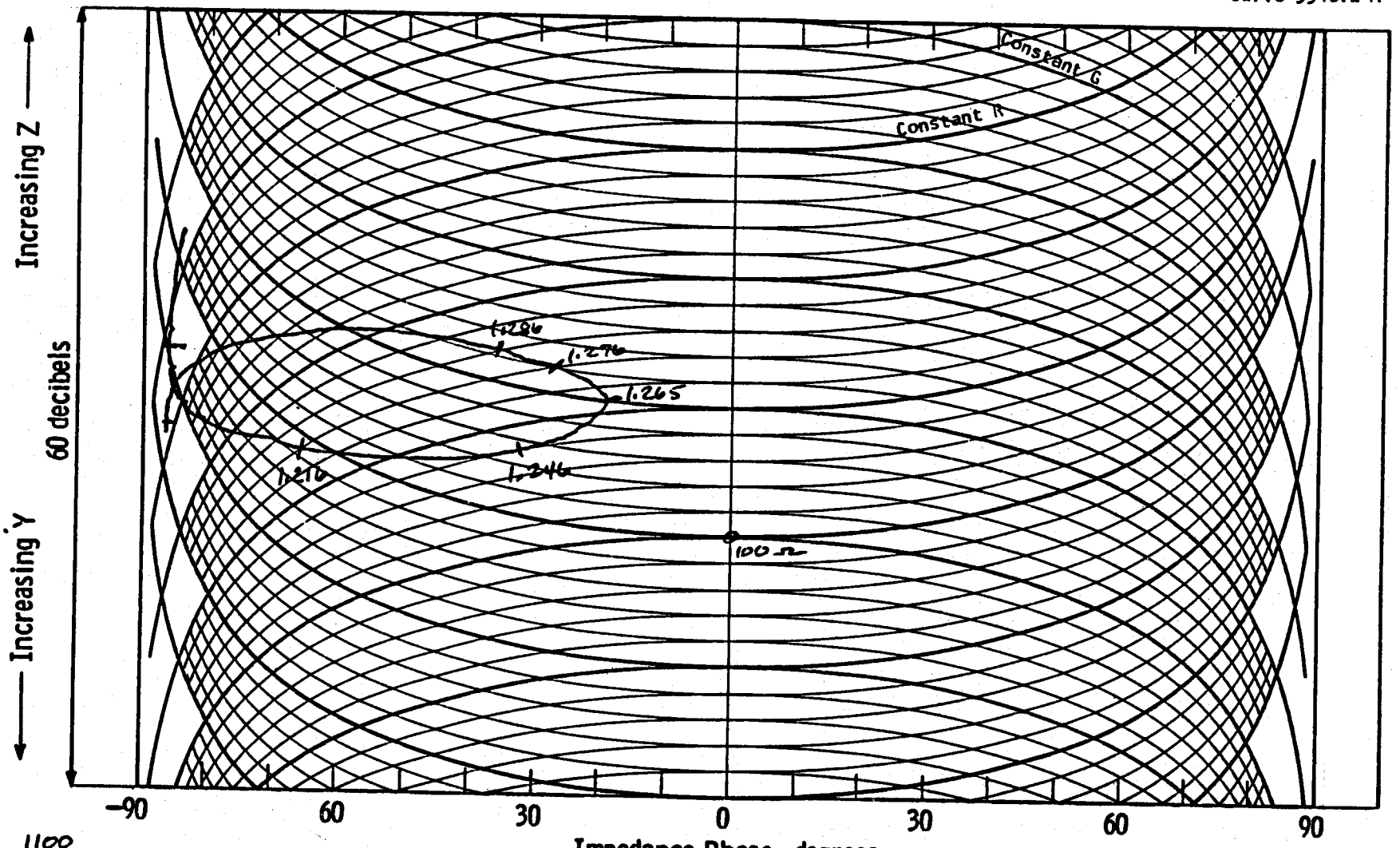

Fig.11.14 Log Vector Impedance Plot (0.3 - 1.5 MHz) for "spare" transducer assembly of Fig. 5. Temperature = 401°F.

Curve 594612-A

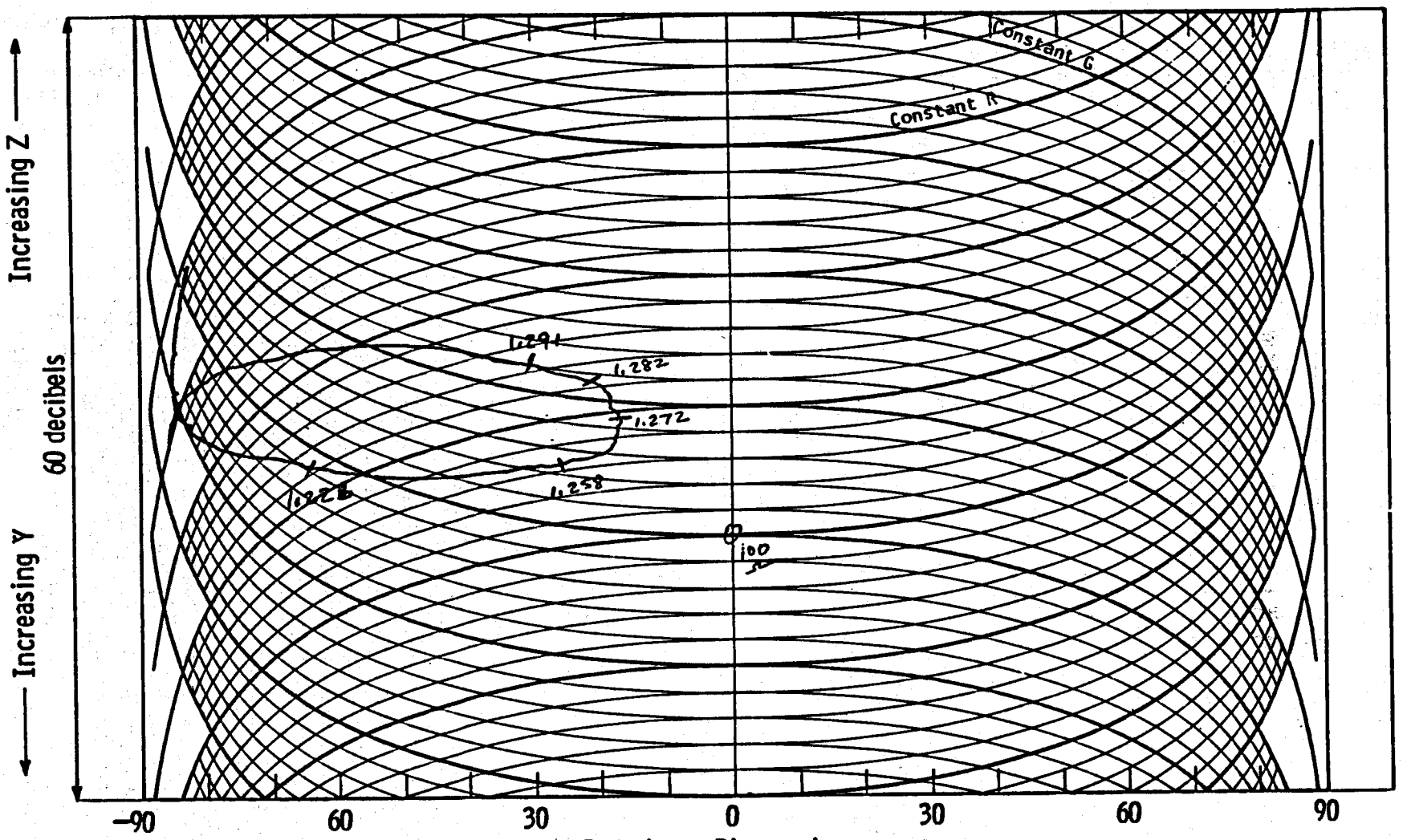

t = 1123
mock-up
in furnace
14.2 mV (505°F)
4 Jan 79

20 db = 10:1 Change

Log Z - Phase Angle Diagram

Fig.11.15 Log Vector Impedance Plot (0.3 - 1.5 MHz) for "spare" transducer assembly of Fig. 5. Temperature = 505°F.

Curve 594612-A

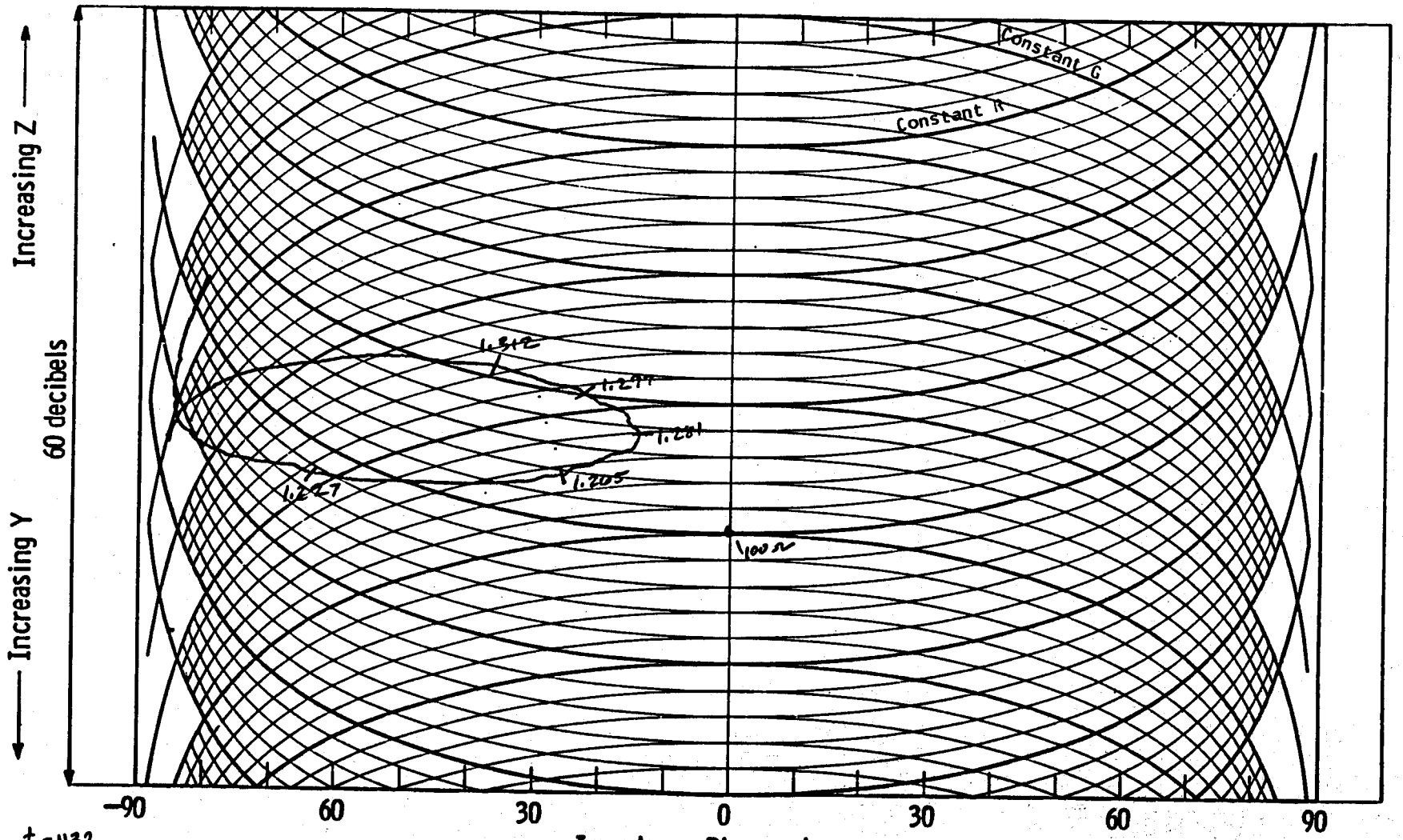

Fig.11.16 Log Vector Impedance Plot (0.3 - 1.5 MHz) for "spare" transducer assembly of Fig. 5. Temperature = 604°F.

Curve 594612-A

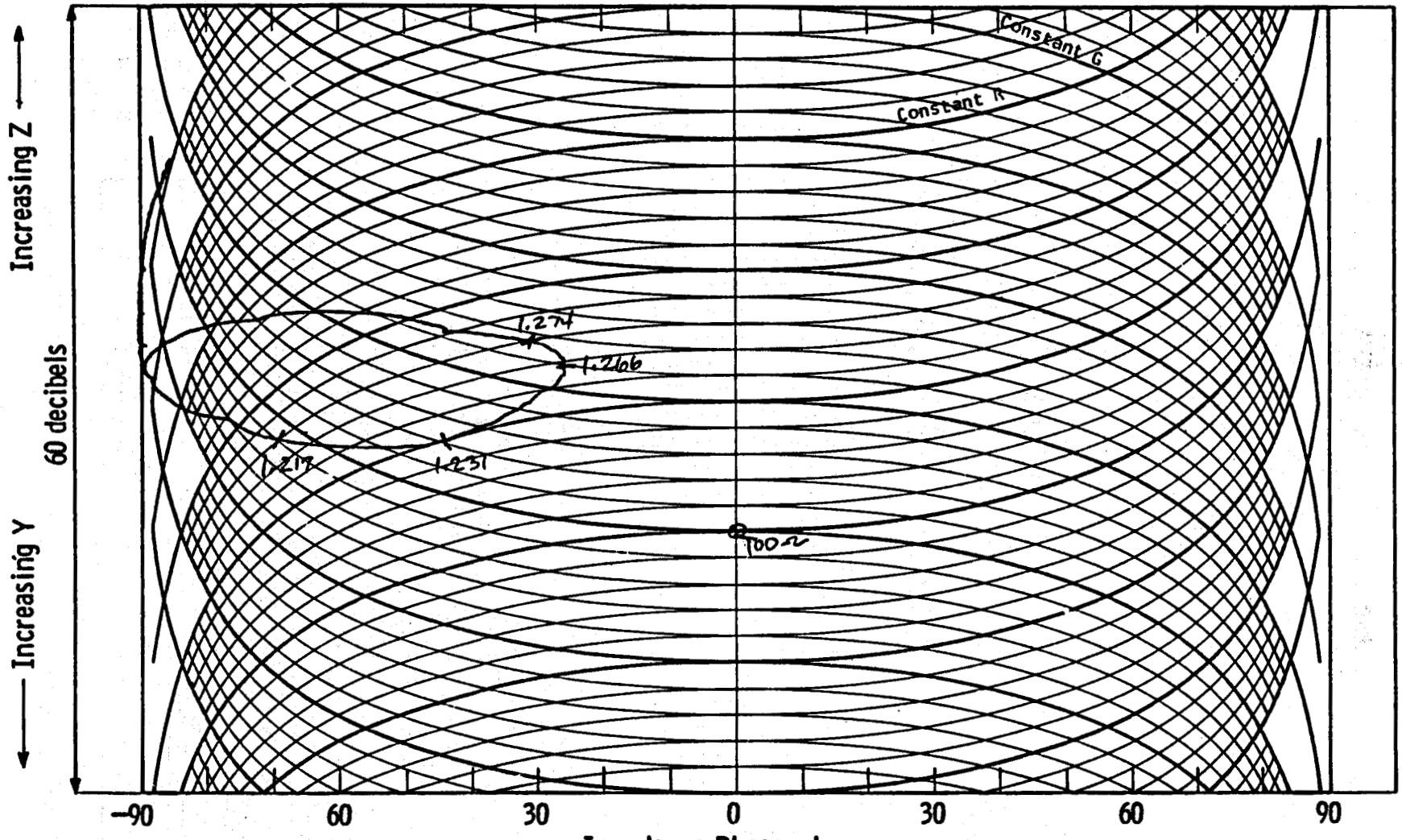

t = 1524

MOCK-UP
AFTER HEATING IN
FURNACE

R.T.

4-JAN 79 20 db = 10:1 Change

Log Z - Phase Angle Diagram

Fig.11.17 Log Vector Impedance Plot (0.3 - 1.5 MHz) for "spare" transducer assembly of Fig. 5, at R.T., following thermal cycle test.

Curve 594612-A

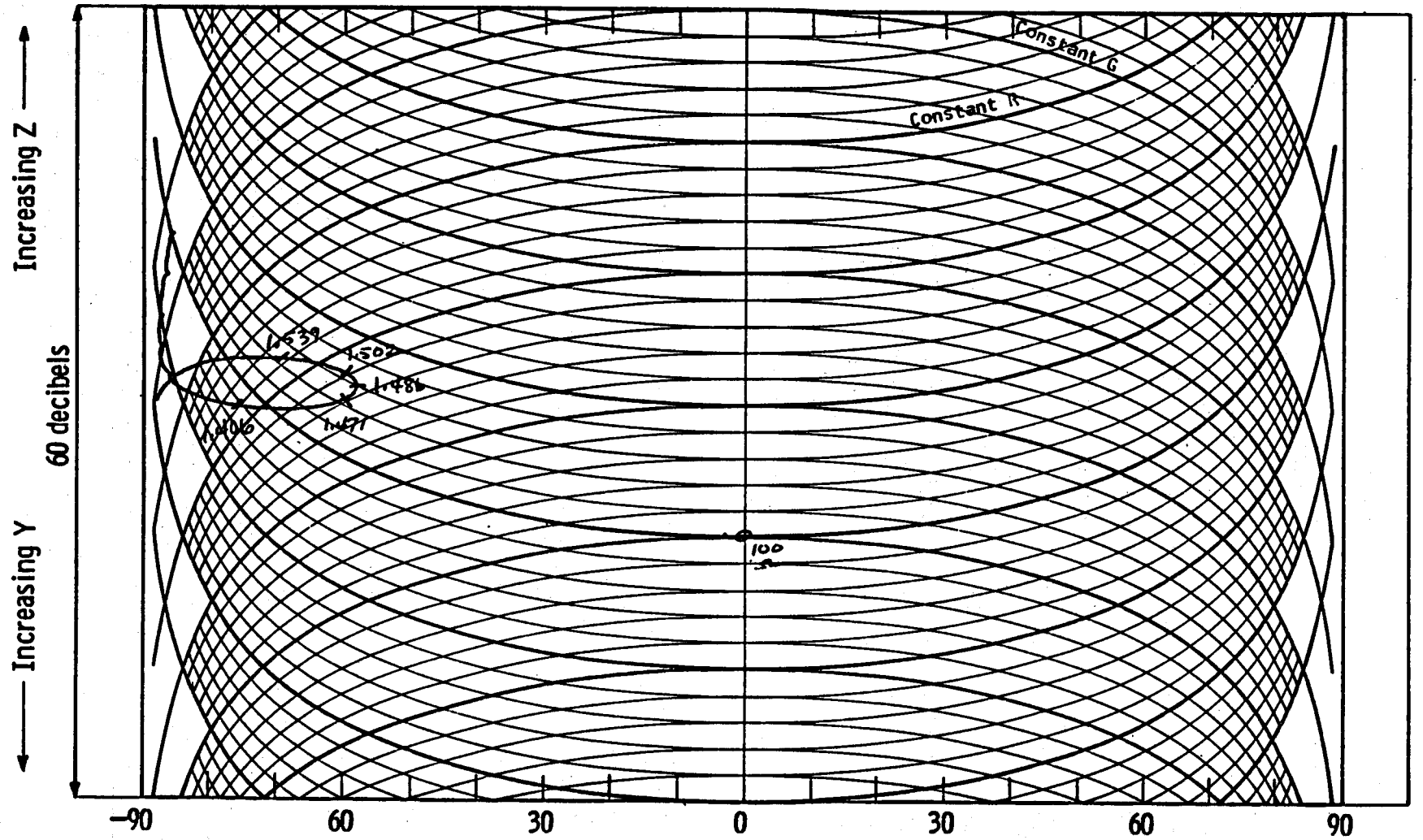

AUTOCLAVED
XDCR ASSEMBLY.
@ RT.

Fig.11.18 Log Vector Impedance Plot (0.3 - 1.5 MHz) for autoclaved sensor, in air, at R.T.

4 JAN 79.

20 db = 10:1 Change

Log Z - Phase Angle Diagram

TABLE II-II

Test Device[1]	Time	Temp.	f_o[2]	f_u[3]	f_L[4]	Q[5]
1	1000	R.T.	1.248	1.287	1.225	20.13
1	1041	214°F	1.249	1.277	1.214	19.83
1	1049	335	1.243	1.275	1.212	19.73
1	1100	401	1.246	1.276	1.216	20.77
1	1123	505	1.258	1.282	1.226	22.46
1	1132	604	1.265	1.297	1.227	18.07
1	1206	492	1.256	1.283	1.219	19.63
1	1217	458	1.254	1.280	1.216	19.59
1	1524	R.T.	1.231	1.274	1.217	21.60
2	-	R.T.	1.293	1.313	1.258	23.51
3	-	R.T.	1.471	1.539	1.406	11.06

Notes:

(1) Test Devices: 1 = Spare assembly in furnace; 2 = Unmounted lead metaniobate disc; 3 = Autoclaved transducer assembly.

(2) f_o = "resonant" frequency

(3) f_u = upper half-power frequency

(4) f_L = lower half-power frequency

(5) $Q = \dfrac{f_o}{\text{Bandwidth}} = \dfrac{f_o}{f_u - f_L}$

The K-81 lead metaniobate material used in this project was supplied by Keramos Incorporated of Lizton, Indiana. Keramos was contacted regarding the radical changes in the material properties which became apparent above 480°F. Keramos confirmed that at temperatures exceeding roughly 500°F, the dissipation and resistivity of K-81 increases sharply but that the peizoelectric properties of the material remain intact. This corroborates the measurements which were made on K-81 discs in the nitrogen furnace after the autoclave test. This indicates that K-81 lead metaniobate can be considered a suitable piezoelectric material

for a geothermal BHTV, provided that the high-temperature shifts in electrical properties are factored into the design of the transmit and receive electronics.

12. CONCLUSIONS

1) The presently manufactured BHTV sensor is not well suited for direct exposure to the geotherml environment specified by DOE (275°C, 7000 psi, and corrosive geofluid).

2) Although wrapping the conventional Vespel window with TFE Teflon tape (USGS - Water Resources) has extended the temeprature tolerance of Vespel, its hydrolytic behavior represents a major reliability problem in future applications.

3) A thin metal acoustic window can provide comparable acoustic sensor performance without the concurrent risk of chemical attack by the corrosive geofluid.

4) Perfluoroalkylpolyethers such as Brayco 812 and Kyrtox 143 appear to be acceptable as internal coupling fluids, from standpoints of temperature, pressure, and acoustic properties.

5) Lead metaniobate piezoelectric material such as is presently used in the BHTV is acceptable provided that transmit and receive circuitry offer suitably low electrical impedances.

6) Tungsten-powder-filled refractory cement is an excellent high-temperature damping (backing) material which is machineable and is compatable with above coupling fluid.

7) Epotek H-20E silver conductive epoxy can be used for mechanical and electrical bonds within the sensor at temperatures of 275°C.

8) The difficulties experienced during autoclave demonstration tests of the experimental sensor are explainable and can be overcome.

9) The sensor concept developed under this contract is capable of providing those functions required of a BHTV at temperatures up to 275°C, pressures up to 7000 psi, and in the presence of corrosive fluids.

13. RECOMMENDATIONS

1) The perfluoroalkylpolyether (Brayco 812) fluid evaluated during the sensor autoclave demonstration test provided those acoustic coupling features fundamental to BHTV sensor operation. However, apparent fluid depolymerization resulting in substantial void fraction when returned to 1 atmosphere was observed. The evidence indicates that depolymerization was due to a chemical reaction with an oxide of a carbon steel mechanical within the sensor compartment. The conventional BHTV sensor housing could probably be modified to accommodate the generated gas while maintaining adequate acoustic sensor operation. Alternatively, the carbon steel could obviously be replaced by a stainless steel or Inconel alloy. However, both of these approaches ignore a more general set of potential fluid related problems. In addition to being acceptable from the standpoint of the acoustic sensor, the fluid must also be compatible with several other devices (materials) located in the sensor housing. These devices include an electric motor, slip-rings, gear box, flux gate magnetometer, and a market switch. Also, other fluid properties such as lubricity, viscosity, and dielectric strength are expected to impact on the operation of these other devices.

It is therefore recommended: that a comprehensive study be undertaken to assess fluid compatibility with all sensor compartment devices under conditions of 275°C and 7000 psi. The objectives of this work should include 1) identification and characterization of fluid compatibility problems, 2) identification of alternatives for overcoming such problems, and 3) assessment of impact of alternatives on tool complexity, reliability, and performance.

2) The acoustic performance of a 0.002" thick Inconel 718 acoustic window are demonstrated to be comparable to the conventional Vespel window (0.1" thick). Lab tests demonstrated that this level of

performance was achievable with metal window segments of both flat and cylindrical (3-3/8" dia.) geometry. In order to incorporate this geotherml window design in an actual BHTV tool, an acceptable cylindrical window manufacturing process must be devised.

It is therefore recommended: that some additional work be done to identify a manufacturing process for producing a complete, thin-walled, cylindrical shell, Inconel 718 acoustic window. Window fabrication from sheet stock may be possible in light of the success attained with electron beam welding techniques in this project. Alternatively, it may be possible to machine a 0.002" wall tube from oversize tubing stock. Other methods should also be investigated. This work should include identifying a means for sealing the window to the body of the televiewer tool. Kalrez o-rings and othe gasket type seals appear to be promising, but flange design details remain to be established.

3) Although the piezoelectric electro-mechanical transduction process of lead metaniobate is maintained at 275°C, certain electrical circuit equivalent parameters were demonstrated to change dramatically and influence apparent performance. Persuant investigation revealed that the effects of these parameter changes can be counteracted by tailoring the design of the associated transmit and receive electronics.

It is therefore recommended: that BHTV electronic circuitry designers be made aware of the apparent need for providing suitably low transmitter output impedance, low receiver input impedance, and for incorporating a simple high-pass network (e.g., parallel inductor) across the piezoelectric disc element.

14. REFERENCES

1. L. E. Baker, R. P. Baker, and R. G. Hughen, "Report of the Geophysical Measurements in Geothermal Wells Workshop", Sandia Laboratories Energy Report No. SAND 75-0608 (December 1975).

2. R. F. Kehrman, J. W. Wonn, "Sensor Application Survey - Technical Report. Task 1", submitted to DOE/DGE by Westinghouse Electric Corp., May 1977. Contract No. EY-76-C-02-4082. TID-27941.

3. J. Zemanek, et. al., "Borehole Televiewer, New Logging Concept for Fracture Location and Other Types of Borehole Inspection", J. Petroleum Technology, Vo. 21, No. 6, June 1969, pp. 762-74.

4. R. J. Urick, Principles of Underwater Sound for Engineers, McGraw-Hill, New York, 1967, pp.16-22.

5. R. H. Bolt, T. F. Hueter, Sonics, John Wiley & Sons, New York, 1955, p. 43.

6. "Technical Bulletin No. L6" (Krytox 143), E. I. DuPont, Wilmington Delaware.

APPENDIX I - ELECTROACOUSTIC CHARACTERIZATION OF BOREHOLE TELEVIEWER

Over the period of June 23-27, 1977, measurements were made on two borehole televiewer tools (3-3/8" and 1-3/4" diameters). This work was done with the cooperation of the U. S. Geological Survey (Water Resources Department) in laboratories at the Denver Federal Center.

Objectives: Quantitatively determine

1) output pressure level and waveform,
2) receiver sensitivity
3) resolution, and
4) beam patterns.

Apparatus:

Two Simplec Manufacturing (Dallas, Texas) BHTV tools were available for testing. One tool was 1-3/4" and the other was 3-3/8" diameter. Both tools incorporated 1/2" diameter lead metaniobate piezoelectric elements ("crystals") and high temperature Vespel window. The larger diameter tool intially had a single layer of teflon tape spiral-wrapped over the acoustic window.

Fixturing was provided for scanning a transmit/receive reference transducer (or various targets) around the BHTV sensor in a plane perpendicular to the tool axis. Figure 1 shows the 3-3/8" diameter tool with the lower centralizer section removed for the purposes of these tests. A simple fixture (see Figure 2) was designed to accommodate both tooling sizes and to provide for rotating (scanning) various devices about either the tool or the internal piezoelectric element axis. This was accomplished by a length of 2" angle with a perpendicular plate welded near one end. Multiple holes in the plate provided the various required rotation axes.

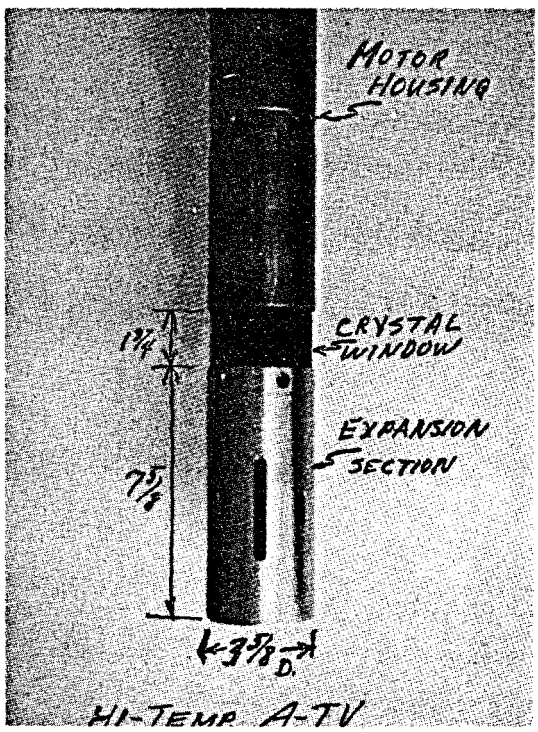

Figure 1. 3-5/8" Diameter BHTV (USGS Photo)

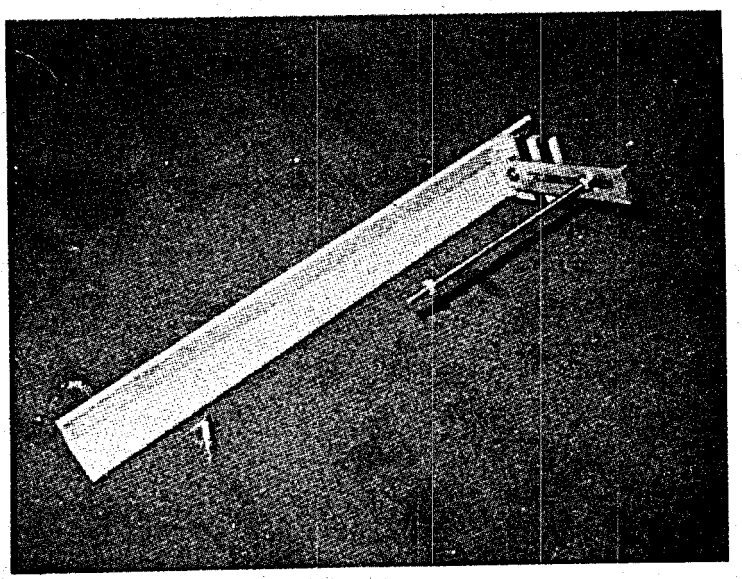

Figure 2. Scanning Fixture

A slotted rotating arm attaches to the plate by bolt and jamb nuts. The appropriate hole in the plate is selected according to the rotational axis desired. An all-thread post provides adjustable positioning of various devices along the tool axis and radial distance from tool is adjustable according to post location along the slot. The fixture is firmly attached to the tool using two hose clamps. Figure 2 shows the completed fixture and Figure 3 shows it attached to the 3-3/8" diameter tool and supporting a calibration sensor.

Other mechanical test hardware included 1/8" and 1/4" diameter spherical brass reflectors attached to the ends of 4-40 all-thread posts. These reflectors are useful in measuring the resolving capacity of the BHTV.

The downhole electronics package for the 1-3/4" diameter tool was used in conjunction with both tools tested.

The calibration transducer (see Figure 4) used is an Automation Industries #57A2788, incorporating a piezoelectric lithium sulphate disc 0.375" diameter with a 10 MHz, low-Q resonance. The response of this transducer is uniform and flat below 5 MHz. The receive sensitivity has been measured at -124 dB re 1 volt/μBar with a 6' cable attached. When used in the transmit mode, this transducer produces on-axis pressure of 76 μBar per volt of drive at a distance 25.4 cm from the crystal. RF excitation was provided to the calibration transducer by a tone burst transmitter with phase lock loop circuitry for frequency stability and with a low output impedance for minimizing load effects.

Signals received by the BHTV crystal were measured either directly across the crystal through a 6' length of coaxial cable or as an amplified version available on the front panel of the BHTV surface package. Signal levels were determined by inspection of the oscilloscope used as the read-out. Polaroid pictures of the CRT were taken to record much of the data.

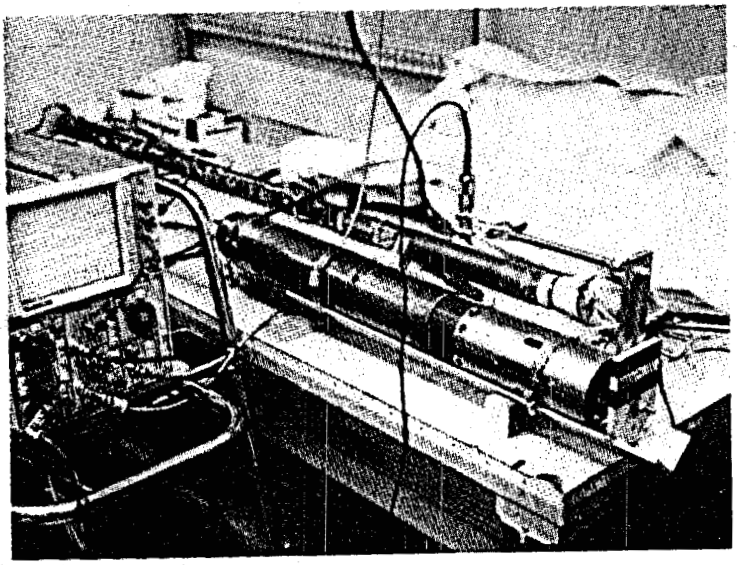

Figure 3. Fixture and Reference Sensor Installed on BHTV @ USGS.

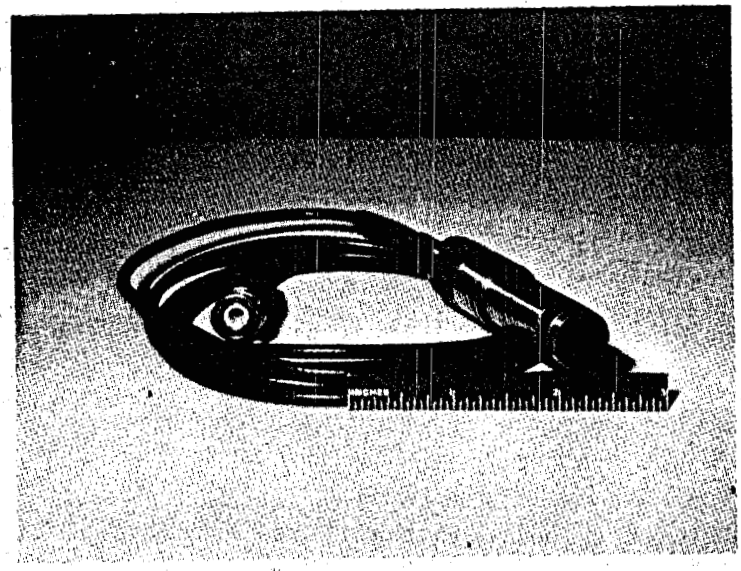

Figure 4. Calibration Sensor

Method

All measurements were made with the BHTV sensor section immersed in a 2 ft. diameter (water-filled) test tank as shown in Figure 5 and with the internal crystal stationary (no rotating). BHTV crystal beam patterns were made by rotating the Automation Industries transducer (receiver) about the crystal axis. Resolution measurements were made by rotating spherical reflectors about the tool axis as though they were targets located on a concentric borehole wall. Figures 6 and 7 show the calibration transducer and a spherical reflector (respectively) mounted on the BHTV while immersed in the test tank.

The original test plan included varying the spacing between two small spheres to determine at what spacing the two targets merged into one. In order to get the spheres close enough for these measurements, they had to be small (1/8" dia.) and the reflected signal levels from such small targets was found to be insufficient for meaningful data. Therefore, this test component was deleted. This was not considered to be a major problem since similar information can be obtained from the transmit/receive beam pattern of the single larger sphere.

Angular position of the test devices relative to the BHTV crystal axis was measured using a protractor and referencing the available geometrical features of the apparatus. By repetition of a few measurements, the tolerance of angular position data appeared to be no worse than $\pm$ 1/4°. Angle data were rounded off to the nearest 1/2°.

Test Results and Discussion

3-3/8" Diameter Tool: Initially the exterior of the Vespel window was wrapped with .6 mils of teflon tape. This was part of a prior experimental effort to provide means for protecting the window. It was not known whether the taped window had been down hole but it was considered worthwhile to measure its effect on the acoustic transmission characteristics. As such, a beam pattern of the transmit signal was made with the tape in place and a few points checked again after the tape was removed.

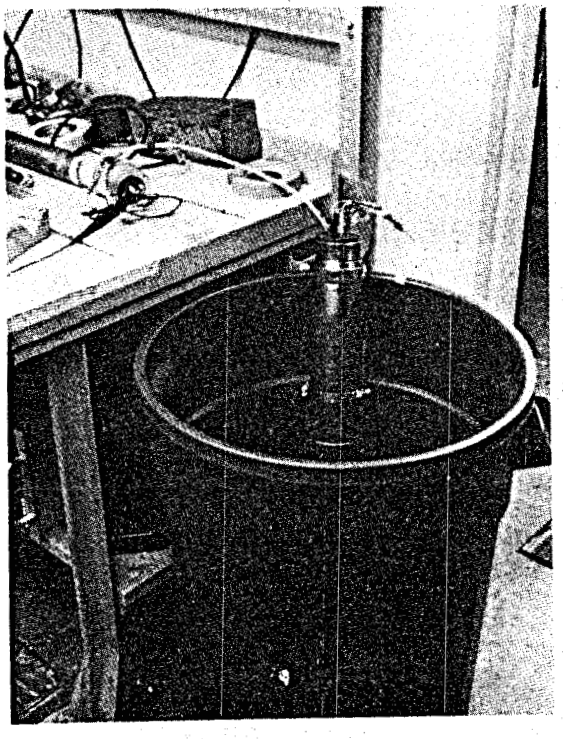

Figure 5. BHTV in Test Tank

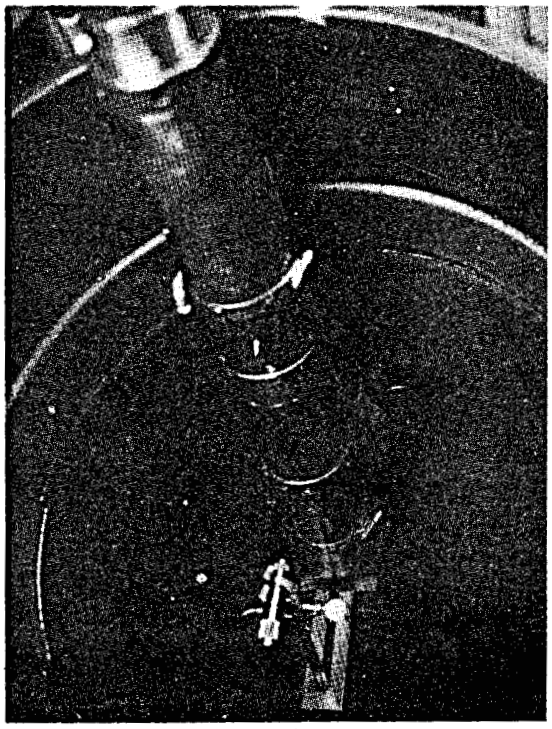

Figure 6. BHTV and Calibration Sensor in Tank

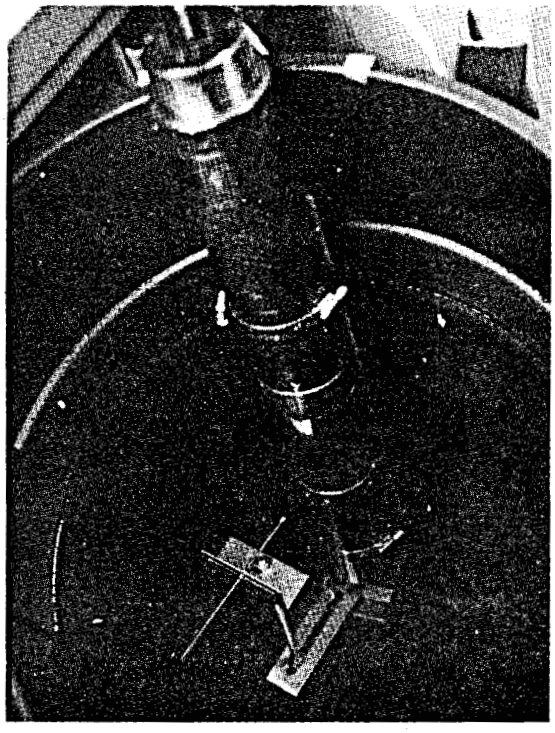

Figure 7. BHTV and 1/4" Diameter Spherical Target in Tank

The solid line of Figure 8 shows the measured beam pattern of the transmitting crystal with the teflon tape. The reference receiver was located 4-3/4" from the tool exterior in an effort to measure the far-field pattern. The approximate near/far field crossover occurs at 3-1/4" from the BHTV crystal. The on-axis received signal (0 dB reference level) was 430 mV p-p and is shown in Figure 9. This corresponds to an rms pressure of 2.4×10^5 μBar. The half-power (-3dB) beam width is $5\text{-}1/2^{\circ}$. Calculated beamwidth for an equivalent piston source is $\sim 6.9^{\circ}$ and the small difference is expected to be related to the effects of the various intermediate materials and their curvature. The data taken after carefully removing the tape and adhesive is shown by broken line in Figure 8. Signal levels are slightly higher with the tape vs. without and the beam somewhat broader. The on-axis variation (0.6 dB) may be attributed to experimental error, but the shape variation is not. While these variations are interesting, they are small enough to be of little practical significance in the realm of tool performance. Therefore, an explanation was not pursued.

Figure 10 shows a BHTV transmit/receive beam pattern. For this data, the BHTV is used in the normal "transceive" mode and a 1/4" sphere is used as a target. It is evident that the beam is narrower (3°) than that of Figure 8. This is expected since for this test, the angular response shown in Figure 8 effects the beam once when the pulse is transmitted and again upon receiving the reflected pulse. The beam pattern of Figure 10 is considered to be the most relevant in that it replicates the process of borehole imaging. With a reflector-to-tool range of 1.5", this simulates conditions in a 6-3/8" diameter borehole.

Referring to Figure 9, the launched waveform consists of a first arrival pulse containing ~2-1/2 cycles of 1.5 MHz, followed by several lower level replicas which appear to persist in excess of 10 μseconds. These trailing signals are likely to be due to internal reverberation within the televiewer. Some of this reverberation is expected to find its way into the BHTV receiver channel via the crystal and degrade the SNR of the tool.

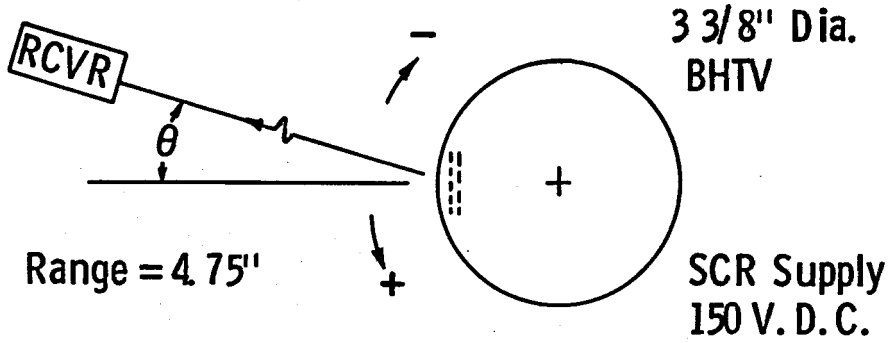

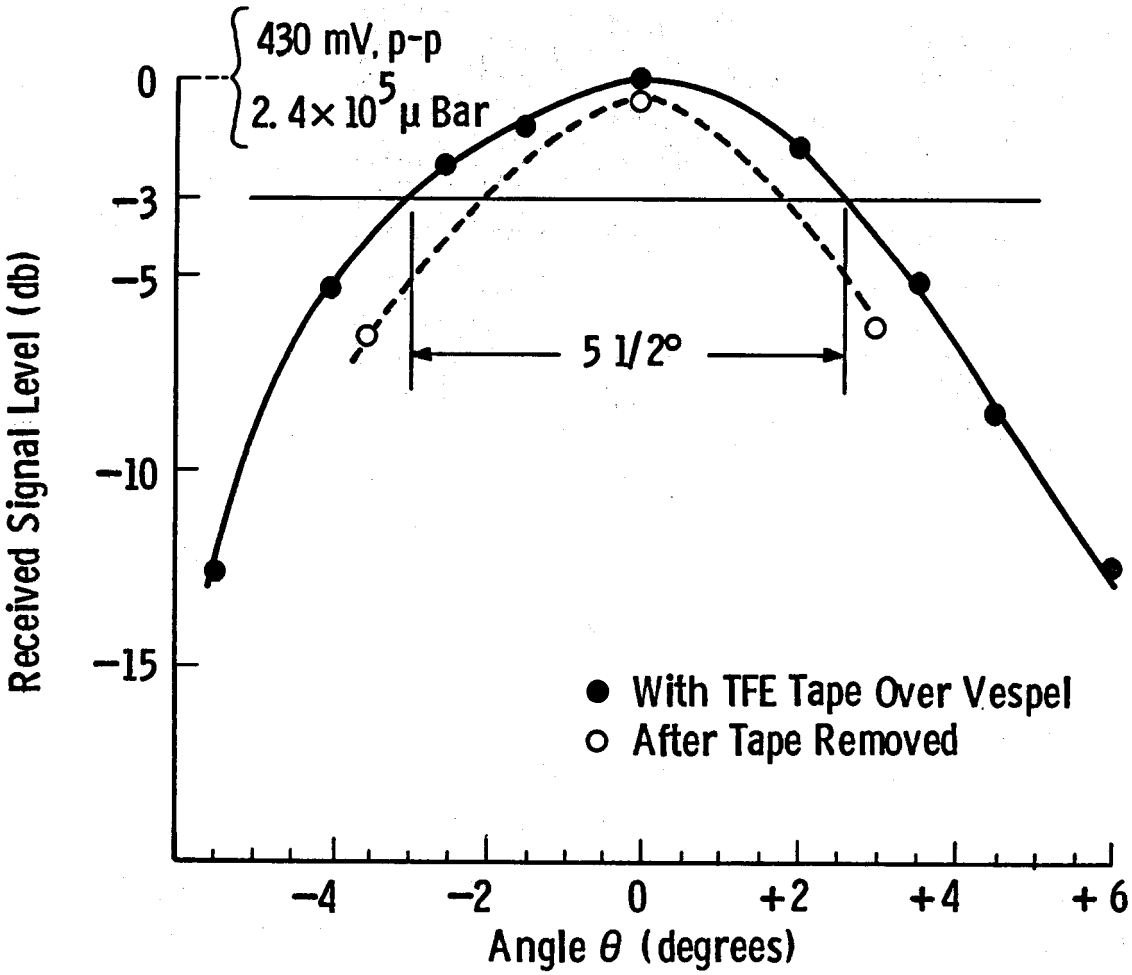

Fig. 8—Transmit beam pattern; 3-3/8" tool; 4.75" range, with and without Teflon tape over Vespel window

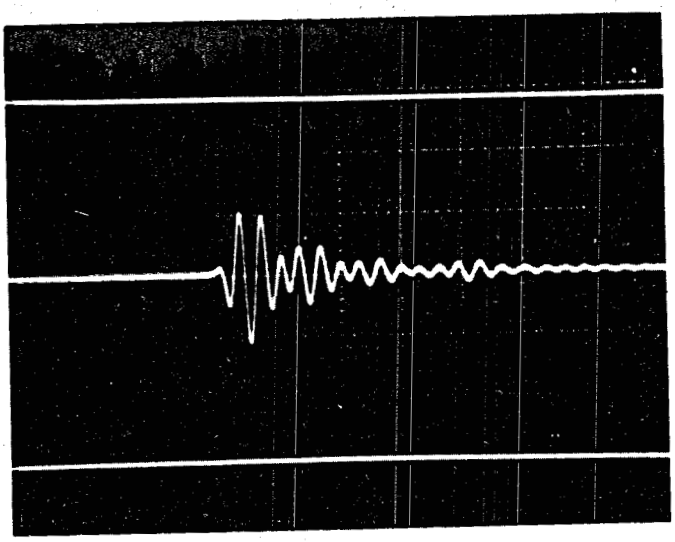

Figure 9. On-Axis Pressure Pulse; 3-3/8" Tool; With Teflon Tape. (H = 2 μsec/div; V = 0.2 Volts/div.)

Curve 715666-A

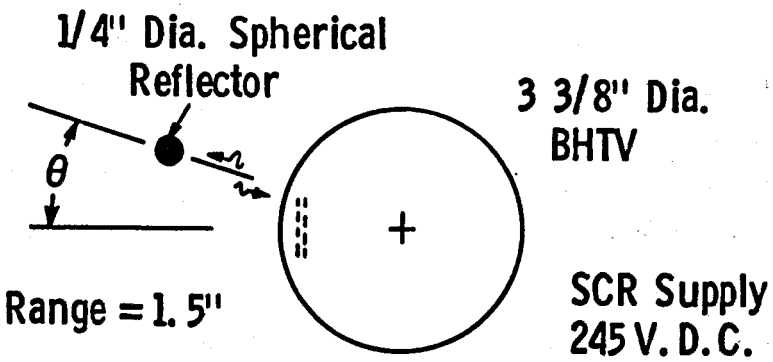

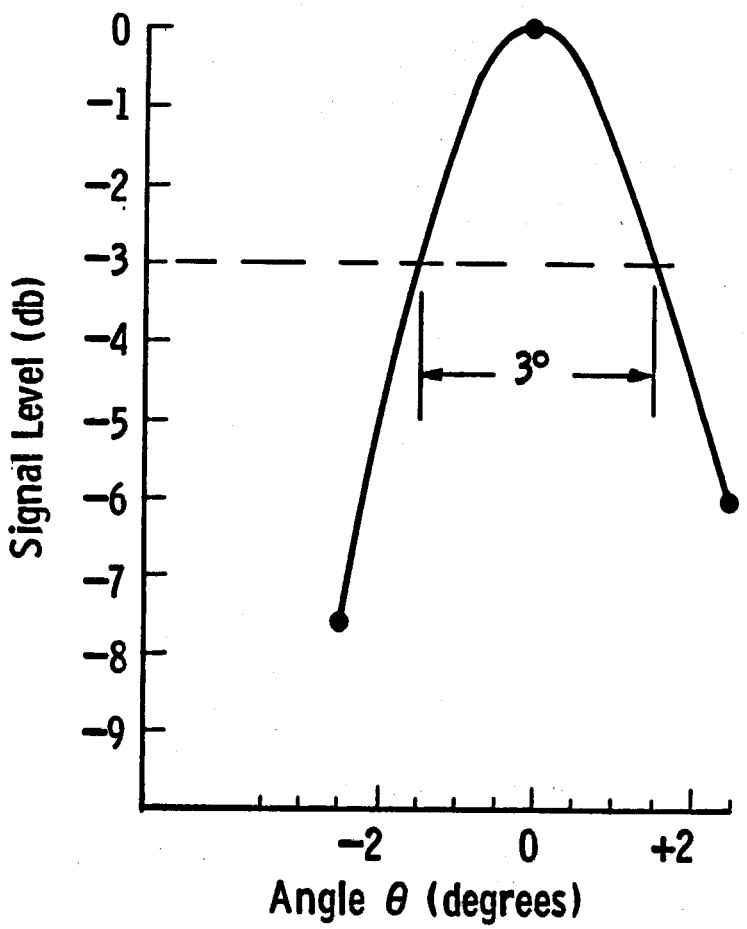

Figure 10. Transmit/receive beam pattern; 3-3/8" tool; 4.75" range.

BHTV receiver sensitivity was measured by transmitting a known, gated, sinusoidal pressure wave with the calbration transducer and noting the received voltage across the BHTV crystal. The crystal was loaded by "o feet of coaxial cable. For this measurement, the faces of the calibration and BHTV crystals were parallel and separated by about 4-3/4".

The output of the calibration transducer was previously determined to be 76.1 μBar per volt of drive at a 10" range. With an excitation level of 30 Volts p-p, the pressure at 10" is 2.3×10^3 μBar (p-p). As the far field pressure is inversely proportional to range, the actual pressure at the BHTV window should be 10/4.75 times the pressure at 10" range. The actual pressure input to the BHTV is then 4.8×10^3 μBar (p-p).

Figure 11 shows the waveform across the BHTV receiving crystal in response to the above pressure wave. The amplitude is 100 mV (p-p). A receiver sensitivity can be calculated by dividing this voltage by the applied input pressure.

$$\frac{\text{Voltage}}{\text{Pressure}} = \frac{100 \text{ mV}}{4.8 \times 10^3 \ \mu\text{Bar}} = 2.1 \times 10^{-5} \frac{\text{Volts}}{\mu\text{Bar}}$$

The terms of the more conventional free-field voltage sensitivity (FFVS), -94 dB re 1 Volt/μBar.

1-3/4" Diameter Tool: A similar set of measurements were made for the 1-3/4" diameter tool. As both tools use identical crystals the data was expected to be similar to that of the 3-3/8" diameter tool with most differences attributable to increase curvature of the window and more compact arrangement of internals (i.e., damping block, etc.).

The far-field (one-way) beam pattern is shown in Figure 12 and exhibits a half-power beamwidth of 5-1/2°. The on-axis signal (0 dB reference level) was 490 mV peak-to-peak and is shown in Figure 13. This corresponds to a calculated rms pressure of 2.7×10^5 μBar.

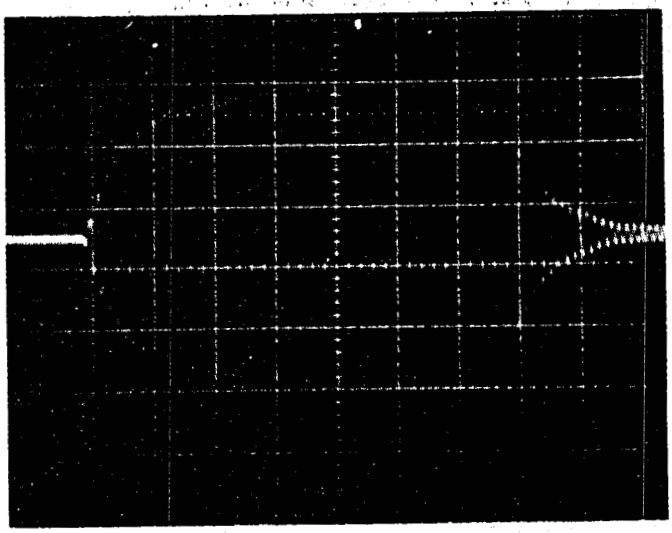

Figure 11. Receiver Sensitivity Waveform; 3-3/8" Tool
(H = 5 μsec/div.; V = 20 mV/div.)

Curve 715665-A

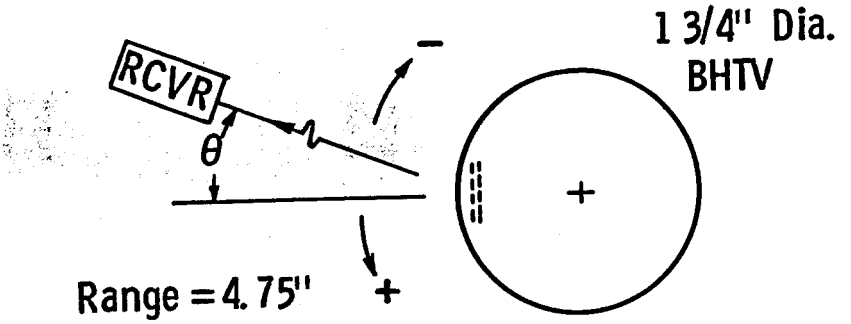

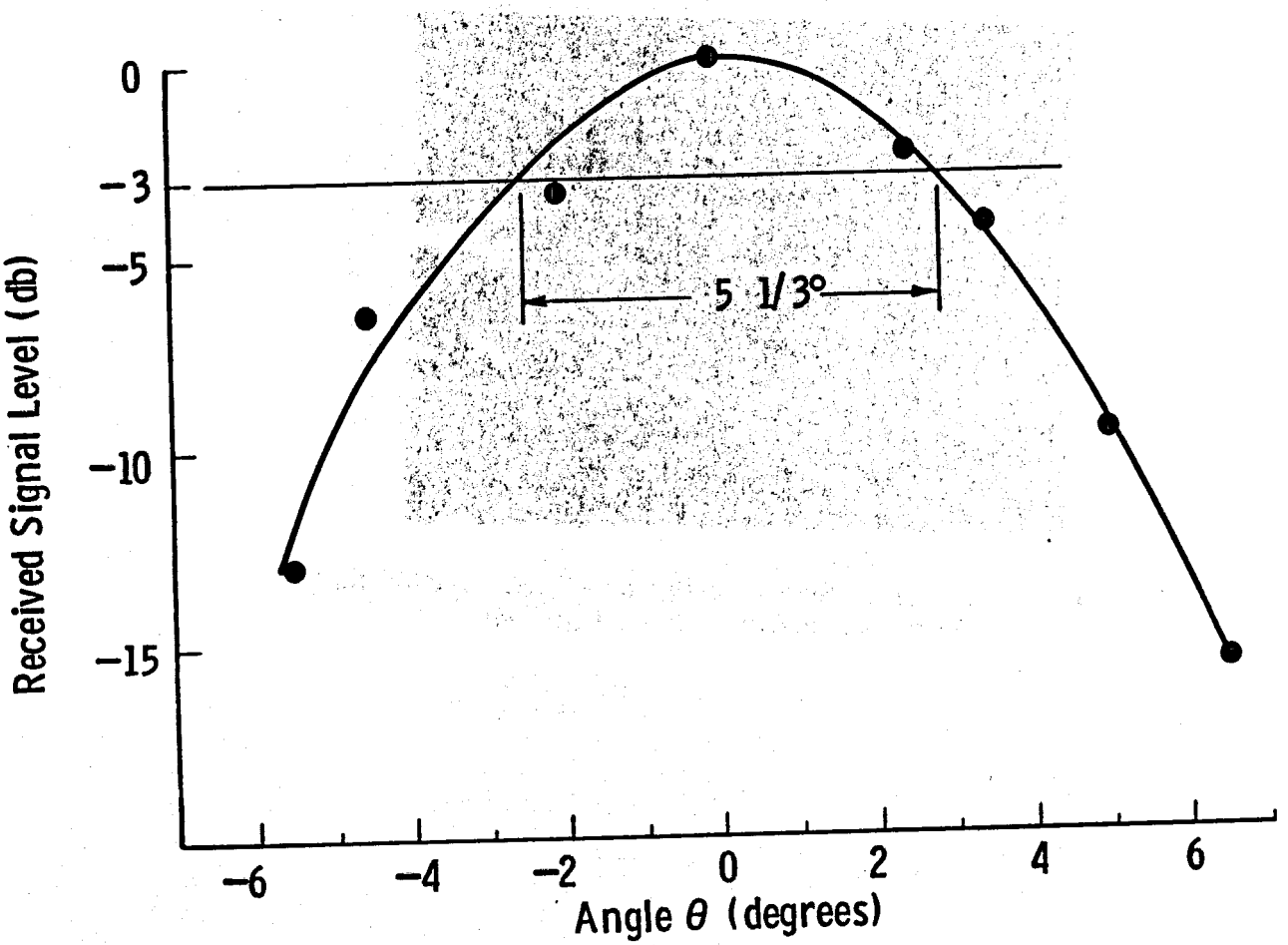

Fig. 12—Transmit beam pattern; 1-3/4" tool; range - 4.75"

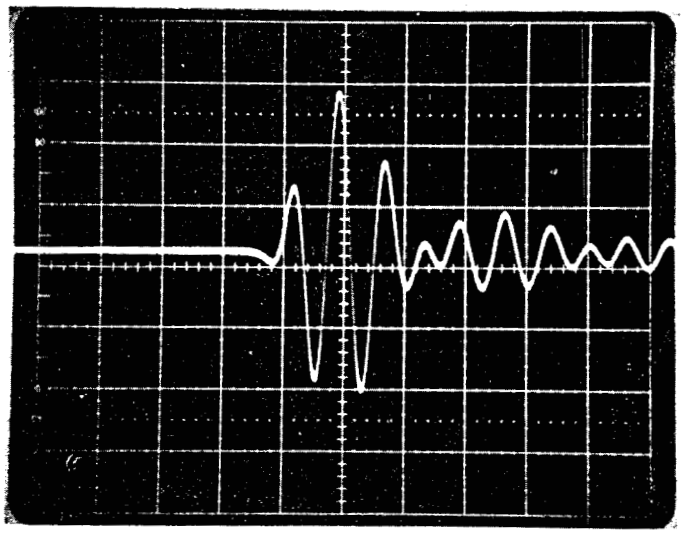

Figure 13. On-Axis Pressure Pulse; 1-3/4" Tool
(H = 1 μsec/div.; V = 0.1 Volt/div.)

The transmit/receive beam pattern was measured again using the 1/4" diameter spherical target at 1.5" range and is shown in Figure 14. This pattern shows a main lobe and significant output in two other directions, $+17^{\circ}$ and -22°. If these outputs were actual side lobes characteristics of a circular piston source, they would be located at $\pm 11^{\circ}$ (approximately) and should appear at similar times since target-to-crystal distance remained constant. Actual arrival times were significantly later than on-axis arrivals. It is therefore believed that these lobes may be the result of significant amounts of acoustic energy launched into the BHTV, reflecting from internals, and propagating out through the window. That similar lobes are not apparent on the 3-3/8" tool is expected to be related to the geometry differences. The smaller tool provides less room for damping materials and internal absorbing sound paths are shorter and therefore less effective. This may suggest that internal reverberation is more of a problem in the smaller diameter tool. In practice, the significant time delay allows for range gating to preclude reception of signals in the directions of the undesired lobes. If this were not so, "ghosting" or multiple images would be evident in BHTV output under all but poorest SNR conditions.

The target was then moved out to 4.75" to check for variation in beam size as a function of range. The beam pattern (see Figure 15) is somwhat narrower at the optimum range of 1.5" ($3-1/3^{\circ}$ @ 4.75" vs. $2-1/3^{\circ}$ @ 1.5") as predicted by the results of a computer simulation by Zemanek.[1]

The increased target-to-transducer distance resulted in reduced echo levels and the off-axis lobe energy was not detectable above the background electronic noise.

The receiver sensitivity of the 1-3/4" tool was measured in the same way as the 3-3/8" tool. 30 volts (p-p) excitation as applied to the

---

[1]Zemanek, J.: "Beam Behavior Within the Nearfield of a Vibrating Piston,", J. Acoustic Society of America (1971), 181-191, Vol. 49, No.1.

Curve 715668-A

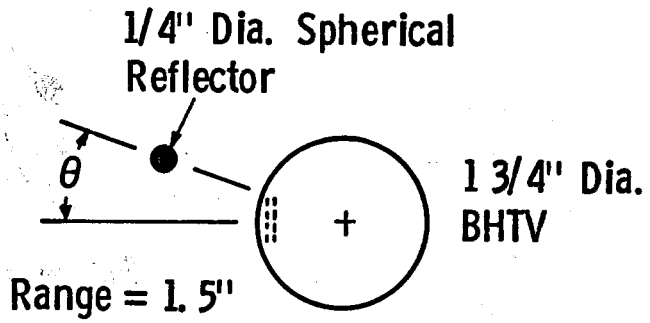

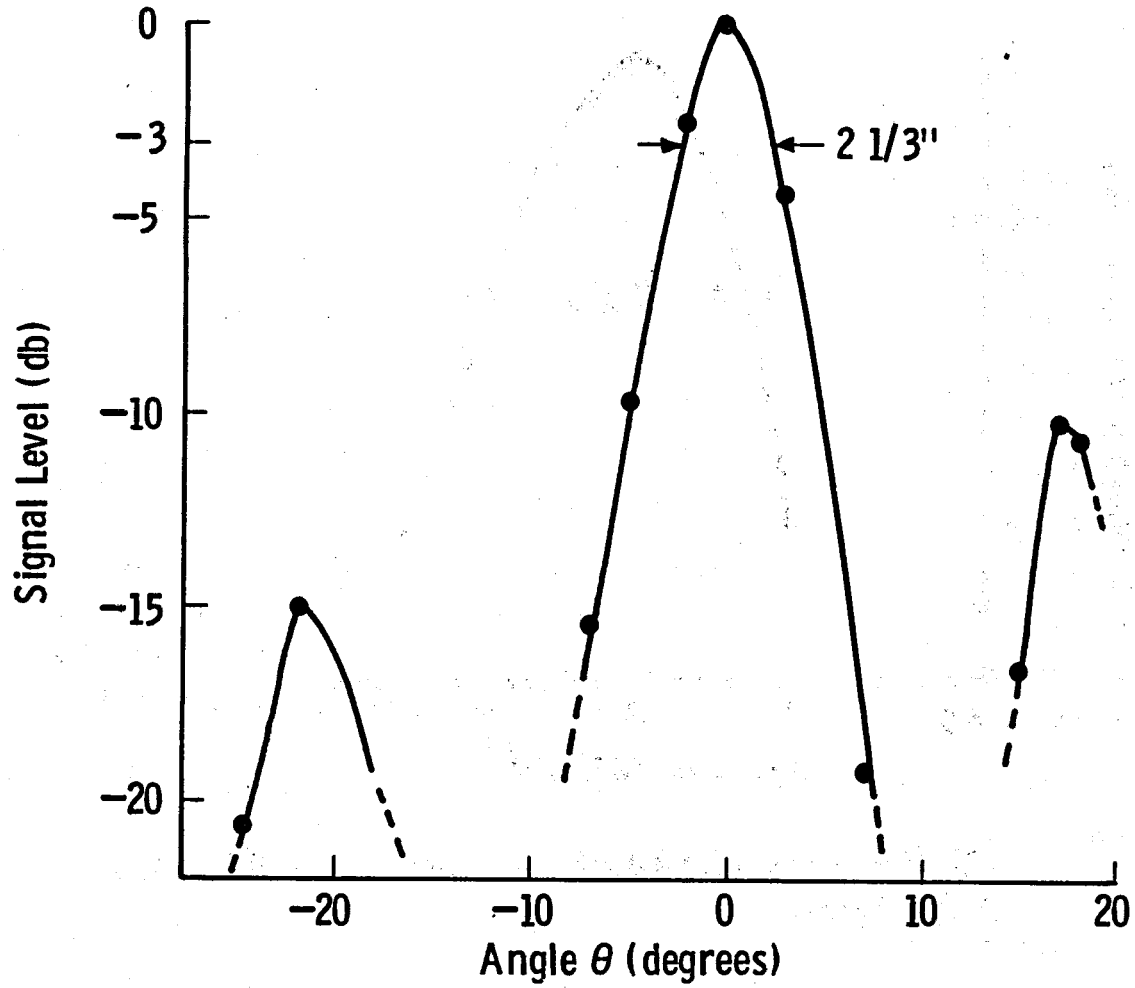

Fig. 14—Transmit/receive beam pattern; 1-3/4" tool; 1.5" range

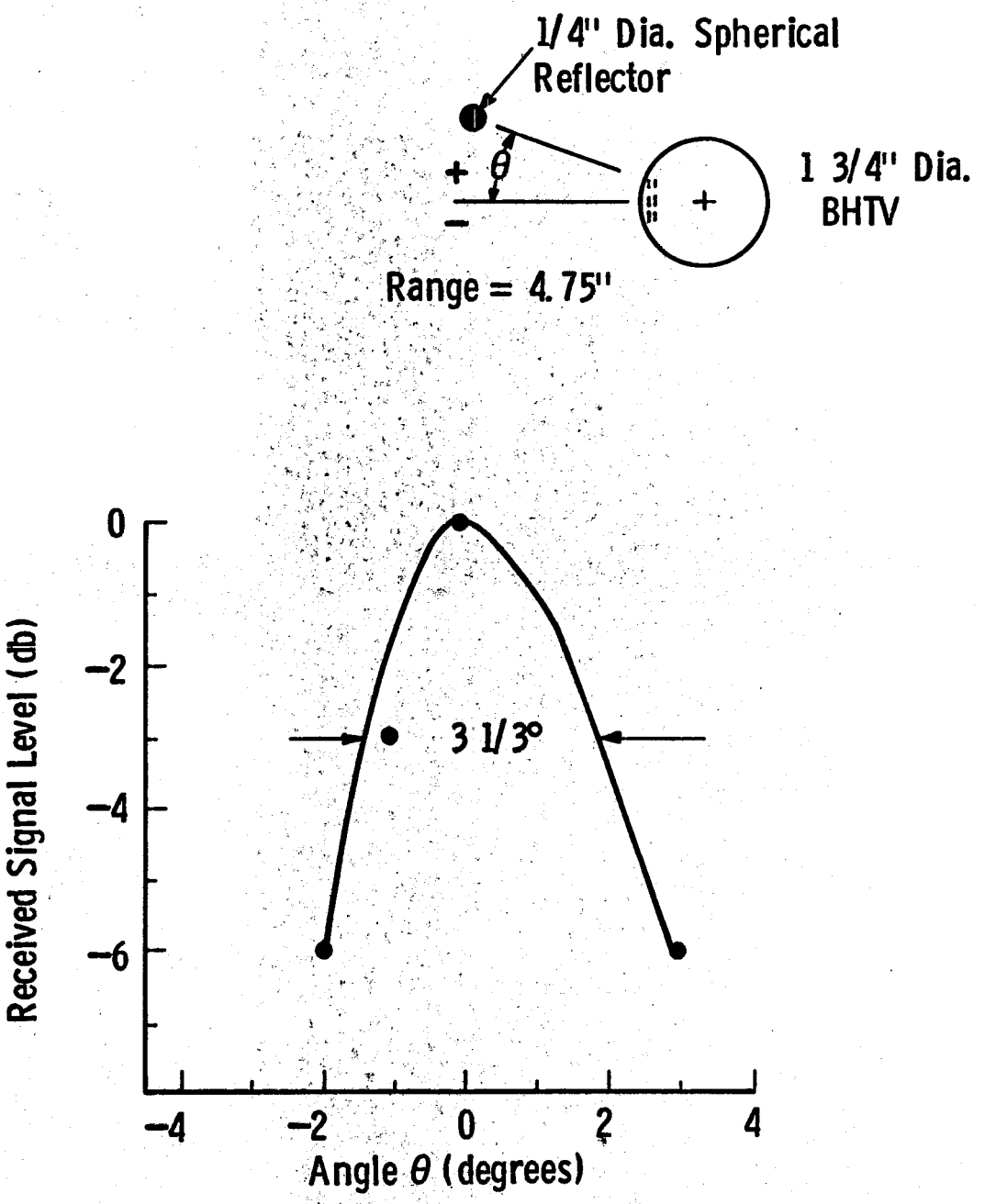

Fig. 15—Transmit/receive beam pattern; 1-3/4" tool; 4.75" range

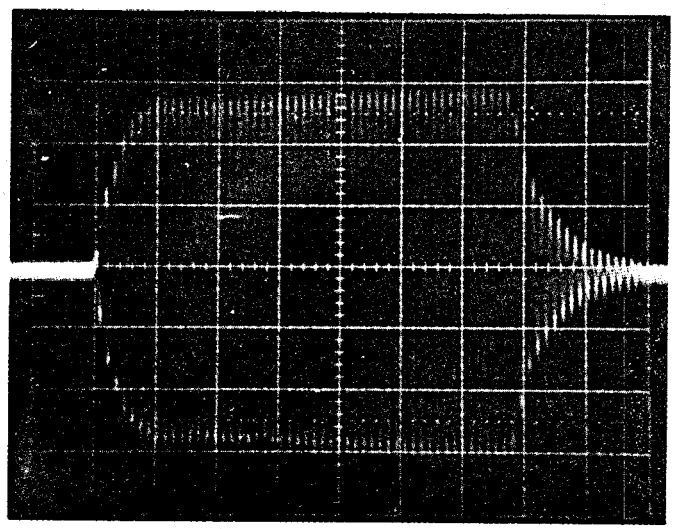

Figure 16. Receiver Sensitivity Waveform; 1-7/8" Tool
(H = 5 μsec/div.; V = 10 mV/div.)

reference transducer located 4.75" from the BHTV window. Figure 16 shows the resulting received voltage across the BHTV crystal. The received signal level is 58 mV p-p which is considerably lower than that of the larger tool. The reason for this difference is unknown although it may be attributable to the relatively severe curvature of the window. The calculated receiver sensitivity is 1.21×10^{-5} volts per μBar (or -98.4 dB re 1 volt per μBar.

APPENDIX II - PRELIMINARY MATERIALS SCREENING TESTS

Introduction

A number of materials and components were considered candidates for use in construction of a geothermal well logging sensor. Although these items were selected on the basis of both previous elevated-temperature design experience and a review of current product literature, their endurance in the intended service environment was uncertain. Testing was therefore required to screen the survivability of these materials and components when immersed for a lengthly time in a high-temperature high-pressure chemically corrosive geothermal liquid environment, while being physically assembled in a service-simulative but non-operative fashion.

This appendix describes two preliminary materials screening tests. The information presented includes materials and components tested, test procedures, and post-test analysis of specimens. The relevant Autoclave Test Plan (ST-001) is found in Appendix III.

SCREENING TEST NO. 1

I. CANDIDATE MATERIALS AND COMPONENTS

Four 316 stainless steel test capsules were prepared. Each capsule was 6-1/4-inches long and comprised a 6-inch length of 1-inch Schedule 80 pipe fitted with two 1-5/8-inch diameter tubular end caps. Three of the capsules had their ends sealed with plastic and elastomeric candidate window materials, and developed candidate high temperature oils along with sundry candidate transducer material and component samples. These capsules were designated as A, B and C. The fourth capsule was permitted to free flood to the autoclave liquid environment and contained candidate plastic plotting and encapsulating materials. This capsule was designated as D.

A photograph of Capsule A that was taken prior to autoclave testing is shown in Figure 1. The elastomeric candidate acoustic window material is clearly seen as a black convex surface at the top of the capsule.

Test capsules A, B and C each had an identical assortment of candidate solid materials and components, and differed only in the type of high temperature oil enveloped. Capsule A had Mobil Jet Oil II, Capsule B had Dow Corning DC-210H silicone oil and Capsule C and Dow Corning DC-550 high-phenyl silicone oil. A description of the candidate solid material and component assortment is given below.

Fig. 1. Pre-test Photograph of Test Capsule A

Candidate Solid Material and Component Assortment for Test Capsules A, B and C

1. Rudimentary Piezoceramic Transducer Assemblies

Each assembly consisted of a fragment of thin silver-electroded lead metaniobate piezoceramic adhesively bonded with high temperature electrically conductive epoxy to a 1/2-inch cube of candidate transducer backing material.

The lead metaniobate piezoceramic had a thickness resonant frequency of 2.0 MHz and was K81 material as supplied by Keramos, Inc.; 104 North Church Street; Lizton, IN 46149. The high temperature electrically conductive epoxy was Epo-Tek H20E as supplied by Epoxy Technology, Inc.; 65 Grove Street, Watertown, MA 02172.

1.1 Tungsten-filled Alumina Cement Transducer Backing Material

A candidate tungsten-filled high-alumina cement transducer backing material was fabricated by the Westinghouse R&D Ceramics and Glasses Group. The nominal batch formula for this material is as follows:

(a) Alcoa Calcium Aluminate Cement CA-25. (High alumina cement manufactured by the Aluminum Company of America.) Weight: 24.0 pounds, Volume: 0.124 cubic feet.

(b) Harbison-Walker GP-71 Fused Silica Poweder (Fine grained fused silica powder manufactured by Glasrock Products Group; Harbison-Walker Refractories; Division of Dressen Industries, Inc.) Weight: 18.0 pounds; Volume: 0.131 cubic feet.

(c) Fine Grained Tungsten Powder. (Tungsten metal powder as manufactured by Atlantic Equipment Engineers of Bergenfield, New Jersey; Catalog No. WP 355; 100 mesh crystalline tungsten metal powder.) Weight: 220.0 pounds; Volume: 0.183 cubic feet.

(d) Water. Weight: 20.0 pounds; Volume: 0.321 cubic feet.

This mixture has a nominal slurry density of 372 pounds per cubic foot and contains 83.97 percent of tungsten on a weight basis.

Test Capsules A, B and C each contained a specimen comprised of a fragment of lead metaniobate piezoceramic adhesively bonded with electrically conductive epoxy to a 1/2-inch cube of the above specified tungsten-filled high-alumina cement.

1.2 Tungsten-filled Stycast 2762FT Epoxy

A candidate tungsten-filled Stycast 2762 FT epoxy tranducer backing material was fabricated. The batch formula for this material is as follows.

(a) Stycast 2762 FT high-temperature epoxy as supplied by Emerson & Cuming, Inc.; Canton, MA 02021. Resin: 100.0 grams. Catalyst #17: 10.0 grams.

(b) Fine grained tungsten powder (Atlantic Equipment Engineers; Catalog WP 355). Weight: 333 grams.

The curing cycle for this mixture was 2 hours at 100°C followed by 4 hours at 150°C.

Test Capsules A, B and C each contained a specimen comprised of a fragment of lead metaniobate piezoceramic adhesively bonded with electrically conductive epoxy to a 1/2-inch cube made of the above specified tungsten-filled Stycast 2762 FT epoxy.

1.3 Tungsten-filled Duralco 700 Epoxy

A candidate tungsten-filled Duralco 700 epoxy transducer backing material was fabricated. The batch formula for this material is as follows:

(a) Duralco 700 high-temperature epoxy as supplied by Cotronics Corp.; 3379 Shore Parkway, Brooklyn, NY 11235. Resin: 75.0 grams. Catalyst: 13.5 grams.

(b) Fine grained tungsten powder (Atlantic Equipment Engineers; Catalog WP 355). Weight: 250 grams.

The curing cycle for this mixture was 2 hours at 100°C followed by 4 hours at 150°C.

Test Capsules A, B and C each contained a specimen comprised of a fragment of lead metaniobate piezoceramic adhesively bonded with electrically conductive epoxy to a 1/2-inch cube made of the above specified tungsten-filled Duralco 700 epoxy.

2. Potting Materials

Test Capsules A, B and C each contained a 1/2-inch cubical sample of each of the high temperature epoxy potting materials described below.

2.1 Stycast 2762 FT

Stycast 2762 FT high-temperature epoxy as supplied by Emerson & Cuming, Inc. Resin: 100.0 grams. Catalyst #17: 10.0 grams. The curing cycle is 2 hours at 100°C followed by 4 hours at 150°C.

2.2 Duralco 700

Duralco 700 high-temperature epoxy as supplied by Cotronics Corp. Resin: 75.0 grams. Catalyst: 13.5 grams. The curing cycle is 2 hours at 100°C followed by 4 hours at 150°C.

3. Insulated Wire Specimens

Test Capsules A, B and C each contained a sample of each of the following types of high temperature insulated wire.

3.1 Mica Glass Insulated Nickel Wire

Continental/Anaconda Type MG-300-22 No. 22 AWG solid nickel wire with mica glass insulation (gray colored insulation).

3.2 Silicon Dioxide Insulated Nickel Wire

Gulton Duroflex I No. 22 AWG solid nickel wire with silicon dioxide fiber insulation (white colored insulation).

Comment: It should be noted that when this wire is cut, the braided fibrous insulation always flares out in the region of the cut.

3.3 TFE Teflon Insulated Copper Wire

Type EE TFE Teflon insulated No. 22 AWG 7 x 30 stranded copper hookup wire as supplied by Belden Wire Company.

3.4 Silicon Dioxide Insulated Nickel Wire with Termini-Constrained Insulation

Gulton Duroflex I No. 22 AWG solid nickel wire with silicon dioxide fiber insulation (white colored insulation).

Comment: The insulation near the termini of each wire sample was constrained with a 5- to -7 turn wrap of 304 stainless steel wire prior to cutting so as to prevent flare-out.

3.5 FEP Teflon Insulated Copper Wire

FEP Teflon insulated No. 24 AWG solid copper hookup wire as supplied by Teledyne Thermatics Corp.

Comment: It should be noted that this insulation was mistakenly though to be TFE Teflon at the time of test.

4. Window Materials

Test Capsules A, B and C were each end-sealed with the following plastic and elastomeric candidate acoustic window materials.

4.1 Kalrez Elastomer

Kalrez is an elastomeric analogue of Teflon fluorocarbon resin. By virtue of its exceptional resistance to corrosive-fluid and high-temperature environments, it extends the use of elastomers beyond traditional application limits. In some cases, it is suitable for long-term service at 500°F and intermittent service to 600°F.

Kalrez is supplied by E. I. DuPont De Nemours and Co., Inc.; Elastomer Chemicals Department, E353312; Wilmington, DE 19898.

Each test capsule was sealed at one end with a 1/16-inch thick by 1.25-inch diameter Kalrez disk.

4.2 TFE Teflon Plastic

Each test capsule was sealed at one end with a 1/16-inch thick by 1.25-inch diameter disk made of the TFE Teflon fluorocarbon resin.

5. Piezoceramic Slivers

Test Capsules A, B and C each contained three slivers of lead metaniobate piezoceramic having fired-on silver electrodes. Each sliver was encased within the individual protective cage made of 304 stainless steel screening.

Comment: These samples were used for testing the individual survivability of the fired-on silver electrodes.

6. Inert Solid Filler Material

Test Capsules A, B and C each contained a large quantity of inert solid filler material in addition to the solid materials and components being tested. The purpose of this filler was to minimize the volume of contained oil, and thereby minimize the chance of window rupture due to thermal expansion of the oil.

The filler material used was T-61, 14-28 mesh, Tabular Alumina as supplied by the Aluminum Company of America.

Test Capsule D, which was permitted to free flood to the autoclave liquid environment, contained the candidate plastic potting and encapsulating materials described below.

1.0 Potting Materials

Test Capsule D contained a 1/2-inch cubical sample of each of the following high temperature epoxy potting materials: Stycast 2762 FT; and Duralco 700. The recipes and curing cycles for these samples were identical to those of their duplicates that went into capsules A, B and C.

2.0 Vespel Coupon Samples

Vespel is a high-temperature polyimide resin supplied by E. I. Dupont De Nemours and Co. of Wilmington, DE.

Test Capsule D contained two 1/2-inch by 1/2-inch by 27/32-inch Vespel coupon samples.

3.0 Vespel Block Sample

Test Capsule D contained a single 1/2-inch by 1/2-inch by 27/32-inch Vespel block sample.

4.0 TFE Teflong Coupon Samples

Test Capsules D contained two 1/16-inch by 1/16-inch by 27/32-inch TFE Teflon Coupon samples.

II. AUTOCLAVE TEST DESCRIPTION

The autoclave test was carried out from 10 January 1978 until 12 January 1978 by Pressure Chemical Company; 3419 Smallman Street; Pittsburgh, PA 15201. Work was performed in accordance with Technical Requirements Description No. ST-001, Revision A, Autoclave Test Plan (see end of this Appendix) and the following two specific items: (1) at the discretion of Westinghouse Electric Corporation, any phase of the contracted testing may be witnessed by Westinghouse personnel; and (2) Westinghouse shall supply 0.040-inch diameter Monel 400 wire in lieu of the 0.035-inch 304 stainless steel wire called out in Sections 3.4 and 4.1 of ST-001, Revision A.

Conformance of both the autoclave test and resultant test data to the requirements of ST-001, Revision A, is reviewed below. The format followed is to first cite a specific section of ST-001, Revision A, and then to describe what was done in accordance with the cited section.

With reference to section 4.1, the four test capsules were fastened to the outside surface of the autoclave's internal cooling coil using 0.040-inch diameter Monel 400 wire. The test capsules were positioned to be 2-1/2-inches below the autoclave liquid level while undergoing test. Photographs of the mounted test capsules appear in Figures 2-3.

The following comments pertain to Section 4.2.

(a) The deionized water was deaerated for 24-hours with nitrogen prior to use.

(b) Prior to pressurized leak testing of the autoclave system, the specified autoclave-liquid ingredients were charged to the autoclave with the exception of the $Na_2S \cdot 9\ H_2O$ and a small amount of water. The ingredients were charged under an argon gaseous blanket and an argon-gas liquid purge. Following charging, the solution was purged with argon for an additional 30-minutes after which the autoclave head was fastened into place while the argon atmosphere was still maintained.

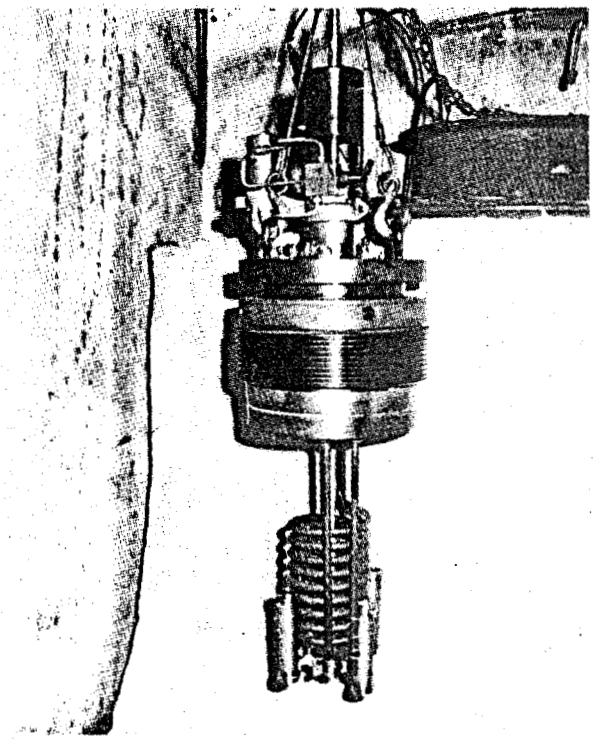

Fig. 2. Test Capsules Fastened to Autoclave Cooling Coil

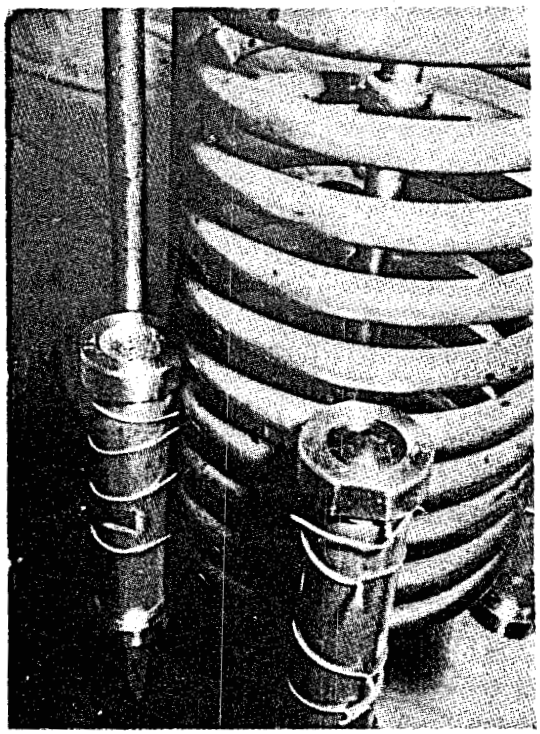

Fig. 3. Test Capsules Fastened to Autoclave Cooling Coil.

Foreground: Top view of Test Capsule C showing Kalrez window.

Background: Free-flooding Test Capsule D

(c) The autoclave system was slowly pressurized to 6000 psig over a 2-1/2-hour period, held at 6000 psig for 1/2-hour, and then depressurized. Since no pressure drops were observed during the 1/2-hour hold period, the autoclave seal was pronounced to be satisfactory.

(d) Following the pressure test, the $Na_2S \cdot 9H_2O$ was dissolved in the remaining small amount of water, and the solution was poured into the depressurized autoclave via a small add-port. This solution was also prepared and charged under an argon gaseous blanket.

With reference to Section 4.3, the volume of the autoclave liquid was 22,902 milliliters and the volume of the autoclave cover gas was 10,743 milliliters.

With reference to Section 4.4, the pre-test pH of the autoclave liquid was 4.8 at 22°C (71.60°F).

The following comments pertain to Section 4.5.

(a) The temperature of the autoclave-liquid system was first slowly raised to 250°F during an overnight period of 12-hours, whie the pressure was maintained at 100 psig.

(b) The temperature of the autoclave-liquid system was next raised to 523°F over a 7-hour period, during which time the autoclave liquid was continuously stirred. During this time the autoclave pressure had risen of its own accord from 100 to 1200 psig.

(c) With the autoclave fluid temperature at 523°F, argon gas was used to increase pressure from 1200 to 7000 psig. The total elapsed time from the start of initial heating to the attainment of 523°F, 7000 psig test conditions was 19-hours.

The following comments pertain to Section 4.6.

(a) The first three hours of this phase of testing can best be described as a test-condition stabilization period. During

this time the pressure recording showed a mean of 6,801.33 psig and a standard deviation of 259.99 psig, while the temperature recording showed a mean of 512.64°F and a standard deviation of 6.41°F.

(b) The last 14-1/2-hours of this phase of testing can be described as being the specified test period itself. During this time the pressure recording showed a mean of 6,989.05 psig and a standard deviation of 39.95 psig, while the temperature recording showed a mean of 523.59°F and a standard deviation of 2.27°F.

With reference to Section 4.7, the total time for the test-condition removal phase was 5-1/2-hours.

With reference to Section 4.8, the post-test pH of the autoclave liquid was 3.9 at 80°F.

The following comments pertain to Section 5.1.

(a) Prior to the start of testing, the primary instrument thermocouple was calibrated in an oil bath at 527°F against a standard thermometer. The thermocouple accuracy was determined to be $\pm$ 2°F at 527°F. Since the autoclave liquid was continuously stirred during the test, the accuracy with which temperature was measured is therefore $\pm$ 2°F (E = 2°F).

(b) During the specified test period, the temperature recording showed a mean of 523.59°F and a standard deviation of 2.27°F (σ = 2.27°F). Since 99.7 percent of all data lies within $\pm$ 3σ of the mean, the steadiness with which temperature was maintained during the specified test period was $\pm$ 6.81°F (3σ = 6.81°F).

(c) The precision with which temperature was both known and maintained during the specified test period can be taken as being equal to the sum-of-the-squares of both the temperature-measurement accuracy and the temperature-data steadiness, i.e.

$$\pm A = \pm\sqrt{(E)^2 + (3\sigma)^2}$$

$$= \pm 7.10^{\circ}F.$$

(d) The autoclave-liquid temperature during the specified test period can therefore be descirbed as having a mean of 523.59°F and of being maintained within a precision of ± 7.10°F.

(e) Prior to the start of testing, the autoclave's pressure transmitter was calibrated against a Heise Bourdon-tube pressure gage having an accuracy of ± 30 psig. The accuracy with which pressure was measured is therefore ± 30 psig (E = 30 psig).

(f) During the specified test period, the pressure recording showed a mean of 6,989.05 psig and a standard deviation of 39.95 psig (σ = 39.95 psig). Since 99.7 percent of all data lies within ± 3σ of the mean, the steadiness with which pressure was maintained during the specified test period was ± 119.85 psig (3σ = 119.85 psig).

(g) The precision with which pressure was both known and maintained during the specified test period can be taken as being equal to the sum-of-the-squares of both the pressure-measurement accuracy and the pressure-data steadiness, i.e.,

$$\pm A = \pm\sqrt{(E)^2 + (3\sigma)^2}$$

$$+ \pm 123.55 \text{ psig.}$$

(h) The autoclave pressure during the specified tes period can therefore be described as having a mean of 6,989.05 psig and of being maintained within a precision of ± 123.55 psig.

With reference to Section 5.2, the pre-test pH was 4.8 at 22°C (71.60°F) and the post-test pH was 3.9 at 80°F.

With reference to Section 5.3, the liquid volume was 22,902 milliliters and the gaseous volume was 10,743 milliliters.

With reference to Section 5.4, the pre-test room ambient temperature was 64°F and the post-test room ambient temperature was also 64°F.

III. Post-test Analysis of Materials and Components

When the test capsules were viewed at Pressure Chemical Company at the completion of testing, it was immediately seen that all of the Kalrez window discs had failed. Post-test photographs of the mounted test capsules appear in Figures 4-5, where the failed windows are clearly seen. The TFE Teflon windows at the capsule bottoms were intact, thereby retaining the test specimens within their respective test capsules. With reference to Figures 4-5, the white colored speckling seen on both the test capsules and autoclave cooling coil is due to some tabular alumina that had washed out of the opened capsules during testing.

Following the taking of post-test in situ photographs, the test capsules were removed from the autoclave cooling coil and taken back to the Westinghouse R&D Center where an autopsy was performed. Also taken for autopsic analysis were the Kalrez window fragments that were found to be floating atop the autoclave liquid.

Figures 6-8 are photographs of the sites where the Kalrez windows had failed in Test Capsules A, B and C respectively. For comparison, a pre-test top view photo of Test Capsule A is shown in Figure 9. It should be noted that despite the fact that their Kalrez windows had failed, all three test capsules appeared at this time to have retained a sizable amount of their respective test oils.

The top portion of the Figure 10 photograph shows the Kalrez window fragments that were fished out of the autoclave liquid, while the bottom portion shows an untested and undamaged Kalrez window for comparison. It was found to be impossible to identify any of these fragments with a specific test capsule.

All of the Kalrez window fragments were severely bloated (swelling) at the time of their retrieval from the autoclave liquid, as can be seen from the edge-view photo of a fragment shown in Figure 11. Although most of the fragments were intially almost double their original thickness, nearly all contracted to about a 12-percent thickness increase upon subsequent cleaning. Some of the cleaned fragments had a puffy appearance and were very compliant when prodded.

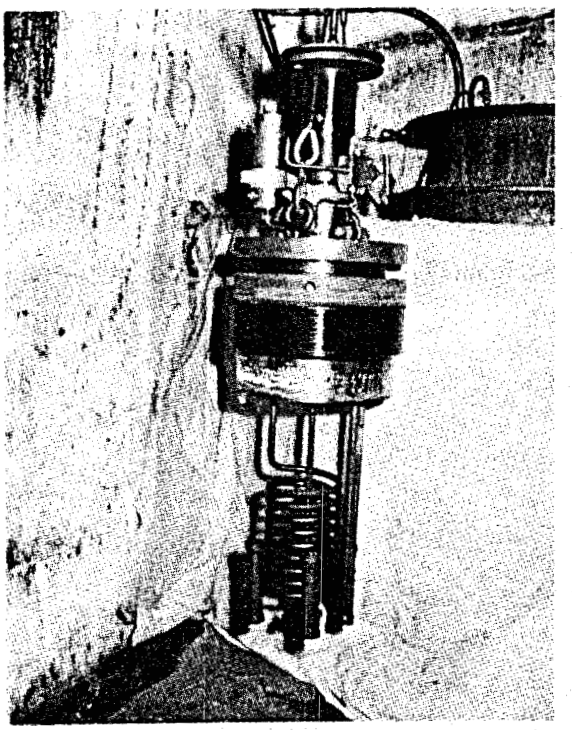

Fig. 4. Post-test Photograph of Test Capsules Fastened to Autoclave Cooling Coil

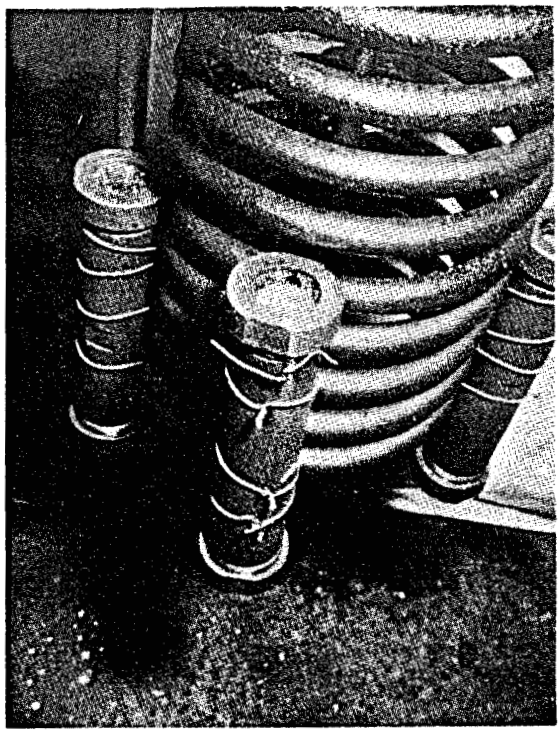

Fig. 5. Post-test Photograph of Test Capsules Fastened to Autoclave Cooling Coil

Foreground: Top view of Test Capsule C showing failed Kalrez window.

Background: Free-flooding Test Capsule D.

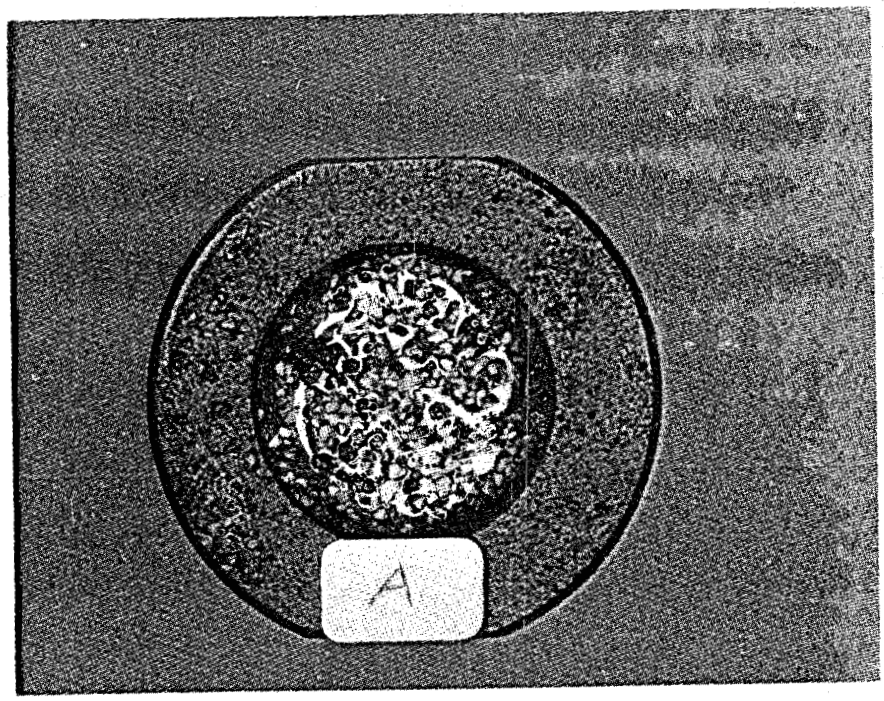

Fig. 6. Top view of Test Capsule A showing where Kalrez window had failed.

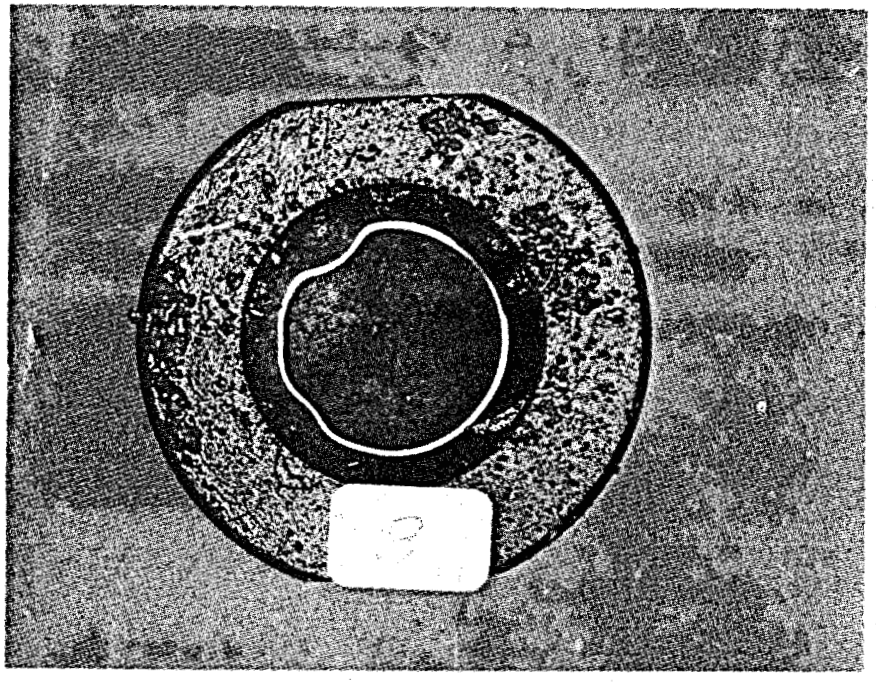

Fig. 7. Top view of Test Capsule B showing where Kalrez window had failed.

Note: Flashtube reflection off the oil meniscus is shown as a ring-like feature in the photograph.

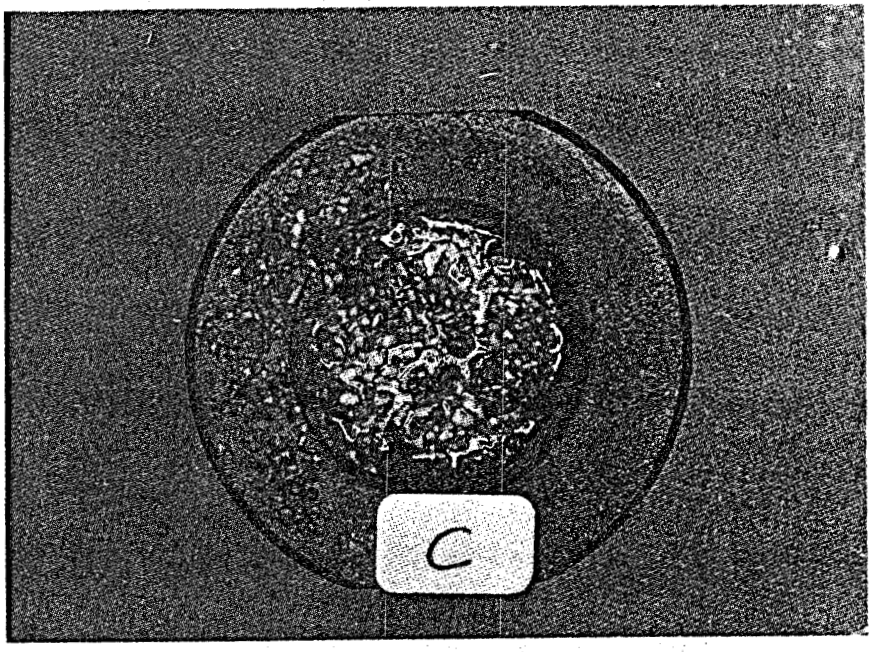

Fig. 8. Top view of Test Capsule C showing where Kalrez window had failed.

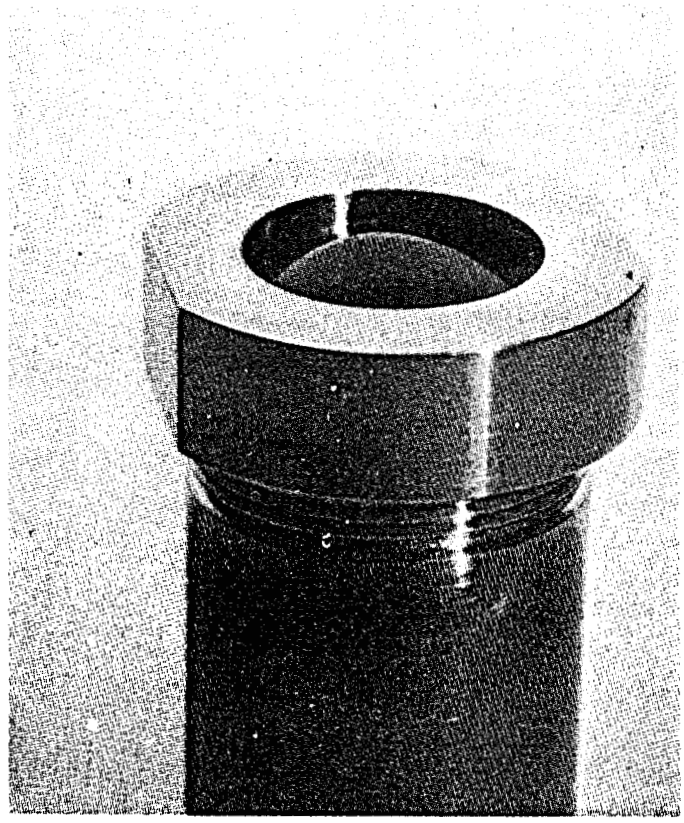

Fig. 9. Pre-test photograph of Test Capsule A showing intact Kalrez window.

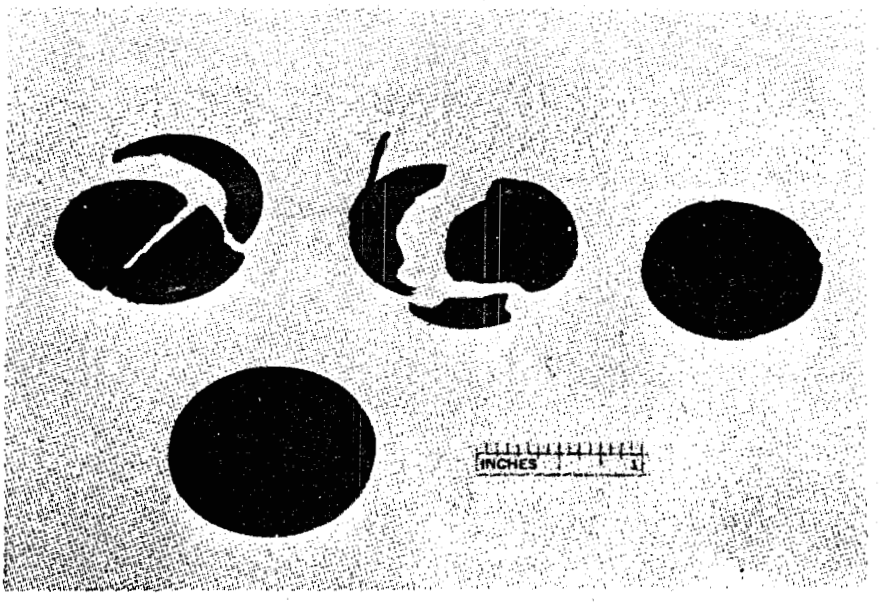

Fig. 10. Top: Fragments of the three Kalrez windows that had failed.

Bottom: Untested and undamaged Kalrez window.

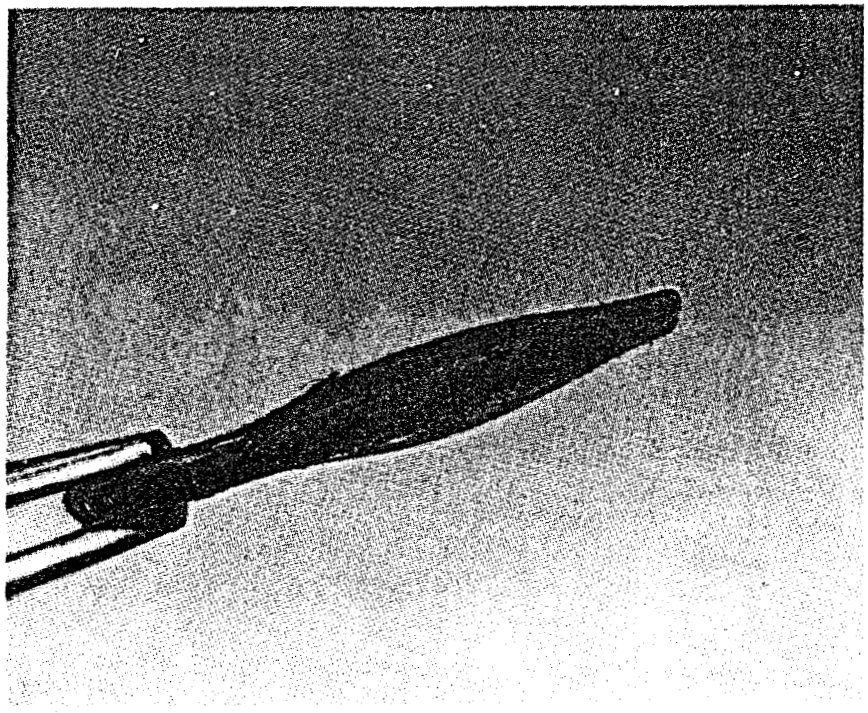

Fig. 11. Edge view of failed and bloated Kalrez window.

The mechanism by which the Kalrez windows failed could not be readily determined from the test results. Although failure can be described as the tearing of Kalrez material, it isn't clear whether this tearing was caused by test oil expansion, Kalrez swelling in the autoclave liquid test environment or a synergistic combination of both mechanisms.

Test Capsules A, B and C were next emptied of their contents. At this point these contents could best be described as sludge comprised of specified test components, tabular alumina and oil. With reference to Test Capsules B and C, the individual test components were clearly identifiable within the sludge and they along with the tabular alumina were uniformly coated with silicone oil. The tabular alumina of Test Capsule D, however, was not uniformly coated with oil and contained relatively large black lumps that probably comprised coagulated Mobil Jet Oil II, dissolved epoxy residue and badly decomposed remnants of the epoxy test components.

The individual test components from Test Capsules A, B and C were next cleaned up and examined for damage. Post-test photographs of these components appear in Figures 12-17. The condition of these components will now be described with the exception of the Kalrez windows which were discussed near the beginning of this section.

Candidate Solid Material and Component Assortment for Test Capsules A, B and C

1. Rudimentary Piezoceramic Transducer Assemblies

1.1 Tungsten-filled Alumina Cement Transducer Backing Material

This specimen emerged from the test in fairly good condition for Test Capsules A, B and C. Although coated with a hydrocarbon residue, the cube retained both its shape and dimensions fairly well. The piezoceramic element remained firmly bonded to the cube, indicating that the Epo-Tek H20E electrically conductive epoxy is satisfactory even under failed window conditions. When prodded with a pair of tweezers, the piezoceramic's fired-on outer silver electrode remained firmly adherent; however, the Epo-Tek H20E had hardened somewhat from its original consistency.

This element is shown at the extreme left in Figures 12, 14 and 16.

1.2 Tungsten-filled Stycast 2762FT

This element completely disintegrated in the Mobil Jet Oil II environment of Test Capsule A. With reference to Test Capsules B and C, the relative ease with which material could be scraped off of the cube's surface showed that the Stycast 2762FT had undergone both embrittlement and partial decomposition.

This element appears second from the left in Figures 14 and 16.

1.3 Tungsten-filled Duralco 700 Epoxy

This element completely disintegrated in Test Capsule A, and became both embrittled and partially decomposed in Test Capsules B and C.

This element appears third from the left in Figures 14 and 16.

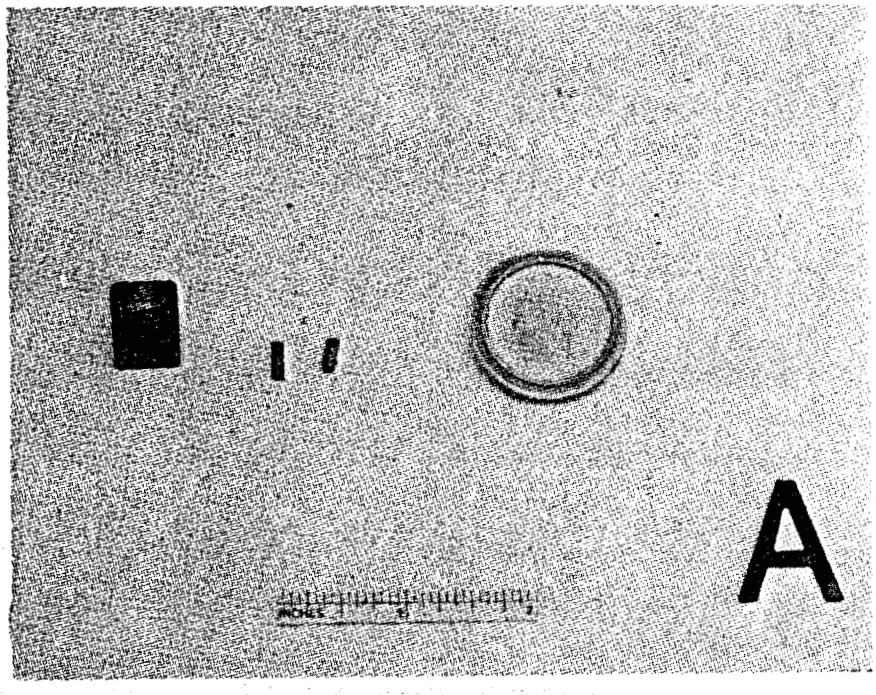

Fig. 12. Post-test Photograph of Test Capsule A Contents with Exclusion of Wire Samples

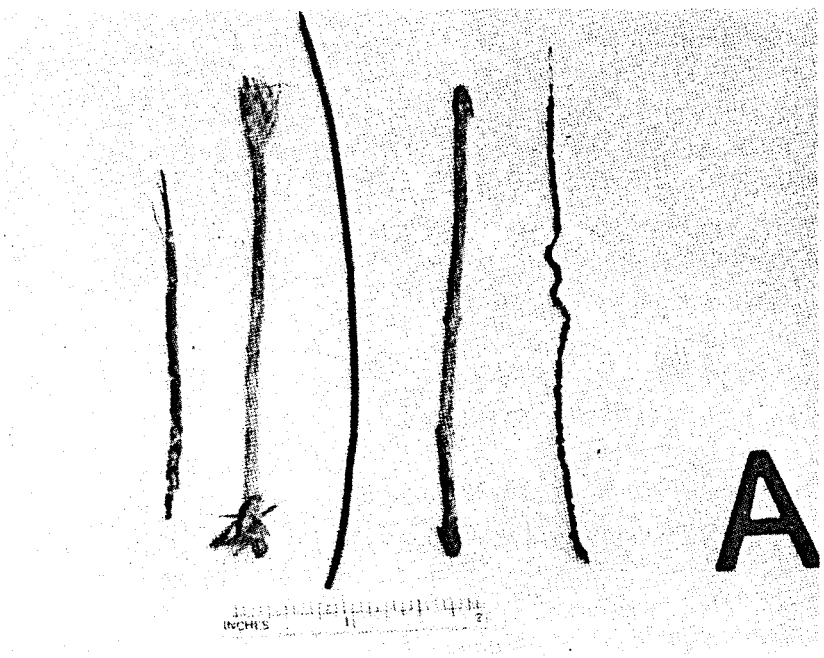

Fig. 13. Post-test Photograph of Test Capsule A Wire Samples

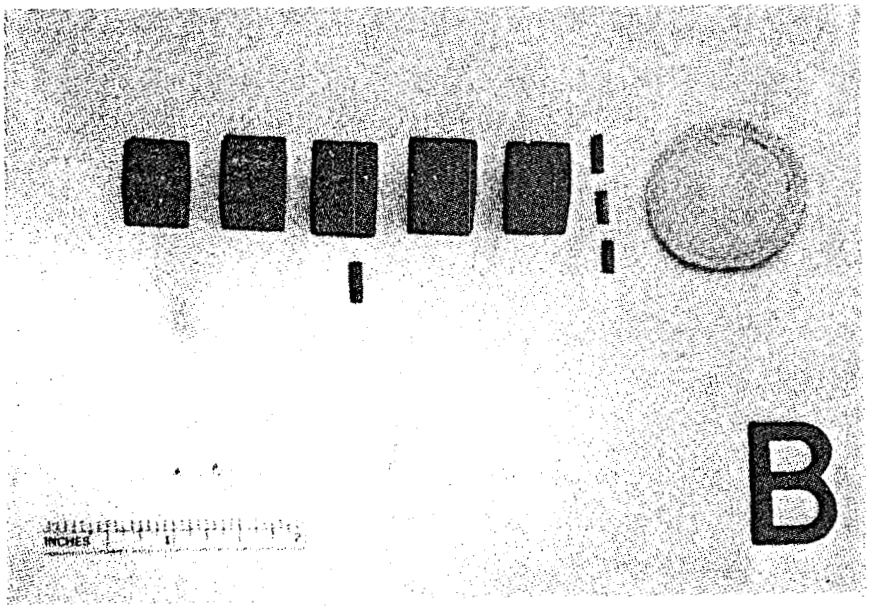

Fig. 14. Post-test Photograph of Test Capsule B Contents with Exclusion of Wire Samples

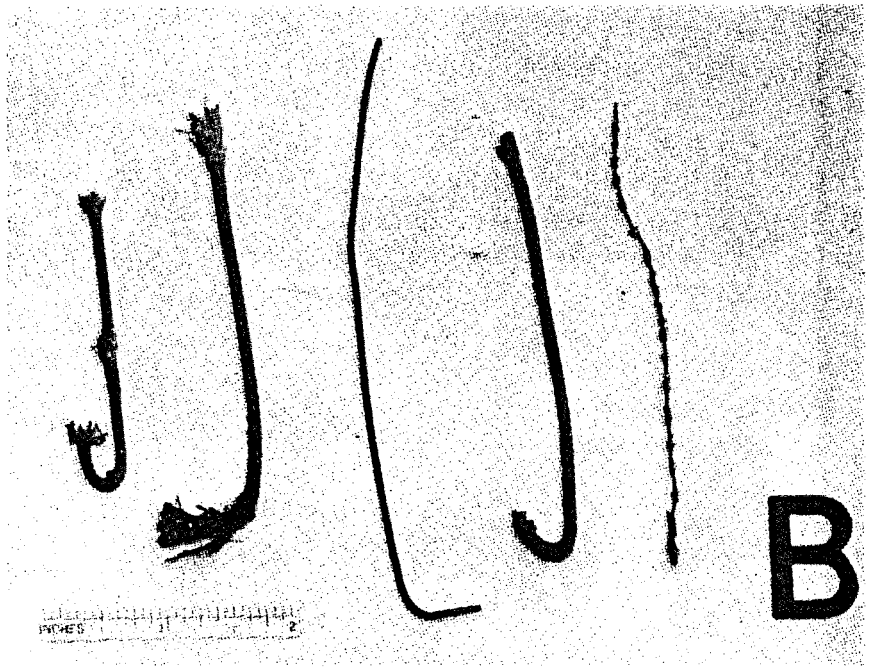

Fig. 15. Post-test Photograph of Test Capsule B Wire Samples

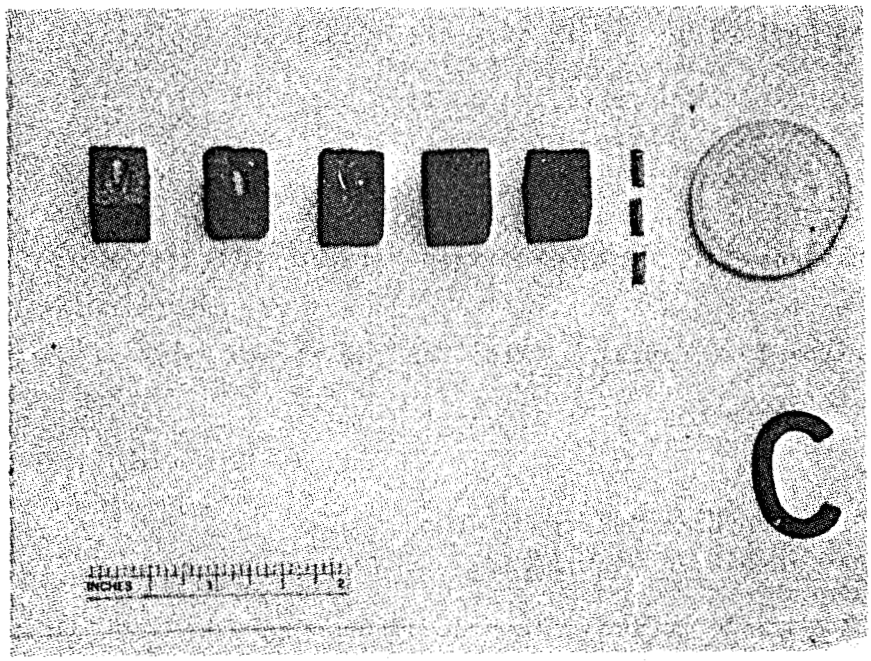

Fig. 16. Post-test Photograph of Test Capsule C Contents with Exclusion of Wire Samples

2. Potting Materials

2.1 Stycast 2762FT

This element completely disintegrated in Test Capsule A, and became both embrittled and partially decomposed in Test Capsules B and C. The element from Test Capsule B also had relatively large surface cracks, indicating that the Dow Corning DC-210H silicone oil of Test Capsule B may be more reactive and less protective than the Dow Corning DC-550 high-phenyl silicone oil of Test Capsule C.

This element appears fourth from the left in Figures 14 and 16.

2.2 Duralco 700

This element completely disintegrated in Test Capsule A, and became both embrittled and patially decomposed in Test Capsules B and C. The element from Test Capsule B also had relatively large surface cracks.

This element appears fifth from the left in Figures 14 and 16.

3. Insulated Wire Specimens

3.1 Mica Glass Insulated Nickel Wire

This sample became highly decomposed in the Mobil Jet Oil II environment of Test Capsule A. The insulation of the sample from Capsule B was coated with hydrocarbon residue, whereas the sample from Test Capsule C survived in best shape.

This element is shown at the extreme left in Figures 13, 15 and 17.

3.2 Silicon Dioxide Insulated Nickel Wire

This sample survived fairly well in Test Capsules A, B and C. However, the sample from Test Capsule B was coated with a hydrocarbon residue.

This element appears second from the left in Figures 13, 15 and 17.

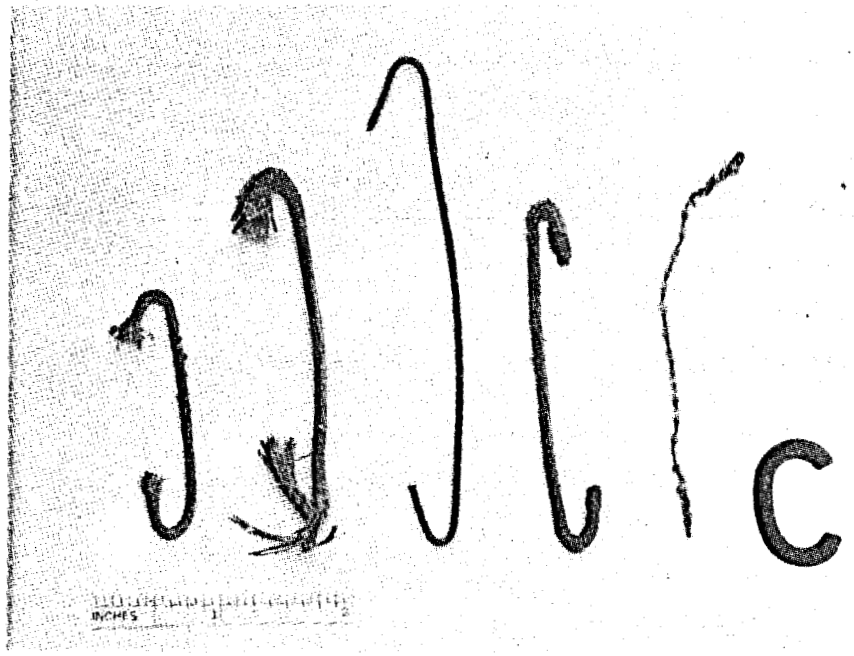

Fig. 17. Post-test Photograph of Test Capsule C Wire Samples

3.3 TFE Teflon Insulated Wire

This specimen emerged from the test in very good condition for Test Capsules A, B and C. No coating of hydrocarbon residue was observed. Aside from some unexplained shortening at both ends, the stranded copper wire showed no signs of damage. The shortening may be attributed to the Teflon having been stretched beyond the wire terminus during the wire-snipping oepration.

This element appears third from the left in Figures 13, 15 and 17.

3.4 Silicon Dioxide Insulated Nickel Wire with Termini-Cosntrained Insulation

This sample survived fairly well in Test Capsules A, B and C. However, the sample from Test Capsule B was coated with a hydrocarbon residue.

This element appears fourth from the left in Figures 13, 15 and 17.

3.5 FEP Teflon Insulated Copper Wire

This wire specimen emerged from all three test capsules in very poor shape. The FEP Teflon insulaion was completely disintegrated.

This element appears to the extreme right in Figures 13, 15 and 17.

4. Window Materials

4.1 Kalrez Elastomer

The condition of the Kalrez windows was previously discussed at the beginning of this section.

4.2 TFE Teflon Plastic

The TFE Teflon window was found to be in fairly good condition from Test Capsules A, B and C. Although somewhat deformed structurally, these disks showed no signs of either embrittlement or of having been chemically attacked. With reference to the structural deformation, the disk's formerly flat surfaces had dimpled into a spherical contour. There was visible evidence of material flow in the region of the seal.

The element appears to the extreme right in Figures 12, 14 and 16.

5. Piezoceramic Slivers

The piezoceramic slivers from all three test capsules were found to be structurally intact. However, the fired-on silver electrodes showed various signs of chemical attack that ranged from mild pitting to complete electrode separation. This is assumed due to window failure and admission of autoclave fluid.

These elements appear second from the right, as a group of three, in Figures 12, 14 and 16.

Finally, the contents of free-flooding Test Capsule D were emptied. With reference to the Figure 18 photograph of these contents, the TFE Teflon coupons appear as the two upper left-most objects, the Duralco 700 epoxy cube appears as the upper right-most object, the Vespel block appears as the one remaining upper object, and the Vespel coupons appear as the only two lower objects. The Stycast 2762FT epoxy cube was totally disintegrated and dissolved during the test.

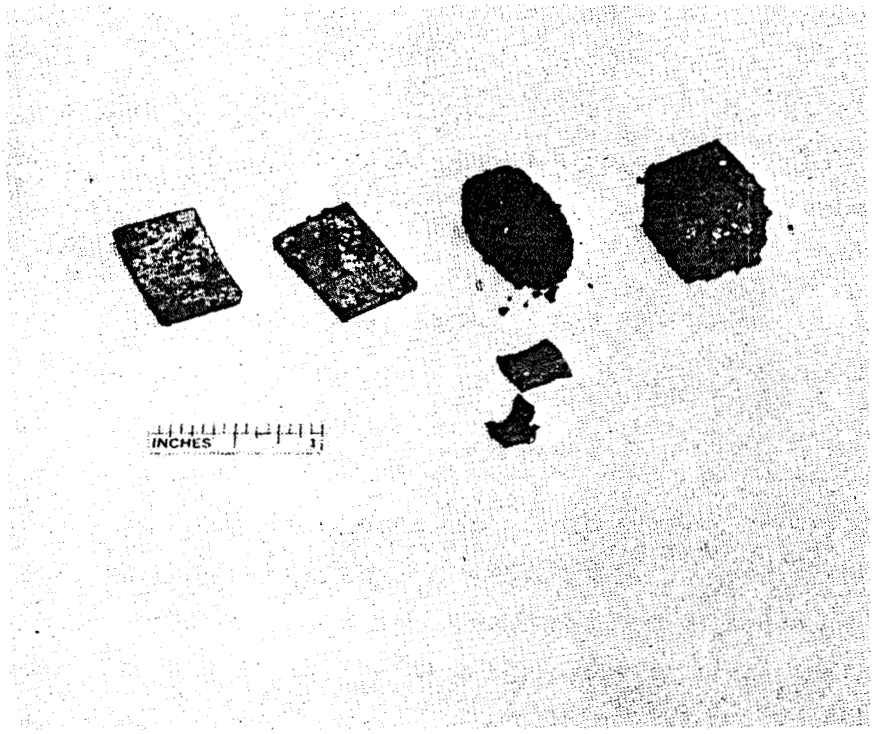

Fig. 18. Post-test Photograph of Test Capsule D Contents

Aside from being coated with a hydrocarbon residue, the TFE Teflon coupon samples showed little sign of damage. After being cleaned of this residue and inspected, it was observed that their mean length had increased from 0.8603-inch to 0.8660-inch, their mean width had increased from 0.5320-inch to 0.5375-inch, and their mean thickness remained constant at 0.067-inch. The coupons were easily flexed and didn't appear to be embrittled.

Although still structurally intact, the Duralco 700 epoxy cube was embrittled. It was very easy to prod surface material loose with a pair of tweezers.

Both the block and coupon samples of Vespel polyimide resin were highly embrittled and decomposed. Embrittlement was such that only slight pressure was sufficient to fracture the material. The bottom portion of Figure 19 shows the embrittled and decomposed Vespel samples, while the top portion shows untested and undamaged samples for comparison.

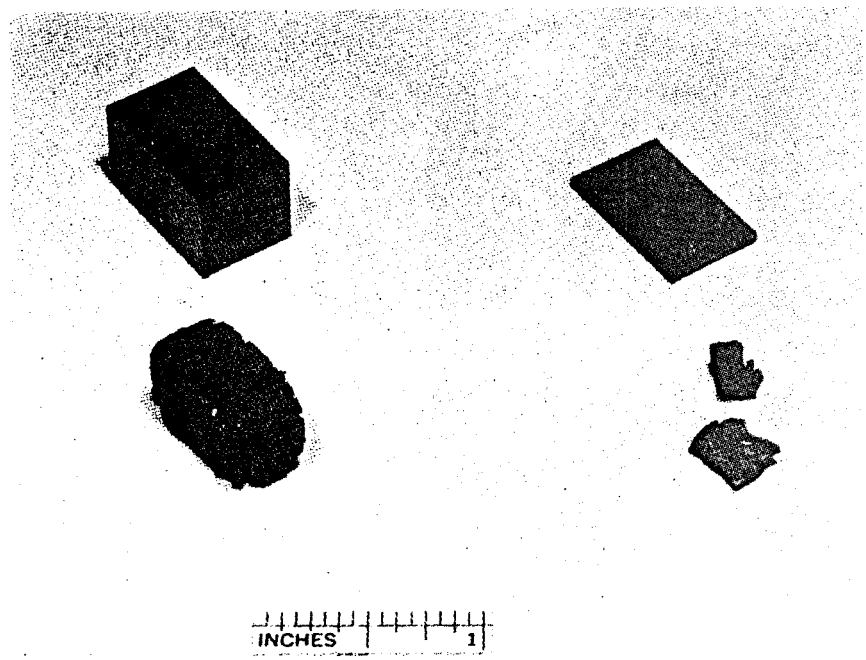

Figure 2.3 — Top: Untested (control) block and coupon samples of Vespel.
Bottom: Vespel block and coupon samples after autoclave testing.

SCREENING TEST NO. 2

I. Candidate Materials and Components

Five 316 stainless steel test capsules were used. Each capsule was 6-1/4-inch long and comprised a 6-inch length of 1-inch Schedule 80 pipe fitted with two 1-5/8-inch diameter tubular end caps. Four of the capsules had their ends sealed with TFE Teflon candidate plastic window material, and eveloped candidate high temperature oils along with sundry candidate transducer material and component samples. These capsules were designated as A, B, C and E. The fifth capsule was permitted to free flood to the autoclave liquid environment and contained a different assortment of candidate material and component samples. This capsule was designated as D

A pre-test photograph of Test Capsules A and B is shown in Figure 1, with Capsule A on the left and Capsule B on the right. Likewise, a pre-test photograph of Test Capsules E and C is shown as Figure 2, with Capsule E on the left and Capsule C on the right. Capsules A, B and C are blackened because they were used in the first autoclave screening test, whereas Capsule E is shiny because it was newly fabricated for this second autoclave test.

Test Capsules A, B, C and E each had an identical assortment of candidate solid materials and components, and differed only in the type of high temperature oil enveloped. Capsule A had Mobil Jet Oil II, Capsule B had Dow Corning DC-210H silicone oil, Capsule C had Dow Corning DC-550 high-phenyl silicone oil. A description of the candidate solid material and component assortment is given below.

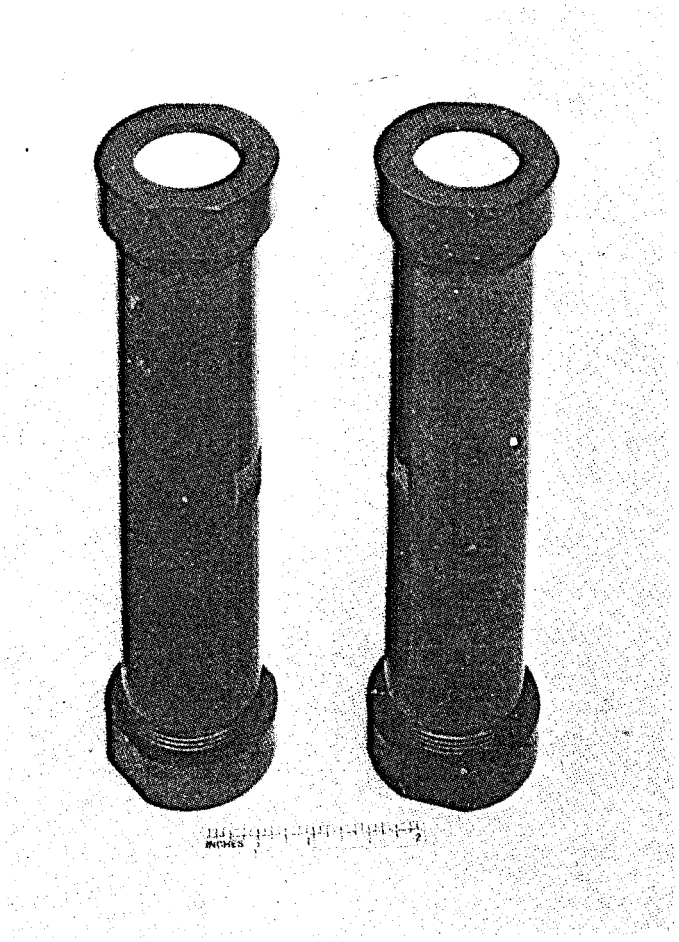

Figure 1. Pre-test Photograph of Test Capsules A and B.
Right: Test Capsule B.
Left: Test Capsule A.

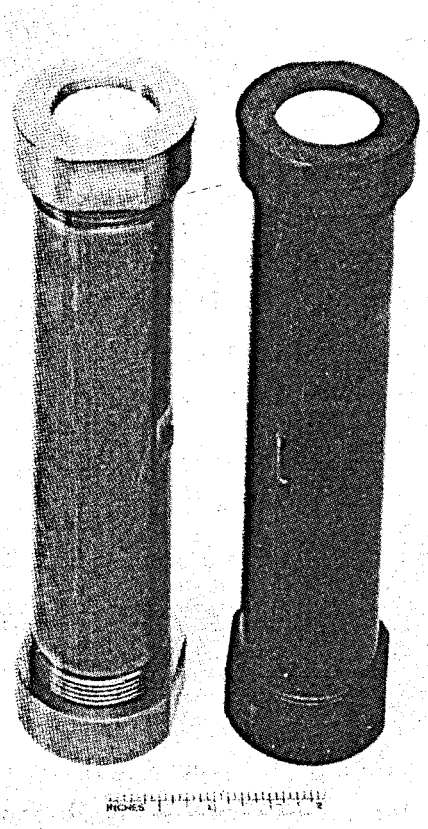

Figure 2. Pre-test Photograph of Test Capsules E and C.
Right: Test Capsule C.
Left: Test Capsule E.

Candidate Solid Material and Component Assortment for Test Capsules A, B, C and E

1. Rudimentary Peizoceramic Transducer Assembly

The assembly consisted of a fragment of thin silver-electroded lead metaniobate piezoceramic adhesively bonded with high temperature electrically conductive epoxy to a 3/8-inch cube of tungsten-filled-cement candidate transducer backing material.

The lead metaniobate piezoceramic had a thickness resonant frequency of 2.0 MHz and was K81 material as supplied by Keramos, Inc.; 104 North Church Street; Lizton, IN 46149. The high temperature electrically conductive epoxy was Epo-Tek H20E as supplied by Epoxy Technology, Inc.; 65 Grove Street; Watertown, MA 02172.

The tungsten-filled high-alumina cement candidate transducer backing material was fabricated by the Westinghouse R&D Ceramics and Glasses Group. The nominal batch formula for this material is as follows:

(a) Alcoa Calcium Aluminate Cement CA-25. (High Alumina cement manufactured by the Aluminum Company of America.) Weight: 24.0 grams.

(b) Harbison-Walker GP-71 Fused Silica Powder. (Fine grained fused silica powder manufactured by Glasrock Products Group; Harbison-Walker Refractories; Division of Dressen Industries, Inc.) Weight: 18.0 grams.

(c) Fine Grained Tungsten Powder. (Tungsten metal powder as manufactured by Atlantic Equipment Engineers of Bergenfield, New Jersey; Catalog No. WP355; 100 mesh crystalline tungsten metal powder.) Weight: 220.0 grams.

(d) Water. Weight: 20.0 grams.

Test Capsules A, B, C and E each contained one rudimentary piezoceramic transducer assembly as described above.

2. Potting Materials

Test Capsules A, B, C and E each contained an 11/32-inch by 11/32-inch by 1/2-inch rectangular parallelpiped sample of each of the high temperature epoxy potting materials described below.

2.1 Stycast 2762FT

Stycast 2762FT high-temperature epoxy as supplied by Emerson & Cuming, Inc.; Canton, MA 02021. Resin: 100.0 grams. Catalyst #17: 10.0 grams. The curing cycle is 2 hours at 100°C followed by 4 hours at 150°C.

2.2 Duralco 700

Duralco 700 high-temperature epoxy as supplied by Cotronics Corp.; 3370 Shore Parkway; Brooklyn, NY 11235. Resin: 75.0 grams. Catalyst: 13.5 grams. The curing cycle is 2 hours at 100°C followed by 4 hours at 150°C.

3. Hookup Wire

Test Capsules A, B, C and E each contained a 5-inch length of Type EE TFE Teflon insulated No. 22 AWG 7X30 stranded copper hookup wire as supplied by Belden Wire Company.

In preparing these specimens, care was taken to assure that the TFE Teflon insulation was flush with the copper-wire termini.

4. TFE Teflon Windows

Test Capsules A, B, C and E were each end-sealed with 1/16-inch thick by 1.25-inch diameter disks made of TFE Teflon fluorocarbon resin. Each capsule required two disks; one for each capsule end.

5. Material Coupons

5.1 TFE Teflon

Test Capsules A, B, C and E each contained a 1/16-inch by 1/2-inch by 1-inch rectangular parallelepiped coupon sample of TFE Teflon fluorocarbon resin.

5.2 Type 304 Stainless Steel

Test Capsules A, B, C and E each contained a 0.031-inch by 1/2-inch by 1-inch rectangular parallelepiped coupon sample of Type 304 stainless steel.

6. Inert Solid Filler Material

Test Capsules A, B, C and E each contained a large quantity of inert solid filler material in addition to the solid materials and components being tested. The purpose of this filler was to minimize the volume of contained oil, and thereby minimize the chance of window rupture due to thermal expansion of the oil.

The filler material used was T-61, 14-28 mesh, Tabular Alumina as supplied by the Aluminum Company of America.

The following specific tasks were performed during the preparation and filling of Test Capsules A, B, C and E for this second autoclave test.

(a) With reference to Test Capsules A, B and C which were previously used during the first autoclave test, the sealing surfaces at their tubular-body termini were remachined so as to assure good sealing when compressed against the TFE Teflon windows.

(b) Vacuum was used as an aid when filling each test capsule with oil so as to assure gas purgation. The volume of oil actually absorbed within each test capsule was monitored and recorded as follows:

Test Capsules A:	40.0 milliliters (+0, -2.0 ml).
Test Capsule B:	35.0 milliliters (+0, -2.0 ml).
Test Capsule C:	35.0 milliliters (+0, -2.0 ml)
Test Capsule D:	35.0 milliliters (+0, -2.0 ml)

(c) Each TFE Teflon window was affixed in the following manner: (a) the tubular cylinder was topped up with oil so as to form a convex meniscus; (b) the TFE Teflon window was placed atop the oil meniscus; (c) the TFE Teflon window was loosely attached to the tabular cylinder with an end cap to the point where the window began to compress slightly; (d) the end cap was firmly tightened to the tubular cylinder with the aid of a wrench. It was observed that all end caps were revolved by about 1/8-turn during the wrench-tightening operation.

(d) Vacuum was pulled on all four assembled test capsules so as to assure the integrity of the Teflon-to-metal end seals. It was observed that all seals were secure.

Test Capsule D, which was permitted to free flood to the autoclave liquid environment, contained the candidate material and component samples described below.

Candidate Material and Component Assortment for Free-Flooding Test Capsules D

1. High-Temperature Elastomeric Materials

1.1 Kalrez

Kalrez is an elastomeric analogue of Teflon fluorocarbon resin. By virtue of its exceptional resistance to corrosive-fluid and high-temprature environments, it extends the use of elastomers beyond traditional application limits. It is suitable for long-term service at 500 to 500°F and intermittent service to 600°F.

Kalrez is supplied by E. I. DuPont De Nemours and Co.; Inc.; Elastomer Chemical Department, E343312; Wilmington, DE 19898.

Test Capsule D contained two 1/16-inch by 1/2-inch by 1-inch coupon samples of Vespel.

1.2 AFLAS-150

AFLAS-150 is a fluorinated elastomer, based on tetrafluoroethylene-propylene copolymer, that possesses outstanding thermal and chemical stability. AFLAS-150 has been used continuously at temperatures to 200°C (329°F), and intermittently at temperatures to 300°C (572°F).

AFLAS-150 is supplied by Asahi Glass Co., Ltd; 1-2, Marunouchi 2 Chome; Chiyoda-Ku, Tokyo, Japan.

Test Capsule D contained two 0.132-inch by 3/4-inch by 3/4-inch coupon samples of AFLAS-150.

1.3 Ethylene Propylene

Ethylene propylene elastomer possesses good thermal and chemical stability. It can be used continuously at temperatures to 350°C.

A test sample was obtained from Seals Eastern, Inc.; 134 Pearl Street; Red Bank, NJ 07724.

Test capsule D contained two 1/16-inch by 3/8-inch by 2-inch coupon samples of ethylene propylene.

1.4 Phosphonitrilic Fluoroelastomer

Firestone PNF compound R-210818 phosphonitrilic fluoroelastomer is a semi-inorganic rubber having good thermal and chemical stability. It can be used continuously at temperatures to 300°F.

A sample of PNF compound R-210818 was obtained for testing from the Phosphazene Marketing Group; The Firestone Tire and Rubber Company; 1200 Firestone Parkway; Akron, OH 44317.

Test Capsule D contained two 0.050-inch by 3/8-inch by 1-1/4-inch coupon samples of Firestone PNF compuond R-210818 phosphonitrilic fluoroelastomer.

2. Metal Coupons

2.1 Type 304 Stainless Steel

Test Capsule D contained two 0.031-inch by 1/2-inch by 1-inch coupon samples of Type 304 stainless steel.

2.2 Inconel 718

Test Capsule D contained two samples of each of the following dimensioned coupons of Inconel 718: (a) 0.003-inch by 3/8-inch by 1-inch; (b) 0.004-inch by 3/8-inch by 1-1/2-inch; (c) 0.005-inch by 3/8-inch by 2-inch.

3. High-Temperature Plastic Materials

3.1 TFE Teflon

Test Capsule D contained two 1/16-inch by 1/2-inch by 1-1/2-inch coupon samples of TFE Teflon.

3.2 Astrel 360

Astrel 360 is a high-temperature plastic made by 3M Company; 3M Center; St. Paul, MN 55101. A sample of Astrel 360 was supplied for testing through the Westinghouse Research Insulation Chemistry Group.

Test Capsule D contained two 1/8-inch by 5/16-inch by 1-1/8-inch coupon samples of Astrel 360.

3.3 Polybutadiene

Polybutadiene plastic possesses good thermal and chemical stability. It can be used continuously at temperatures to 500°F.

A sample of polybutadiene was made for testing by the Westinghouse Research Insulation Chemistry Group. This sample had an uneven nominal thickness of 1/8-inch, with the unevenness caused by a slight tilt of the mold used to cure the plastic.

Test Capsule D contained two 3/8-inch by 7/8-inch by 1/8-inch coupon samples of polybutadiene.

3.4 Graphite-Carbon-Glass Filled TFE

The addition of graphite, carbon and glass filler materials to plain TFE Teflon improves its elevated-temperature mechnical strength at the expense of some degradation in its chemical resistance and gaseous impermeability. Filled TFE Teflon of this type is used by the Bal-Seal Engineering Company in the construction of some types of high pressure mechanical seals.

A 3/4-inch diameter by 2-inch long solid right-circular cylindrical sample was obtained from the Bal-Seal Engineering Company; 17592 Sherbrook Drive; Tustin, CA 92680.

Test Capsule D contained two 3/4-inch diameter by 1/10-inch thick disk-like coupon samples of graphite-carbon-glass filled TFE Teflon.

3.5 Doryl-Glass-Mica Composite

The Westinghouse Research Insulation Chemistry Group supplied a small sheet of doryl-glass-mica composite material. This composite possess good thermal and chemical stability.

Test Capsule D contained two 1/16-inch by 3/4-inch by 7/8-inch coupon samples of doryl-glass-mica.

4. Potting Materials

Test Capsule D contained one 11/32-inch by 11/32-inch by 1/2-inch rectangular parallelpiped sample of each of the following high temperature epoxy potting materials: Stycast 2762 FT and Duralco 700. The recipes and curing cycles for these sampls were identical to those of their duplicates that went into Capsules A, B, C and E.

5. TFE Teflon Insulated Single-Conductor Copper Wire

The permeability of TFE Teflon to geothermal-environment liquids and gases is of interest. To study this phenomenon, a sample of TFE Teflon insulated single conductor silver-plated copper wire was acquired.

Test Capsule D contained two 5-inch long samples of No. 22 AWG TFE Teflon insulated single conductor silver-plated copper wire conforming to MIL-W-16878D as manufactured by Alpha Wire Products Company.

6. Bal Seal

Bal Seals are spring-loaded TFE Teflon assemblies that are intended to replace O-rings in high-temperature high-pressure chemically

corrosive application environments. Both pure and filled TFE Teflon materials are used in their construction along with sundry metallic spring materials. Bal Seals are manufactured by Bal-Seal Engineering Company; 17592 Sherbrook Drive, Tustin, CA 92680.

Test Capsule D contained one sample of each of the following Bal-Seal assemblies: (a) a light-duty reciprocating seal made of plain TFE Teflon with stainless steel spring; and (b) a light-duty reciprocating seal made of grahite-filled TFE Teflon with stainless steel spring.

In addition to the materials and components that were tested while contained within Test Capsules A, B, C, D and E, the components described below were tested while directly exposed to the autoclave liquid environment. These components were affixed with Monel 400 wire to the autoclave cooling coil for testing.

Component Assortment for Direct-Exposure Testing Within Autoclave Liquid Environment

1. Metal Bellows

The conventional BHTV sensor incorporates a metal bellows to serve as a transducer-oil accumulator. The physical survivability of a metal bellows in a geothermal liquid environment is therefore of interest.

A Type 347 stainless steel bellows was acquired for testing from Metal Bellows Corporation; 1075 Providence Highway; Sharon, MA 02067. They can also supply Inconel units.

2. Swagelok-Rod Assemblies

A means is needed for reliably affixing the metal bellows transducer-oil accumulator to the sensor body. A Swagelok tube fitting is a candidate for this application.

In order to test the quality of Swagelok-fitting seals in a geothermal liquid environment, a structural assembly was designed that comprised a joined Swagelok pair sealed at both ends with solid stainless steel rods so as to form a small capsule filled with air. The flattened rod end surfaces at the interior of the capsule cavity were polished prior to assembly; the intent being that during post-test analysis a leaked seal would be identified through observed corrosion and discoloration of these surfaces.

A total of four Swagelok-rod assemblies were prepared for testing; two which utilized 1/8-inch diameter rods and two which utilized 1/4-inch diameter rods. The Swageloks were fabricated of Type 316 stainless steel and the solid rods were fabricated of Type 304 stainless steel.

The Swagelok tube fittings were obtained from Crawford Fitting Company; 29500 Solon Rd.; Solon, OH 44139.

3. Stainless Steel Hose Clamps

Geothermal-environment compatible hose clamps may be useful for affixing a tubular acoustic window to the sensor body. Ordinary stainless steel hose clamps are unacceptable because, although they may employ stainless steel bands, their screws are made of cadmium-plated carbon steel.

Two all-stainless-steel hose clamps were acquired for testing from Breeze Corporations, Inc.; 100 Aero-Seal Drive; Saltsburg, PA 15681. These clamps employ a band made of Type 302 stainless steel.

A pre-test photograph of the component assortment for direct-exposure testing within the autoclave liquid environment is shown as Figure 3. Here the metal bellows appears in the upper right-hand corner, the hose clamps appear in the upper left-hand corner, the 1/4-inch Swagelok-rod assemblies appear in the lower left-hand corner, and the 1/8-inch Swagelok-rod assemblies appear in the lower right-hand corner.

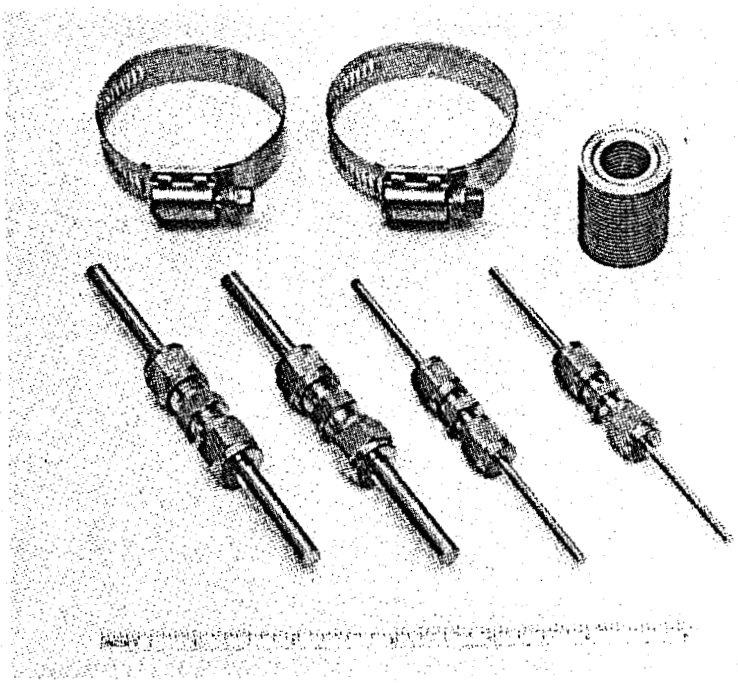

Figure 3. Pre-test Photograph of Component Assortment for Direct-Exposure Testing Within Autoclave Liquid Environment.

II. AUTOCLAVE TEST DESCRIPTION

The second autoclave test was carried out from 06 March 1978 until 08 March 1978 by Pressure Chemical Company, 3419 Smallman Street, Pittsburgh, PA 15201. Work was performed in accordance with technical Requirements Description No. ST-001, Revision A, Autoclave Test Plan (see end of this Appendix), and the following four specific items:

(1) At the discretion of Westinghouse Electric Corporation, any phase of the contracted testing may be witnessed by Westinghouse personnel.

(2) Westinghouse shall supply 0.040-inch diameter Monel 400 wire in lieu of the 0.035-inch diameter 304 stainless steel wire called out in Sections 3.4 and 4.1 of ST-001, Revision A.

(3) Westinghouse shall supply five (5) test capsules in lieu of the four (4) capsules as called out in Sections 3.4 and 4.1 of ST-001, Revision A.

(4) Westinghouse shall also supply the following items to be affixed with Monel 400 wire to the autoclave cooling coil:

(a) Assemblies comprised of 316 stainless steel Swageloks affixed to 304 stainless steel rods; four (4) units each.

(b) Hose-clamps comprised of 302 stainless steel bands and 305 stainless steel screws; two (2) units each.

(c) Bellows fabricated of 347 stainless steel; one (1) unit each.

Conformance of both the autoclave test and resultant test data to the requirements of ST-001, Revision A, is reviewed below. The format followed is to first cite a specific section of ST-001, Revision A, and then to describe what was done in accordance with the cited section.

With reference to Section 4.1 of ST-001 and the four specific items cited, the five test capsules along with the Swagelok-rod assemblies, hose clamps and metal bellows were fastened to the outside surface of the autoclave's internal cooling coil using 0.0040-inch diameter Monel 400 wire. The test capsules were positioned to be 2-1/2-inches below the autoclave liquid level while undergoing test. Photographs of the mounted items appear in Figure 4 through 9.

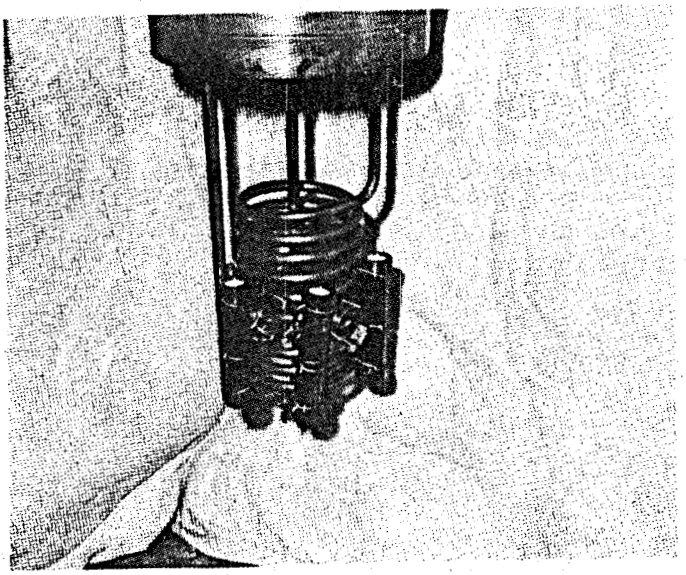

Fig. 4. Pre-Test Photograph of Test Capsules Fastened to Autoclave Cooling Coil

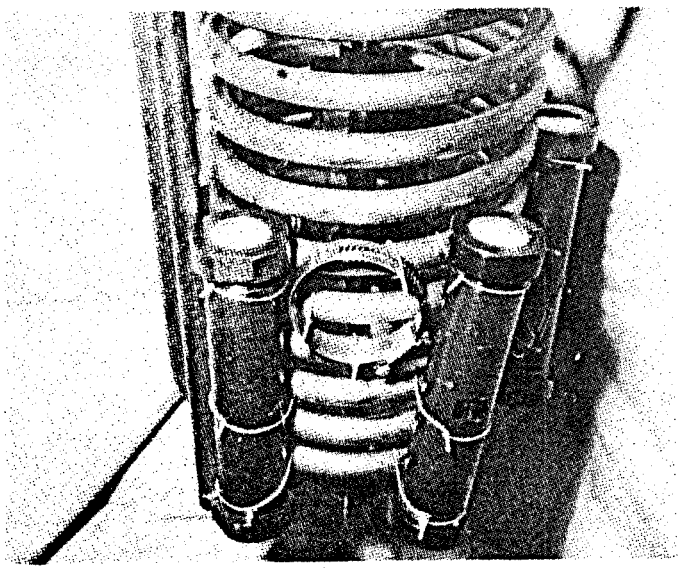

Fig. 5. Pre-Test Photograph of Test Capsules Fastened to Autoclave Cooling Coil

Left: Test Capsule A

Middle: Hose Clamp #1

Right: Test Capsule B

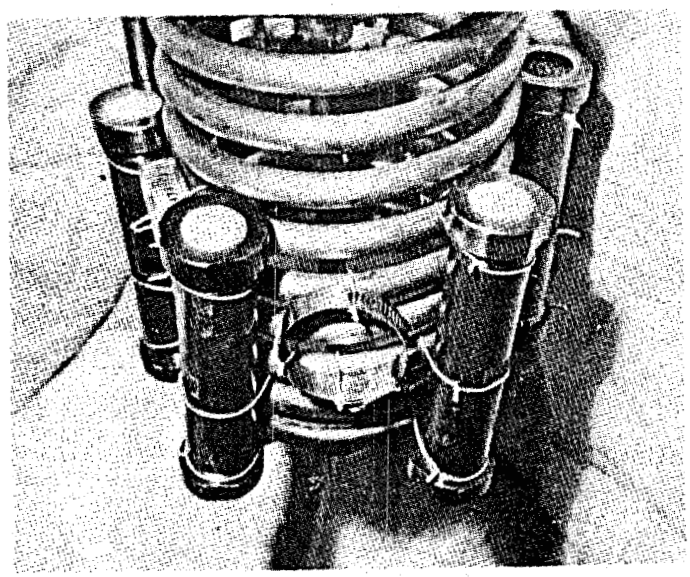

Fig. 6. Pre-Test Photograph of Test Capsules Fastened to Autoclave Cooling Coil

Left: Test Capsule B

Middle: Hose Clamp #2

Right: Test Capsule C

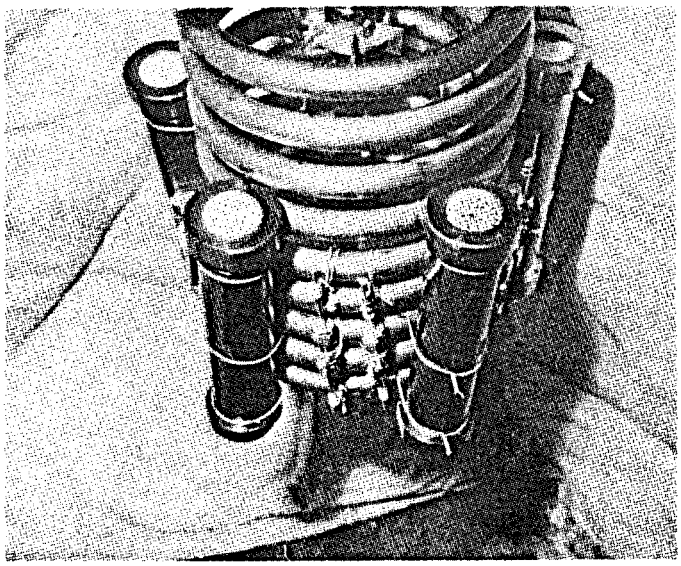

Fig. 7. Pre-Test Photograph of Test Capsules Fastened to Autoclave Cooling Coil

Left: Test Capsule C

Middle: 1/8 inch Swagelok-rod Assemblies

Right: Test Capsule D

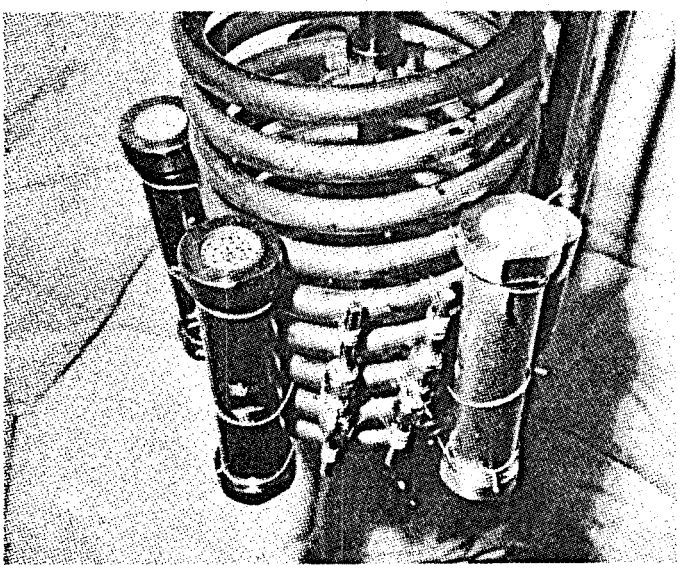

Fig. 8. Pre-Test Photograph of Test Capsules Fastened to Autoclave Cooling Coil

Left: Test Capsule D

Middle: 1/4 inch Swagelok-rod Assemblies

Right: Test Capsule E

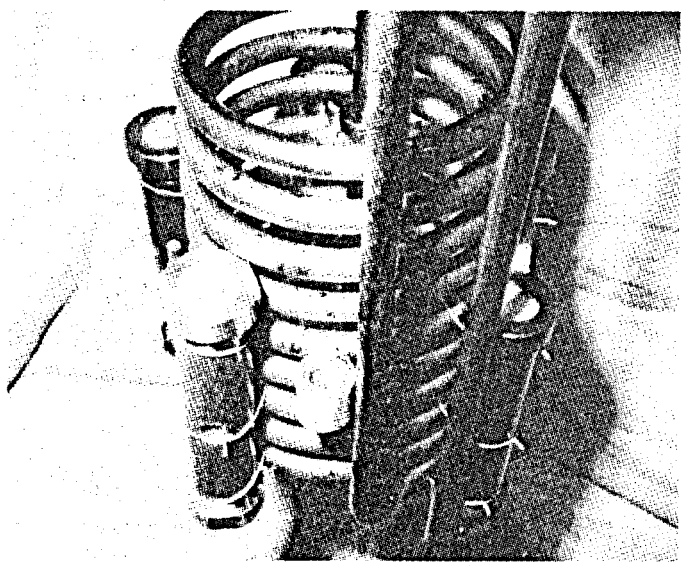

Fig. 9. Pre-Test Photograph of Test Capsules Fastened to Autoclave Cooling Coil

Left: Test Capsule E

Middle: Metal Bellows

Right: Test Capsule A

The following comments pertain to Section 4.2:

(1) The deionized water was deaerated for 80 hours with nitrogen prior to use. (This was done during the weekend preceding the test.)

(2) Prior to pressurized leak testing of the autoclave system, the specified autoclave-liquid ingredients were charged to the autoclave with the exception of the $Na_2S \cdot 9H_2O$ and a small amount of water. The ingredients were charged under a nitrogen gaseous blanket. Following charging, the solution was purged with nitrogen for 30 minutes after which the autoclave head was fastened into place while the nitrogen blanket was maintained.

(3) The autoclave system was slowly pressurized with nitrogen to 7500 psig, held at between 7500 and 7300 psig for 1/2 hour, and then depressurized. Since no significant pressure drop was observed during the 1/2 hour hold period, the autoclave seal was pronounced to be satisfactory.

(4) Following the pressure test, the $Na_2S \cdot 9H_2O$ was dissolved in the remaining small amount of deaerated deionized water, and the solution was poured into the depressurized autoclave via a small add-port. This solution was also prepared and charged under a nitrogen gaseous blanket.

(5) Following the charging of the $Na_2S \cdot 9H_2O$ and water solution, nitrogen gas was purged from the autoclave using argon gas. The autoclave liquid was then mixed for 5 minutes, after which a sample was removed for pH testing. The autoclave was again purged with argon and then pressurized with argon to 100 psig. This pressure was maintained overnight from 06 March to 07 March 1978.

With reference to Section 4.3, the volume of the autoclave liquid was 22,902 milliliters and the volume of the autoclave cover gas was 10,510.5 milliliters. (The 232.50 milliliter decrease in cover gas volume from the 10,743 milliliters recorded for the first autoclave test is due to the increase in test-piece volume.)

With reference to Section 4.4, the pre-test pH of the autoclave liquid was 5.5.

The following comments pertain to Section 4.5.

(1) With the autoclave still pressurized at 100 psig as set the night before, power was applied to the autoclave's electric heaters at 5:15 AM on 07 March 1978. At this time the heater control was set at 250°F. The room ambient temperature was recorded as 64°F.

(2) At 7:03 AM, 1.80 hours later, the autoclave liquid temperature reached 258°F, while the autoclave pressure remained at 100 psig. At this time the heater control was set to 550°F and argon gas was used to increase autoclave pressure to 1400 psig.

(3) At 8:45 AM, 1.70 hours later, the autoclave liquid temperature was measured at 550°F. The autoclave pressure had also risen of its own accord to 2000 psig.

(4) The 5-hour period from 8:45 AM until 1:45 PM can best be described as a test-condition attainment phase. During this time argon gas was used to gradually increase autoclave pressure to 7000 psig, while the temperature control was adjusted to bring the autoclave liquid temperature to 527°F. Also, during this time the measurement thermocouples were temporarily removed from their well and recalibrated against a thermometer in a 527°F silicone oil bath. The total elapsed time from the start of heating at 5:15 AM until the attainment of 527°F, 7000 psig test conditions at 1:45 PM was 8.50 hours.

The following comment pertains to Section 4.6.

(1) The specified test period lasted 17.17 hours from 1:45 PM on 07 March 1978 until 6:55 AM on 08 March 1978. During this time, the pressure recording showed a mean of 7,009.34 psig and a standard deviation of 13.02 psig, while the temperature recording showed a mean of 529.60°F and a standard deviation of 2.43°F.

With reference to Section 4.7, the total time for the test-condition removal phase was 5.08 hours.

With reference to Section 4.8, the post-test pH of the autoclave liquid was 4.9.

The following comments pertain to Section 5.1.

(1-a) The primary instrument thermocouple was calibrated in a silicone oil bath at 527°F against a standard thermometer. The thermocouple accuracy was determined to be $\pm$ 2°F at 527°F. Since the autoclave liquid was continuously stirred during the test, the accuracy with which temperature was measured is therefore $\pm$ 2°F (E = 2°F).

(1-b) During the specified test period, the temperature recording showed a mean of 529.60°F and a standard deviation of 2.43°F (σ = 2.43°F). Since 99.7 percent of all data lies within $\pm$ 3σ of the mean, the steadiness with which temeprature was maintained during the specified test period was $\pm$ 7.29°F (3σ = 7.29°F).

(1-c) The precision with which temperature was both known and maintained during the specified test period can be taken as being equal to the square root of the sum-of-the-squares of both the temperature-measurement accuracy of the temperature-data steadiness, i.e.

$$\pm A = \pm \sqrt{(E)^2 + (3\sigma)^2}$$

$$= \pm 7.56^{\circ}F$$

(1-d) The autoclave-liquid temperature during the specified test period can therefore be described as having a mean of 529.60°F and of being maintained within a precision of ± 7.56°F.

(2-a) Prior to the start of testing, the autoclave's pressure transmitter was calibrated against a Heise Bourdon-tube pressure gage having an accuracy of ± 30 psig. The accuracy with which pressure was measured is therefore ± 30 psig (E = 30 psig).

(2-b) During the specified test period, the pressure recording showed a mean of 7,009.34 psig and a standard deviation of 13.02 psig (σ = 13.02 psig). Since 99.7 percent of all data lies within ± 3σ of the mean, the steadiness with which pressure was maintained during the specified test period was ± 39.06 psig (3σ = 39.06 psig).

(2-c) The precision with which pressure was both known and maintained during the specified test period can be taken as being equal to the square root of the sum-of-the-squares of both the pressure-measurement accuracy and the pressure-data steadiness, i.e.

$$\pm A = \pm \sqrt{(E)^2 + (3\sigma)^2}$$

$$= \pm 49.25 \text{ psig}$$

(2-d) The autoclave pressure during the specified test period can therefore be described as having a mean of 7,009.34 psig and of being maintained within a precision of ± 49.25 psig.

With reference to Section 5.2, the pre-test pH was 5.5 and the post-test pH was 4.9.

With reference to Section 5.3, the liquid volume was 22,902 milliliters and the gaseous volume was 10,510.5 milliliters.

With reference to Section 5.4, the pre-test room ambient was 64°F and the post-test room ambient temperature was also 64°F.

III. POST-TEST ANALYSIS OF MATERIALS AND COMPONENTS

At the completion of autoclave itesting on 08 March 1978, photographs were taken of the mounted test items so as to record their post-test in situ appearance. These are shown in Figures 10 through 15.

Following the taking of the post-test in situ photographs, the test capsules and directly-exposed component assortment were removed from the autoclave cooling coil and taken to the Westinghouse R&D Center for post-test analysis. Once there, these parts were immediately cleaned and photographed. These photographs are shown in Figures 16 through 22.

Due to the convexity of the TFE Teflon windows of Test Capsules A, B, C, and E as seen in the photographs of Figures 16 through 19, it was apparent that the oil contained within all four test capsules had thermally expanded during the test. With reference to Figure 17, it also appeared at this stage of the post-test analysis that one of the TFE Teflon windows of Test Capsule had cracked and leaked during testing.

With reference to Figure 22, superficial examination of the hose clamps, metal bellows, and Swagelok-rod assemblies at this stage of the post-test analysis showed them to be discolored but otherwise structurally intact.

Test Capsules A, B, C, and E were next opened and emptied of their contents. While the test capsules were being opened, it was observed that all of their end caps were loosened. The loosening probably was caused by the extrusion of the TFE Teflon windows out from under the end caps, in response to the force of the thermally expanding capsule oil during test.

At this point the contents of the capsules could best be described as sludge comprised of individual test components, tabular alumina and oil. The surviving individual test components were then removed for subsequent cleaning and examination. It should be noted at this point that no epoxy specimens were recovered from Test Capsule A.

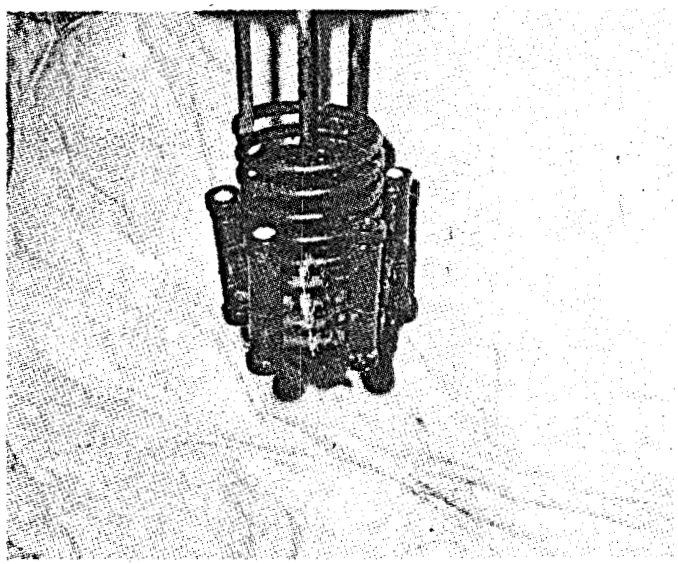

Fig. 10. Post-Test Photograph of Test Capsuled Fastened to Autoclave Cooling Coil

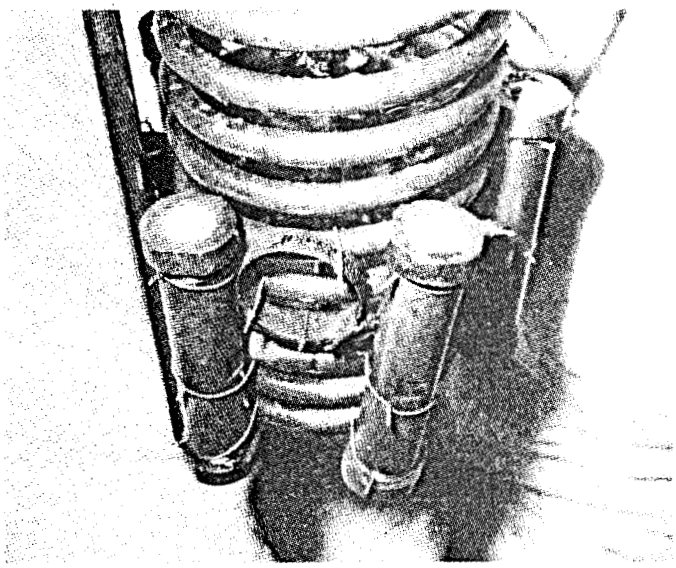

Fig. 11. Post-Test Photograph of Test Capsuled Fastened to Autoclave Cooling Coil

Left: Test Capsule A

Middle: Hose Clamp #1

Right: Test Capsule B

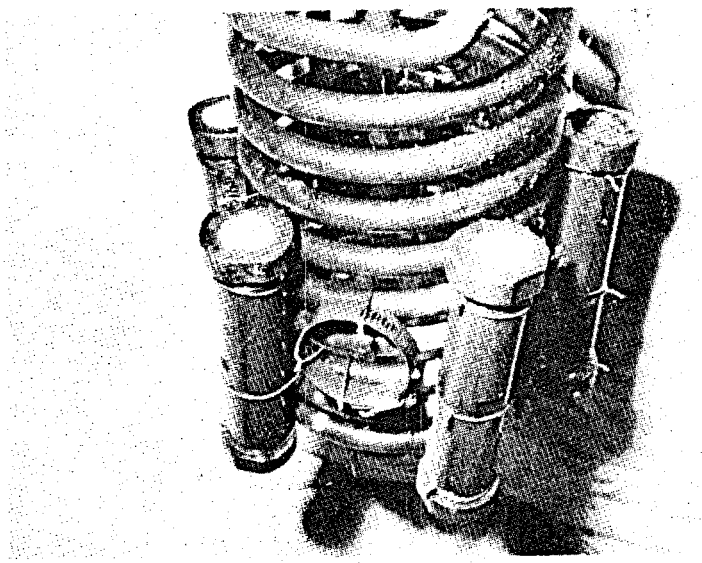

Fig. 12. Post-Test Photograph of Test Capsules Fastened to Autoclave Cooling Coil

Left: Test Capsule B

Middle: Hose Clamp #2

Right: Test Capsule C

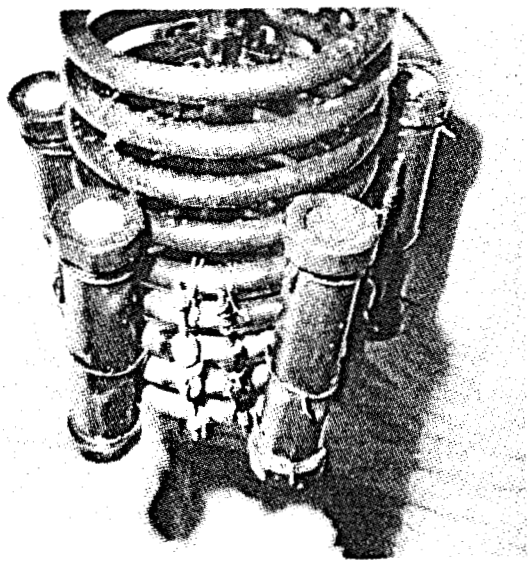

Fig. 13. Post-Test Photograph of Test Capsules Fastened to Autoclave Cooling Coil

Left: Test Capsule C

Middle: 1/8 inch Swagelok-rod Assemblies

Right: Test Capsule D

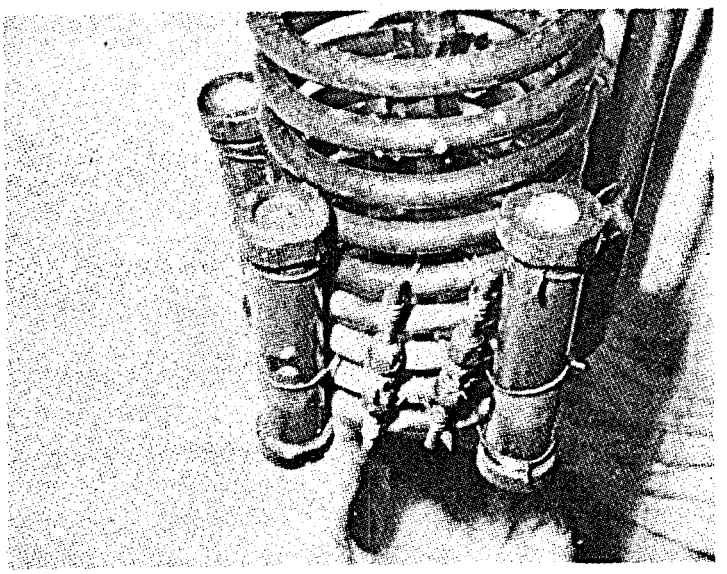

Fig. 14. Post-Test Photograph of Test Capsules Fastened to Autoclave Cooling Coil

Left: Test Capsule D

Middle: 1/4 inch Swagelok-rod Assemblies

Right: Test Capsule E

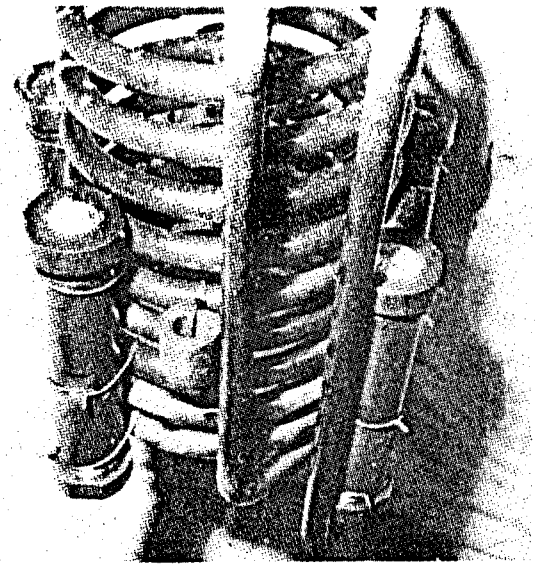

Fig. 15. Post-Test Photograph of Test Capsules Fastened to Autoclave Cooling Coil

Left: Test Capsule E

Middle: Metal Bellows

Right: Test Capsule A

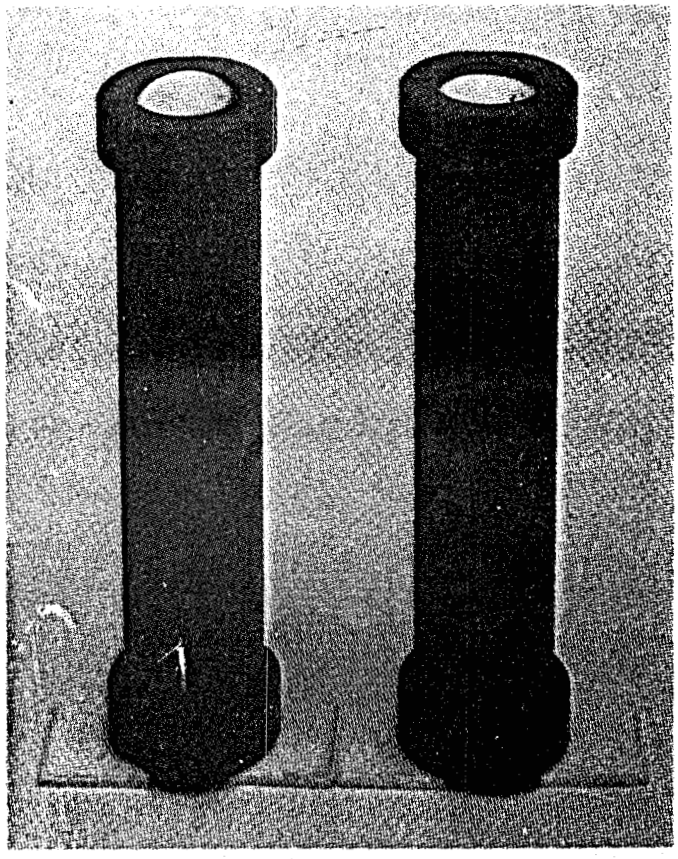

Fig. 16. Post-Test Photograph of Test Capsules A and B

Left: Test Capsule A, End Cap A1 Facing Upward

Right: Test Capsule B, End Cap B1 Facing Upward

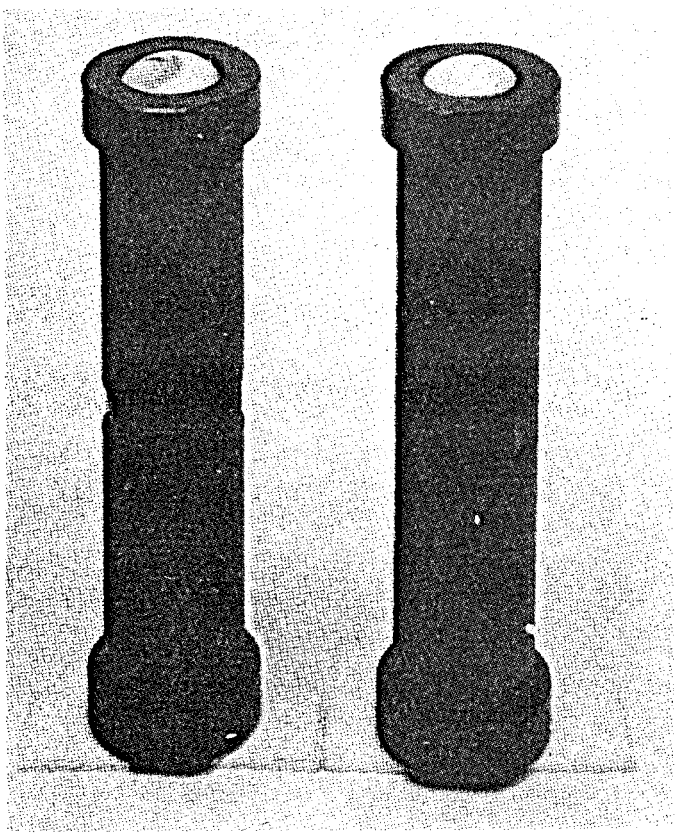

Fig. 17. Post-Test Photograph of Test Capsules A and B

Left: Test Capsule A, End Cap A2 Facing Upward

Right: Test Capsule B, End Cap B2 Facing Upward

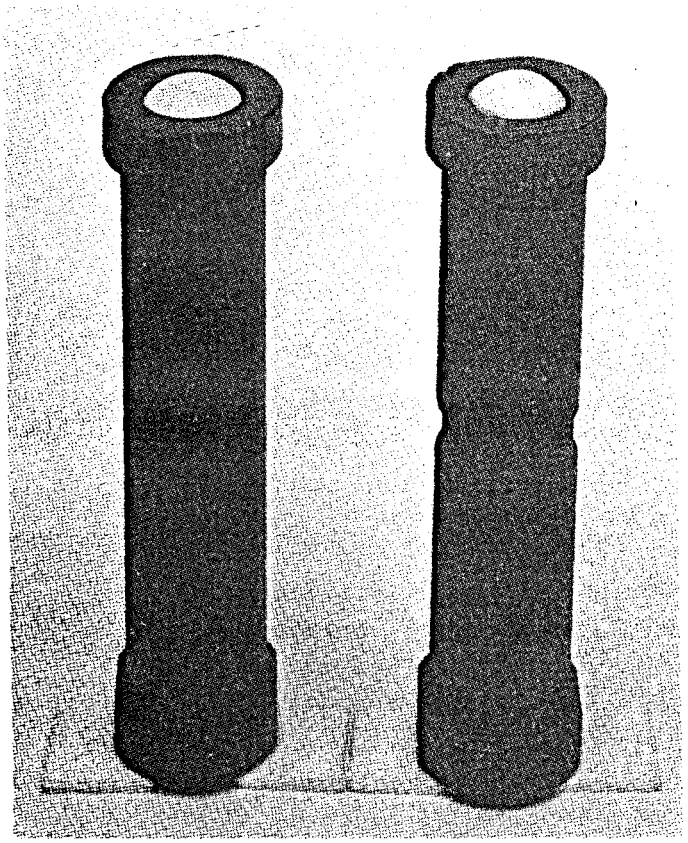

Fig. 18. Post-Test Photograph of Test Capsules C and E

Left: Test Capsule C, End Cap C1 Facing Upward

Right: Test Capsule E, End Cap E1 Facing Upward

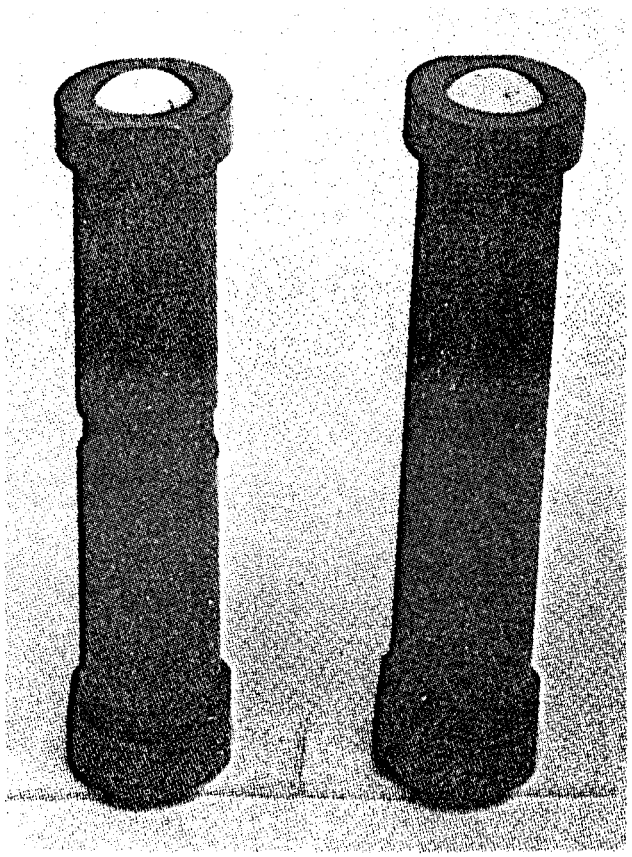

Fig. 19. Post-Test Photograph of Test Capsules C and E

Left: Test Capsule C, End Cap C2 Facing Upward

Right: Test Capsule E, End Cap E2 Facing Upward

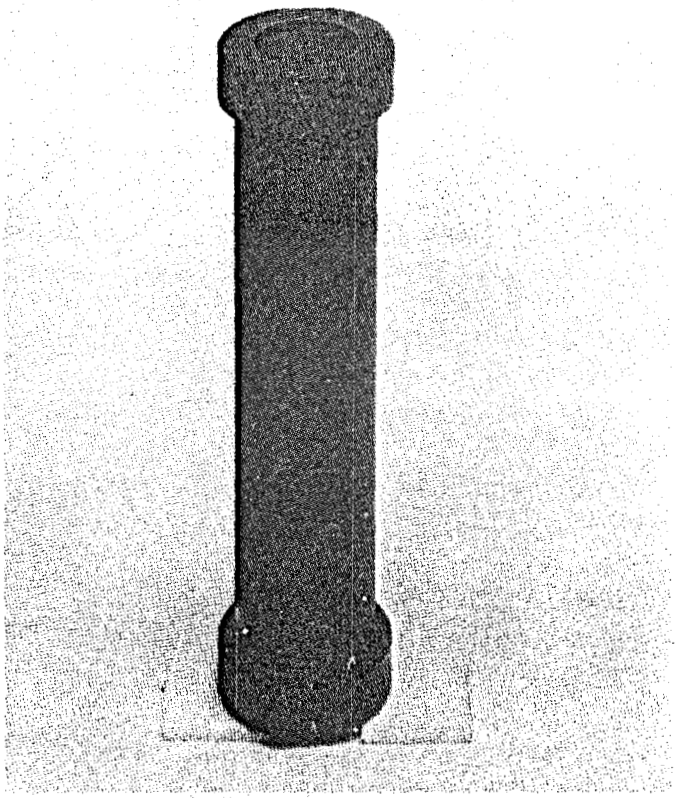

Fig. 20. Post-Test Photograph of Free-Flooding Test Capsule D, End Cap D1 Facing Upward

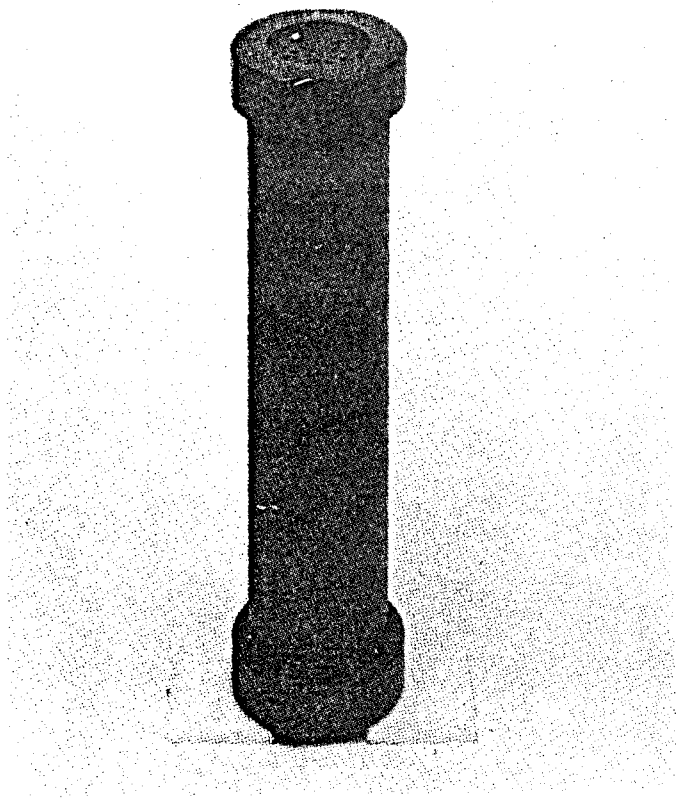

Fig. 21. Post-Test Photograph of Free-Flooding Test Capsule D, End Cap D2 Facing Upward

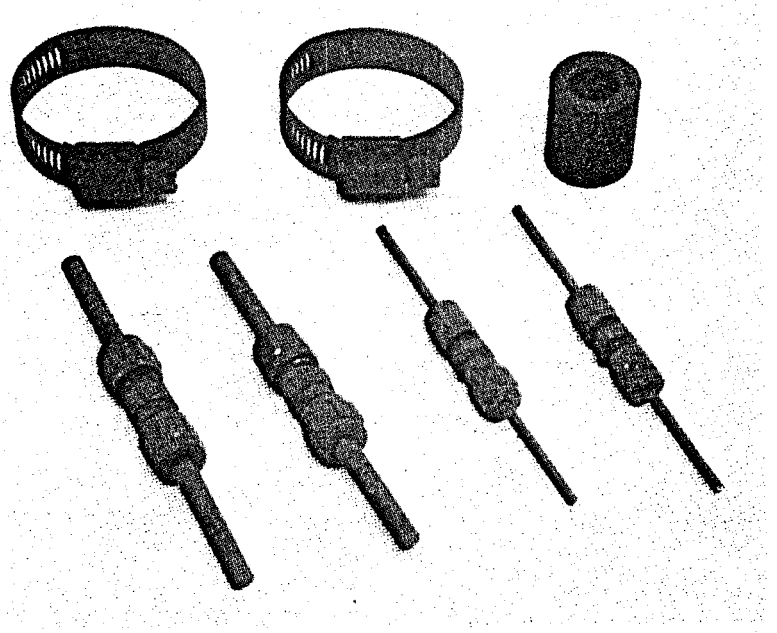

Fig. 22. Post-Test Photograph of Component Assortment Subjected to Direct-Exposure Testing Within Autoclave Liquid Environment

The remaining oil and tabular alumina sludge from Test Capsules A, B, C, and E was examined next. That from Test Capsule A was very dark in color and highly viscous, that from Test Capsule B was slightly darkened and moderately viscous, and that the Test Capsules C and E was white in color and had the same moderate viscosity as the sludge recovered from Test Capsule B.

Test Capsule A was filled with Mobil Jet Oil II both in this test and in the first test of 10-12 January 1978. In both tests, no epoxy specimens were recovered and the remaining sludge was dark in color and highly viscous. This evidence suggests that Mobil Jet Oil II may itself decompose at elevated temperature, that it may fail to protect the chosen epoxy specimens from elevated temperature destruction, and that it may possibly aid in the elevated temperature destruction of the chosen epoxy specimens.

Test Capsule B was filled with Dow Corning DC-210H silicone oil both in this test and in the first test of 10-12 January 1978. In both test, the remaining sludge was slightly darkened in color but retained its pre-test moderate viscosity. This darkening suggests that Dow Corning DC-210H may either decompose slightly at elevated temperature or may fail to fully protect the chosen epoxy specimens from elevated temperature decomposition.

Test Capsule C was filled with Dow Corning DC-550 high-phenyl silicone oil both in this test and in the first test of 10-12 January 1978. In both tests the remaining sludge retained its pre-test color and moderate viscosity. This evidence suggests that Dow Corning DC-550 high-phenyl silicone oil may hold up well in an elevated temperature environment.

Test Capsule E was filled with Dow Corning DC-710 high-phenyl silicone oil. The remaining sludge retained its pre-test color and moderate viscosity. This evidence suggests that Dow Corning DC-710 high-phenyl silicone oil may hold up well in an elevated temperature environment.

The individual test components from Test Capsules A, B, C, and E were next cleaned up and examined for damage. Post-test photographs of these components appear in Figures 23 through 26.

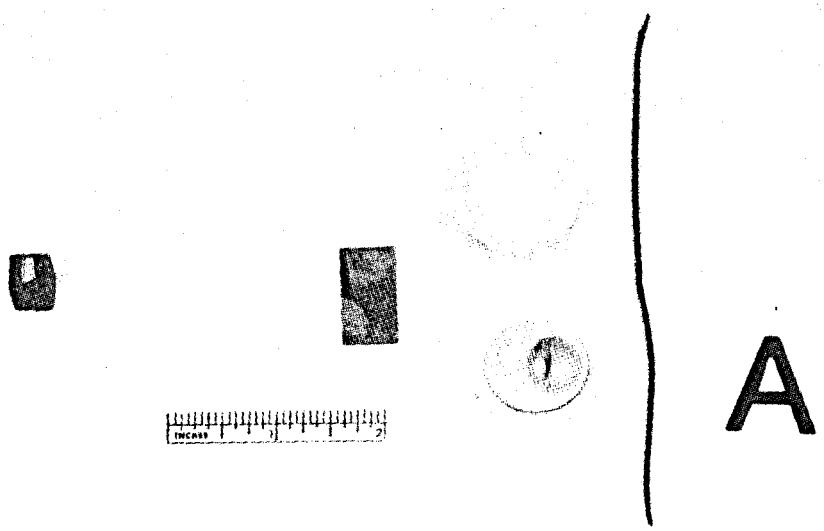

Fig. 23. Post-Test Photograph of Test Capsule A Contents

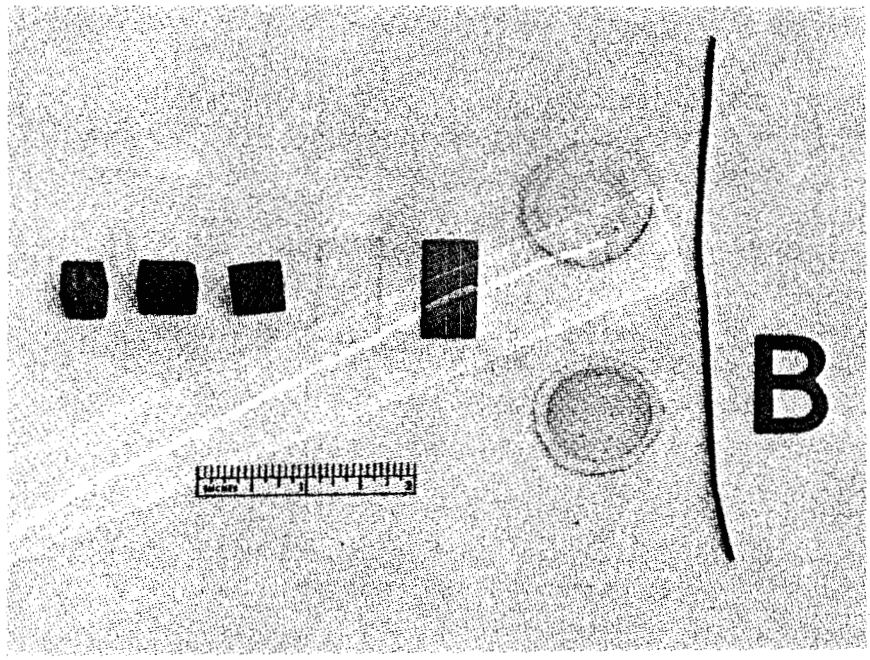

Fig. 24. Post-Test Photograph of Test Capsule B Contents

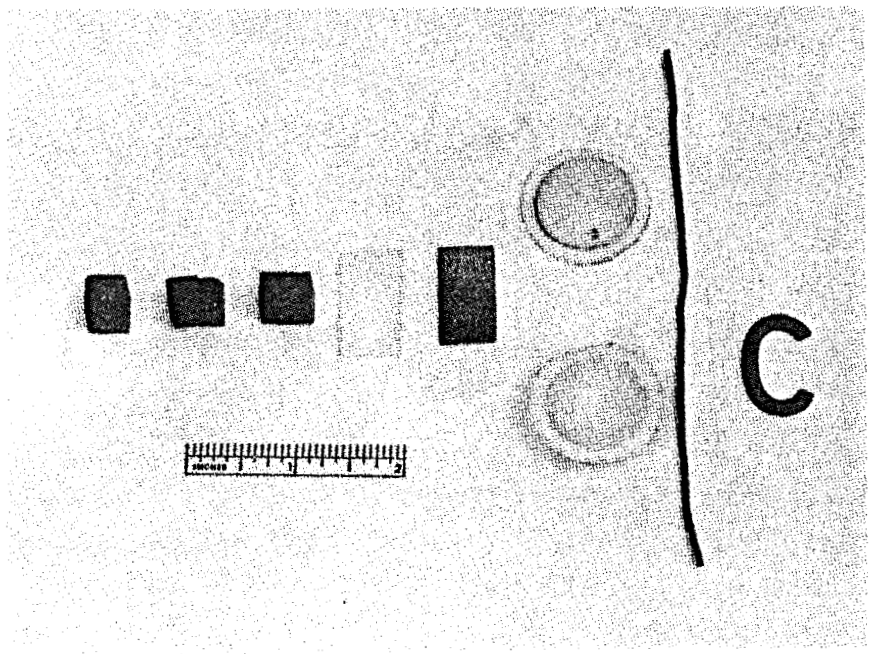

Fig. 25. Post-Test Photograph of Test Capsule C Contents

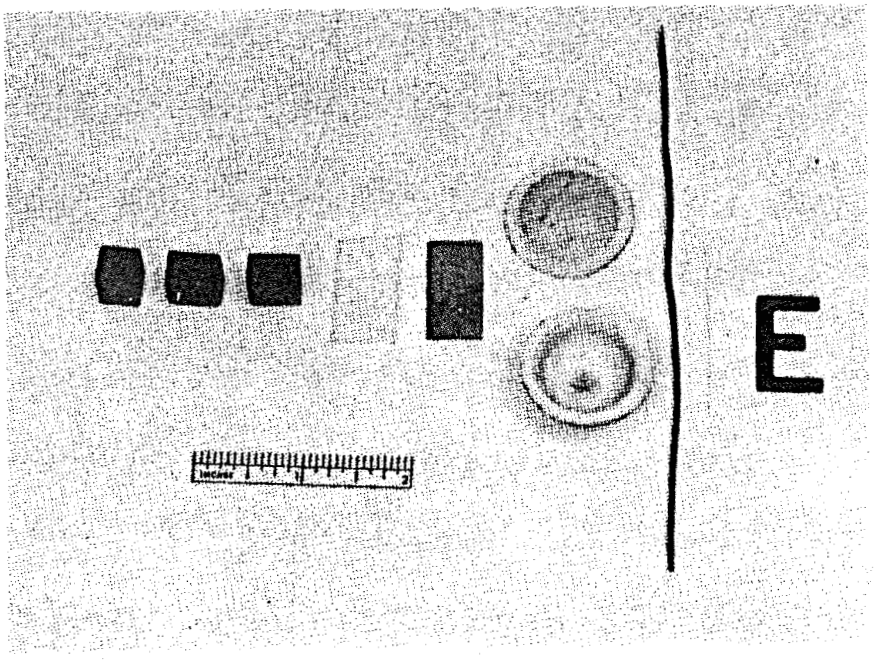

Fig. 26. Post-Test Photograph of Test Capsule E Contents

Candidate Solid Material and Components Assortment for Test Capsules A, B, C, and E

1. Rudimentary Piezoceramic Transducer Assembly

This specimen emerged from the test in fairly good condition for Test Capsules A, B, C, and E. Although coated with a hydrocarbon residue, the 3/8 inch cube of tungsten-filled alumina cement retained both its shape and dimensions fiarly well. The piezoceramic element remained firmly bonded to the cube, indicating that the Epo-Tek H20E electrically conductive epoxy is satisfactory. When prodded with a pair of tweezers, the piezoceramic's fired-on outer silver electrode remained firmly adherent; however, the Epo-Tek H20E had hardened somewhat from its original consistency.

This element is shown at the extreme left in Figures 23 through 26.

2. Potting Materials

2.1 Stycast 2762FT

This element completely disintegrated in Test Capsule A, but emerged in fairly good condition from Test Capsules B, C, and E. The surviving samples had only slight dimensional changes and discoloration, but showed no marked embrittlement or gross decomposition.

This element appears third from the left in Figures 23 through 26.

2.2 Duralco 700

This element completely disintegrated in Test Capsule B, became partially decomposed and dimensionally changed in Test Capsules B, C, and E. Its condition was somewhat worse than that of the Stycast 2762FT.

This element appears second from the left in Figures 23 through 26.

3. Hookup Wire

Superficially, the TFE Teflon insulated wire specimen emerged from the test in very good condition for Test Capsules A, B, C, and E. No embrittlement, decomposition, or hydrocarbon-residue coating were observed.

When prepared, the wire specimens were all cut to 5-inch straight lengths and care was taken to assure that the insulation was flush with the copper-wire termini. Post-test measurements on all four specimens showed that the copper wire itself had a mean length of 5.13 inches with a 0.005 inch standard deviation, while its Teflon insulation had a mean length of 5.44 inches with a 0.150 inch standard deviation. This information suggests that the stranded copper wire may have untwisted during elevated temperature test and that its TFE Teflon insulation may have simultaneously expanded due to oil absorption. These phenomena may also explain the apparent shortening of copper wire as reported in the first (10-12 January 1978) autoclave test.

This element appears to the far right of Figures 23 through 26.

4. TFE Teflon Windows

The TFE Teflon windows of Test Capsules A, B, C, and E were grossly deformed. The formerly flat surface of each disk-like window had dimpled into a spherical contour. Some of the windows were cracked and discolored at the sites where they had ruptured under the presssure of the thermally-expanding test capsule oil. Ohterwise, these windows showed no signs of either embirttlement or of having been chemically attached.

The TFE Teflon windows appear second from the right in Figures 23 through 26.

5. Material Coupons

5.1 TFE Teflon

The TFE Teflon coupon samples recovered from Test Capsules A, B, C, and E were in very good shape. They were clean in appearance and showed only slight dimensional increases. They showed no signs of either embrittlement or of having been chemically attacked.

With reference to the dimensional changes, the mean values for the pre-test length (l), width (w), and thickness (t) dimensions along with the standard deviations (σ) are as follows: (1) l = 1.065 inch (σ_l = 0.016 inch); (2) w = 0.561 inch (σ_w = 0.007 inch); t = 0.0635 inch (σ_t = 0.0000 inch). The corresponding post-test values are as follows: (1) l = 1.069 inch (σ_l = 0.014 inch); (2) w = 0.566 inch (σ_w = 0.007 inch); (3) t = 0.651 inch (σ_t = 0.0005 inch).

The TFE Teflon coupon samples appear fourth from the right in Figures 23 through 26.

5.2 Type 304 Stainless Steel

The Type 304 stainless steel coupon samples recovered from Test Capsules A, B, C, and E were in very good shape. Except for some slight tarnishing, they were clean in appearance. They showed no dimensional changes and no signs of gross chemical attack.

The Type 304 stainless steel coupon sample is shown third from the right in Figures 23 through 26.

Candidate Material and Component Assortment for Free-Flooding Test Capsules D

1. High-Temperature Elastomeric Materials

1.1 Kalrez

The Kalrez coupon samples recovered from free-flooding Test Capsules D were slightly swollen and had some surface cracking, but were still very pliable.

With reference to their dimensional changes, the mean values for the pre-test length (l), width (w), and thickness (t) dimensions along with their standard deviations (σ) are as follows: (1) l = 1.051 inches (σ_l = 0.021 inch); (2) w = 0.480 inches (σ_w = 0.006 inch); (3) t = 0.060 inch (σ_t = 0.000 incch). The corresponding post-test values are as follows: (1) l = 1.123 inches (σ_l = 0.021 inch); (2) w = 0.517 inches (σ_w = 0.006 inch); (3) t = 0.067 inch (σ_t = 0.000 inch).

The Kalrez coupon samples occupy the extreme-left and second-from-left positions in the bottom row of Figure 27.

1.2 AFLAS-50

The recovered AFLAS-150 coupon samples were swollen and had some surface cracking. In addition, their surfaces were covered with a large number of small-sized dimples.

With reference to the dimensional changes, the mean values for the pre-test length (l), width (w), and thickness (t) dimensions along with their standard deviations (σ) are as follows: (1) l = 0.734 inches (σ_l = 0.006 inch); (2) w = 0.708 inches (σ_w = 0.002 inch); (3) t = 0.132 inches (σ_t = 0.000 inch). The corresponding post-test values are as follows: (1) l = 0.769 inches (σ_l = 0.012 inch); (2) w = 0.738 inches (σ_w = 0.004 inch); (3) t = 0.173 inches (σ_t = 0.010 inch).

The AFLAS-150 coupon samples occupy the third-from-left and fourth-from-left positions in the bottom row of Figure 27.

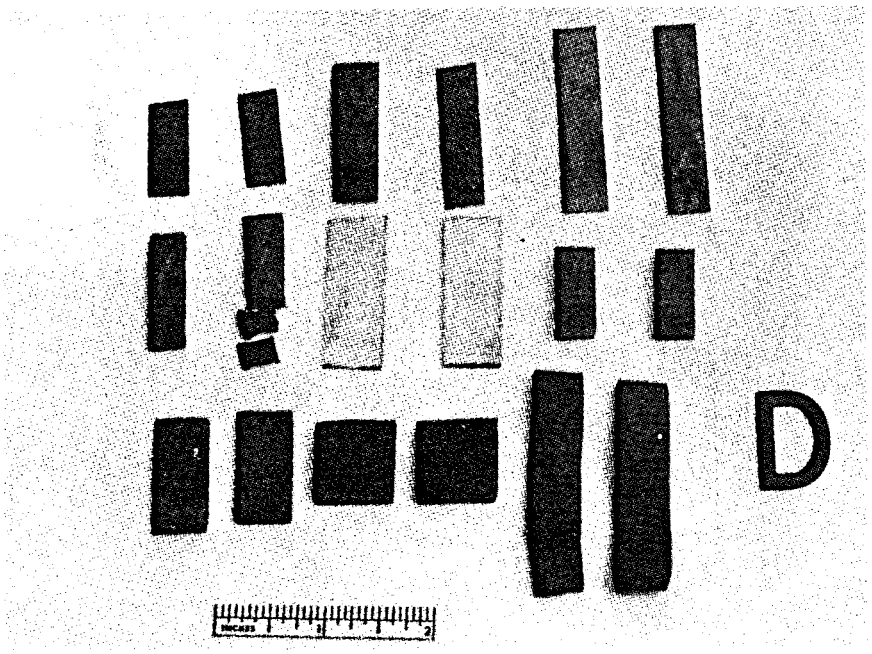

Fig. 27. Post-Test Photograph of Test Capsule D Contents (Group 1 of 2)

1.3 Ethylene Propylene

The recovered ethylene propylene coupon samples somewhat swollen and had some surface cracking. In addition, they felt gummy.

With reference to their dimensional changes, the means and standard deviations for their pre-test dimensions are as follows: (1) l = 1.987 inches (σ_l = 0.000 inches); (2) w = 0.410 inches (σ_w = 0.018 inches); (3) t = 0.082 inches (σ_t = 0.001 inches). The corresponding post-test values are as follows: (1) l = 2.200 inches (σ_l = 0.004 inch); (2) w = 0.486 inches (σ_w = 0.016 inches); (3) t = 0.173 inches (σ_t = 0.010 inches).

The ethylene propylene coupon samples occupy the extreme-right and second-from-right positions in the bottom row of Figure 27.

1.4 Phosphonitrilic Fluoroelastomer

The recovered phosphonitrilic fluoroelastomer coupon samples were embrittled to the point where they could be easily fractured when touched.

The phosphonitrilic fluoroelastomer coupon samples occupy the extreme-left and second-from-left positions in the middle row of Figure 27.

2. Metal Coupons

2.1 Type 304

The recovered Type 304 stainless steel coupon samples were blackened but otherwise were in very good shape. They showed no measurable dimensional changes, although they were slightly pitted in spots.

The Type 304 stainless steel coupon sampls are shown in the extreme-right and second-from-right positions in the top row of Figure 28.

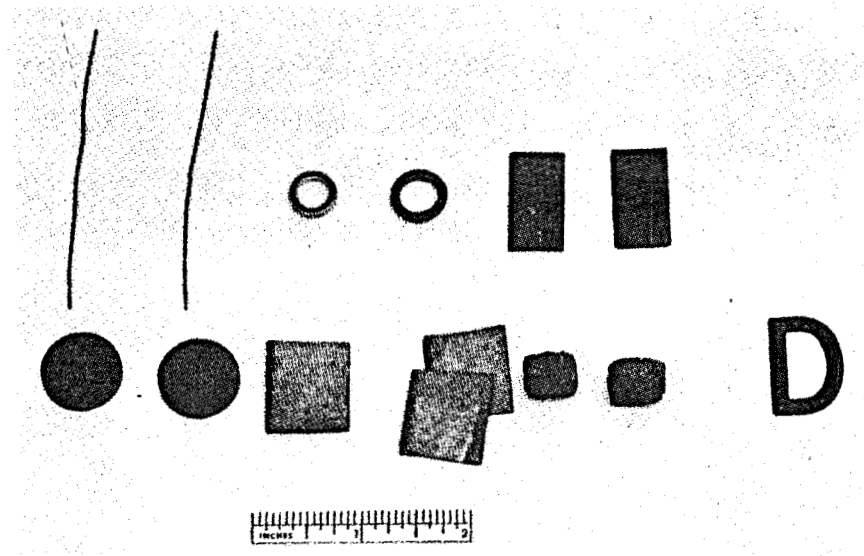

Fig. 28. Post-Test Photograph of Test Capsule D Contents (Group 2 of 2)

2.2 Inconel 718

The Inconel 718 coupon samles recovered were in very good shape. Except for some slight tarnishing, they were clean in appearance. They showed no dimensional changes and no signs of gross chemical attack.

The Inconel 718 coupon samples occupy the entire top row of Figure 27.

3. High-Temperature Plastic Materials

3.1 TFE Teflon

The recovered TFE Teflon coupon samples were in very good shape. They were only slightly discolored and showed only slight dimensional increases. They showed no signs of embrittlement or of having been chemically attacked.

With reference to their dimensional changes, the means and standard deviations for their pre-test dimensions are as follows:

(1) $l = 1.567$ inches ($\sigma_l = 0.025$ inches);
(2) $w = 0.536$ inches ($\sigma_w = 0.002$ inches);
(3) $t = 0.0635$ inches ($\sigma_t = 0.000$ inches).

The corresponding post-test values are as follows:

(1) $l = 1.569$ inches ($\sigma_l = 0.023$ inches);
(2) $w = 0.544$ inches ($\sigma_w = 0.004$ inches);
(3) $t = 0.065$ inches ($\sigma_t = 0.000$ inches).

The TFE Teflon coupon samples are the two white samples at the center of Figure 27.

3.2 Astrel 360

The Astrel 360 coupon samples completely decomposed during the test. No remains of these samples were recovered.

3.3 Polybutadiene

The recovered polybutadiene coupon samples were in fair shape. They were no longer transparent, but had crystallized and were now translucent. In addition, they were warped and exhibited some surface cracking. Because of the warping and the non-uniformity of the pre-test thickness dimension, it was impossible to make reliable post-test dimensional measurements.

The polybutadiene coupon samples occupy the far-right and second-from-right positions in the middle row of Figure 27.

3.4 Graphite-Carbon-Glass Filled TFE Teflon

The disk-shaped coupons of graphite-carbon-glass filled TFE Teflon were recovered in very good shape. They showed no apparent degradation.

With reference to their dimensional changes, the mean values for the pre-test diameter (d) and thickness (t) dimensions, along with their standard deviations (σ) are as follows:

(1) $d = 0.749$ inches ($\sigma_d = 0.000$ inches);
(2) $t = 0.100$ inches ($\sigma_t = 0.003$ inches).

The corresponding post-test values are as follows:

(1) $d = 0.752$ inches ($\sigma_d = 0.001$ inches);
(2) $t = 0.102$ inches ($\sigma_t = 0.002$ inches).

These disk-shaped coupons are shown in the lower left corner of Figure 28.

3.5 Doryl-Glass-Mica Composite

The recovered doryl-glass-mica composite samples were found to be stripped of epoxy. One sample's remnants comprised only two clean mica sheets. Although the other sample comprised two epoxy-bonded mica sheets, its exterior epoxy coating was completely gone.

The doryl-glass-mica composite samples occupy the third-from-left and fourth-from-left positions in the bottom row of Figure 28.

4. Potting Materials

The recovered Stycast 2762FT and Duralco 700 epoxy samples were badly decomposed and were not individually identifiably. These epoxy potting material samples occupy the far-right and second-from-right positions in the bottom row of Figure 28.

5. TFE Teflon Insulated Single-Conductor Copper Wire

Superficially, the TFE Teflon insulated single-conductor wire specimens emerged from the test in very good condition. No embrittlement, decomposition, or hydrocarbon-residue coating were observed.

When prepared, the wire specimens were all cut to 3-inch straight lengths and care was taken to assure that the insulation was flush with the copper-wire termini. Post-test measurements on both specimens showed that the length of the single-conductor copper wire itself remained at 3.00 inches but that the length of its TFE Teflon insulation had increased to a mean value of 3.18 inches with a standard deviation of 0.04 inches. This information suggests that the TFE Teflon insulation may have expanded due to absorption to autoclave liquid at elevated temperature.

The copper wire's silver coating was found to be completely blackened. This suggests that corrosive substances, among which sulfur may be included, had attacked the silver after first diffusing either along the Teflon-to-wire interface or directly through the Teflon itself. Aside from its blackened silver coating, the copper wire showed no other signs of chemical attack.

The recovered TFE Teflon insulated single-conductor wire specimens are shown in the upper left corner of Figure 28.

6. Bal Seals

Superficially, the Bal Seals emerged from the test in good condition. The Bal Seals are the ring-like objects shwon in the middle of the top row in Figure 28.

The component assortment that had been affixed to the autoclave cooling coil for testing was examined next. A post-test photograph of this assortment is shown in Figure 22. The condition of these components will now be described with reference to the listing given in Section II of this report.

Component Assortment for Direct-Exposure Testing Within Autoclave Liquid Environment

1. Metal Bellows

Superficially, the metal bellows emerged from the test in good condition. Other than being blackened, no evidence of gross chemical attack was seen. When held to a light, no signs of pin-hole cracks were to be seen.

The metal bellows is shown in the upper-right corner of Figure 22.

2. Swagelok-Rod Assemblies

All of the Swagelok seals had held up during testing. No corrosion or discoloration at all was observed on the seal-protected rod surfaces that formed part of the Swagelok-rod capsule's interior cavity.

The Swagelok-rod assemblies occupy the bottom row of Figure 22.

3. Stainless Steel Hose Clamps

The stainless steel hose clamps emerged from the test in good condition. Other than being blackened, no evidence of gross chemical attack was seen. It was possible to tighten and untighten all hose clamps.

The stainless steel hose clamps are shown in the upper-left corner of Figure 22.

APPENDIX III - AUTOCLAVE TEST PLANS

ST-001

1. Introduction

This technical requirements description delineates the steps that must be taken to assure the success of the forthcoming autoclave test of Westinghouse supplied capsules at Pressure Chemical Company, 3419 Smallman Street, Pittsburgh, PA 15201.

2. Objective

The objective is to continuously test Westinghouse supplied capsules in the Westinghouse specified autoclave liquid environment at a pressure of 7000 psi and a temperature of 275°C (527°F) for a period of time equal to or greater than 12 hours. So as to preclude thermal shock to component parts within the Westinghouse supplied capsules, the time required to reach the specified 7000 psi, 275°C (527°F) test conditions from room ambient pressure and temperature shall be no less than 2 hours. Likewise, the time required to return to room ambient pressure and temperature from the specified 7000 psi, 275°C (527°F) test conditions shall be no less than 2 hours.

During the test, the Westinghouse supplied capsules must be completely immersed within the Westinghouse specified autoclave liquid environment.

3. Test Components

3.1 Autoclave

Pressure Chemical Company's 10-gallon 316 stainless steel autoclave (11-1/2-inch I.D. by 19-inch internal length) shall be

utilized. The autoclave shall be fitted with its customary cooling coil, stirring impeller and thermocouple wells.

3.2 Autoclave Liquid

The autoclave liquid shall have the following chemical compositions:

H_2O = 990 g/l	(Note: 1,2)
NaCl = 25.4 g/l	
$NaHCO_3$ = 1.94 g/l (0.023M)	(Note: 3)
$Na_2S \cdot 9H_2O$ = 2.15 g/l (0.00895M)	(Note: 4)
HCl (1M) = 41.0 ml/l (0.0410M)	(Note: 5,6)

Notes:

(1) Deionized water is to be used exclusively.

(2) "g/l" designates "grams/liter."

(3) "M" designates "molar solution;" i.e., a solution containing one gram-mole of solute per liter of solution. Deionized water is to be used exclusively for preparing all required molar solutions.

(4) Westinghouse shall supply the required $Na_2S \cdot 9H_2O$ crystals. Pressure Chemical Company shall supply all other required chemicals.

(5) "ml/l" designates "milliliters/liter."

(6) A 0.0410M solution of HCl shall be prepared by adding 41.0 ml of 1M HCl solution to 1 liter of deionized water.

3.3 Autoclave-Liquid Cover Gas

Argon must be used exclusively as a cover gas. In addition, any cover gas volume must be kept to a minimum since autoclave-liquid dissolved gases will partition between the liquid and vapor phases.

The actual volumes occupied by both the autoclave-liquid and the cover gas at room ambient pressure and temperature prior to the start of testing must be precisely known. This will permit computation of the dissolved gas liquid-vapor phase paritition at the specified 7000 psi, 257°C (527°F) test conditions.

3.4 Test Capsules

Westinghouse shall supply four (4) 300-series stainless steel test capsules. Each capsule shall be comprised of a 1.315-inch diameter tube fitted with two 1-5/8-inch diameter end caps, and shall be 6-1/4-inches in overall length. Each capsule may be conveniently fastened to the outer perimeter of the autoclave's cooling coil by means of stainless steel wire for this purpose.

3.5 Instrumentation

Pressure Chemical Company shall supply all needed instrumentation such as a pressure gage, thermocouple, thermocouple ice-point reference junction, pH meter and strip chart recorder.

4. Test Procedure

4.1 Fastening of Test Capsules

Pressure Chemical Company personnel shall fasten each of the four (4) Westinghouse-supplied test capsules to the outer perimeter of the autclave's cooling coil by means of stainless steel wire. Westinghouse shall supply a spool of 0.035-inch diameter 304 stainless steel wire for this purpose.

4.2 Preparation, Filling and Deaeration of Autoclave Liquid

The autoclave liquid shall have a chemical composition as specified in Section 3.2 of this Technical Requirements Description No. ST-001, Revision A. However since oxygen is likely to have a strong effect on the reactivity of the chemicals in solution, it must be purged from the autoclave liquid to the greatest extent possible.

One suggested purging procedure is as follows: (1) fill the autoclave with deionized water; (2) add only the required NaCl solute; (3) heat the solution while bubbling argon through it; (4) add the remaining required solutes to solution. This purging procedure will assure that the water isn't re-aerated while the NaCl is dissolved into solution by stirring.

Another acceptable purging procedure would be to dissolve all solutes together following the water deaeration, provided that an argon cover gas is maintained so as to preclude re-aeration during stirring.

4.3 Pre-Test Liquid and Cover Gas Volume Measurements

The volume of the autoclave liquid at room ambient pressure and temperature shall be measured prior to the start of testing.

The volume of the autoclave cover gas at room ambient pressure and temperature at the start of testing shall be either: (1) measured; or (2) computed by subtracting the autoclave-liquid volume from the known volume of the autoclave cavity.

4.4 Pre-Test pH Measurement

The pH of the autoclave liquid must be measured prior to the start of testing.

4.5 Application of Pressure and Temperature Test Conditions

So as to preclude thermal shock to component parts within the Westinghouse supplied test capsules, the time require to reach the specified 7000 psi, 257°C (527°F) test conditions from room ambient pressure and temperature shall be no less than 2 hours.

4.6 Maintenance of Pressure and Temperature Test Conditions

The autoclave liquid environment shall be continuously maintained at a pressure of 7000 psi and a temperature of 275°C (527°F) for a period of time equal to or greater than 12 hours.

4.7 Removal of Pressure and Temperature Test Conditions

The time required to return to room ambient pressure and temperature from the specified 7000 psi, 275°C (527°F) test conditions shall be no less than 2 hours.

4.8 Post-Test pH Measurement

The pH of the autoclave liquid must be measured after the finish of testing.

5. Required Test Data

5.1 Pressure and Temperature

A continuous-time strip chart record of pressure and temperature shall be provided. The test-condition application, meaintenance and removal phases as called out in Sections 4.5, 4.6 and 4.7 of this Technical Requirements Description No. ST-001, Revision A, must be clearly delineated on the record. The precision with which pressure has been measured must be clearly delineated on the record. The precision with which temperature has been both measured and maintained within the autoclave liquid volume must be clearly delineated on the record. The record must also contain anecdotal observations.

5.2 pH

Both the pre-test and post-test measured pH values must be written on the pressure-temperature strip chart record.

5.3 Pre-Test Liquid and Cover Gas Volume

The volume of the autoclave liquid at room ambient pressure and temperature at the start of testing must be written on the pressure-temperature strip chart record.

The volume of the autoclave cover gas at room ambient pressure and temperature at the start of testing must be written on the pressure-temperature strip chart record.

5.4 Pre-Test Room Ambient Temperature

The room ambient temperature at the start of the testing must be written on the pressure-temperature strip chart record.

ST-005

Introduction

This technical requirements decription delineates the steps that must be taken to assure the success of the forthcoming autoclave test of a Westinghouse supplied sensor assembly at Pressure Chemical Company, 3419 Smallman Street, Pittsburgh, PA 15201.

Objective

The test objectives are 1.) test overall suitability of the sensor package concept under simulated geothermal borehole conditions, 2.) determine electroacoustic performance characteristics of the sensor under simulated geothrmal borehole conditions.

The first objective can be met by compliance with those sections relating to the autoclave liquid preparation and test procedures. The second objective will be met by operating the sensor in the pulse-echo mode during selected intervals in the test cycle. To accomplish this, special features are provided in the test sensor for bringing electrical leads out of the autoclave. In addition, special "target" structures will be located within the vessel.

Test Components

Autoclave

Pressure Chemical Company's 10-gallon 316 stainless steel autoclave (11-1/2 inch I.D. by 19-inch internal length) shall be utilized. The autoclave shall be fitted with its customary cooling coil and thermocouple wells. The customary stirring impeller and shaft shall be removed to provide for a replacement shaft which is an integral part of the Westinghouse supplied sensor assembly.

Autoclave Liquid

The autoclave liquid shall have the following chemical composition:

H_2O = 999 g/l	(Note: 1,2)
NaCl = 25.4 g/l	
$NaHCO_3$ = 1.94 g/l (0.023M)	(Note: 3)
$Na_2S \cdot 9H_2O$ = 2.15 g/l (0.00895M)	(Note: 4)
HCl (1M) = 41.0 ml/l (0.0410M)	(Note: 5,6)

Notes:

(1) Deionized water is to be used exclusively.

(2) "g/l" designates "grams/liter."

(3) "M" designates "molar solution;" i.e., a solution containing one gram-mole of solute per liter of solution. Deionized water is to be used exclusively for preparing all required molar solutions.

(4) Westinghouse shall supply the required $Na_2S \cdot 9H_2O$ crystals. Pressure Chemical Company shall supply all other required chemicals.

(5) "ml/l" designates "milliliters/liter."

(6) A 0.0410M solution of HCl shall be prepared by adding 41.0 ml of 1M HCl solution to 1 liter of deionized water.

Autoclave-Liquid Cover Gas

Argon must be used exclusively as a cover gas. In addition, any cover gas volume must not exceed 25 percent of total vessel volume.

The actual volumes occupied by both the autoclave-liquid and the cover gas at room ambient pressure and temperature prior to the start of testing must be precisely known. This will permit computation of the dissolved gas liquid-vapor phase partition at the specified 7000 psi, 257°C (527°F) test conditions.

Acoustic Sensor Assembly

Westinghouse will supply one acoustic sensor assembly consisting of a sensor housing, a volumetric expansion bellows, and a modified stirring shaft. The sensor assembly is detailed in Westinghouse drawing 1154C51. This design will locate the upper flange at approximately the level of the top cooling coil.

Acoustic Target Asemblies

Westinghouse will supply several assemblies which will provide simulated borewall targets for evaluting sensor performance. A typical assembly will consist of one or more wire rods attached to a small metal plate which will be attached to adjacent cooling coil windings using corrosion-resistant wire.

Instrumentation

Pressure Chemical Company shall supply all needed instrumentation such as a pressure gage, thermocouple ice-point reference junction, pH meter and strip chart recorder.

Wesitnghouse will provide all instrumentation necessary for evaluating electroacoustic performance of the sensor.

TEST PROCEDURE

Test Sequence

A single test cycle is anticipated, consisting of reaching test conditions, maintaining test conditions for specified time, and returning to ambient room conditions. Westinghouse personnel will make electroacoustic measurements of sensor performance as deemed necessary throughout the test cycle.

Sensor Assembly Placement

Correct assembly placement will be automatic as the integral replacement stirring shaft is installed in the packing seal. Careful handling throughout and minimal mechanical abuse during shaft seating are mandatory. Westinghouse personnel must witness sensor assembly placement.

Acoustic Target Assembly Placement

Exact locations of target assemblies will be specified in terms of evaluation and azimuth. Target assemblies will attach to the I.D. of the cooling coil, approximately 3-inches below the top coil. Westinghouse personnel will be available to assist in this step and must witness and approve final placements of target assemblies.

Preparation, Filling and Deaeration of Autoclave Liquid

The autoclave liquid shall have a chemical composition as specified in Section 3.2 of this Technical Requirements Description No. ST-005. However, since oxygen is likely to have a strong effect on the reactivity of the chemicals in solution, it must be purged from the autoclave liquid to the greatest extent possible.

One suggested purging procedure is as follows: (1) fill the autoclave with deionized water; (2) add only the required NaCl solute; (3) heat the solution while bubbling argon through it; (4) add the remaining required solutes to solution. This purging procedure will assure that the water isn't re-aerated while the NaCl is dissolved into solution by stirring.

Another acceptable purging procedure would be to dissolve all solutes together following the water deaeration, provided that an argon cover gas is maintained so as to preclude re-aeration during stirring.

Pre-Test Liquid and Cover Gas Volume Measurements

The volume of the autoclave liquid at room ambient pressure and temperature shall be measured prior to the start of testing.

The volume of the autoclave cover gas at room ambient pressure and temperature at the start of testing shall be either: (1) measured; or (2) computed by subtracting the autoclave-liquid volume from the known volume of the autoclave cavity.

Pre-Test pH Measurement

The pH of the autoclave liquid must be measured prior to the start of the testing.

Application of Pressure and Temperature Test Conditions

The time required to reach the specified 7000 psi, 275°C (527°F) test conditions from room ambient pressure and temperature shall be minimized.

Maintenance of Pressure and Temperature Test Conditions

The autoclave liquid environment shall be continuously maintained at a pressure of 7000 psi and a temperature of 275°C (527°F) for a period of time equal to or greater than 4 hours.

Removal of Pressure and Temperature Test Conditions

The time required to return to room ambient pressure and temperature from the specified 7000 psi, 275°C (527°F) test conditions shall be minimized.

Post-Test pH Measurement

The pH of the autoclave liquid must be measured after the finish of testing.

REQUIRED TEST DATA

Pressure and Temperature

A continuous-time strip chart record of pressure and temperature shall be provided. The test-conditions application, maintenance and removal phases must be clearly delineated on the record. The precision with which pressure has been measured must be clearly delineated on the record. The precision with which temperature has been both measured and maintained within the autoclave liquid volume must be clearly delineated on the record. The record must also contain anecdotal comments describing encountered difficulties as well as noteworth observations.

pH

Both the pre-test and post-test measured pH values must be written on the pressure-temperature strip chart record.

Pre-Test Liquid and Cover Gas Volume

The volume of the autoclave liquid at room ambient pressure and temperature at the start of testing must be written on the pressure-temperature strip chart record.

The volume of the autoclave cover gas at room ambient pressure and temperature at the start of testing must be written on the pressure-temperature strip chart record.

Pre-Test Room Ambient Temperature

The room ambient temperature at the start of testing must be written on the pressure-temperature strip chart record.

Acoustic Sensor Performance

All electroacoustic performance data will be generated by Westinghouse personnel.

TEST WITNESSING

At the discretion of Westinghouse Electric Corporation, any phase of the contracted testing may be witnessed by Westinghouse personnel.

PRESSURE VS. TEMPERATURE PRECAUTION

Sensor assembly heating without simultaneous application of external pressure will result in excessive internal gas expansion, exceeding deisgn limits and risking test success. This precaution stipulates that whenever the test assemblies are in the autoclave and exposed to temperature exceeding 100°F, sufficient cover gas pressure be applied and maintained to control the gas volume internal to the test assemblies. The minimum allowable pressure at any temperature greater than 100°F is that required to insure a maximum gas volume of approximately 1/2 of the ambient room temperature gas volume. The maximum allowable pressure is 7000 psi.

U.S. GOVERNMENT PRINTING OFFICE: 1980—640-258/1979